A MULTI-SCALE APPROACH TO UNDERSTANDING DESERT PIEDMONTS USING COSMOGENIC ISOTOPES AND CENTIMETER-SCALE SURVEYING

A Thesis Presented

by

Kyle Keedy Nichols

to

The Faculty of the Graduate College

of

The University of Vermont

In Partial Fulfillment of the Requirements
for the Degree of Master of Science
Specializing in Geology

March, 2000

Accepted by the Faculty of the Graduate College, The University of Vermont, in partial fulfillment of the requirements for the degree of Master of Science, specializing in Geology.

Thesis Examination Committee:

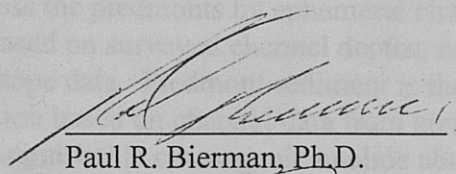

Advisor
Paul R. Bierman, Ph.D.

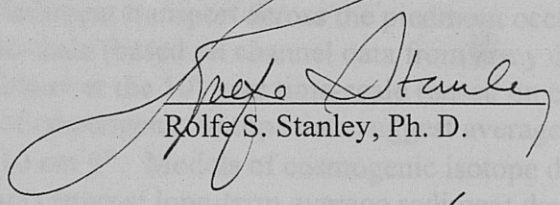

Rolfe S. Stanley, Ph. D.

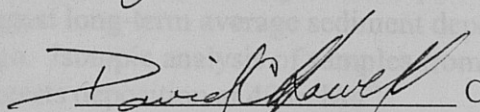

Chairperson
David C. Howell, Ph.D.

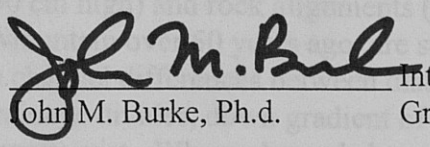

Interim Dean,
John M. Burke, Ph.d. Graduate College

Date: November 10, 1999

ABSTRACT

A multi-scale analysis of the Iron and Granite Mountain piedmonts, eastern Mojave Desert, provides a unique view of piedmont behavior. Centimeter-scale mapping of an abandoned World War II training camp (Camp Iron Mountain) reveals surface process rates averaged over 54 years and quantifies the recovery of an ephemeral channel drainage network from intense disturbance. Cosmogenic isotope data, collected on the Iron and Granite Mountain piedmonts, average surface process rates over the 10^4 year time-scale. Together, these data constrain the rate and spatial distribution of surface processes that modify desert piedmonts.

Based on cosmogenic isotope estimates, the Iron and Granite Mountains erode at an average of 37 m Ma^{-1} and 39 m Ma^{-1}, respectively, equivalent to sediment yields to their adjacent piedmonts of 0.127 m^3 y^{-1} m^{-1} and 0.098 m^3 y^{-1} m^{-1}. Sediment is transported across the piedmonts by ephemeral channels in a uniformly thick active layer (20 to 30 cm) based on surveyed channel depths, measurements to the B-horizon, and cosmogenic isotope data. Piedmont sediment is thoroughly mixed on the 10^2 year time-scale, a conclusion based on channel data from areas disturbed by the army (> 100 years) and from indistinguishable cosmogenic nuclide abundances of amalgamated sediment from channels and terraces (< 1000 years).

Sediment transport across the piedmont occurs in episodic events over the decadal year time-scale (based on channel data from army disturbed areas) but is regular and predictable over the 10^4 year time-scale (based on cosmogenic isotope data). Interpretive models of cosmogenic isotope data suggest average down piedmont sediment velocities of 35 ± 10 cm y^{-1}. Models of cosmogenic isotope data from one soil pit (2.25 km from rangefront) suggest long-term average sediment deposition at 15 m Ma^{-1} until 5,000 to 15,000 years ago. Isotopic analysis of samples from another soil pit, 4.75 km from the rangefront, suggests deposition at 40 m Ma^{-1}.

Disturbance of desert surfaces can have lasting affects on ephemeral drainage networks lasting decades to centuries. Visual observations suggest that more than 50% of small berms (20 to 50 cm high) and rock alignments (clasts 10 to 20 cm high), left by the army at Camp Iron Mountain over 50 years ago, are still intact. These features account for most measurable channel differences between disturbed and undisturbed plots. Small berms act as local drainage divides, down gradient of which there is a zone (20 to 40 m wide) where no channels exist. Where channels have developed below intact berms, channels are smaller than channels in undisturbed plots. Rock alignments outline walkways and divert water more than 20° from the steepest piedmont gradient. Smoothed and compacted walkways promote channel initiation with over 75% of all walkways containing channel heads. Overall, undisturbed channels are ~1 m wider and 1.5 cm deeper than disturbed channels.

CITATIONS

Material for this thesis has been accepted for publication to *Environmental Legacy of Military Operations*, a special volume of the Geological Society of America's Reviews in Engineering Geology, on September 7, 1999 in the following form:

Nichols, Kyle K., and Bierman, Paul R. Fifty-four years of ephemeral channel response to two years of intense World War II military activity, Camp Iron Mountain, Mojave Desert, California. Geological Society of America. Environmental Legacy of Military Operations.

AND

Material for this thesis has been submitted for publication to *Geomorphology* on September 10, 1999 in the following form:

Nichols, Kyle K., Bierman, Paul R., and Caffee, Marc W. Understanding desert piedmonts using *in situ*-produced ^{10}Be and ^{26}Al. Geomorphology.

ACKNOWLEDGEMENTS

Many different people and organizations contributed to making this thesis possible. I would like to thank Dr. Russell Harmon of the Army Research Office for funding this research under ASSERT grant #DAAG559710180 and U.S. Army Research grant #DAAH049610036.

The quality and quantity of data presented in this thesis is in large part due to my excellent field assistants. I would like to thank Christine Massey and my advisor, Paul Bierman, for strong backs, strong legs, and great endurance in the desert heat while collecting the four-kilometer long transect samples and the valley samples. Thanks to Mary Kay Nichols who trekked many kilometers to help dig shallow soil pits. Finally, thanks to Darrin Santos who braved crippling blisters, oppressive heat, flat-tires, and testy GPS equipment to help collect much of the data.

The laboratory analyses required the help of many people. Ben Copans in part, aided separation of quartz from other minerals. Susan Neis' consistent and precise work in the Cosmogenic Isotope Laboratory, produced quality targets for the accelerator mass spectrometer. Finally, Marc Caffee, John Southon, and many other personnel at Lawrence Livermore National Laboratory helped make successful analyses of ^{10}Be and ^{26}Al on the AMS.

I would like to mention the timely completion of the two journal articles in this thesis are in part due to Russell Harmon and Marwan Hassan who graciously invited me to submit a manuscript of the research I presented at the 1998 Geological Society of

America Meeting (Harmon) and the 1999 International Conference on Drainage Basin Dynamic and Morphology (Hassan).

I would like to thank Erik Clapp for discussing the use of cosmogenic isotopes in sediment and thought provoking discussions concerning my data.

I would like to acknowledge that the initial idea for this project came from my advisor, Paul Bierman. I would like to thank Paul for his patience and his countless hours of advising, teaching, and editing (always with a smile) which made this project a terrific learning experience.

Finally, I would like to thank my family for their many sacrifices over the past two years. Thanks to my parents, Erwin and Patricia Nichols, who taught me the value of an education, and were always willing to take care of Erin and Jake in my absence. Thanks to Erin and Jacob Laing who forced me to step away from this thesis to play and have fun. Lastly, I want to thank my wife, Mary Kay, who supported me every step of the way, and would not let me settle for anything but my best.

America Meeting (Harmon) and the 1999 International Conference on Drainage Basin Dynamic and Morphology (Hassan).

I would like to thank Erik Clapp for discussing the use of cosmogenic isotopes in sediment and thought provoking discussions concerning my data.

I would like to acknowledge that the initial idea for this project came from my advisor, Paul Bierman. I would like to thank Paul for his patience and his countless hours of advising, teaching, and editing (always with a smile) which made this project a terrific learning experience.

Finally, I would like to thank my family for their many sacrifices over the past two years. Thanks to my parents, Erwin and Patricia Nichols, who taught me the value of an education, and were always willing to take care of Erin and Jake in my absence. Thanks to Erin and Jacob Laing who forced me to step away from this thesis to play and have fun. Lastly, I want to thank my wife, Mary Kay, who supported me every step of the way, and would not let me settle for anything but my best.

TABLE OF CONTENTS

CITATIONS II

ACKNOWLEDGEMENTS III

TABLE OF CONTENTS V

LIST OF TABLES VIII

LIST OF FIGURES IX

CHAPTER 1: INTRODUCTION 1

- FIELD AREA 1
- RECENT HISTORY OF THE IRON AND GRANITE MOUNTAIN PIEDMONTS 3
- COSMOGENIC ISOTOPE OVERVIEW 4
- SIGNIFICANCE OF RESEARCH 4
- OUTLINE 6

CHAPTER 2: LITERATURE REVIEW 12

- DESERT PIEDMONTS 12
  - Alluvial fans 13
    - Tectonic setting 13
    - Deposition processes 14
    - Empirical relationships 15
    - Climate change 16
    - Big Picture 17
    - What is lacking in the literature 17
  - Pediments 18
    - Pediment processes 19
    - Morphometric analyses 22
  - Anthropogenic influences on desert processes 23
- COSMOGENIC ISOTOPES 26
  - Background 26
  - Basin-wide erosion rates and grain-size influence 27
  - Terrace sediment and fluvial sediment 30
  - Soil generation rates and dating soils 31

CHAPTER 3: PAPER SUBMITTED TO SPECIAL VOLUME OF REVIEWS IN ENGINEERING GEOLOGY 34

- ABSTRACT 34
- INTRODUCTION 35
- METHODS 38
  - Survey Methods 39

Plot locations 39
Data Reduction 40
RESULTS 41
Depth, Width, and Cross-sectional Area Data 41
Channel Area and Drainage Density 42
Channel Orientations 43
DISCUSSION 43
Control Plots 44
Walkway Plots 44
Road Plots 46
Process model 47
CONCLUSIONS 50
ACKNOWLEDGMENTS 51
REFERENCES CITED 51
FIGURE CAPTIONS 53

CHAPTER 4: JOURNAL ARTICLE SUBMITTED TO *GEOMORPHOLOGY* 75

ABSTRACT 75
1.0. INTRODUCTION 77
2.0. RESEARCH AREA 78
3.0. COSMOGENIC ISOTOPES 79
4.0. METHODS 80
4.1. Sediment collection for ^{10}Be and ^{26}Al analysis 80
4.1.1. Valley Samples 80
4.1.2. Transect Samples 81
4.1.3. Soil Pit samples 82
4.2. Laboratory methods 82
4.3. Reproducibility 83
5.0. RESULTS 84
5.1. Transect data 84
5.2. Well-mixed layer 86
5.3. Soil pit data 87
5.4. Sediment generation rate estimates 87
6.0. INTERPRETIVE MODELS OF SEDIMENT TRANSPORT AND PIEDMONT HISTORY 88
6.1. Sediment transport model 89
6.2. Soil pit models 93
6.3. Sediment transport velocities and piedmont surface processes 95
6.3.1. Surface of transport 96
6.3.2. Deposition 96
6.3.3. Erosion 97
6.3.4. A plausible scenario 98
7.0. WHAT WE HAVE LEARNED 99
8.0. APPENDIX 101
9.0. ACKNOWLEDGEMENTS 102
10.0. REFERENCES CITED 103
FIGURE CAPTIONS 105

CHAPTER 5: INTEGRATING DIFFERENT TEMPORAL- AND SPATIAL-SCALES 129
FUTURE DIRECTION OF RESEARCH 133
COMPREHENSIVE BIBLIOGRAPHY 135
APPENDIX A: SURVEY DATA 148
APPENDIX B: BASE STATION COORDINATES 257
APPENDIX C: GRAIN SIZE DATA 258

LIST OF TABLES

CHAPTER 3

TABLE 1. CHANNEL DEPTHS FOR CONTROL, WALKWAY,AND ROAD PLOTS 56

TABLE 2. CHANNEL WIDTHS FOR CONTROL, WALKWAY, AND ROAD PLOTS 57

TABLE 3. CHANNEL CROSS-SECTIONAL AREAS FOR CONTROL, WALKWAY, AND ROAD PLOTS 58

TABLE 4. CHANNEL AREAS FOR CONTROL, WALKWAY, AND ROAD PLOTS 59

TABLE 5. DRAINAGE DENSITIES FOR CONTROL, WALKWAY, AND ROAD PLOTS 60

CHAPTER 4

TABLE 1. ^{10}Be and ^{26}Al data for the Iron and Granite Mountain piedmonts 110

TABLE 2. Distribution of geomorphic unit samples 112

TABLE 3. ^{10}Be and ^{26}Al erosion rates and associated sediment production rates 113

LIST OF FIGURES

CHAPTER 1

Figure 1. Location map of the Mojave Desert and the Iron and Granite Mountains (black dots) in southern California. 8

Figure 2. Topographic map of the Iron and Granite Mountain piedmonts. 9

Figure 3. Average grain size of piedmont transects as a function of distance from rangefront. 10

Figure 4. Location of the Desert Training Center (shaded in gray) in the southwestern United States. 11

CHAPTER 3

Figure 1A. Location of the Desert Training Center (shaded in gray) in the southwestern United States 61

Figure 1B. Topography of the Iron Mountain piedmont and the Iron Mountains 62

Figure 1C. Aerial photograph of Camp Iron Mountain area and location of all plots at approximately same scale as 1B 63

Figure 2. Photograph of Camp Iron Mountain after a sandstorm 64

Figure 3. Distribution of channel depths and widths for control, walkway, and road plots 65

Figure 4. Rose diagrams of channel orientations 66

Figure 5. Maps of all Control Plots 67

Figure 6. Low-level oblique aerial photograph of channels breaching walkway rock alignments at Camp Iron Mountain 68

Figure 7. Maps of all Walkway Plots 69

Figure 8. Low-level oblique aerial photograph of Camp Iron Mountain showing road berms channeling flow 70

Figure 9. Photograph of the smooth surface below an intact road berm on map C-4 71

Figure 10. Photograph of a wide, braided channel down gradient of a breached berm in R-1 72

Figure 11. Maps of all Road Plots. 73

Figure 12. Channel widths and depths as a function of distance from channel head 74

CHAPTER 4

Figure 1A. Location of the Iron and Granite Mountains in the Mojave Desert, California 114

Figure 1B. Oblique aerial photograph of the Iron and Granite Mountains and respective piedmonts looking to the southwest 115

Figure 2. Map of the Iron and Granite Mountain piedmonts 116

Figure 3. Grain size and carbonate distribution of sediment collected from Iron and Granite Mountain piedmonts 117

Figure 4. Photograph of ephemeral channels and terraces located near IMT-3 118

Figure 5. Reproducibility of sediment samples 119

Figure 6. ^{10}Be and ^{26}Al data are well-correlated ($r^2 = 0.98$) 120

Figure 7. Transect (closed symbols) and valley (open symbols) data from Iron (circles) and Granite (squares) Mountain piedmonts 121

Figure 8. Different geomorphic units along the same transect have similar nuclide abundances 122

Figure 9. Soil pit samples have increasing nuclide abundances at depth 123

Figure 10. Continuity models for A) mass balance and B) nuclide balance divide the piedmont into transport segments of a unit width, the ATL thickness, and an arbitrary length 124

Figure 11. Stable surfaces (squares) and eroding surfaces (circles) have nuclide abundances that decrease at depth 125

Figure 12. Predicted deposition rates using A.) ^{10}Be and B.) ^{26}Al data for soil pit 1 (circles) and soil pit 2 (squares) 126

Figure 13. ^{10}Be data for Iron Mountain piedmont (diamonds and thick black line) and predicted results of endmember processes 127

Figure 14. ^{10}Be data for Iron Mountain piedmont (open circles) and predicted results of steady deposition (15 m Ma^{-1}) followed by 5000 years of transport (black dashes) 128

CHAPTER 1: Introduction

This study investigates the processes that modify desert piedmonts at different temporal and spatial scales. By investigating both the small-scale geomorphology (by measuring individual ephemeral channels in eighteen, 3600 m^2 plots), and the large-scale geomorphology (by measuring cosmogenic isotopes in sediment over a 16 km^2 area), I have developed a better understanding of desert piedmont processes. The study site, the Iron and Granite Mountain piedmonts in the Mojave Desert, is unique in that I can use past military activity to determine the rate at which ephemeral channels modify the piedmont surface on human time-scales and use cosmogenic isotopes to determine the long-term (10^3 to 10^4 years) rate at which ephemeral channels modify the surface.

For over 100 years, geomorphologists have been trying to determine the processes that form and modify desert piedmonts. Much of the research is based on observations and theories, but little quantitative data. Needless to say, there is little agreement on the rate, style, and distribution of active processes on desert piedmonts. In this thesis I address piedmonts using two methods to quantify different scales and rates of surface modification. Each method can stand alone, but when combined they provide a more complete temporal and spatial understanding of desert piedmonts.

Field Area

The Iron and Granite Mountains are located in the eastern Mojave Desert in southern California (Figure 1). The Mojave Desert is bound by the San Andreas Fault to the south and the Garlock Fault to the north. The eastern edge of the Mojave Desert is

not clearly defined but is usually stated as the Colorado River. Some previous studies have excluded the Iron and Granite Mountains from the Mojave Desert (Spaulding and Graumlich, 1986; Spaulding et al., 1983) and considered them part of the Sonoran Desert. Consistent with most research of the area, I include the field area as part of the Mojave Desert.

The Iron and Granite Mountains are a granitic core complex of Cretaceous age (Miller et al., 1981). The mountains are surrounded on all sides by low-gradient piedmonts covered with sediment. The field area is located on the eastern piedmont of the Iron Mountains and the northern piedmont of the Granite Mountains (Figure 2). The piedmonts are low-angle (~2°), extend >10 km from each rangefront to Danby Lake playa, and meet the rangefront at a sharp angle. Sediment grains on both piedmonts are mostly between 0.5 and 1.0 mm. There is no evidence of grain-size fining away from the mountains (Figure 3).

The piedmonts are planer features dissected by shallow, ephemeral channels. The piedmonts do not usually have pavements or rock varnish, indicating that they are active surfaces. An exception includes some small relict surfaces near the Iron Mountain rangefront (< 2.5% of the piedmont area) that do have poorly developed pavements, rock varnish, and are dissected by deeper channels (0.5 to 5 m).

I chose the Iron and Granite Mountain piedmonts to quantify large-scale surface processes, for a number of reasons: 1) The piedmonts are wide enough (> 4 km) and long enough (> 4 km) to obtain a spatial distribution of sediment samples. 2) The surface of each piedmont is uniform and planer allowing me to assume that the flux of sediment neither converges nor diverges. 3) The piedmonts are adjacent to each other, which

allows me to assume that each piedmont has experienced the same relative climatic and tectonic histories. 4) The source rocks are granites, which has abundant quartz for the cosmogenic isotope analyses.

Recent history of the Iron and Granite Mountain piedmonts

In May 1942, General George S. Patton, Jr. established the Desert Training Center (DTC) to train American troops in desert warfare for the battles in North Africa during World War II (Henley, 1989). The DTC consisted of 12 temporary base camps spread throughout 42,000 km^2 of the Mojave and Sonoran Deserts (Figure 4). One of these camps, Camp Iron Mountain (the location of the small-scale geomorphology project, Chapter 3) was situated on the Iron Mountain piedmont, and a second camp, Camp Granite, was situated on the Granite Mountain piedmont.

The base camps were the living centers for the troops. The base camps, or "tent cities", consisted of a series of tents, a grid of roads, and rock outlines of walkways, tents, and roads. After the military dismantled the camps, in May 1944, the only features left were the roads, road berms, and the rock alignments.

I chose to study Camp Iron Mountain because it is the best preserved of the base camps. The location is remote and the surface has experienced minimal human disturbance since 1944. A fence was constructed around Camp Iron Mountain in the early 1980s, which prevents entry of off road vehicles into the camp (BLM, 1986). The combination of the military activity at Camp Iron Mountain and the geology of the Iron and Granite Mountain piedmonts are ideal for a multi-scale analysis of desert piedmont processes and rates.

Cosmogenic isotope overview

Cosmogenic isotopes are produced when cosmic rays strike Earth's surface. For example, when cosmic rays interact with quartz, ^{10}Be and ^{26}Al are produced among other isotopes. These isotopes can be used as cosmic ray dosimeters, if the rate at which they are produced is known. The production rates of these isotopes are atoms to tens of atoms per year. With recent advances in accelerator mass spectrometry (AMS), detection of these isotopes is possible from as little as 10^3 years of surface exposure to over 10^6 years of surface exposure. Thus, cosmogenic isotopes are potentially useful for quantifying many surface processes over the 10^3 to 10^6 year time-frame.

Cosmogenic isotopes have been used to approach many geomorphic problems. The most common applications include dating bedrock exposure and measuring bedrock erosion rates (Brook et al., 1993; Marsella, 1998). However, new applications using cosmogenic isotopes in sediment, such as quantifying basin-wide erosion rates, soil production rates, terrace ages, and soil ages are becoming more common (Anderson et al., 1996; Bierman and Steig, 1992; Small et al., 1999). The growing popularity of cosmogenic isotopes, as a geomorphic tool, will continue to inspire new and interesting applications. In chapter 2, I discuss the theory and use of cosmogenic isotopes in sediment.

Significance of research

My research is the first to quantify previously poorly constrained process rates of desert piedmont modification and the response of an ephemeral drainage network to human disturbance. This research is also important because it demonstrates the benefits

of a multi-scale approach to understanding both recent and long-term desert process rates. Although, different scales of piedmont processes have been investigated in the past, none have quantified the different temporal and spatial scales for one piedmont. Usually, short-term rates are discussed for small-scale processes, or long-term rates are discussed for large-scale processes.

I revisit piedmonts using cosmogenic ^{10}Be and ^{26}Al to measure rates of surface change over different temporal and spatial scales. This is the first study with data suggesting that ephemeral channels rework the upper transport surface on 10^2 year time-scales. I use ^{10}Be and ^{26}Al to quantify long-term deposition rates, sediment transport rates, and the time represented by unconformities exposed in soil pits dug in desert piedmonts. I use survey data that documents channel formation over the past 54 years to measure the recovery of an ephemeral drainage network after intense human disturbance.

This new application of in situ-produced ^{10}Be and ^{26}Al, provides new data and a simple technique to quantify desert piedmont sediment transport rates. Most quantitative studies of desert piedmonts involve copious morphometric measurements of piedmont morphology in order to infer piedmont processes (Bull, 1977; Cooke, 1970; Cooke and Reeves, 1972; Hooke, 1967; Mammerickx, 1964). Conversely, arid region active process studies require many years of data collection to average rare events and obtain average process rates (Greenbaum et al., 1999; Lekach and Schick, 1999). Such monitoring may continue for decades before significant geomorphic events are observed. The new cosmogenic isotope technique allows for rapid data collection (weeks) and rapid return of results (six months to a year) to obtain process rates averaged over the 10^3 to 10^4 year time-scale. This study suggests that two piedmonts with similar characteristics (gradient,

sediment yields, tectonic and climatic histories, and lithologies) have similar sediment transport rates. Further application of this technique on other desert piedmonts with different characteristics will provide valuable data about a wide range of surface processes.

The results of this research are important to the field of desert geomorphology. Because deserts cover ~30% of Earth's surface and piedmonts constitute a large part of deserts (Bull, 1977), understanding rates and processes of piedmont change are integral to understanding much of Earth's surface. Since this is the first study to determine long-term average rates of piedmont processes, it is a step forward in understanding a major portion of Earth's surface.

Outline

The main body of this thesis is the two journal articles presented in chapters three and four. The journal articles contain the methods, the results, and discussions of the study. Chapter 2 is an extensive literature review of desert piedmont processes (deposition, erosion, and response to anthropogenic influences) and the theory and practical uses of cosmogenic isotopes, in particular, as used in sediment. Chapter 3 is an invited journal article resulting from a presentation at the 1998 Geological Society of America annual meeting in Toronto, Canada. The article is submitted to a special volume of Reviews in Engineering Geology concerning geology and the military. This paper explains the effects of military activities on the Iron Mountain piedmont fifty-four years after military training exercises ceased. Chapter 4 is another invited journal article resulting from a May 1999 presentation at the International Conference on Drainage Basin Dynamics and Morphology, in Jerusalem, Israel. This paper explains the use of *in*

situ-produced cosmogenic isotopes to quantify many previously unknown rates of process that modify desert piedmonts, such as average sediment transport velocities, sediment deposition rates, and effective time-spans of unconformities. Chapter 5 is a comprehensive results section relating the two articles to each other. Included, is a brief discussion suggesting the future direction of related research. A comprehensive bibliography section follows chapter 5. At the end of the document are appendices of all data not presented in chapters three and four.

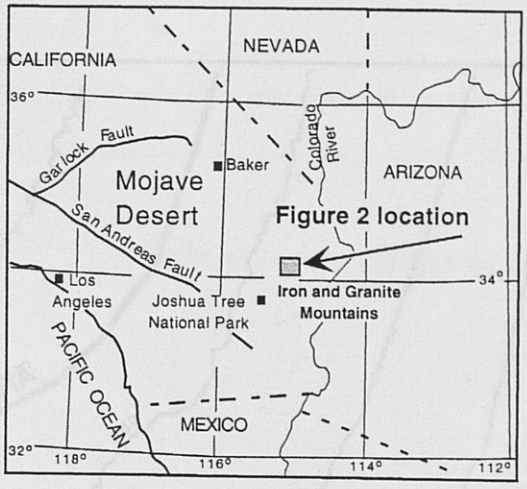

Figure 1. Location map of the Mojave Desert and the Iron and Granite Mountains (gray square) in southern California.

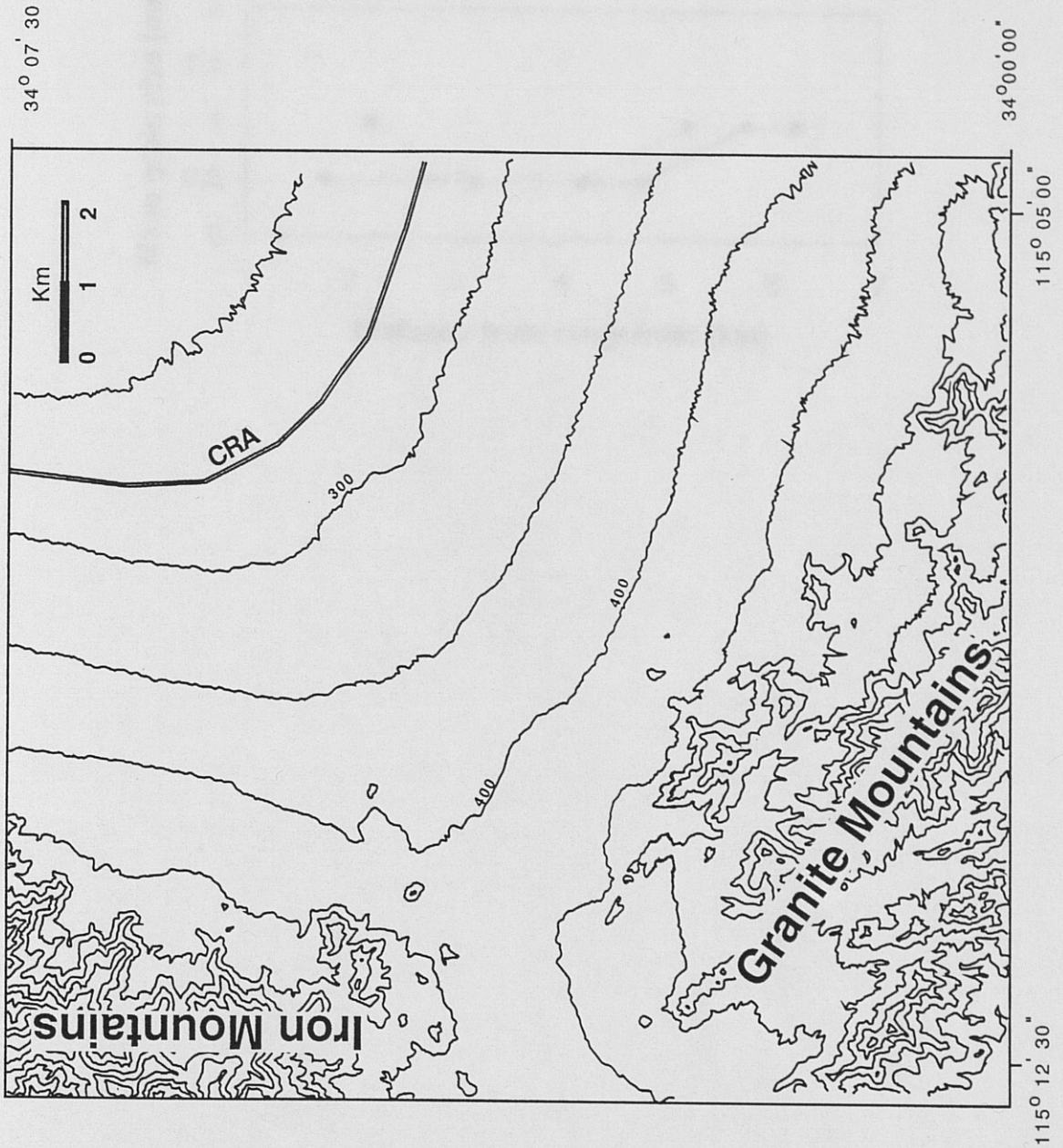

Figure 2. Topographic map of the Iron and Granite Mountain piedmonts. CRA = Colorado River Aqueduct. Contour interval is 50 m. Map based on the Granite Pass and East of Granite Pass U.S.G.S. 1:24,000 quadrangles, 1985.

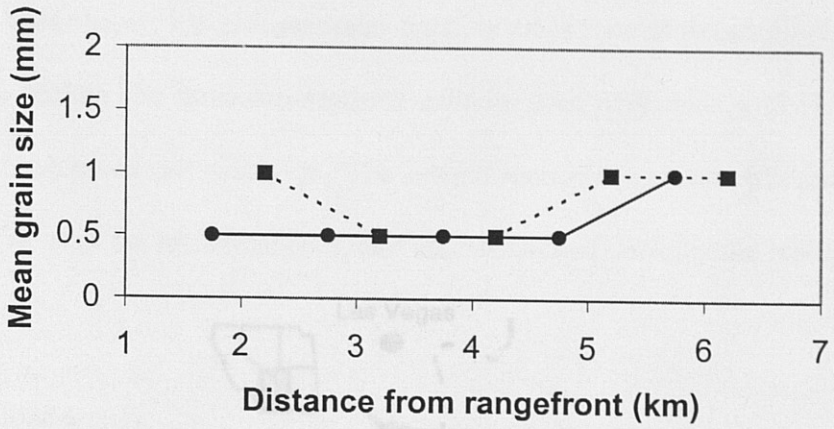

Figure 3. Average grain size of piedmont transects as a function of distance from rangefront. Circles represent Iron Mountain transects; squares represent Granite Mountain transects.

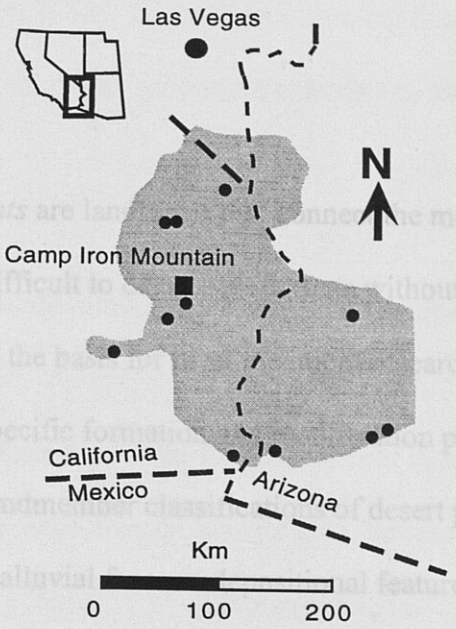

Figure 4. Location of the Desert Training Center (shaded in gray) in the southwestern United States. Circles are temporary base camps, Camp Iron Mountain shown by solid square.

CHAPTER 2: Literature Review

This chapter has two sections. First, is the review of desert piedmont literature, which is broken into three sub-sections, *alluvial fans*, *pediments*, and *anthropogenic influence* on piedmont processes. The second section is a review of cosmogenic isotopes, where I discuss the history, theory, and case studies of cosmogenic isotopes measured in sediment.

Desert piedmonts

Desert piedmonts are landforms that connect the mountainous areas to the adjacent plains. It is difficult to discuss piedmonts without first presenting a few terms and definitions that are the basis for most piedmont research. This is often problematic, as each term implies specific formation and modification processes.

There are two endmember classifications of desert piedmonts: *alluvial fans* and *pediments*. Generally, alluvial fans are depositional features and pediments are erosional features. Often, piedmonts have both depositional and erosional areas (Hadley, 1967). Understanding piedmonts is made difficult by natural complexities and the long history of the landforms (Dohrenwend, 1987; Oberlander, 1974). Such complexities (different climates, tectonic settings, lithologies, drainage basin characteristics, and drainage networks) make it difficult to develop a general model or hypothesis that fits all piedmonts (Bull, 1977; Cooke and Warren, 1973; Lecce, 1990; Oberlander, 1974). Difficulties in understanding desert piedmonts are highlighted by Oberlander (1974) who coined the term 'pediment problem' and Lecce (1990) who coined the term 'alluvial fan

problem' in describing the expansive, but imprecise body of knowledge of alluvial fan and pediment processes.

Alluvial fans

Alluvial fans are a common desert landform that vary in size, shape, formation processes, parent lithology, base level change, and climatic history. Thus, a large volume of literature is devoted to alluvial fans, predominately of the American southwest (Lecce, 1990; Nilsen and Moore, 1984). Since the alluvial fan literature is so expansive and in large part repetitive, I will review important concepts of fan processes rather than individual papers.

Tectonic setting

Alluvial fans are ubiquitous in the American southwest particularly in the basin and range province (Bull, 1977; Cooke and Warren, 1973; Dohrenwend, 1987; Hooke, 1968; Hooke, 1972), although alluvial fans are present in many different tectonic and climatic settings. Many large alluvial fans form in, but are not limited to, tectonically active areas (Bull, 1977; Denny, 1967; Dohrenwend, 1987). When mountains are uplifted, streams respond by incising into the mountains to adjust to a lower baselevel. Thus, the uplift of the mountains provides ample sediment for alluvial fans.

Other alluvial fans form in tectonically quiet settings. Here, fan growth is a result of natural incision of mountain masses (Bull, 1977; Dohrenwend, 1987). Other factors (climate, base level, and drainage basin characteristics) influence the style of deposition in tectonically quiet setting (Bull, 1977; Dohrenwend, 1987; Hooke, 1967; Hooke, 1968).

Deposition processes

There are two deposition processes that form alluvial fans. Fluvial deposition characterized is by well-sorted sediment deposited by streams. Debris flow deposition is characterized by poorly sorted sediment. I will briefly describe the importance of each process below.

The deposition of sediment in alluvial fans was long thought, and is still stated in some introductory geology textbooks (Tarbuck and Lutgens, 1996; Thompson and Turk, 1991), to be a result of gradient change from steep gradients in the mountains to low gradients at mountain front. Although such gradient changes can be responsible for deposition, it has been shown that there are not significant gradient differences between many mountain basins and adjacent alluvial fans (Bull, 1964). Where gradients are similar, deposition is caused by the hydraulic response as flow leaves the confines of the channel and spreads out causing decreases in depth and velocity which cause deposition (Bull, 1977; Dohrenwend, 1987). Deposition is also caused by decreases in water velocity and water volume due to infiltration, which is common on well-sorted alluvial fan deposits of the southwest (Bull, 1977; Denny, 1967; Hooke, 1967).

The second mechanism responsible for deposition on alluvial fan is debris flows. Debris flows are common in small steep basins made of weak lithologies such as mudstone and low-grade metamorphic rocks (Harvey, 1984). Alluvial fans formed from debris flows are characterized by poorly sorted sediment in a fine-grained matrix (Bull, 1977; Harvey, 1984; Hooke, 1968). Topography of debris flow fans is usually hummocky due to debris flow lobes and levees (Whipple and Dunne, 1992). Although,

many debris-flow fans are documented in California (Whipple and Dunne, 1992), such fan characteristics are not representative of the Iron and Granite Mountain piedmonts.

Empirical relationships

Many empirical relationships relate alluvial fan area to drainage basin area for arid-region alluvial fans (Bull, 1964; Bull, 1977; Denny, 1967; Hooke, 1967). Other empirical relationships establish depositional histories by measuring slopes of fans (Bull, 1977; Denny, 1967; Dohrenwend, 1987; Hooke, 1967). Data suggest that the aerial extent of active deposition can occupy as little as 5% of total fan area (Bull, 1977; Hooke, 1967).

Extensive work in the arid southwest show that fan area is related to the drainage basin area by:

$$A_f = cA_d^n$$

where A_f is the fan area, c is a coefficient that depends on climate, lithology, tectonics, and available space, A_d is the drainage basin area, and n is the slope of the regression line of A_f vs. A_d on a log-log plot (Bull, 1964; Denny, 1967; Hooke, 1968). Values for n are approximately 0.9 for southwestern alluvial fans (indicating that some sediment is stored in basin valleys), while values for c vary between 0.15 and 2 (Bull, 1977; Hooke, 1968). Low c values represent resistant rock lithology, blocky weathering, and tectonically active areas, while high c values represent weak lithologies, back tilted piedmonts, and tectonically quiet rangefronts (Dohrenwend, 1987). It is the c value that is important to determine to understand processes on alluvial fans.

Alluvial fans have two important slope characteristics. First, slopes are usually concave with the apex slope similar to the slope of the mountain basins. Second,

although slopes are concave, slopes are usually segmented (having many separable slope values) and not a smooth curve (Bull, 1977; Denny, 1967; Hooke, 1972). The segments are a result of the fluvial system responding to changes in tectonics, base-level, climate, fan head trenching, and/or sediment load. Such slope segments are helpful in determining past depositional histories of individual fans. The areas of active fan deposition could either be near the apex or near the toe of the fan, depending on the combinations of fan processes (Bull, 1977; Denny, 1967; Dohrenwend, 1987). For example, tectonic activity will uplift the mountain mass and deposition will occur at the apex of the fan, while lowering of local baselevel would result in deposition near the toe of the fan (Bull, 1977; Denny, 1967).

Climate change

The effects of climate change on alluvial fans are well documented by geomorphic and soil stratigraphy studies. Much focus on climate change centers on the Pleistocene-Holocene transition (Bull, 1991; Bull and Schick, 1979; Mayer and Bull, 1981; McFadden et al., 1989; Wells et al., 1987). Bull and Schick (1979) proposed that during the wetter Pleistocene, sediment and water was retained on hillslopes by vegetation and stream power was less. After a change to drier conditions in the Holocene, vegetation became sparse which allowed for more runoff and increased stream power. Higher stream power stripped the hillslopes of soil and segmented (eroded) many alluvial fans in tectonically quiet areas (Bull, 1991; Wells et al., 1987). Evidence for a difference in stream power between the Pleistocene and the Holocene is found in the sediment size and sediment distribution on alluvial fans. Sediment transported during the

Pleistocene was finer grained and grain size decreased less rapidly down fan than the sediment transported during the Holocene (Mayer and Bull, 1981).

Big Picture

Within large areas of the southwest, alluvial fans have been exposed to the same effects of regional tectonism and climate. However, all alluvial fans are not identical in such regions. Alluvial fan process is an intricate interaction of tectonism and climate along with specific variables (lithology, drainage basin size, channel gradient, percent of basin eroded, type of sediment, and location of storm cells) that have great spatial variability within these regions (Wells and Harvey, 1987). Dohrenwend (1987) might best sum up the interaction of the above processes when he stated that the morphometery of alluvial fans is largely controlled by drainage basin characteristics and that the surface morphology is strongly influenced by climate change.

What is lacking in the literature

As stated before, much of the alluvial fan literature is based on empirical relationships founded on present-day measurements. Yet some fans, such as the Milner Creek fan of the White Mountains, could be 700,000 years old (Beaty, 1970). It is optimistic to extrapolate alluvial fan processes over such time-spans. There is a need to determine long-term averaged rates that extend past the last major climate change to understand better the long-term processes acting on alluvial fans. Such rates involve sediment yield from drainage basins, sediment deposition rates, and sediment residence time.

The alluvial fan literature repeatedly states that adjacent alluvial fans converge to form an alluvial plain or bajada (Beaty, 1970; Bull, 1977; Cooke and Warren, 1973;

Denny, 1967; Dohrenwend, 1987; Lecce, 1990). However, little research has been conducted to understand the processes of alluvial plains. The only discussion of such zones is a random walk of channels model that predicts similar discharges for each channel on the alluvial plain (Rachocki, 1981). Although alluvial plains are combinations of alluvial fans, they may be formed or modified by different processes and rates, and thus should be studied to determine their relationship to alluvial fans.

Pediments

Cooke and Warren (1973) refer to the pediment literature as an "...appalling volume of literature...". By 1973, there were over 950 papers written about pediments (Whitaker, 1973), and numerous additional papers in the 26 years since. The first reference to a pediment was in Gilbert's landmark paper on the Geology of the Henry Mountains (1877). Later in the 19th century, McGee observed and described sheetfloods on pediments in Arizona (1897). Since these first pediment references, the term has been used for numerous different surfaces. The term pediment was so loosely used that Whitaker (1979) wrote a paper describing all of the pediment definitions in the literature and stated his definition of a pediment. Two common characteristics of most pediment definitions are: 1) pediments are erosional surfaces, and 2) pediments are low angle features with high angle backing slopes. The expansive pediment literature and the different pediment definitions make an extensive review of the pediment literature difficult.

The problem of pediment formation is complex. Some researchers have used morphometric relationships to infer pediment formation processes (Parsons and Abrahams, 1984; Schumm, 1962). Others, state that pediments are landforms relict from

pre-Quaternary times, and that present-day morphometric relationships characterize pediment modification, not pediment formation (Cooke and Warren, 1973; Dohrenwend, 1987; Oberlander, 1972; Oberlander, 1974). A fundamental problem is that human-time scales are too short to monitor pediment formation. Some geomorphologists have relied on time markers, such as basalt flows, to date pediments (Oberlander, 1972). Others have monitored and observed small-scale pediment formation to determine process and rates (Mabbutt, 1966; Mabbutt, 1977; Schumm, 1962). Even after 900 published papers, there still is not an agreed upon formation or modifying process (Whitaker, 1973). In the following sections, I will review the leading hypotheses of pediment formation and review specific papers that describe morphometric relationships of pediments.

Pediment processes

Geomorphologists have been trying to determine the processes that can erode mountain masses, maintain the sharp angle between pediment and mountain, and erode low angle bedrock floors for over 100 years. Gilbert (1877) was the first to discuss pediments which he termed 'hills of plantation'. The pedimentation process that Gilbert described later became known as lateral plantation. Lateral plantation was favored by many subsequent geomorphologists who expanded upon Gilbert's initial research (Howard, 1942). Lateral plantation involves a low-angle slope of erosion (and transport) that connects mountain mass erosion and lowland deposition. Streams migrate laterally to erode and transport sediment from the mountain mass to the lowlands while smoothing the rock surface. Streams also migrate and undercut the rangefront causing parallel retreat.

Other geomorphologists believe that hillslope weathering and removal of sediment by rill action and sheetfloods is the dominant pedimentation process. McGee (1897) made the first account of a sheetflood on a pediment. McGee wrote a vivid description of the erosive power of sheetfloods, which strongly influenced later geomorphologists (Lawson, 1915; Rich, 1935). Rilling and sheetfloods generate parallel hillslope retreat by weathering, wash, and mass movement. The angle between the pediment and the mountain front remains constant due to the angle of repose of boulders. The debris from the mountain-pediment (or piedmont) junction is removed by rill action and sheetflood events and deposited below the pediment in the basin. Sheetfloods would also flatten the exposed bedrock surface. As mountain denudation continued, less sediment would be delivered to the expanding pediment surface and the pediment area would increase.

Paige (1912), expanding upon Gilbert's lateral plantation hypothesis, put forth a third pediment forming process, exhumation. Paige stated that residual alluvial patches on a surface flanking an escarpment suggested the pediment was originally buried and was later uplifted by faulting. Once the pediment was uplifted, steams unearthed the rock surface by the lateral plantation. Lawson (1915) also supports exhumation in his research, but favors sheetfloods for the removal of detritus.

A variation of the exhumation origin by later geomorphologists is mantle controlled plantation (Mabbutt, 1966; Moss, 1977). This process invokes a mantle of sediment that holds moisture longer than exposed bedrock. The water quickens the chemical weathering of the underlying bedrock. Runoff from mountain basins collects in sediment at the rangefront, and thus chemical weathering is greatest at the mountain-

pediment junction (Mabbutt, 1966). Such rapid weathering can maintain the mountain-pediment angle which is intrinsic in most pediment definitions (Whitaker, 1979). Protrusions of bedrock under the sediment mantle are subject to enhanced weathering that would account for the smoothness of pediments (Mabbutt, 1966). The sediment mantle is removed by sheet-flow induced stripping events.

Moss (1977) proposed a similar theory of bedrock weathering under a sediment mantle. In Arizona, Moss found a pediment with a 60-m grus mantle. Moss states that lateral plantation can transport grus but not produce the uneven bedrock surfaces found below the grus. Instead, differential water moisture in the grus causes differential weathering, and thus uneven bedrock surfaces. Moss casts doubt on the hypothesis of parallel mountain retreat, which was so firmly believed since Gilbert (1877). Moss contends that erosion rates of rangefronts (8 m Ma^{-1}) are too slow to produce large pediments that extend up to 3 km away from the mountains. Instead, the downwasting of mountains by weathering can better explain large pediments.

Parsons and Abrahams (1984) further challenged the parallel retreat model. Parsons and Abrahams state that few mountain fronts are linear, while most mountain fronts have embayments. Parsons and Abrahams assume that the rate of divide removal is not significantly less than rate of mountain front retreat. They hypothesize that removal of embayment divides can account for a higher piedmont junction retreat rate than erosion of a linear mountain mass. Parsons and Abrahams believe that although channels can swing abruptly after exiting rangefronts and erode up to half of the mountain front in some mountains, hillslope processes usually affect a greater part of the mountain front than channel processes.

Morphometric analyses

Few papers have been published on the morphometric analysis of pediments and fewer papers have good data sets (Cooke and Warren, 1973). Many of the early pediment papers were based on observations (Gilbert, 1877; McGee, 1897) and theory (Gilbert, 1877; Lawson, 1915; McGee, 1897; Paige, 1912). Measurements of pediments are absent in most of the literature until the 1960s when researchers began measuring morphologic relationships (Cooke, 1970; Cooke and Reeves, 1972; Mammerickx, 1964; Schumm, 1962).

Schumm (1962) compiled 8 years of erosion data on miniature pediments in the Badlands of South Dakota. Schumm concluded that erosional processes such as lateral plantation formed pediments. However, this study actually measured pediment modification not pediment formation. Also, it is difficult to relate the pedimentation of a miniature, clay pediment to large, hard rock pediments of the southwest. Nevertheless, Schumm was one of the first to attempt a quantitative analysis of pediment systems.

Mammerickx (1964) was the first to synthesize pediment data from the Mojave and Sonoran Deserts. Mammerickx concluded that pediment slopes are not related to drainage basin size, lithology, or grain size. The most important factors in pediment morphometery are tectonic activity and the cyclic formation of pediments (due to climate change) creating inset pediments. Mammerickx also is the first to note that pediments in the less tectonically active Sonoran Desert are larger than pediments in the more tectonically active Mojave Desert. Later geomorphologists support this finding (Cooke, 1970; Cooke and Warren, 1973; Dohrenwend, 1987). This paper shows that pediments with different characteristics produce different morphometries.

Cooke (1970) studied 53 mountain masses and their associated piedmonts and pediments in the western Mojave Desert to determine quantitative relationships and infer pediment processes. Cooke determined that slopes (average of 2°35') are independent of pediment length, basin area, and lithology. Cooke believes that although morphometric analyses do not answer many pediment questions, they provide more precise relationships between local variables (lithology, drainage basin) and regional variables (tectonics and climate). Cooke claims that the lack of consistent pediment relationships is possibly due to the pediments being exposed after mountain-piedmont relationships were established, rather than concurrently. This idea supports the exhumation process of Paige (1912) described above.

Cooke and Reeves (1972) quantify the slope of pediments and the relationship of sediment size as a function of distance from the mountains. Results suggest that slope generally decreases as a function of distance from the mountain front, but at different rates for different lithologies. Sediment size relationships are more variable. Cooke and Reeves believe that smaller grains are transported while larger grains are weathered from local bedrock. Cooke and Reeves did not discuss pedimentation processes in this paper.

Anthropogenic influences on desert processes

The desert literature contains numerous studies of anthropogenic influence on desert processes. Most detail the influence on soil properties (Iverson, 1980; Iverson et al., 1981; Prose, 1985; Webb et al., 1986; Wilshire and Webb, 1980) and on the distribution and recovery of vegetation (Lathrop, 1983; Prose et al., 1987; Schlesinger et al., 1989). I will discuss the anthropogenic influence on desert soils, as soils most directly affect the surface processes on desert piedmonts.

Desert environments change slowly due to small amounts of precipitation, infrequent overland flow, and few bioturbating animals (Cooke and Warren, 1973). Thus, human disturbance of desert soils is measurable long after the disturbance has taken place (Prose, 1985; Webb et al., 1986; Wilshire and Webb, 1980). Webb et al. (1986) used soil penetration measurements to evaluate the soil compaction from vehicles, foot traffic, and animals, at five ghost towns in Death Valley, California. They determined that soil compaction is measurable in four of five Death Valley ghost towns up to 75 years after they had been completely abandoned. Granitic soils and high elevations soils were most resistant to compaction. Soils at lower elevations, and soils derived from dacitic and rhyolitic rocks, on average need a century to recover to pre-disturbance compaction levels.

Prose (1985) made similar measurements of soil compacted by army tanks at seven former military training areas in California. The soil compaction measurements made in tank tracks were statistically higher than the measurements of adjacent untracked soil for all seven sites. Less than 50% of all attempted penetration measurements (tracked and untracked) penetrated the soil below 30 cm due to the carbonate accumulation of the K-horizon. Only two of seven sites had higher soil density measurements for tank-tracked soils compared to untracked soils, suggesting that increased soil compaction is not always associated with increased soil density. Prose noted that small rills developed in the tank tracks on low slopes (~1°), suggesting that decreased infiltration capacity accelerated erosion. Prose concludes that up to a century is required to eliminate the effects of compaction.

Iverson (1980) studied the effects of simulated rainfall on erosion of desert hillslopes modified by off-road vehicles (ORV). Iverson found that ORV use 1) decreased soil infiltration capacity by compacting soil pore spaces, 2) loosened surficial soil and removed vegetation and disturbed desert pavements thus making more sediment available for transport, 3) channelized runoff down vehicle tracks, and 4) smoothed microtopographic roughness elements that normally reduce runoff velocity. Any one of the changes listed above could accelerate erosion of desert hillslopes.

Steeper slopes, for both disturbed and undisturbed sediment, generate more erosion than shallower slopes. ORV use decreases sediment infiltration capacity and increases erosion of poorly sorted, gravelly soils that normally retain runoff and decrease erosion when undisturbed. Desert hillslopes used by ORVs have sediment yields 10 to 20 times higher than similar undisturbed slopes.

Iverson et al. (1981) studied the effects of ORVs on 1) soil bulk density and infiltration capacity, and 2) runoff and erosion process in the Mojave Desert. Results show that the bulk density of soil increases logarithmically in response to number of ORV passes and may extend to a depth of several decimeters. Iverson et al. assume that the increase in bulk density is due to the destruction of pore spaces, which decreases infiltration capacity.

Rainfall infiltration experiments on undisturbed desert surfaces suggest rainfalls of 40 to 60 mm h^{-1} for 20 minutes are needed to obtain overland flow. Rainfall data suggest that such intensities may only occur once a decade for many desert surfaces. However, ORV-disturbed soils are subject to erosion at rainfall intensities < 10 mm h^{-1}.

Cosmogenic isotopes

The use of cosmogenic isotopes, in particular ^{10}Be and ^{26}Al, as a geomorphic tool to determine long-term process rates became feasible only recently. Although there was an attempt to use cosmogenic ^{36}Cl in 1955 (Davis and Schaeffer, 1955), measuring most cosmogenic isotopes did not become practical until accelerator mass spectrometry (AMS) allowed for measurement of small numbers of atoms (Bierman, 1994). Today, cosmogenic nuclides (^{3}He, ^{10}Be, ^{21}Ne, ^{26}Al, and ^{36}Cl) are applied to problems such as, but not limited to, measuring bedrock erosion rates, measuring basin-wide average erosion rates (Bierman and Steig, 1996; Clapp et al., 1997; Clapp et al., 1999; Granger et al., 1996), dating glacial events (Brook et al., 1993; Gosse et al., 1995b; Gosse et al., 1995a; Marsella, 1998; Phillips et al., 1990), determining sediment production (Bierman and Steig, 1996; Brown et al., 1995; Clapp, in review a; Clapp et al., in review b; Granger et al., 1996; Heimsath et al., 1999; Monaghan et al., 1992; Small et al., 1999), investigating arroyo cycling (Clapp et al., 1997; Clapp et al., in review a; Phillips et al., 1998), determining source areas of sediment (Clapp, in review b), dating soils (Phillips et al., 1998), and determining fault displacement rates (Gran et al., in review). I will focus on ^{10}Be and ^{26}Al measured in sediment.

Background

Quartz-rich sediment, at and near Earth's surface, is continuously exposed to cosmic ray bombardment, which produces the rare isotopes ^{10}Be and ^{26}Al (Bierman, 1994; Lal, 1988; Nishiizumi et al., 1989). The intensity of Earth's magnetic field has fluctuated over time, thus altering the production rate of cosmogenic isotopes (Bierman, 1994). The orientation of Earth's magnetic field also affects production rates (Lal, 1991).

Cosmic rays are deflected more strongly at low latitudes, where the field is perpendicular to the incoming cosmic rays, than at high latitudes where the field lines are parallel to the incoming cosmic rays (Lal, 1991). Likewise, a thicker atmosphere interacts more strongly with cosmic rays and decreases production rates. Thus, production rates of ^{10}Be and ^{26}Al are least near the equator and at sea level.

Sediment can be used as a cosmic ray dosimeter. Lal (1991) discusses the latitude and altitude corrections, and estimates ^{10}Be and ^{26}Al production to within ± 10% (Clark et al., 1995; Larsen, 1996; Nishiizumi et al., 1989). Because rocks and sediments integrate the production of cosmogenic isotopes, the effects of changing production rates dampens over time. Presently, attempts at developing corrections for changing magnetic field strength are under way (Clapp and Bierman, 1996). Since production rates due to differing magnetic fields are integrated over time and we know production rates and the latitude and altitude corrections, we can use quartz to trace near surface sediment histories (Lal and Arnold, 1985).

Basin-wide erosion rates and grain-size influence

Lal and Arnold (1985) first proposed using cosmogenic isotopes in sediments to determine steady-state sedimentation histories. Surprisingly, little research utilized sediment until 1992 when an abstract was presented at the Geological Society of America (Bierman and Steig, 1992). In 1996, Bierman and Steig discussed a theoretical model for determining basin-wide erosion rates using sediment from mountain valleys, and Brown et al. (1995) and Granger et al. (1996) provided field examples. The model proposed by Bierman and Steig (1996) is based on the work of Lal (1988), and Lal (1991), and requires that 1) the rate of erosion is constant but not necessarily spatially

uniform, 2) the basin is in isotopic steady state, 3) the sediment is well-mixed, 4) mass loss is due to surface lowering, and 5) the concentration of the mineral selected for isotopic analysis is spatially uniform throughout the basin. Once these assumptions have been met, basin-wide erosion rates are determined using:

$$m = \frac{\Lambda P_{eff}}{C}$$

where m is the basin-wide mass lowering rate (g cm^{-2} y^{-1}), Λ is the attenuation factor (g cm^{-2}), P_{eff} is the basin-wide production rate (atoms g^{-1} y^{-1}), and C is the average isotope concentration of sediment leaving the basin (atoms g^{-1}).

Field verifications of the above technique are becoming more numerous. Granger et al. (1996) determined that erosion rates from two small catchments are within one standard deviation of independent estimates of long-term deposition rates (over 16,000 years) of the adjacent alluvial fans. Clapp (in review a) measured an erosion rate of 102 ± 24 m Ma^{-1} in the semi-arid Arroyo Chavez area of northern New Mexico. Independent erosion rate estimates for the same basin, based on a sediment budget (146 ± 25 m Ma^{-1}), and nearby basins based on hypsometric dating (~100 m Ma^{-1}), are in good agreement with the cosmogenic isotope measurements. Additional work by Clapp et al. (1999) in Israel show that long-term erosion rates determined using cosmogenic isotopes (29 ± 6 m Ma^{-1}) are less than erosion rates based on a 17-year sediment budget (46 m Ma^{-1}). Field observations within the basin suggest that sediment is currently being exported from fluvial terraces, which would increase the apparent erosion rate calculated from the short-term sediment budget. These three estimates of basin-wide erosion rates agree with checks of either, deposited sediment (Granger et al., 1996), or other independently

estimated basin-wide erosion rates (Clapp et al., 1997; Clapp et al., 1999; Clapp et al., in review a). Thus, the Bierman and Steig (1996) technique appears to be valid for small, arid drainage basins.

Clapp et al. (in review b) applied the basin-wide erosion technique to a large, lithologically heterogeneous drainage basin in southern Arizona. Clapp et al. conclude that in large basins, such as Yuma Wash, channel sediment may be reworked from older deposits. Data from this study show that isotope abundances decrease down the main stem of Yuma Wash. Field evidence suggests that the sediment is reworked from thick terrace and alluvial fan units that might be old enough for isotopic decay to have erased previous exposure histories. Mixing nuclide-rich sediment from drainage basins with nuclide-poor sediment from the thick terrace and alluvial fan units accounts for the decrease of nuclide abundance down wash. Analyses of tributary basins, however, produced consistent estimates of highland erosion rates basin-wide. This study suggests that the basin-wide erosion technique works for small basins (few km^2) without much storage, but does not work for large basins (>100 km^2) if there is great sediment storage potential.

Brown et al. (1995) analyzed sediment from a drainage basin in Puerto Rico. Results from this study suggest that all grain-sizes must be analyzed in order to determine basin-wide erosion rates. However, deep-seated (2 m) landslides erode a large portion of the sediment in the Puerto Rico field area. Such landslide events mix nuclide-rich surface sediment with nuclide-poor sediment from depths of 2 m where production is much less than surface production. Landslides are rapid episodic events that transport a wide variety of grain sizes, while more continuous erosion mechanisms such as soil

creep, sheetwash, and surficial weathering transport finer grained material over longer periods of time. Thus, one expects to find differences in nuclide abundance in different grain sizes for material transported by landslides.

In arid and semi-arid environments where Clapp et al. (1997,1999, in review a, in review b) and Granger (1996) worked, sediment is not as likely to be transported by landslides due to lack of a thick colluvial cover. Sediment transport in arid environments occurs in pulses that transport many different grain sizes together. Short durations and rapid infiltration of flow do not allow preferential transport of fine grains (Laronne et al., 1994; Laronne and Reid, 1993; Reid and Laronne, 1995). Clapp et al. (1997, 1999, in review a, in review b) analyzed different grain sizes in each of their studies. Results from all three studies show that nuclide abundances and thus, basin-wide erosion rates are independent of grain size for arid and semi-arid drainage basins.

Terrace sediment and fluvial sediment

Research on terrace sediments suggests when working in depositional environments one should address the pre-depositional abundance of cosmogenic isotopes (inheritance) (Anderson et al., 1996). Anderson et al. (1996) use a technique in which they amalgamated sediment clasts collected from the surface and from a known depth and measure the nuclide abundances to back calculate the terrace age. The technique is dependent upon the critical assumptions that deposition was rapid, all sediment in the terrace had identical initial nuclide abundances, and that deposition was recent enough so that decay is not a factor. The production at depth relationship (at 2 to 3 meters) is used to determine the nuclide inheritance of terrace sediment. The difference between the measured nuclide abundance of the surface sample and the estimated nuclide inheritance

is used to calculate a terrace age. Anderson et al. conclude that nuclide inheritance of terrace sediment can be significant. Although, this paper introduced a new method for using cosmogenic isotopes, I feel the method needs greater sampling resolution to be accepted as robust. Analyzing only two samples, even though amalgamated, could lead to gross error in calculating production at depth curves if the sediment were not deposited rapidly or the two samples did not have identical inherited nuclide abundances.

An alternative to dating fluvial terraces to determine fluvial downcutting rates, is to date cave-deposited alluvium (Granger et al., 1997). Granger et al. (1997) used the differential decay of ^{10}Be and ^{26}Al to date cave-deposited alluvium and estimate the downcutting rates for the New River in Virginia. Assuming that sediment is deposited with minimal prior burial history and an initial $^{26}Al/^{10}Be$ ratio is close to 6.0 (Nishiizumi et al., 1989), current $^{26}Al/^{10}Be$ ratios can be used to estimate emplacement times of sediment in abandoned caves. Granger et al. caution that sub-surface production by neutron spallation and muon capture can distort calculated burial times. Distortions of calculated burial time increase as burial time increases. Granger et al. (1996) conclude that sediment deposited in caves ranges from 0.29 ± 0.18 Ma for a cave 12 m above the river to 1.47 ± 0.22 Ma for a cave 29 m above the river. Associated long-term incision rates for the New River average 27 ± 4.5 m Ma^{-1}.

Soil generation rates and dating soils

The literature describing basin-wide erosion rates usually discusses sediment generation rates as well (Clapp et al., 1999; Clapp et al., in review a; Clapp et al., in review b; Granger et al., 1996). By knowing basin-wide erosion rates, the area of the basin, and the density of rock, one can calculate sediment generation rates assuming

steady-state. Other methods utilizing cosmogenic isotopes to date soils and estimate soil production are discussed below.

All of the sediment generation literature discussed above analyzed *in situ*-produced cosmogenic isotopes. However, fallout ^{10}Be, produced in the atmosphere, was first used to determine soil production rates (McKean et al., 1993; Monaghan et al., 1992). Monaghan et al. (1992) developed rigorous models of soil mass balance and ^{10}Be abundance balance to determine bedrock-to-soil conversion rates in California. Monaghan et al. conclude that soil generation rates are between 150 and 270 m Ma^{-1}, and that soil creep is capable of removing soil from the hillslopes at a rate equivalent to the uplift rate of the California coast. McKean et al. (1993) also used a mass balance model to determine soil production of a hillslope in the same region of California. McKean et al. determined that soil production was 260 m Ma^{-1} and that soil creep rate is proportional to surface gradient. Not surprisingly, both estimates (McKean et al., 1993; Monaghan et al., 1992) of soil production, based on similar mass balance models for the same region of California, agree.

A similar mass and nuclide balance approach to estimating soil production rates was tested on an alpine hillslope using *in situ*-produced cosmogenic ^{10}Be and ^{26}Al (Small et al., 1999). Small et al. calculated mean sediment production rates of 14.3 ± 4.0 m Ma^{-1} based on ^{10}Be, and 13.0 ± 4.0 m Ma^{-1} based on ^{26}Al. Sediment generation rates of regolith produced under a sediment mantle are nearly twice the rate of sediment produced from bare rock. The difference in weathering rates is due to the regolith holding water longer than bare rock. The water speeds the chemical and physical weathering of bedrock. It should be noted that the difference in erosion rates between mantled bedrock

and exposed bedrock discussed in this paper contradict the Mabbutt (1966) hypothesis discussed above. Mabbutt states that bedrock protrusions are areas of focused erosion, thus smoothing topography, while Small et al. measured differences in erosion rates that promote the generation of topography.

Phillips et al. (1998) used cosmogenic ^{21}Ne depth profiles to date soil development in New Mexico. Phillips et al. conclude that determining soil ages is best accomplished in fine-grained alluvium that was deposited rapidly with similar nuclide abundance. The ages of the Qt2 and Qt4 Rendija Canyon terraces are 144 ± 17 ka and 63 ± 8 ka, respectively and agree with independent age estimates based on soil profile development. More importantly, Phillips et al. suggest that the depth profile method of cosmogenic isotopes is a powerful tool to detect depositional unconformities and constrain the origin and genetic association of pedogenic features. Phillips et al. however, did not quantify unconformities in their soil profiles.

CHAPTER 3: Paper submitted to special volume of Reviews in Engineering Geology

In press, Environmental and Engineering Geology Impacts on Military Operations

Revised

July 13, 1999

Fifty-four years of ephemeral channel response to two years of intense World War II military activity, Camp Iron Mountain, Mojave Desert, California

Kyle K. Nichols and Paul R. Bierman
Department of Geology
University of Vermont
Burlington, Vermont 05405
kknichol@zoo.uvm.edu
(802) 656-3398
(802) 656-0045 (fax)

ABSTRACT

During World War II, U.S. Army personnel lived, trained, and executed mock battles on low gradient piedmonts (~2°) in the Mojave Desert. For example, Camp Iron Mountain (established in 1942 by General George S. Patton, Jr. and used until 1944) housed up to 20,000 Army personnel at any specific time. The camp is located on the large alluvial piedmont that extends from the Iron Mountains and is drained by shallow ephemeral channels.

At this camp, we made 18 detailed topographic maps in order to compare drainage networks of 6 undisturbed control plots and 12 plots disturbed by army activities. There are significant differences between the morphometery of small-scale, ephemeral, drainage networks on control plots, on plots bisected by stone-walled walkways, and on plots down gradient of former army roads. Control plot channels are wider (2.05 ± 1.48 m) and deeper (8.8 ± 4.5 cm) than channels in walkway plots (width: 1.19 ± 0.71 m, depth: 7.4 ± 4.1 cm) and in road plots (width: 1.18 ± 0.61 m, depth: 7.2 ± 6.7 cm).

The military's modification of the landscape affected subsequent channel originations and orientations. Channel heads were found in 76% of the compacted and smoothed walkways. In walkway plots, 80% of walkways caused the orientation of channels to deviate from the steepest piedmont gradient by more than 20°. After more than 50 years, road berms still act as local drainage divides. Down gradient of each intact road berm, there is a wide (20 to 40 m) zone in which no channels exist. Where channels have developed below intact road berms, they are smaller than channels in undisturbed control plots. Down gradient of breached road berms, wide, braided channels are common. Fifty-four years after camp abandonment, the channel network at Camp Iron Mountain has yet to recover, primarily because rock alignments and road berms continue to influence drainage patterns and local gradients.

INTRODUCTION

A significant amount of military training is done in arid regions where rates of surface processes are slow and surface change is often episodic and thus difficult to

observe and quantify. The military, as a steward of large tracts of land, is required by Army Regulation AR 200-2 to monitor the environmental effects of training exercises in arid regions (Prose, 1985). In order to place in perspective the effect of military maneuvers on the desert environment, one must understand rates of geomorphic processes and the rate at which natural systems recover from disturbance. Because many desert processes are so slow, results of short-term monitoring are often inconclusive (Abrahams et al., 1984). A longer-term perspective may be gained by studying areas where military activity occurred over a known and discrete time frame. Such data may allow identification and implementation of training protocols that minimize environmental impact.

From 1942 to 1944, the US Army established twelve temporary base camps and living quarters in the Desert Training Center (Fig. 1A). Camp Iron Mountain (~ 6 km^2) was built on a low-gradient piedmont surface extending > 10 km from the Iron Mountains to Danby Lake playa in the Mojave Desert (Fig. 1B). At this camp, the Army constructed an extensive (4 km by 1.5 km) grid of roads (Fig. 1C). During road construction, berms (30 to 40 cm high) were built on both sides of each road. Troops outlined walkways, tents, and roads with angular granitic clasts ranging in size from 10 to 20 cm (Fig. 2). After two years of continuous use, the Army dismantled the camps in May 1944 (Henley, 1989). Today, the only evidence of occupation is the presence of road berms, rock alignments, rock designs, and other artifacts, in various states of deterioration.

The Iron Mountains are Cretaceous granite (Miller et al., 1981). The piedmont meets the mountain front at a sharp angle and is dominated by granular granitic alluvium

(grus); median grain size is 2 mm. The piedmont slopes uniformly ~2° to the east where Camp Iron Mountain is located (Fig. 1B). Shallow, 10-cm deep ephemeral channels form gentle channel-terrace topography and dissect the surface.

The Iron Mountain piedmont receives an average of 7.9 cm of precipitation a year (NOAA, 1982). Late summer thunderstorms and mid-winter cyclonic events produce the majority of precipitation. Most precipitation infiltrates the grus. Runoff occurs only during rare, high-intensity rainfall events. Iverson et al. (1981) determined that runoff events in the western Mojave Desert probably occur about once per decade in undisturbed areas and more frequently in disturbed areas. As overland flow moves down the piedmont, some of the flow infiltrates the unsaturated grus (Bull, 1991; Ritter, 1978).

In areas where no channels exist, sheetwash is the dominant overland flow mechanism (Horton, 1945). Sheetwash continues until flow depth is great enough so that 1) a critical basal shear stress is reached and channel incision begins (Montgomery and Dietrich, 1994), or 2) raindrops cannot obliterate incipient channels as they begin to concentrate flow (Dunne, 1980). Small channels then form and transport sediment until the sediment load becomes greater than the transport capacity. When deposition occurs, caused by flow loss (infiltration) or a decrease in local gradient, many of the small channels diffuse into the planar surface. Such discontinuous channel morphologies dominate inside Camp Iron Mountain.

Historic photographs document that constant foot, vehicle, and tank traffic destroyed most, if not all, of the small channels during the occupation of Camp Iron Mountain (Fig. 2). Thus, we can reasonably assume a surface absent of channels inside the camp when our experiment began in May, 1944. We assume that road berms and

rock alignments were intact at the time of evacuation. Because the area is remote and the nearest populated town is more than 55 kilometers away (Desert Center, California, population 120), post-army activity is limited to natural processes (overland flow and bioturbation) and occasional off-road vehicle (ORV) use. Around 1980, a fence was constructed around Camp Iron Mountain that stopped all ORV traffic (Bureau of Land Management, 1986).

Camp Iron Mountain provides a unique opportunity to investigate the redevelopment of an ephemeral channel network after two years of intense military training. We collected data 54 years after camp abandonment in May, 1998. In this paper, we use our observations and data, in conjunction with previous research illustrating that human influence increases soil density (Prose, 1985; Webb et al., 1986), soil compaction, and soil surface smoothness (Iverson, 1980; Iverson et al., 1981), to develop a process model of channel response to military activity on low-gradient arid landscapes.

METHODS

In order to determine whether environmental impacts persist half a century after the U.S. Army abandoned Camp Iron Mountain, we compared ephemeral channel depths, widths, areas, orientations, and drainage densities in three types of experimental plots (60 m by 60 m square areas). *Control plots* are representative of undisturbed conditions and are outside Camp Iron Mountain. *Walkway plots* contain rock alignments and are representative of disturbed conditions inside the camp. *Road plots* contain road berms at the up-gradient boundary and are also representative of disturbed conditions inside the camp. By comparing data gathered from these different types of plots, we determine the

degree to which past military activities still affect the desert surface, in particular, the geometry of ephemeral channels that drain the Iron Mountain piedmont.

Survey Methods

We outlined plot boundaries using a Pentax PCS-2 total station to delineate 60-m orthogonal sides on all plots except Control Plot 3 where we used a tape and compass survey. We used flags to outline all channels within plot boundaries. Each plot was surveyed using a Trimble 4400 real time kinematic differential Global Positioning System (GPS), precise to within several centimeters horizontally and ~1 cm vertically. We surveyed topography using a five-meter grid spacing and surveyed each channel by making a series of cross-sections, with the exception of Control Plot 3 and Road Plot 1 where cross-sections were not measured. Each cross-section consisted of two bank-top points, two bank-bottom points, and any points of significant topographical change within the channel. In places where channel banks could not be defined, the channel margins were labeled as wash banks. In walkway plots, we also surveyed all rock alignments. For each plot, an average of 454 topographic data points were collected.

After surveying each plot, we contoured the data at ten-centimeter intervals. Before removing the channel boundary flags, we field checked maps of each plot to verify the accuracy of channel locations. We made observations of characteristics, inside and outside each plot, that influence channel morphology. We made a photographic record of each plot, and noted photograph locations and orientations on each map.

Plot locations

We randomized the selection of all plot locations within characteristic areas. Control plots were located outside Camp Iron Mountain. Walkway plots were inside the

camp and contained visible rock alignments and no roads. We chose walkway plot locations by walking inside the camp until we could see rock alignments extending approximately 80 m in all directions. To minimize bias, we walked 20 additional steps, in the same direction, before setting up the plot boundaries. All road plots contained a road berm that formed the up-gradient boundary. Road plots did not contain roads or rock alignments, except for one plot that contained a 10-m rock alignment. We chose the road plots by walking along a road until we could not see rock alignments for at least 60 m.

Data Reduction

We used cross-section data to calculate channel depths, widths, and channel cross-sectional areas. Channel depths are defined as bank-bottom elevations subtracted from bank-top elevations. We used the GPS northing (N) and easting (E) coordinates and following equation to define the channel widths:

$$W = ((E_L - E_R)^2 + (N_L - N_R)^2)^{1/2} \quad (1)$$

where W is the width, E_L is left bank easting coordinate, E_R is right bank easting coordinate, N_L is left bank northing coordinate, and N_R is right bank northing coordinate. Cross sectional areas are defined as the channel width multiplied by the average channel depth.

We used our high-resolution topographic maps to determine channel surface areas, drainage densities, and channel orientations. We digitized each map to calculate the total area of each plot occupied by channels. Drainage densities for plots are defined as the sum of channel lengths divided by the plot area (Dunne and Leopold, 1978). The drainage densities for channels inside old walkways (inside the walkway plots) are

defined as the sum of channel lengths inside old walkways divided by the old walkway area. Since most channels in the plots are linear, we determined channel orientation by measuring each representative channel orientation with respect to north. For channels with curvature, we measured the average direction of flow determined by connecting the upstream end of the channel to the downstream end of the channel.

RESULTS

Visual observations made at Camp Iron Mountain imply that human influences on the surface morphology persist 54 years after the camps were abandoned. Detailed topographic mapping shows differences in channel characteristics between control and experimental plots. The data support visual observations that ephemeral channel networks have not recovered to background conditions more than a half-century after Army abandonment.

Depth, Width, and Cross-sectional Area Data

On average, control plot channels are significantly deeper (99.9% confidence level) than walkway ($t = 6.27$, $df = 1396$, $P < 0.001$) and road ($t = 7.63$, $df = 1397$, $P < 0.001$) plot channels, and have an average depth of 8.9 ± 4.5 cm ($n = 756$). Average channel depths in walkway and road plots are 7.4 ± 4.1 cm ($n = 647$) and 7.2 ± 6.7 cm ($n = 653$), respectively (Table 1). Channel depths in walkway and road plots are not statistically different ($t = 0.65$ $df = 1272$, $P > 0.52$). Data for all plots are right skewed (Fig. 3).

Channels in control plots are significantly wider (99.9% confidence level) than channels in walkway ($t = 9.29$, $df = 428$, $P < 0.001$) and road ($t = 8.53$, $df = 531$, $P <$

0.001) plots. Control plot channel widths average 2.05 ± 1.48 m (n = 319). Average channel widths for walkway and road plots are 1.19 ± 0.71 m (n = 418) and 1.18 ± 0.61 m (n = 224), respectively (Table 2). Widths of channels in walkway and road plots are not statistically different ($t = 0.58$, $df = 372$, $P > 0.56$). Control plot channels have a greater range in widths compared to widths in disturbed plots. Data are skewed to the right for all plots (Fig. 3).

Control plot channels have, on average, statistically larger cross-sectional areas than walkway ($t = 8.01$, $df = 409$, $P < 0.001$) and road ($t = 11.04$, $df = 385$, $P < 0.001$) plot channels (Table 3). The average cross-sectional area for control plot channels is 0.157 ± 0.039 m^2 (n = 288). The average cross-sectional areas for walkway and road plot channels are 0.077 ± 0.031 m^2 (n = 331) and 0.086 ± 0.060 m^2 (n = 198), respectively. Road plot channels have statistically larger cross-sectional areas than walkway plot channels ($t = 5.01$, $df = 449$, $P < 0.001$).

Channel Area and Drainage Density

Control plots channel areas are statistically larger than walkway channel areas at the 90% confidence level ($t = 2.07$, $df = 9$, $P < 0.1$), and road channel areas at the 70 % confidence level ($t = 1.26$, $df = 9$, $P < 0.3$). Channels in control plots cover an average of 733 ± 297 m^2, 20% of the average control plot area. Walkway plot channels cover an average of 432 ± 199 m^2, 12% of the average walkway plot area. The average road plot channel area is 490 ± 367 m^2, 14% of the average road plot area (Table 4). Walkway and road plot channel areas are not statistically different ($t = -0.34$, $df = 9$, $P > 0.5$).

Control plot drainage densities are not statistically different than walkway plot drainage densities ($t = 0.68$, $df = 9$, $P > 0.5$). The average drainage density for control

plots is 0.096 ± 0.036 m/m^2, while walkway plots have an average drainage density of 0.084 ± 0.027 m/m^2. Road plots have an average drainage density of 0.067 ± 0.023 m/m^2 (Table 5). Road plot drainage densities are statistically smaller than control plot drainage densities at the 80% confidence level ($t = 1.71$, $df = 9$, $P < 0.2$) and walkway plot drainage densities at the 70% confidence level ($t = 1.19$, $df = 10$, $P < 0.3$).

Channel Orientations

Channels are usually oriented down the Iron Mountain piedmont's steepest gradient, 103 ± 16° based on a plot by plot analysis of our topographic maps. Walkway plot channel orientations are bimodal (Fig. 4). In fact, more channels in walkway plots have the same orientation as walkways (126°) than have the orientation of the average steepest gradient (103°). Control plot channels exhibit the largest range of orientations (101 ± 20°), but control plots are more widely distributed across the piedmont surface than walkway and road plots (Fig. 1C). Road plot channels have the smallest range of orientations (103 ± 11°), following the steepest piedmont gradient and consistent with the smooth surface topography below the intact road berms.

DISCUSSION

Camp Iron Mountain has been recovering from a discrete environmental impact for the past 54 years. Our data for ephemeral channels show that recovery is far from complete. There remain measurable and distinct differences between channel characteristics in control and experimental plots. The differences are primarily due to the presence of rock alignments, road berms, and the smoothing and compaction of the surface. By diverting shallow overland flow and changing surface roughness, human

activity has altered surface water flow patterns within the camp as indicated by measurements made in the experimental plots. Our data support the conclusions of Iverson (1980) that ORV use, or in this study, military activity, reduces infiltration and changes the roughness of desert surfaces.

Control Plots

Control plots are representative of undisturbed conditions on the Iron Mountain piedmont. Control plots are located both upslope and downslope of Camp Iron Mountain. The average channel depths, channel widths, channel areas, channel orientations, and drainage densities are similar for all control plots (Tables 1 through 5).

On average, control plot channels are almost a meter wider and are more continuous than walkway and road plot channels, thus providing for greater channel areas and drainage densities (Tables 4 and 5). Control plot channels are on average 1.5 cm deeper than average walkway and road plot channel depths (Table 1). Average channel orientations deviate little (101 ± 20°) even though control plot 6 is located at the convergence of the Iron Mountain and Granite Mountain piedmonts. The internal consistency of the control plot data, despite the distance between plots (up to 3 km), supports the observation that the Iron Mountain piedmont is a homogeneous planar surface experiencing similar ephemeral channel processes along its entire length and width (Fig. 5).

Walkway Plots

Channel characteristics in walkway plots are influenced strongly by the combination of rock alignments and the compaction and smoothing of roughness elements caused by two years of foot traffic on the walkways. Up-gradient of some

walkway areas, there are discontinuous rock alignments that disperse overland flow and impede channel incision. Where channels have incised, rock alignments influence the orientation of flow. Eighty percent of all walkway rock alignments act as a barricade to flow and cause channel orientations to deviate at least 20° from the steepest gradient. Small channels that form in, or just up gradient of walkways, have orientations along the walkway (Fig. 6), until either the walkway ends, the flow has enough power to breach the rock alignment, or sediment load exceeds the transport capacity and the channels diffuse into the surface. Larger channels usually have flow directions controlled by overall topography, regardless of the presence of rock alignments (Fig. 7).

Interestingly, walkway plot channel areas are approximately half that of the control plot channel areas, while drainage densities are similar. Channel areas differ and drainage densities are similar because the more numerous, smaller, and discontinuous walkway channels (Fig. 7) have approximately the same total channel length as the less frequent, wider, and more continuous control plot channels (Fig. 5).

Compacting the soil and smoothing surface roughness elements aids in the incision of new channels (Iverson, 1980). Compaction decreases infiltration capacities (Hillel, 1980) and allows runoff at lower precipitation intensities and durations. Smooth surfaces generate greater flow velocities than rough surfaces, increasing basal shear stresses and promoting channel incision. Prose (1985) found that soils at Camp Iron Mountain were compacted enough after only one pass of a medium-sized tank to promote rill and gully formation within the tank tracks. The walkways experienced two years of foot traffic, which was effective in smoothing roughness elements and compacting the soil. Over 76% of walkways have channels that start within them, due presumably to

decreased infiltration capacities and the smooth surface. Many of these channels dissipate further down gradient, but some channels extend beyond the plot boundaries.

Road Plots

Most literature on the impact of roads on drainage networks centers on logging roads in mountainous regions. Logging roads cause increased erosion rates and landslide initiation (Montgomery, 1994), more peaked hydrographs (Wemple et al., 1996), and changes in channel morphology. We, however, are investigating the effects of temporary roads, established on a low-gradient surface in an arid-environment. Our data do not suggest increased erosion rates, landslide initiation, or more peaked hydrographs, but do reveal changes in channel morphologies.

Channel characteristics of road plots are strongly influenced by the presence of paired road berms up-gradient. Road berms act as local drainage divides, channeling and diverting overland flow. The paired berms around each road collect surface runoff and concentrate flow until either a cross road of steeper gradient is encountered, or there is enough water to breach the berm and flow unconfined down the steepest gradient (Fig. 8). Intact road berms divert water away from some road plots. Down gradient of the intact road berms there is usually a zone (20 to 40 m) where shallow sheetflow must dominate and channels are absent (Fig. 9). Down gradient of a berm breach, the flow disperses and forms a braided channel (Fig. 10). The presence of wide, braided channels accounts for the larger average and standard deviation in cross-sectional area and channel area for road plots in comparison to the walkway plots (Tables 3 and 4). However, the relatively few channels in road plots, (compared to walkway plots) accounts for a lower drainage density (Fig. 11).

Channel orientations in road plots are less variable than channel orientations in walkway and control plots (Fig. 4). The road plot channels have a uniform surface with few flow obstructions. Most channels in road plots develop within the plots (Fig. 11), their orientation controlled directly by the steepest local gradient. The uniform surface, the closer spatial distribution of road plots when compared to the control plots, and the fact that most channels in road plots are developed within the plot account for the low variance in road plot channel orientations.

Process model

In order to generalize our results in a qualitative model, we must understand the surface processes affecting the Iron Mountain piedmont. Such a qualitative model must not only be consistent with our understanding of desert surface processes, but must also explain our observations at the camp and the observations of others (Iverson, 1980; Iverson et al., 1981; Prose, 1985; Webb et al., 1986). By understanding the dominant physical processes occurring on desert surfaces, we can suggest ways to minimize the impact of military training in arid regions.

Iverson (1980) concluded that ORV use in the western Mojave Desert compacted and smoothed microtopography which led to hydraulic responses that increased soil erosion in disturbed areas. At Camp Iron Mountain, tanks, vehicles, and troops compacted and smoothed the soil (Prose, 1985). The compacted soil has fewer and smaller pores and thus lower infiltration rates. Reduced infiltration increases the volume and frequency of overland flow (Iverson et al., 1981). Troops and vehicles smoothed microtopography, which normally acts to disperse flow energy, and cause localized sediment deposition. Iverson (1980) found a 13-fold decrease in surface roughness after

just a few passes of an ORV. As a result of soil compaction and surface smoothing, overland flow volumes increase, along with the potential for channel incision, especially on heavily impacted areas such as walkways.

Walkways, the most compacted and smoothed features we mapped, have the highest frequency of channel heads (Santos, 1999). As argued above, this observation is consistent with soil compaction and surface smoothing. Iverson (1980) noted a strong positive correlation between runoff power and sediment yield ($r^2 = 0.78$) for desert surfaces. Increased sediment yield at Camp Iron Mountain is expressed by channel formation. The abundance of channel heads on walkways suggests that runoff power must be higher on walkways than elsewhere. Compacting and smoothing walkway surfaces decreased infiltration, increased local discharge, and thus increased runoff power.

Control plot channels are mostly continuous through the plots, have larger widths and depths, and thus larger channel cross-sectional areas than channels in disturbed plots. For alluvial rivers, larger channel cross-sectional areas correspond to larger drainage areas (Dunne and Leopold, 1978). However, the piedmont experiences overland flow and does not have clearly defined drainage divides, except for road berms. Unlike their larger cousins, individual widths and depths of piedmont channels, do not change significantly or predictably as a function of distance from channel head (Fig. 12). Linear models of such relationships have low slopes and channel widths and depths are poorly correlated with distance from the channel head. Thus, channel widths and depths change little as a function of channel length and the size of the local drainage area does not control the size of the channels on the piedmont. Rather, the channels appear to attain a

"steady state" size at which incoming overland flow and precipitation balance infiltration losses.

Low drainage densities of road plots are a direct result of intact road berms. Road berms collect runoff and divert water to intersections with roads that are sub-parallel to slope, thereby limiting overland flow in areas down gradient of intact berms. In these flow-deprived areas, sheetwash dominates for 20 to 40 m down gradient of the road berm, where there are few or no channels. This zone, absent of channels, lowers the drainage densities for road plots compared to control and walkway plots. At the location where basal shear stress reaches a critical threshold, or rainsplash is unable to obliterate incipient channels (usually 20 to 40 meters from the road berm), channel initiation occurs and channel heads are abundant.

Rock alignments act as barricades to flow. Rock alignments, which outline walkways, are usually orientated 20° from the steepest average gradient of the Iron Mountain piedmont. When small flows encounter the large rock clasts (or when channels form inside walkway boundaries), the water is forced along the alignments until the rock alignment ends, the flow acquires enough power to breach the rock alignment, there is a gap in the alignment, or the channel diffuses into the surface. The most common channel orientation in walkway plots is along the rock alignments, and some channels flow inside walkways for the entire length of the plot.

The length of time that the drainage network will continue to be affected by past Army activities is difficult to determine. Webb et al. (1986) suggested that soil densities might take more than a century to recover to natural values after disturbance. Iverson (1980), Iverson et al. (1981), and Prose (1985) conclude that soil lost by erosion in desert

environments is probably unrecoverable on human time scales. We observed that more than half of the road berms and rock alignments are still intact more than 50 years after camp abandonment. Since soil compaction is probably only half way to recovery and rock alignments and road berms will be present for the next 50 years, drainage networks should be affected for at least that long and possibly longer.

Persisting army effects might have been significantly reduced by simple remediation at the time of camp abandonment. Because the topography was smooth within camp boundaries and the roads were already compacted (Prose, 1985), grading the road berms at abandonment would have eliminated local drainage divides without further disturbing the surface. Also, removal of the rock alignments would have eliminated the stone-walled flow boundaries. Neither of these techniques, however, addresses compaction or smoothing of roughness elements, which are more difficult to remediate. Nevertheless, the removal of road berms and rock alignments in 1944 would have greatly reduced many of the lingering hydraulic differences demonstrated by our data.

CONCLUSIONS

Camp Iron Mountain is located on a uniform, low gradient, piedmont surface where sediment is transported primarily in shallow, discontinuous, ephemeral streams. After two intense years of military activity and 54 subsequent years of recovery, channels in affected areas still have not returned to natural geometries due to: 1) the persisting network of road berms and rock alignments and 2) soil compaction and smoothing. Road berms concentrate runoff and cause zones where channels are absent below intact road berms. Where berms are breached, wide, braided channels dominate. Discontinuous rock alignments disperse flow and inhibit channel formation. Continuous rock

alignments influence the orientation and increase the frequency of small channels, but not large channels. Compacted and smoothed walkway surfaces change channel morphologies. Destroying road berms and rock alignments when temporary camps are abandoned will likely minimize the long-term impact of army maneuvers.

ACKNOWLEDGMENTS

We thank D. Santos and C. Massey for field assistance, H. Wilshire for the low-level oblique aerial photographs, D. Howell for statistical assistance, and D. Montgomery, S. Gran, A. Noren, K. Jennings, D. Santos and an anonymous reviewer whose edits improved an earlier version of this manuscript. U.S. Army Research Office grants DAAG559710180 and DAAH04-96-1-0036 funded this research.

REFERENCES CITED

Abrahams, A. D., Parsons, A. J., Cooke, R. U., and Reeves, R. W., 1984, Stone movement on hillslopes in the Mojave Desert, California: A 16-year record: Earth Surface Processes and Landforms, v. 9, p. 365-370.

Bull, W. B., 1991, Geomorphic responses to climate change: New York, Oxford University Press, 326 p.

Bureau of Land Management, 1986, Desert Training center California-Arizona Maneuver Area interpretive plan: Bureau of Land Management, California District.

Dunne, T., 1980, Formation and controls of channel networks: Progress in Physical Geography, v. 4, p. 211-239.

Dunne, T., and Leopold, L. B., 1978, Water in environmental planning: San Francisco, W. H. Freeman, 818 p.

Henley, D. C., 1989, "The land that God forgot..." The saga of Gen. George Patton's Desert Training Center, Western American History Series, 54 p.

Hillel, D., 1980, Fundamental of soil physics: New York, Academic Press, 486 p.

Horton, R., 1945, Erosional development of streams and their drainage basins: hydrophysical approach to quantitative morphology: Bulletin of the Geological Society of America, v. 57, p. 275-370.

Iverson, R. M., 1980, Processes of accelerated pluvial erosion on desert hillslopes modified by vehicular traffic: Earth Surface Processes, v. 5, p. 369-388.

Iverson, R. M., Hinckley, B. S., Webb, R. M., and Hallet, B., 1981, Physical effects of vehicular disturbances on arid landscapes: Nature, v. 212, p. 915-917.

Miller, D. H., Howard, K. A., and Anderson, J. L., 1981, Mylontic gneiss related to emplacement of a Cretaceous batholith: U..S. Geological Survey Open File Report.

Montgomery, D. R., 1994, Road surface drainage, channel initiation, and slope instability: Water Resources Research, v. 30, no. 6, p. 1925-1932.

Montgomery, D. R., and Dietrich, W. E., 1994, Landscape dissection and drainage area-slope thresholds, *in* Krikby, M. J., ed., Process Models and Theoretical Geomorphology: New York, John Wiley & Sons Ltd., p. 221-246.

National Oceanic and Atmospheric Administration, 1982, Monthly normals of temperature, precipitation, and heating and cooling degree days 1951-1980, California.: NOAA (National Oceanic and Atmospheric Administration).

Prose, D. V., 1985, Persisting effects of armored military maneuvers on some soils of the Mojave Desert: Environmental Geology Water Science, v. 7, p. 163-170.

Ritter, D. F., 1978, Process geomorphology: Dubuque, Iowa, WM. C. Brown, 603 p.

Santos, D. L., 1999, The effects of two years of intense military activity on the source areas, source-basin lengths and initiation of channels in Camp Iron Mountain of the U.S. Army's former Desert Training Center, Mojave Desert, California [Senior thesis]: University of Vermont.

Webb, R. H., Steiger, J. W., and Wilshire, H. G., 1986, Recovery of compacted soils in Mojave Desert ghost towns: Soil Science Society of America Journal, v. 50, p. 1341-1344.

Wemple, B. C., Jones, J. A., and Grant, G. E., 1996, Channel network extension by logging roads in two basins, Western Cascades, Oregon: Water Resources Bulletin, v. 32, no. 6, p. 1195-1207.

FIGURE CAPTIONS

Figure 1. A. Location of the Desert Training Center (shaded in gray) in the southwestern United States. Circles are temporary base camps, Camp Iron Mountain shown by solid square. B. Topography of the Iron Mountain piedmont and the Iron Mountains. IM = Iron Mountains, CRA = Colorado River Aqueduct. Contour interval is 50 m. Map based on the Granite Pass, California 7.5' U.S.G.S. quadrangle, 1985. C. Aerial photograph of Camp Iron Mountain area and location of all plots at approximately same scale as 1B. Roads are orthogonal. C = Control Plots, W = Walkway Plots, and R = Road Plots (U.S.G.S. aerial photograph NAPP 6822-240 10/2/95).

Figure 2. Photograph of Camp Iron Mountain after a sandstorm. Rock alignments are visible in front of tents. After camp abandonment, rock alignments were left intact.

Foot and vehicle traffic has obliterated ephemeral channel network. National Archives photo #111-SC-145201.

Figure 3. Distribution of channel depths and widths for control, walkway, and road plots. The black bar represents mean value.

Figure 4. Rose diagrams of channel orientations. The light gray arrow represents the average orientation of the steepest topographic gradient for all plots. Each successive larger circle represents five channels with the same orientation. A. Control plots B. Walkway plots (smaller, double barbed arrow represents walkway orientation) C. Road plots.

Figure 5. Maps of all Control Plots. Scale bar and direction are in C-6. Contour interval = 0.2 m. Elevations in maps are precise to ±1 cm, but real elevations are ± 30 m, due to systematic GPS inaccuracy.

Figure 6. Low-level oblique aerial photograph of channels breaching walkway rock alignments at Camp Iron Mountain (from H. Wilshire). Arrow(s) from: RA point to rock alignments; RB point to road berms and SG points down steepest gradient. Walkways are approximately 1.5 m wide.

Figure 7. Maps of all Walkway Plots. Scale bar is in W-6. Contour interval = 0.2 meters. Walkways are gray and channels are black. Elevations in maps are precise to ±1 cm, but real elevations are ± 30 m, due to systematic GPS inaccuracy.

Figure 8. Low-level oblique aerial photograph of Camp Iron Mountain showing road berms channeling flow. Crossroads that are orientated down steeper gradients become wide washes. Roads are approximately 7 m wide. SG = steepest gradient (from H. Wilshire).

Figure 9. Photograph of the smooth surface below an intact road berm on map C-4. This area, devoid of channels, is dominated by sheetwash. Bush in center of photograph is approximately 2 m high.

Figure 10. Photograph of a wide, braided channel down gradient of a breached berm in R-1. Bush in front left is approximately 80 cm high.

Figure 11. Maps of all Road Plots. Scale bar and direction are in R-6. Contour interval = 0.2 meters. Road berms form the up gradient boundary. Area where channel heads are absent is 20 m to 40 m wide. Location of Figure 9 photograph is noted in R-4. Location of Figure 10 photograph is noted in R-1. Elevations in maps are precise to ±1 cm, but real elevations are ± 30 m, due to systematic GPS inaccuracy.

Figure 12. Channel widths and depths as a function of distance from channel head. Low slopes of linear models and poor correlation imply that channels widen slightly but do not appear to deepen significantly down piedmont.

TABLE 1. CHANNEL DEPTHS FOR CONTROL, WALKWAY,AND ROAD PLOTS

Plot	Control (cm)	Walkway (cm)	Road (cm)
1	10.7 ± 5.4 (126)	6.5 ± 2.8 (100)	9.0 ± 4.0 (222)
2	7.4 ± 2.5 (59)	8.4 ± 4.1 (125)	6.1 ± 2.9 (127)
3	9.9 ± 5.0 (178)	5.5 ± 2.5 (80)	5.8 ± 2.5 (77)
4	7.9 ± 3.9 (155)	7.1 ± 4.4 (120)	7.6 ± 2.9 (69)
5	8.2 ± 4.1 (142)	6.1 ± 3.0 (61)	5.1 ± 2.4 (86)
6	8.1 ± 4.1 (96)	8.8 ± 4.8 (161)	7.7 ± 3.5 (72)
Average of all channels	8.9 ± 4.5 (756)	7.4 ± 4.1 (647)	7.2 ± 6.7 (653)

Note: Average and standard deviations are determined using *n* values in parenthesis.
Paired depths for channel cross-sections are assumed to be independent observations because left and right banks are poorly correlated ($r^2 = 0.05$).

TABLE 2. CHANNEL WIDTHS FOR CONTROL, WALKWAY, AND ROAD PLOTS

Plot	Control (m)	Walkway (m)	Road (m)
1	2.42 ± 1.37 (75)	1.02 ± 0.63 (78)	N.D.*
2	2.02 ± 2.02 (34)	1.10 ± 0.45 (65)	1.15 ± 0.50 (50)
3	N.D.*	1.34 ± 0.97 (58)	0.88 ± 0.57 (41)
4	2.10 ± 1.27 (75)	1.43 ± 0.83 (57)	1.36 ± 0.52 (35)
5	1.94 ± 1.58 (69)	1.09 ± 0.50 (76)	0.63 ± 0.27 (59)
6	1.63 ± 1.31 (55)	1.40 ± 0.69 (84)	2.23 ± 1.44 (38)
Average of all channels	2.05 ± 1.48 (308)	1.19 ± 0.71 (418)	1.18 ± 0.61 (223)

Note: Average and standard deviations are determined using *n* values in parenthesis.
*N.D. = not determined

TABLE 3. CHANNEL CROSS-SECTIONAL AREAS FOR CONTROL, WALKWAY, AND ROAD PLOTS

Plot	Control (m^2)	Walkway (m^2)	Road (m^2)
1	0.219 ± 0.143 (64)	0.046 ± 0.031 (55)	N.D.*
2	0.119 ± 0.105 (30)	0.095 ± 0.058 (65)	0.061 ± 0.047 (48)
3	N.D.*	0.052 ± 0.046 (39)	0.040 ± 0.025 (31)
4	0.152 ± 0.129 (75)	0.101 ± 0.098 (56)	0.106 ± 0.062 (35)
5	0.172 ± 0.174 (67)	0.046 ± 0.040 (40)	0.029 ± 0.022 (59)
6	0.115 ± 0.122 (52)	0.127 ± 0.089 (78)	0.193 ± 0.146 (35)
Average of all channels	0.157 ± 0.039 (288)	0.077 ± 0.031 (331)	0.086 ± 0.060 (198)

Note: Average and standard deviations are determined using *n* values in parenthesis.
*N.D. = not determined

TABLE 4. CHANNEL AREAS FOR CONTROL, WALKWAY, AND ROAD PLOTS

Plot	Control (m^2)	Walkway (m^2)	Road (m^2)
1	1064	287	1160
2	477	302	630
3	603	361	314
4	1100	547	258
5	765	307	152
6	394	787	427
Average	733 ± 297	432 ± 199	490 ± 367

Note: Average and standard deviation are determined using plot values.

TABLE 5. DRAINAGE DENSITIES FOR CONTROL, WALKWAY, AND ROAD PLOTS

Plot	Control (m/m^2)	Walkway (m/m^2)	Road (m/m^2)
1	0.123	0.071	0.100
2	0.052	0.068	0.091
3	0.068	0.056	0.052
4	0.138	0.097	0.049
5	0.124	0.078	0.045
6	0.073	0.132	0.061
Average	0.096 ± 0.036	0.084 ± 0.027	0.066 ± 0.023

Note: Average and standard deviation are determined using the plot values.

Figure 1A

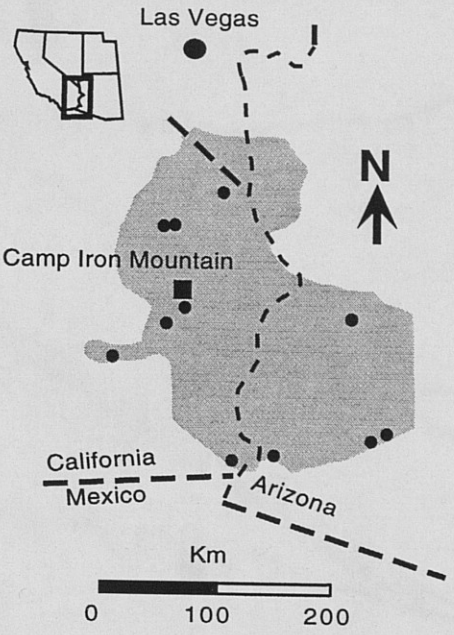
Las Vegas
N
Camp Iron Mountain
California
Mexico
Arizona
Km
0
100
200

Figure 1B

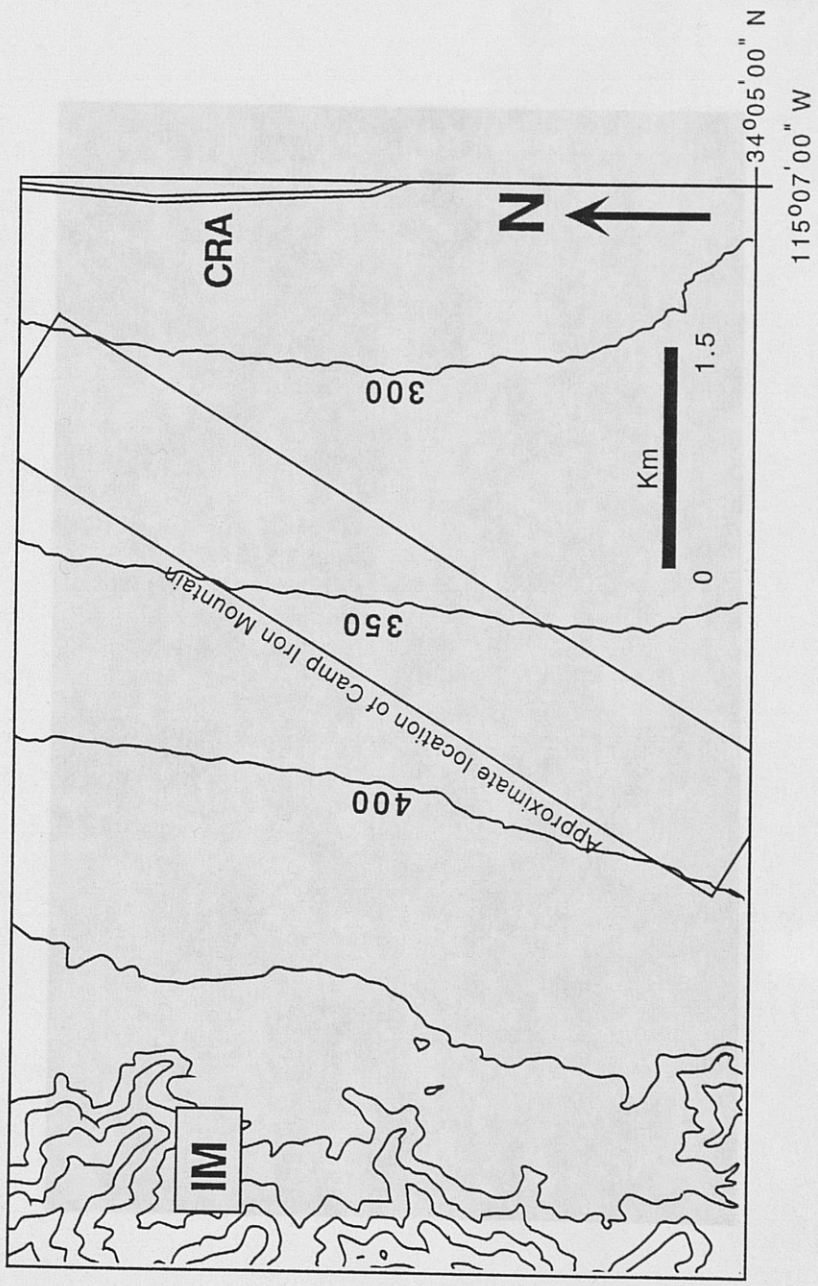
34°05'00" N
115°07'00" W
N
CRA
300
350
400
Approximate location of Camp Iron Mountain
Km
0
1.5
IM

Figure 1C

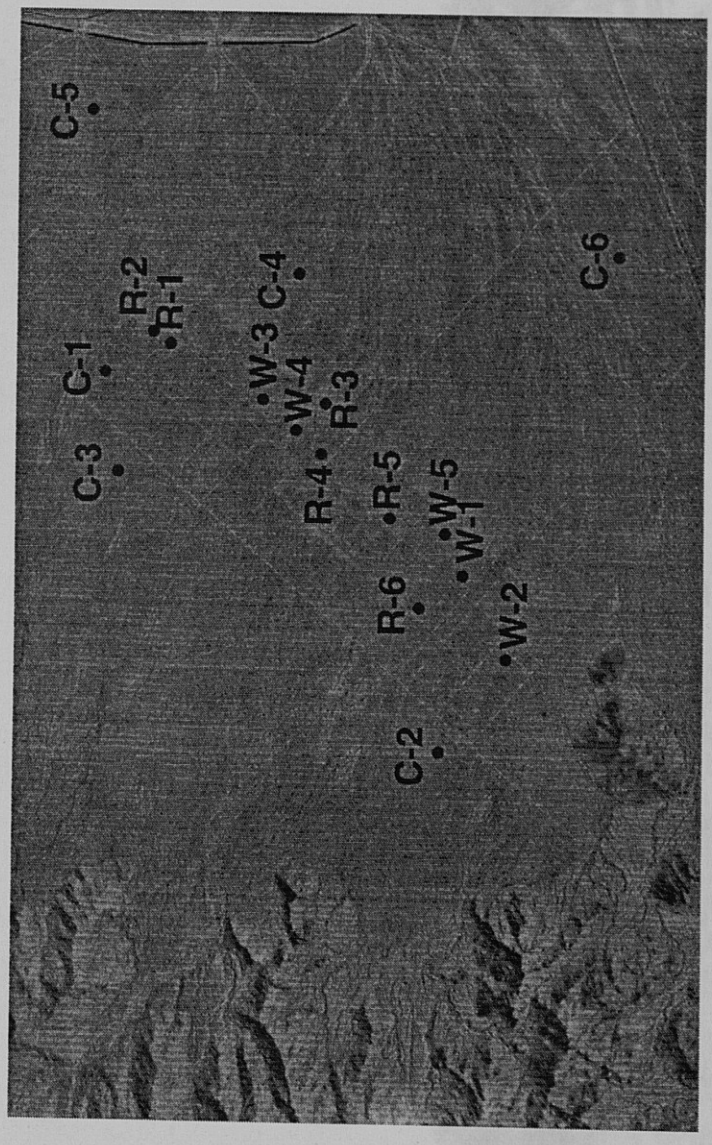

Figure 2

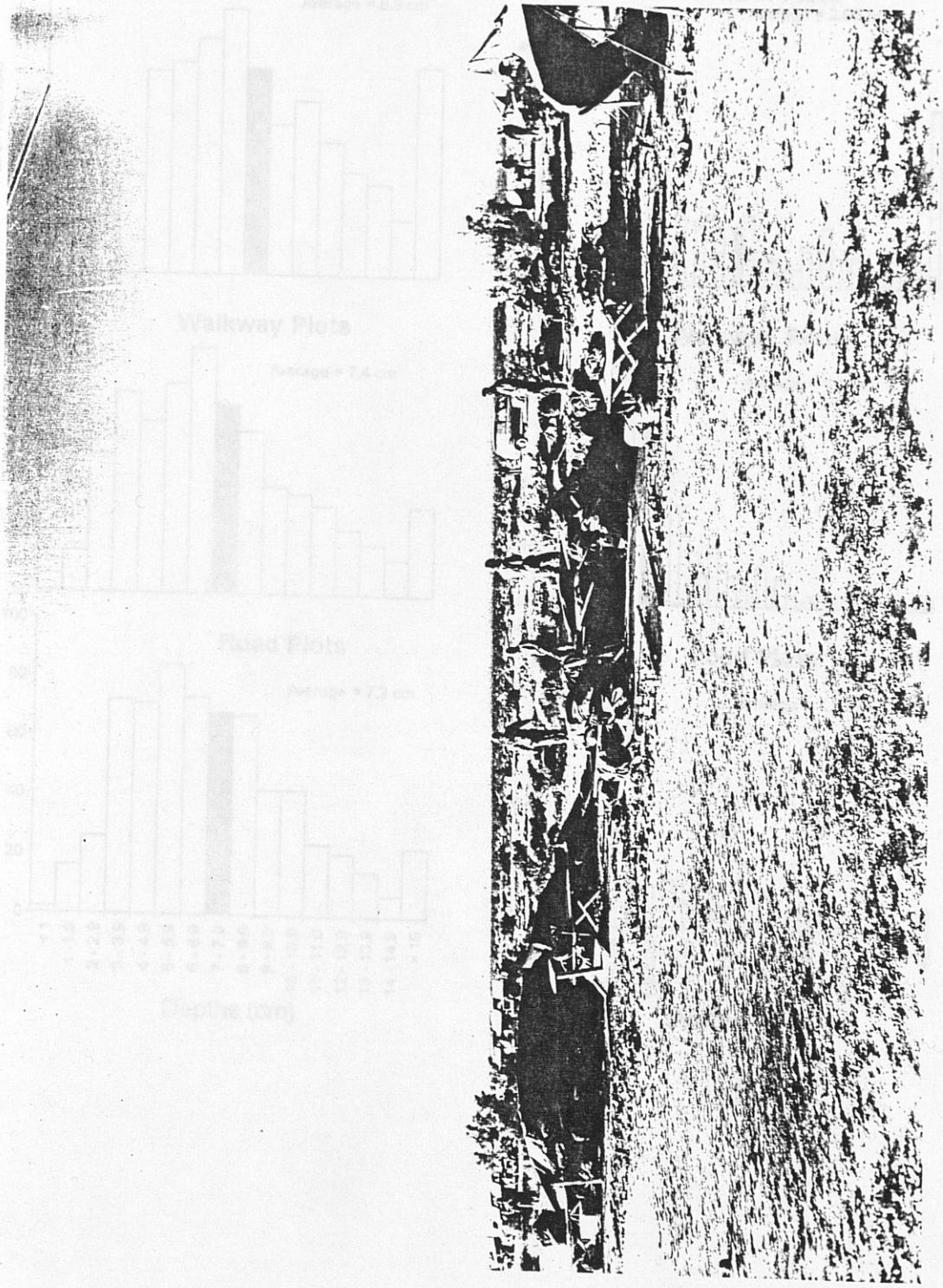

Figure 3

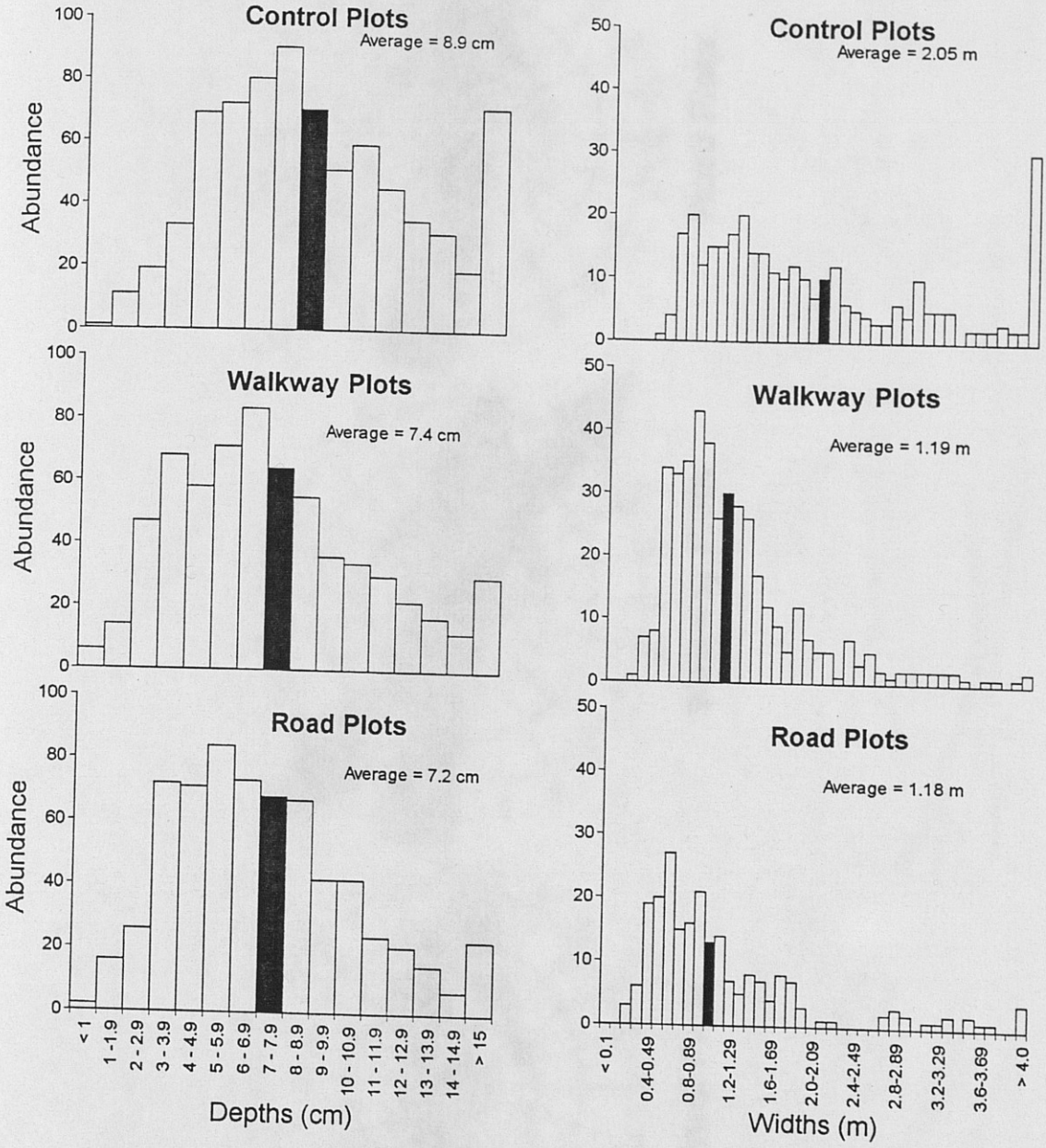
Control Plots
Average = 8.9 cm
Abundance
Walkway Plots
Average = 7.4 cm
Abundance
Road Plots
Average = 7.2 cm
Abundance
< 1
1 - 1.9
2 - 2.9
3 - 3.9
4 - 4.9
5 - 5.9
6 - 6.9
7 - 7.9
8 - 8.9
9 - 9.9
10 - 10.9
11 - 11.9
12 - 12.9
13 - 13.9
14 - 14.9
> 15
Depths (cm)
Control Plots
Average = 2.05 m
Walkway Plots
Average = 1.19 m
Road Plots
Average = 1.18 m
< 0.1
0.4-0.49
0.8-0.89
1.2-1.29
1.6-1.69
2.0-2.09
2.4-2.49
2.8-2.89
3.2-3.29
3.6-3.69
> 4.0
Widths (m)

Figure 4

A.
B.
C.
0
15
30
45
60
75
90
105
120
135
150
165
180
195
210
225
240
255
270
285
300
315
330
345
Control Plots
Walkway Plots
Road Plots

Figure 5

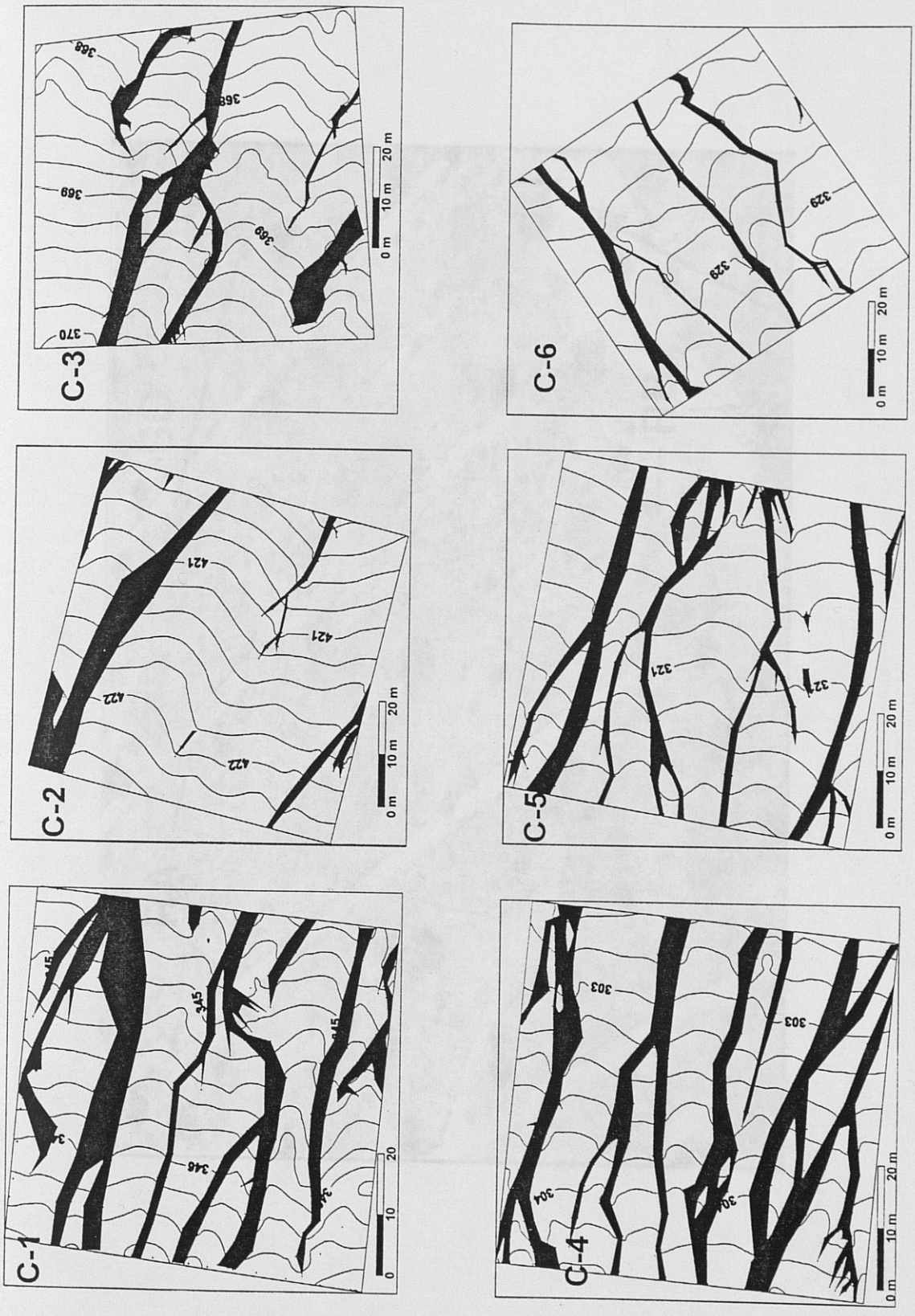
C-3
370
369
368
368
0 m
10 m
20 m
C-6
329
329
0 m
10 m
20 m
C-2
421
421
422
422
0 m
10 m
20 m
C-5
321
321
0 m
10 m
20 m
C-1
345
346
0
10
20
C-4
303
303
304
304
0 m
10 m
20 m

Figure 6

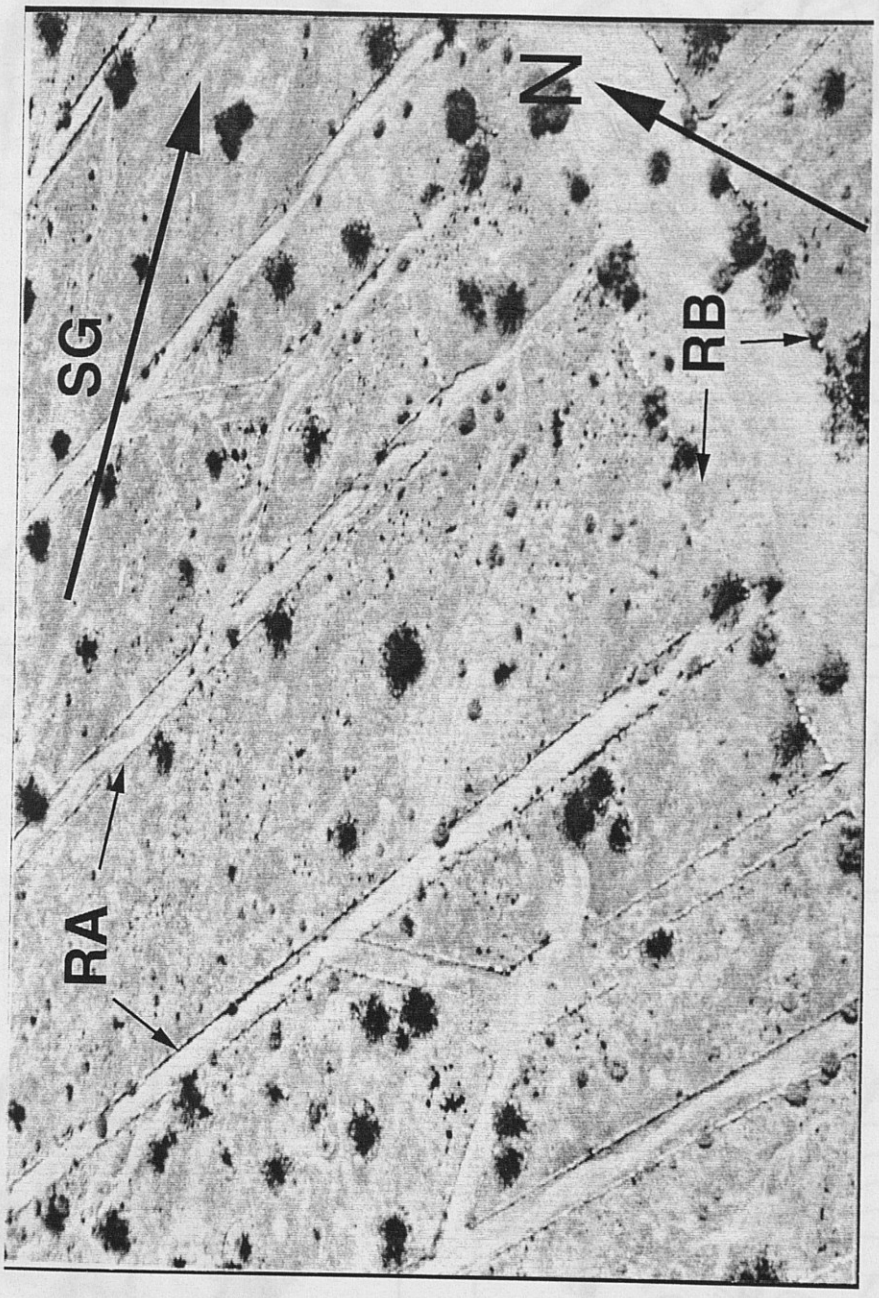

Figure 7

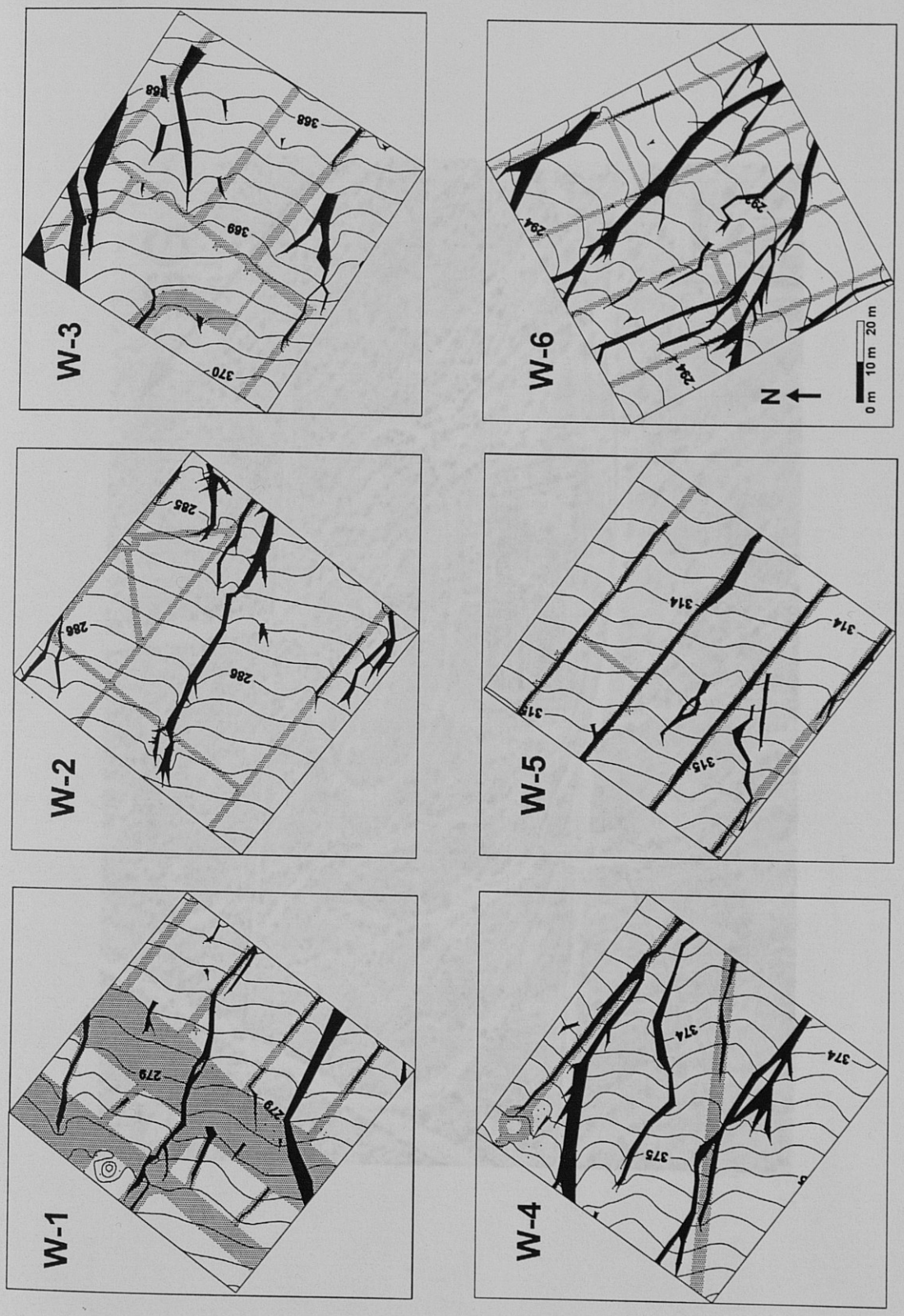
W-1
279
279
W-2
285
286
286
W-3
368
369
370
W-4
374
375
374
W-5
314
315
314
W-6
284
282
284
N
0 m 10 m 20 m

Figure 8

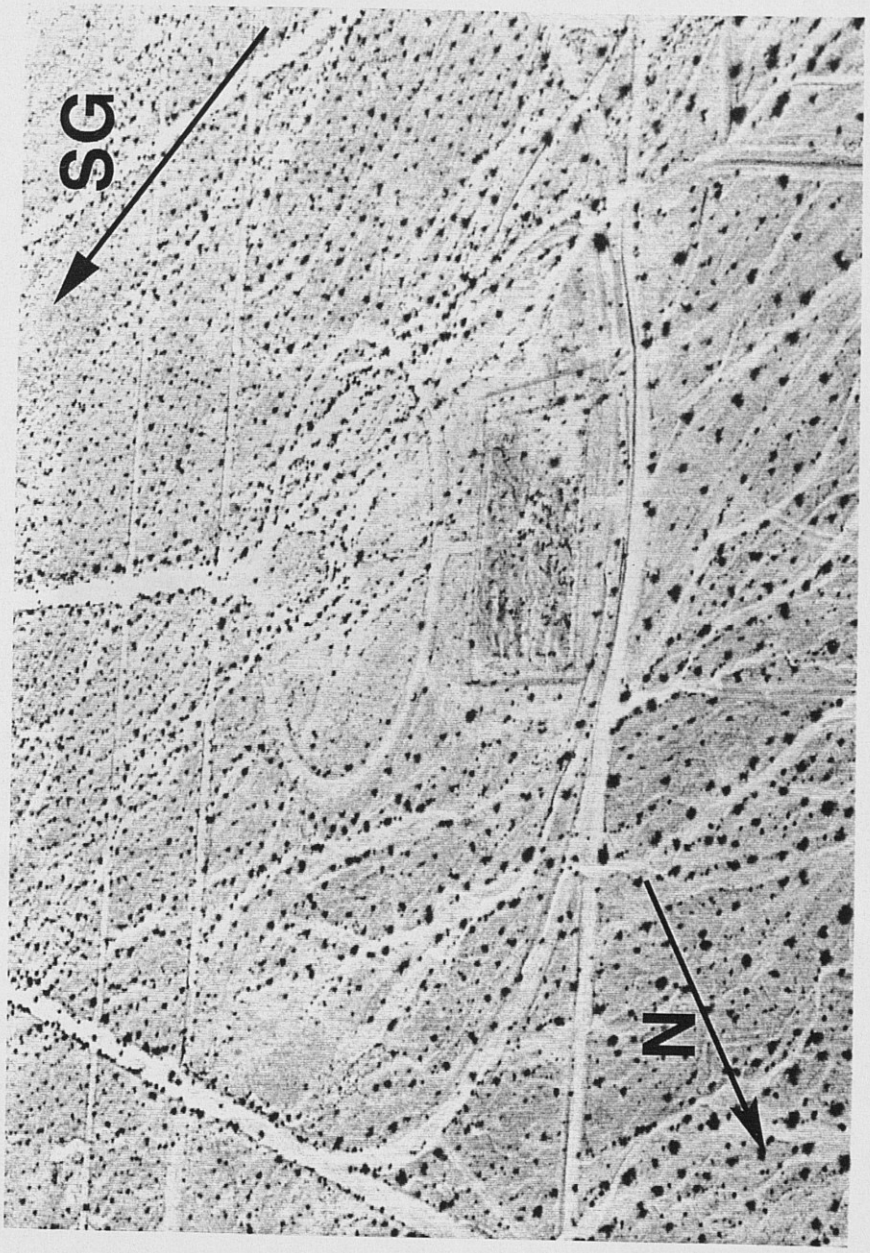

Figure 9

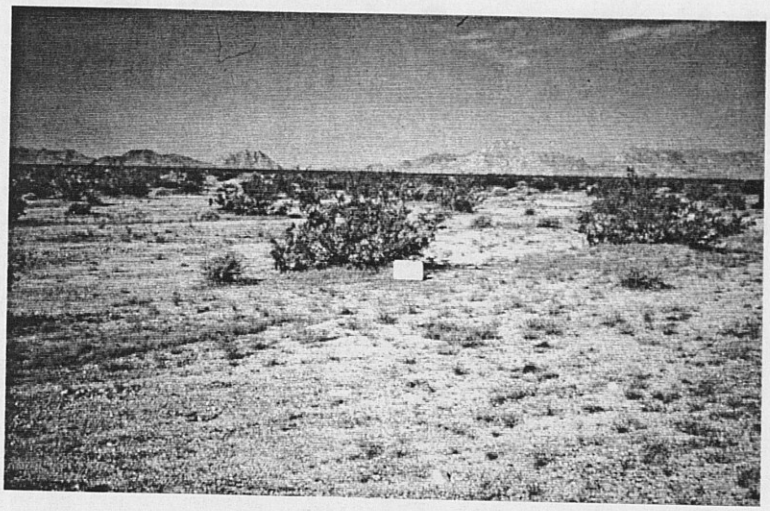

Figure 10

Figure 11

R-1
Road Berm
329
331
Figure 10
R-2
Road Berm
328
329
330
R-3
Road Berm
358
360
360
361
R-4
Road Berm
375
376
376
Figure 9
R-5
Road Berm
388
389
R-6
Road Berm
397
398
N
0 m
10 m
20 m

Figure 12

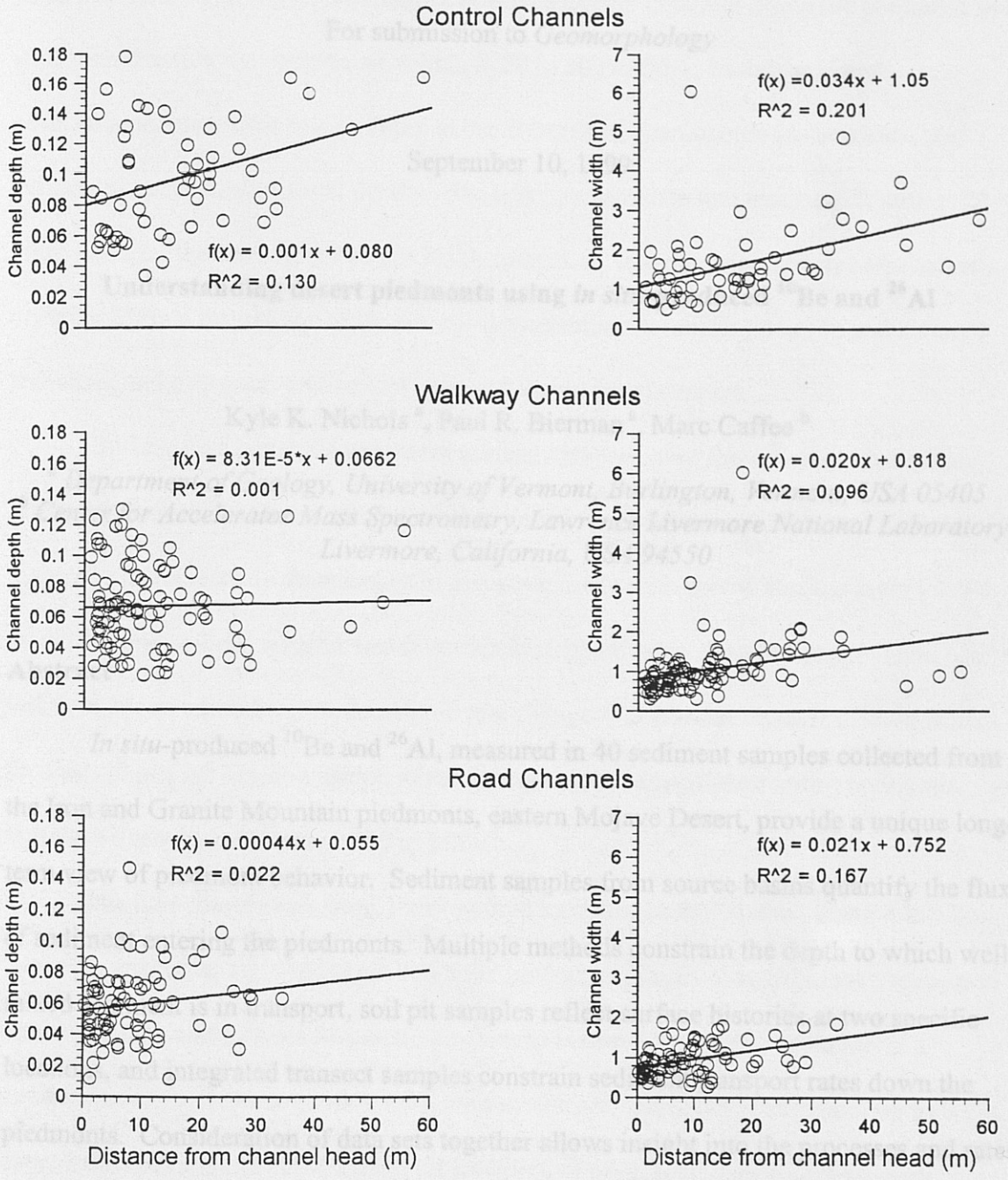
Control Channels
Channel depth (m)
f(x) = 0.001x + 0.080
R^2 = 0.130
Channel width (m)
f(x) =0.034x + 1.05
R^2 = 0.201
Walkway Channels
Channel depth (m)
f(x) = 8.31E-5*x + 0.0662
R^2 = 0.001
Channel width (m)
f(x) = 0.020x + 0.818
R^2 = 0.096
Road Channels
Channel depth (m)
f(x) = 0.00044x + 0.055
R^2 = 0.022
Channel width (m)
f(x) = 0.021x + 0.752
R^2 = 0.167
Distance from channel head (m)
Distance from channel head (m)

CHAPTER 4: Journal article submitted to *Geomorphology*

For submission to *Geomorphology*

September 10, 1999

Understanding desert piedmonts using *in situ*-produced ^{10}Be and ^{26}Al

Kyle K. Nichols [a], Paul R. Bierman [a], Marc Caffee [b]

[a] *Department of Geology, University of Vermont, Burlington, Vermont, USA 05405*
[b] *Center for Accelerator Mass Spectrometry, Lawrence Livermore National Laboratory, Livermore, California, USA 94550*

Abstract

In situ-produced ^{10}Be and ^{26}Al, measured in 40 sediment samples collected from the Iron and Granite Mountain piedmonts, eastern Mojave Desert, provide a unique long-term view of piedmont behavior. Sediment samples from source basins quantify the flux of sediment entering the piedmonts. Multiple methods constrain the depth to which well-mixed sediment is in transport, soil pit samples reflect surface histories at two specific locations, and integrated transect samples constrain sediment transport rates down the piedmonts. Consideration of data sets together allows insight into the processes and rates that modify the Iron and Granite Mountain piedmonts over the 10^4 year time-scale.

Nuclide abundances, measured in Iron and Granite Mountain drainage basin sediment, suggest long-term sediment fluxes onto adjacent piedmonts of 0.127 m^3 yr^{-1}

m^{-1} and 0.098 m^3 yr^{-1} m^{-1}, respectively, equivalent to highland bedrock lowering rates of 37 m Ma^{-1} and 39 m Ma^{-1}. This sediment is transported onto and down the piedmont in a well-mixed active transport layer, which is 20 to 30 cm thick, based on visual observations, measurements of depth to the B-horizon, cosmogenic isotope data, and maximum ephemeral channel depths. Nuclide data mandate that sediment is stored for < 1000 years in low terraces (~ 10 cm high), indicating that the small ephemeral channels on the piedmont migrate quickly, provide a mechanism for mixing terrace and channel sediment, and transport well-mixed sediment down the piedmont.

Soil pit data constrain piedmont surface histories over the 10^4 year time-scale. Interpretive models of increasing nuclide abundances at depth, and a discontinuity to markedly lower nuclide abundances in the isotopically well-mixed surface layer (~20 to 30 cm) in one soil pit, suggest steady sediment deposition on the piedmont (~15 m Ma^{-1}) followed by an unconformity that signifies a change in piedmont behavior. Data from a second soil pit, 2.5 km downslope of the first soil pit, are consistent with continuous sediment deposition at a rate of 40 m Ma^{-1}.

Nuclide abundances from 10 integrated samples, each collected along 4 km-long transects, spaced at 1 km intervals down the piedmonts, imply that sediment transported across the Iron and Granite Mountain piedmonts is dosed by cosmic radiation at a constant rate. Such dosing infers long-term systematic transport of sediment up to 6 km away from the rangefront. A variety of interpretive models suggest that long-term sediment transport rates across the piedmont average between 25 and 50 cm y^{-1}.

Keywords: piedmont, cosmogenic isotope, arid region sediment transport, desert geomorphology, climate change, pediment

1.0. Introduction

Large alluvial piedmonts flank desert mountains around the world. Such surfaces have been studied for over 100 years (Abrahams et al., 1984; Denny, 1967; Doehring, 1970; Mammerickx, 1964; McGee, 1897; Parsons and Abrahams, 1984). Many researchers have tried to determine whether such piedmonts are surfaces of deposition (alluvial fans) or surfaces of erosion (pediments). Even after a century of research, there still is not a satisfactory means by which to classify and understand many piedmont surfaces (Warnke, 1969).

The desert piedmont problem extends beyond piedmont classification to piedmont geomorphic processes as well. Little is known about the rate and style of long-term sediment transport across such piedmont surfaces (Denny, 1967; Hooke, 1968). Runoff is episodic in arid regions; thus, long-term observations, accomplished in only a few places, are necessary to determine representative process rates (Greenbaum et al., 1999; Lekach and Schick, 1999; Yair, 1999). Furthermore, the difficulty in determining accurate sediment generation rates in source basins has precluded quantitative estimates of sediment flux and sediment transport rates across piedmont surfaces.

Changes in piedmont process are routinely attributed to climatic change (Bull, 1991; Dohrenwend, 1987; Mayer and Bull, 1981; Oberlander, 1974). It is hypothesized, but remains uncertain, that soil was stripped off of some hillslopes and transported down gradient as a result of the Pleistocene-Holocene climate transition (Bull, 1991; Bull and Schick, 1979). Increased sediment yield is associated with possible early Holocene

deposition on piedmonts (Wells et al., 1987). Once the sediment supply in mountain basins was depleted, transport capacity of channels increased, and at least some piedmonts were dissected (Wells et al., 1987).

The traditional geomorphic techniques of mapping and monitoring has allowed some geomorphologists to determine surface histories and infer changes in piedmont process (Bull, 1991; Wells et al., 1987). Other researchers have used soil development to understand the age and the history of desert piedmonts (Birkland, 1984; McFadden et al., 1989).

Using in situ-produced cosmogenic ^{10}Be and ^{26}Al, a new sampling strategy, and several interpretive models, we quantify long-term average sediment transport rates across large, planar, piedmont surfaces that extend from the Iron and Granite Mountains in the Mojave Desert, California (Fig. 1). Using ^{10}Be and ^{26}Al in two soil profiles, we determine the Late Pleistocene and Holocene aggradation history at two places on the Iron Mountain piedmont. Application of these techniques elsewhere could lead to a better understanding of arid-region sediment transport rates, surface processes, and the effects of climate change on rates and styles of sediment transport across desert piedmonts.

2.0. Research area

In the Mojave Desert, the Iron and Granite Mountains rise steeply from adjacent > 10-km long, low-gradient (~2°) piedmonts (Fig. 2). The piedmont surfaces consist primarily of grus, 0.5 to 1 mm in diameter having minimal carbonate development with depth (Fig. 3). Small, ephemeral channels, averaging ~10 cm in depth (Nichols and

Bierman, in press), migrate across the planar piedmonts on a time-scale of decades to centuries, and account for the majority of sediment transport. Almost all surface clasts are unvarnished; desert pavements are not commonly developed. These and other field observations suggest that the ephemeral channel network currently reworks over 98% of the piedmont surface. The remainder, directly abutting the rangefront, is relict alluvium exhibiting some pavement development, and incision by channels 0.5 m to 5 m deep. There is no evidence of range-bounding faults, suggesting that the basin and adjacent ranges are not currently tectonically active.

The southern Mojave Desert and the Iron and Granite Mountain piedmonts are extremely dry and warm. Average annual precipitation is 7.9 cm and the mean temperatures for January and July are 12°C and 35°C, respectively (NOAA, 1982). Packrat midden data suggest a change in the paleoclimate from wetter to drier conditions between 10,000 to 8,000 years ago (Spaulding and Graumlich, 1986; Spaulding et al., 1983).

3.0. Cosmogenic isotopes

Cosmic rays bombard Earth's surface and produce a variety of isotopes *in situ* including ^{10}Be and ^{26}Al. Cosmogenic nuclide production rates are greatest at the surface and decrease exponentially with depth (Lal, 1988). For example, production rates at a depth of one meter in sediment ($\rho = 1.55$ g cm^{-3}), are ~37% of surface production. Production rates for ^{10}Be and ^{26}Al, and the adjustments for altitude and latitude, have been estimated to better than 20% (Clark et al., 1995; Lal, 1991; Nishiizumi et al., 1989). We can measure accurately ^{10}Be and ^{26}Al abundances (< 4%) using accelerator mass

spectrometry, and use these nuclides as cosmic-ray dosimeters to record near-surface residence time. Knowing nuclide production rates and using geomorphic models, we interpret ^{10}Be and ^{26}Al activities as monitors of sediment dosing and thus sediment transport rates.

4.0. Methods

4.1. Sediment collection for ^{10}Be and ^{26}Al analysis

To understand and quantify the three-dimensional behavior of the Iron and Granite Mountains and their piedmonts over time we collected three types of sediment samples (Table 1). Measurement of ^{10}Be and ^{26}Al in sediment samples collected from three channels at and near the Iron Mountain rangefront and two channels at the Granite Mountain rangefront, allow quantification of long-term average source-basin lowering rates and the flux of sediment entering the piedmont (Bierman and Steig, 1996; Brown et al., 1995; Granger et al., 1996). Integrated transect samples, located at successive 1-km intervals from the rangefront, reflect changes in average ^{10}Be and ^{26}Al abundance as sediment moves away from the source basins and allow us to determine integrated sediment transport rates. Soil-pit profiles allow us to quantify the depth to which sediment is currently well mixed and provide insight into whether the piedmont is, or has been a surface of deposition, erosion, or transport. Definitions and units for all variables used in following equations are listed at the end of the paper in an appendix.

4.1.1. Valley Samples

We determine long-term basin erosion and sediment generation rates by analyzing sediment samples collected from streams exiting five small, steep, lithologically homogeneous basins in the Iron and Granite Mountains (Fig. 2). The long-term average

sediment generation rate is modeled from the cosmogenic data following the work of Brown et al. (1995), Bierman and Steig (1996), and Granger et al. (1996):

$$m = \frac{\Lambda P}{C_i(0)} \quad (1)$$

4.1.2. Transect Samples

We collected five transect samples spaced at 1-km intervals away from both the Iron and Granite Mountain rangefronts. Each transect sample integrated an equal volume of surface sediment (0 to 10 cm deep) collected from 20 sampling stations, each spaced at ~200 m intervals, along each 4-km transect (Fig. 2). We classified each sampling station according to the geomorphic unit that was sampled (Table 2). Predetermined sampling stations were located in the field using a hand-held Global Positioning System (GPS) with a horizontal uncertainty of ± 20 m.

The piedmont consists of three distinct, low-relief geomorphic units: low terraces, active channels, and animal burrow piles. To determine if low-terrace sediment had been exposed on average longer than channel sediment, and thus, more heavily dosed by cosmic radiation, we sampled both geomorphic units and compared the nuclide abundance (Fig. 4). We also sampled sediment from animal burrow piles to determine the depth from which sediment was transported vertically during burrowing. At each of the 20 sampling stations, along both IMT-1 and IMT-4, we collected an equal volume of sediment from the nearest terrace, channel, and animal burrow sediment pile, and integrated each sample separately.

An older alluvial fan surface was thought to extend into the northern four sampling stations along IMT-0 (Fig 2). Channels were entrenched and the surface had a poorly developed pavement. To determine if the surface were older and contained more highly-dosed sediment, we collected sediment from only the four sampling stations on the alluvial fan surface (IMT-0FAN).

4.1.3. Soil Pit samples

We dug two soil pits (~1 m deep) into the Iron Mountain piedmont (Fig. 2) noting soil stratigraphy, sediment grain size, and soil horizonation. On the basis of soil stratigraphy, we divided each pit into 8 depth intervals that we sampled to determine nuclide abundance. Each interval was continuous, so that the entire pit was represented. We dug 25 additional shallow soil pits along IMT-1, IMT-2H, and IMT-4, to understand better the spatial variability of depth to the B-horizon (Fig. 2).

4.2. Laboratory methods

All samples were sieved into 11 size fractions (>4000 μm, 2000 to 4000 μm, 1410 to 2000 μm, 1000 to 1410 μm, 710 to 1000 μm, 500 to 710 μm, 350 to 500 μm, 250 to 350 μm, 177 to 250 μm, 80 to 177 μm, and < 80 μm) and weighed. We analyzed the 500 to 1000 μm size fraction to minimize inclusion of aeolian input from other basins. We did not analyze different grain sizes because ephemeral channels are not armored and do not preferentially transport smaller grain sizes (Laronne et al., 1994; Laronne and Reid, 1993; Reid and Laronne, 1995). Also, previous research using ^{10}Be and ^{26}Al to analyze different grain sizes of sediment in arid-region streams suggests all grain sizes have statistically similar nuclide abundances (Clapp et al., 1997; Clapp et al., in review). We

assume that the 500 to 1000 μm size we analyzed represents fluvially transported material.

We measured soil density and percent carbonate of all soil pit layers. To measure the density of the soil pit layers, we extracted a known volume of sediment from each layer and weighed each sample. There was no depth dependence in density, and the average density of all strata was 1.55 ± 0.07 g cm^{-3}. We used the Chittick apparatus to measure percent carbonate (Machette, 1986). We classified the carbonate development as Stage I based on the results of the carbonate measurements (Fig. 3) and our soil pit observations.

All samples were ultrasonically etched with 6 N HCl and up to four 1% HF and 1% HNO_3 baths in order to remove any atmospheric ^{10}Be and isolate ≥ 40 g of pure quartz (Kohl and Nishiizumi, 1992). After the addition of 250 μg of Be carrier, we digested the samples with HF. Be and Al were purified using chromatographic techniques. The ^{10}Be/^{9}Be and ^{26}Al/^{27}Al ratios were determined using accelerator mass spectrometry (AMS) at Lawrence Livermore National Laboratory. All measurements were corrected using similar-sized procedural blanks. Blanks were prepared with each batch of seven samples and analyzed at the same time as all other samples using AMS. We calculated ^{10}Be and ^{26}Al abundances from ^{9}Be (added as carrier) and native ^{27}Al measured in duplicate aliquots, removed from HF solutions, by Inductively Coupled Argon Plasma Spectrometry – Optical Emission.

4.3. Reproducibility

The isotope data are reproducible and consistent. Field replication, laboratory replication, and the ^{26}Al/^{10}Be regression validate the method of collecting integrated

samples and the laboratory procedures. Measured yields of ^{10}Be average 100.6 ± 1.1%; measured yields of Al blanks average 99.7 ± 0.9%, indicating high recovery of stable Al. Isotopic abundances of GMT-0A and B, collected independently along the same transect, are statistically indistinguishable for both ^{26}Al and ^{10}Be content (Fig. 5). IMT-3 was analyzed twice; both analyses produced statistically similar results for both ^{26}Al and ^{10}Be (Fig. 5). ^{10}Be and ^{26}Al are well correlated with a ratio of 5.8 ± 0.2 and an intercept of 0.07 ± 0.5 x 10^5 atoms at a 68% confidence level (Fig. 6). Accordingly, we focus discussion on the ^{10}Be data for the remainder of the paper.

5.0. Results

Four independent data sets constrain sediment dynamics of the Iron Mountain and Granite Mountain piedmonts. Integrated transect samples constrain sediment transport rates down the piedmonts, multiple methods constrain the depth to which piedmont sediment is well-mixed, soil pit samples reflect surface histories at two specific sites, and valley samples quantify the flux of sediment entering the piedmonts from the mountain basins. Together, these data provide a three-dimensional view of sediment movement across the Iron and Granite Mountain piedmonts over the 10^4 year time-scale.

5.1. Transect data

Integrated transect samples show a remarkably regular linear increase in nuclide abundance down both piedmonts (Fig.7). For example, moving away from the Iron Mountain rangefront, ^{10}Be abundance increases from 2.26 x 10^5 atoms g^{-1} to 3.67 x 10^5 atoms g^{-1}(r^2 = 0.98). We measured a similar increase in ^{10}Be abundance (r^2 = 0.99) in samples collected away from the Granite Mountain rangefront (Fig. 7A).

The rates at which ^{10}Be abundance increases down slope on the Iron Mountain piedmont ($0.36 \pm 0.03 \times 10^5$ atoms g^{-1} km^{-1}) and the Granite Mountain piedmont ($0.32 \pm 0.02 \times 10^5$ atoms g^{-1} km^{-1}) are statistically indistinguishable. Likewise, the rates at which ^{26}Al increases down slope on the Iron Mountain piedmont ($0.26 \pm 0.03 \times 10^6$ atoms g^{-1} km^{-1}) and on the Granite Mountain piedmont ($0.21 \pm 0.03 \times 10^6$ atoms g^{-1} km^{-1}) are also statistically indistinguishable. From the similarity of these rates we conclude that the geomorphic and sediment transport processes and rates acting on the Iron Mountain piedmont are similar to those acting on the Granite Mountain piedmont, a conclusion consistent with field observations.

Nuclide abundances (^{10}Be and ^{26}Al) of all three low-relief geomorphic units (terraces, channel and burrow piles) are indistinguishable. Data, for Iron Mountain transects 1 and 4 (IMT-1 and IMT-4, respectively), demonstrate that nuclide abundances in low terrace sediment (IMT-1TERR and IMT-4TERR) are statistically identical to the nuclide abundance of active channel sediment (IMT-1CHAN and IMT-4CHAN) for respective transects (Fig. 8). Furthermore, the nuclide abundance of sediment from animal burrows (IMT-1CRIT and IMT-4CRIT) is statistically identical to the nuclide abundances in both the low terrace sediment and the active channel sediment. All these processes efficiently homogenize all sediment on a time-scale comparable or less than the average residence time (<1000 years). This homogenization can only happen if the channels migrate across the surface and the animal burrowing occurs at a depth comparable to stream incision. These nuclide data support the hypothesis that "...shallow distributary channels rapidly fill with sediment and then shift a short distance." (Bull, 1977).

Sediment on the alluvial fan surface (IMT-0FAN) is no more highly dosed than sediment on the active piedmont surface (Table 1), implying that sediment exposure histories are similar regardless of surface topography along IMT-0.

5.2 Well-mixed layer

Four lines of evidence suggest that the upper 20 to 30 cm of sediment on the Iron Mountain piedmont and by inference the Granite Mountain piedmont are vertically well-mixed. 1) The top two samples from soil pit 1 (PIT1 0-10 and PIT1 10-20) and soil pit 2 (average of PIT2 0-14 and PIT2 0-14 DUP, and PIT2 14 –28) have statistically indistinguishable ^{10}Be abundances (Table 1 and Fig. 9). 2) The change from gray bedded sediment to red homogenous sediment at the B-horizon, measured in 25 additional shallow pits along transects IMT-1, IMT-2H, and IMT-4, averages 20 to 30 cm below the surface. Significant reddening of the soil at the B-horizon suggests several thousand years of stability (Birkland, 1984). Therefore, we assume that the top of the B-horizon is a proxy for the maximum thickness of well-mixed sediment (Birkland, 1984; Lekach et al., 1998). 3) Over 9000 topographic measurements of the ephemeral channels, currently the main sediment mixing and transport mechanism, show maximum channel depths between 20 to 30 cm (Nichols and Bierman, in press). 4) Transect samples taken from terrace sediment, channel sediment, and animal burrow piles have statistically similar nuclide abundances, implying thorough mixing over 20 to 30 cm depth on the $< 10^3$ year time scale (Fig. 8). For the remainder of the paper we will refer to the well-mixed layer as the active transport layer (ATL). We believe sediment in this layer is in transport down piedmont because this layer is the same thickness as the maximum channel depths, displays sedimentary structures, and lacks soil development.

5.3. Soil pit data

Eight sediment samples, taken from each of two soil pits, show isotopically well-mixed surface zones, 20 and 28 cm thick, underlain by zones with increasing nuclide abundances as a function of depth (Fig. 9A). ^{10}Be abundances increase from 1.94 ± 0.15 x 10^5 atoms g^{-1} at the surface of soil pit 1 to 4.27 ± 0.26 x 10^5 atoms g^{-1} at the bottom of soil pit 1, and from 4.04 ± 0.12 x 10^5 atoms g^{-1} at the surface of soil pit 2 to 5.13 ± 0.15 x 10^5 atoms g^{-1} at the bottom of soil pit 2. ^{26}Al abundances also increase from the piedmont surface to the soil pit bottoms (Fig. 9B).

We interpret the distinct abundance discontinuity in soil pit 1 as an unconformity representing the transition between the ATL and undisturbed sediment. As expected from transect data (Fig. 7), pit 2, located ~4.75 km from the rangefront, has higher ^{10}Be abundances than pit 1 located ~2.25 km from the rangefront. Pit 2 has a less-well defined step in nuclide abundance at the base of the ATL.

5.4 Sediment generation rate estimates

We determined source-basin sediment generation rates using samples collected from stream valleys draining the Iron and Granite Mountains. Average ^{10}Be abundances collected from valley samples at the margin of the Iron and Granite Mountains are 1.49 ± 0.12 x 10^5 (1σ, n=3) atoms g^{-1} and 1.40 ± 0.05 x 10^5 (1σ, n=2) atoms g^{-1}, respectively. The average ^{26}Al abundances of valley samples for the Iron and Granite Mountains are 1.01 ± 0.06 x 10^6 (1σ, n=3) atoms g^{-1} and 0.90 ± 0.05 x 10^6 (1σ, n=2) atoms g^{-1}, respectively. Erosion rates (^{26}Al and ^{10}Be data) are similar for both mountain ranges, 37 m Ma^{-1} and 39 m Ma^{-1} (Table 3), respectively. The larger Iron Mountains export more sediment to their adjacent piedmont than the smaller Granite Mountains. Average

sediment fluxes from the Iron and Granite Mountains to the respective piedmonts are 0.13 $m^3 y^{-1} m^{-1}$ and 0.10 $m^3 y^{-1} m^{-1}$, respectively (Table 3).

6.0. Interpretive models of sediment transport and piedmont history

In order to quantify piedmont sediment transport velocities and the depositional history of the Iron Mountain piedmont, we developed interpretive mathematical models that track sediment from the time it exits the source basins until it is deposited or it is transported past the last transect (Fig. 10). Our model combines a mass balance model (Fig. 10A) and a nuclide balance model (Fig. 10B) and is derived from earlier models of Monaghan et al. (1992) and Small et al. (1999), which assume plug flow of sediment. At small-scales (e.g. m-scale) and short-time scales (10^1 to 10^2 years) plug flow is not an accurate representation of sediment transport on piedmonts. However, nuclide data imply channels migrate rapidly enough that sediment in channels and sediment in terraces is statistically indistinguishable, while nuclide data of transects are statistically separable. Therefore, at sufficient spatial scales (10^2 to 10^3 m) and time scales (10^2 to 10^3 years), plug flow is representative of large-scale and long-term sediment transport processes on the Iron and Granite Mountain piedmonts.

In order to simplify our models, we make a few assumptions. The piedmonts are planar and we do not consider sediment divergence or convergence (Heimsath et al., 1999). We assume no dissolution of minerals (Small et al., 1999), and the decay of nuclides is unimportant due to short transport times.

6.1 Sediment transport model

Our sediment transport model divides the piedmont into transport segments in order to quantify the velocity of sediment down piedmont (Fig. 10). The general equation for mass balance per unit width, where M = mass, is:

$$M_i + M_p = M_o \tag{2}$$

We expand the mass balance equation by deriving each term. The explicit mass balance equation then becomes:

$$M_i(L) + \int_0^L M_P(x)\,dx = \int_0^H \rho(L,z)\,u(L,z)\,dz \tag{3}$$

where M_i, M_p, ρ, and u vary down slope, and ρ and u vary with depth. The first term represents the flux of sediment into a transport segment at distance L from the rangefront. The second term represents the flux change within each transport segment (positive M_p represents erosion, negative M_p represents deposition, and M_p of zero represents a surface of transport). The right hand side of the equation represents the flux of sediment out of each transport segment.

Eq. (3) can be simplified for the Iron Mountain piedmont because the ATL thickness is constant, the piedmont is planar with no divergence, and we measured a constant sediment density with depth. Because of the uniform nuclide abundances in the ATL we can simplify the spatially variable velocity field assuming a uniform velocity with depth. Eq. (3) then becomes:

$$M_i(L) + \int_0^L M_p(x)\,dx = \rho\hat{u}(L)h \tag{4}$$

By definition, the mean rate of segment mass change at position L is:

$$M_p(L) = \frac{1}{L}\int_0^L M_p(x)\,dx \tag{5}$$

and we combine eqs. (4) and (5) to yield:

$$M_p(L) = \frac{1}{L}(\rho\hat{u}(L)h - M_i(L)) \tag{6}$$

where eq. (6) is the mass change in a segment at distance L in terms of average density, average velocity, ATL thickness, and incoming mass.

We also developed a nuclide balance model similar to the mass balance model (Fig. 10B) where A is the nuclide abundance. The nuclide balance model accounts for the continuing production of nuclides as sediment moves down slope. The general nuclide balance model is:

$$A_i + A_p + P_{ATL} = A_o \tag{7}$$

where the left hand side of the equation represents the nuclide flux entering a transport segment, and the right hand side represents the nuclide flux leaving a transport segment. We can expand A_i and A_p in terms of mass and nuclide abundance. The first terms of eq. (7) at distance L becomes:

$$A_i(L) = C_i(L)\,M_i(L) \tag{8}$$

where A_i represents the nuclide flux entering a transport segment from the upslope transport segment, and the second term becomes:

$$A_p(L) = \int_0^L C_p(x)\, M_p(x)\, dx \tag{9}$$

where A_p represents the nuclide flux from the piedmont. A_p is constant at a given distance (L), and by combining eqs. (5) and (9):

$$A_p(L) = L\, C_p(L)\, M_p(L) \tag{10}$$

Eq. (10) is the nuclide flux in terms of distance down piedmont, nuclide flux of the piedmont at distance L, and mass flux of the piedmont at distance L.

The *in situ* production rate of nuclides in the ATL term of eq. (7) is:

$$P_{ATL}(L) = \rho h \int_0^L P_{avg}(x)\, dx \tag{11}$$

where P_{avg} is the mean production rate throughout the ATL. If we assume that the surface production rate, P_o, is uniform along the piedmont (minimal elevation difference between top transect and bottom transect), the mean production rate in the ATL is:

$$P_{avg}(x) = \frac{1}{h} \int_0^h P_o e^{\left(\frac{-z\rho}{\Lambda}\right)} dz$$

$$P_{avg}(x) = \frac{P_o \Lambda}{\rho h}\left[1 - e^{\left(\frac{-h\rho}{\Lambda}\right)}\right] \tag{12}$$

Combining eqs.(11) and (12) we get:

$$P_{ATL} = \rho h \int_0^L \frac{P_o \Lambda}{\rho h}\left[1 - e^{\left(\frac{-h\rho}{\Lambda}\right)}\right] dz \tag{13}$$

By definition eq. (13) simplifies, and the in situ production rate through the ATL is:

$$P_{ATL} = P_o \Lambda L\left[1 - e^{\left(\frac{-h\rho}{\Lambda}\right)}\right] \tag{14}$$

Finally, the right side of eq. (7) equals the flux of nuclides out of each transport segment:

$$A_o = \int_0^h \rho(L,z)\, C(L,z)\, u(L,z)\, dz \tag{15}$$

Our data suggest that ρ, C, and u are constant with depth through the ATL thus, eq. (15) simplifies to:

$$A_o = \rho h C(L) \hat{u}(L) \tag{16}$$

We can now rewrite eq.(7) by substituting in eqs.(8), (10), (14), and (16):

$$C(x) M_i(x) + L\, C_p(x) M_p(x) + P_o \Lambda L \left[1 - e^{\left(\frac{-h\rho}{\Lambda}\right)} \right] = \rho h C(x) \hat{u}(x) \tag{17}$$

Rewriting eq. (17) to solve for velocity:

$$\hat{u}(x) = \frac{C(x) M_i(x) + L\, C_p(x) M_p(x) + P_o \Lambda L \left[1 - e^{\left(\frac{-h\rho}{\Lambda}\right)} \right]}{\rho h C(x)} \tag{18}$$

Eq. (18) allows us to solve explicitly for the average velocity of sediment down piedmont. We have field measurements of $C(x)$, $M_i(x)$, h, and ρ. All other variables are known, except for $M_p(x)$ and $C_p(x)$. We can quantify $M_p(x)$ by determining the long-term piedmont surface history from the soil pit data, and $C_p(x)$ is estimated by the nuclide

abundance below the ATL for the erosion case and by $C(x)$ for the deposition case. By adjusting M_p, this model allows us to investigate three endmember geomorphic processes: *deposition, erosion,* and *steady transport.*

6.2 Soil pit models

Soil pit data allow insight into past piedmont processes, and thus values for $M_p(x)$. Stable or eroding surfaces have nuclide profiles that decrease exponentially as a function of depth (Fig.11). The Iron Mountain piedmont exhibits nuclide profiles that increase as a function of depth (Fig.9). Therefore, the Iron Mountain piedmont has been neither stable nor eroding over the effective half-lives of the nuclides (10^4 years); rather, in the long-term, the Iron Mountain piedmont has been a surface of deposition (Fig. 11).

The idea of using nuclides to determine sediment deposition was first suggested by Lal and Arnold (1985). Substituting Λ for λ in the last term of the Lal and Arnold (1985) deposition we obtain:

$$N = C_i + \frac{1}{s}\int_0^h P_0 e^{(-z\rho/\Lambda)} dz$$
$$= C_i + \frac{P_0 \Lambda}{s\rho}\left[1 - e^{(-h\rho/\Lambda)}\right] \quad (19)$$

Phillips et al. (1998) also derived the deposition equation; however, data from their field site did not reflect steady-state deposition. At Iron Mountain, we measured increasing nuclide abundance at depth and thus can solve for s (deposition rate), since all variables are either known or measured. Using eq. (19), the ^{10}Be and ^{26}Al data for soil pit 1 suggest long-term steady state deposition rates of ~15 m Ma^{-1} (Fig. 12). The ^{10}Be and ^{26}Al data for soil pit 2 suggest long-term steady state deposition rates of ~40 m Ma^{-1}(Fig. 12). These rates imply that sediment is deposited more slowly closer to the rangefront

and more quickly farther from the rangefront. Although these deposition rates represent only two locations on the piedmont surface, we believe they represent the long-term deposition rates of the surface in the vicinity of each soil pit; otherwise, the piedmont would not be planar and there would be significant topographic relief.

Steady state deposition models do not fit the ATL nuclide abundances (top two points) for pit 1 (Fig. 12); there is a significant step to lower nuclide abundances. If the piedmont were still depositing sediment at the long-term deposition rate, the ATL nuclide abundances would be similar to the abundances predicted by the model. Since the ATL nuclide abundances are lower, we infer an unconformity in deposition. The deposition model reasonably predicts ATL nuclide abundances for soil pit 2, suggesting that sediment deposition is still occurring there at the long-term deposition rate.

The abundance of nuclides in the sediment that arrived at each pit throughout time cannot be known. Therefore, we must assume this value has remained constant in order to calculate the length of time that is represented by the unconformity at pit 1. The ^{10}Be abundance difference between the ATL and the deposited sediment in pit 1 is 1.05×10^5 atoms g^{-1}, suggesting an unconformity of ~16,000 years. The ^{26}Al abundance difference in pit 1 is 5.8×10^5 atoms g^{-1}, which represents an unconformity of ~14,000 years. Alternatively, we can use the regressions from our transect samples (Fig.7) to estimate the ^{10}Be and ^{26}Al abundances of sediment when first deposited. Using this assumption for the ^{10}Be data, the difference between the regression-predicted nuclide abundance and the abundance of deposited sediment in pit 1 is 0.50×10^5 atoms g^{-1}, which represents a ~7500 year unconformity. The difference between the ^{26}Al regression-predicted abundance and the abundance of deposited sediment in pit 1 is 1.6×10^5 atoms g^{-1},

equivalent to a ~4,000 year unconformity. Since we do not know which estimate is correct, we can conclude only that the unconformity in pit 1 probably represents a gap in time between ~6000 and ~15,000 years.

6.3 Sediment transport velocities and piedmont surface processes

We seek to quantify sediment transport velocities across piedmont surfaces. To model such velocities accurately, and thus better understand piedmont processes, we attempt to integrate all available data into a plausible scenario of piedmont history. Temporal changes in piedmont process may cause present-day measurements to misrepresent past processes; such process changes have likely occurred on desert piedmonts over the 10^4 year time scale (Bull, 1991; Cooke and Warren, 1973; Wells et al., 1987). Nevertheless, we attempt to reconcile all our observations in a model that is consistent with nuclide data and field measurements. To do this, we model three endmembers of piedmont behavior, and compare the predicted nuclide abundances with measured data. After we constrain plausible rates of endmember processes, we present a mixed model that combines endmember processes.

For the following endmember scenarios, we determine sediment velocity using eq. (18). Once we determine sediment transport velocity, we predict the abundance of nuclides down piedmont using the following equation:

$$C = \frac{L}{\hat{u}} P_{avg} + C_i(0) \qquad (20)$$

Eq. (20) is valid for the erosion endmember since the percentage of more highly-dosed, previously deposited sediment introduced into the ATL is minimal (~2%) even after 10,000 years of erosion. Eq. (20) will predict nuclide abundances accurately in transect

data if the piedmont processes and rates have been uniform over time. Since this may not the case for the Iron Mountain piedmont, we can estimate sediment transport rates for endmember processes and one of many plausible scenarios consistent with our measured data.

6.3.1. Surface of transport

We determine sediment transport velocities and predicted nuclide abundance down piedmont using the surface of transport endmember, which could account for the unconformity in soil pit 1. Using eq.(18) where $M_p = 0$, and ATL thickness is constant and equal to field values (30 cm), the estimated sediment transport velocity down piedmont is 32 ± 4 cm y^{-1}. The predicted nuclide abundances, determined using eq. (20), are lower than the measured transect data (Fig. 13). This suggests that sediment moving in a steady state ATL, along a surface of transport, is not exposed long enough or near enough the surface to accumulate nuclide abundances such as we measured. The inability of the surface of transport endmember model to accumulate sufficient nuclides implies that either sediment is transported more slowly than the estimated velocity (in violation of mass-flux continuity) or that more highly-dosed sediment is mixed into the ATL.

6.3.2. Deposition

The deposition model for soil pit data (section *6.2*) suggests deposition rates of 15 m Ma^{-1} (soil pit 1) and ~40 m Ma^{-1} (soil pit 2). Using eq. (18) where $M_p = -2.33 \times 10^{-4}$ g cm^{-1} y^{-1} (15 m Ma^{-1}), assuming that $C_p(L)$ = ATL nuclide abundance, and the ATL thickness is uniform (30 cm), sediment velocities range from 28 cm y^{-1} at the rangefront to 6 cm y^{-1} at IMT-4. These estimated velocities predict nuclide abundances that are

lower than the measured IMT-0 abundance, and are higher than the measured abundances of IMT-3 and IMT-4 (Fig 13); furthermore, deposition along the piedmont does not produce the observed linear relation between nuclide abundance and distance. Estimated sediment velocities are thus too fast for sediment at IMT-0 and too slow for sediment at IMT-3 and IMT-4. Even more troubling, higher deposition rates (~40 m Ma^{-1}) result in the deposition of all sediment before the IMT-4; this finding suggests that high deposition rates (40 m Ma^{-1}) are not wide spread across the piedmont. The only depositional scenario that matches the measured transect data requires decreasing deposition rates down piedmont, in direct contradiction to our soil pit data.

6.3.3. Erosion

Although the Iron Mountain piedmont cannot be an erosional surface over the 10^4 year time frame, (section 6.2, Figs. 11 and 12) erosion could account for the unconformity observed in soil pit 1. Surface of transport models predict nuclide abundances that are lower than measured transect data (Fig. 13). In principal, erosion could incorporate more highly-dosed sediment from below the ATL (Fig. 9), into the transported sediment and increase average nuclide abundance. Using eq. (18), where M_p = 7.75 x 10^{-4} g cm^{-1} y^{-1} (erosion of 5 m Ma^{-1}), $C_p(L)$ = nuclide abundance of sediment below ATL at distance L (based on linear extrapolation from soil pits 1 and 2), and ATL thickness is uniform (30 cm), velocities range from 28 cm^{-1} at IMT-0 to 48 cm y^{-1} at IMT-4. Substituting these velocities into eq. (20), the predicted nuclide abundances under eroding conditions are actually lower than those predicted by the surface of transport model. Recall that the percentage of highly-dosed sediment is only ~2% of the total sediment in the ATL after 10,000 years of erosion. The small percentage of highly-

dosed sediment does not raise the average nuclide abundance of the ATL significantly and the faster sediment velocities (required for mass balance) control the nuclide abundance of the ATL.

6.3.4. A plausible scenario

No endmember process predicts accurately the measured nuclide abundances of the transect data. The depositional endmember predicts nuclide abundances higher than the measured transect data; erosion and surface of transport endmembers predict abundances lower than the transect data. Only mixed scenarios are able to predict the measured nuclide abundances and because this is an inverse problem, any solution is non unique.

Since piedmont processes and presumably sediment transport rates change due to climatic forcing (Cooke and Warren, 1973), present-day measured values of ATL thicknesses, basin erosion rates, and piedmont sediment supplies may not represent past values. The following scenario allows us to fit our data reasonably (Fig. 14). We assume that the ATL was a constant thickness (40 cm) during the Pleistocene before the unconformity developed. We also assume a slower erosion rate of the source basins in the Pleistocene (25 m Ma^{-1}) that delivered more highly-dosed sediment to the piedmont. We modeled steady piedmont deposition at 15 m Ma^{-1} up to 4.5 km away from the rangefront and 40 m Ma^{-1} from 4.5 km to IMT-4 followed by a surface of transport starting 5 ka. We used an ATL thickness of 30 cm after 5 ka, and the long-term integrated basin-wide erosion rates during the surface of transport phase (last 5000 years). The predicted nuclide abundances fit the transect data reasonably well, except for underestimating the nuclide abundance at IMT-0 (Fig. 14). The sediment transport

velocities range between 28 and 44 cm y^{-1}. Although this is the best fitting scenario we could produce, it is only one of many possible scenarios that reproduce the transect data reasonably well.

7.0 What we have learned

In situ-produced cosmogenic isotope measurements have begun to constrain piedmont processes and rates that have long resisted definition and quantification. Measuring and interpreting cosmogenic isotopes allows us to quantify rates and determine processes on the 10^3 to the 10^5 year time scale, much shorter than the formation of many desert piedmonts (Cooke and Warren, 1973; Oberlander, 1974). The processes and rates discussed here are relevant to piedmont modification and not piedmont formation.

Nuclide data suggest lateral and vertical sediment mixing processes are important on desert piedmonts. Low-relief geomorphic units have indistinguishable nuclide abundances, suggesting that braided ephemeral channels migrate rapidly (≤1000 years), and mix sediment throughout the ATL. Weak channel banks and rapid changes in discharge are typical of migrating channels in sediment-laden networks (Ritter, 1978). Such rapid channel migration is also possible on an eroding piedmont (pediment); however, little bare rock is exposed beyond IMT-0 and GMT-0. The weak channel banks and rapid changes on discharge of desert piedmonts allow for rapid migration of channels over either, more resistant bedrock or more indurated sediment. Such channel migration could effectively erode the piedmont and maintain a planar morphology without forming

entrenched channels. Gilbert (1877) and Paige (1912) were the first speculate that such a process contributes to pedimentation.

Individual channel morphometeries on the Iron Mountain piedmont do not vary significantly over the piedmont's width or length (Nichols and Bierman, in press). Uniformity of a piedmont drainage network is represented numerically by a "random walk" of channels over uniform lithology (Rachocki, 1981). Results of such a model, show that where alluvial fans coalesce, the drainage becomes an interconnected network of braided channels, the discharge of channels becomes uniform, and the "...coalesced surface forms an alluvial piedmont plain." Our data are consistent with such a depositional system dominated by rapidly migrating channels, a uniform braided drainage, a planer morphology, and a uniform substrate lithology.

Soil-pit nuclide data constrain the depositional history of the Iron Mountain piedmont and allow us to infer possible effects of climate change. Our data suggest a change from sediment deposition to sediment transport at soil pit 1 (~2.25 km from the rangefront) between ~6 ka and ~15 ka. The soil pit data could be consistent with a change in either hillslope or piedmont process at the Pleistocene-Holocene transition (~10 ka). From the research of Bull and Schick (1979) and Bull (1991), one would expect increased sediment yield from the source basins, and possibly increased piedmont deposition rates at major climate changes. Further from the rangefront at pit 2, no such change is observed implying either, the change of process has not reached pit 2 yet, or lower reaches of the piedmont are less sensitive to drainage basin processes. A denser spatial distribution of soil pits would better constrain the piedmont history, albeit at significant expense.

Sediment transport rates across desert piedmonts have, until now, been unknown. Although, there is some uncertainty in nuclide and sediment production rates and in the flux of sediment delivered from the source basins, we now know sediment velocities within a factor of two for the Iron Mountain piedmont. We also know that Iron Mountain sediment is transported in a well-mixed active layer that is well defined by isotopically-mixed sediment, maximum channel depths, and depths to the B-horizon. Although piedmont processes have changed on the Iron Mountain piedmont, every interpretative model, including endmember processes and the plausible scenario, suggests that sediment velocities are 35 ± 15 cm y^{-1}. Such velocities imply that human disturbance or sediment contamination would have long-lasting effects on desert piedmonts.

Although, this investigation focuses on one area, the similar increase of nuclide abundance down both the Iron and Granite Mountain piedmonts suggests that other piedmonts in similar settings may have similar sediment transport rates and processes. Applying this technique to piedmonts with different lithologies, slopes, tectonic settings, and morphologies will provide a better understanding of desert piedmont processes.

8.0 Appendix

Definitions and units for variables:
m = long-term average basin-wide lowering rate (g cm^{-2} y^{-1})
Λ = neutron attenuation factor (g cm^{-2})
P = spatially weighted nuclide production rate (atoms g^{-1} y^{-1})
$C_i(0)$ = nuclide abundance of sediment leaving basin (atoms g^{-1})
M_i = sediment mass flux entering transport segment (g cm^{-1} y^{-1})
M_p = sediment mass flux (±) from piedmont below ATL (g cm^{-1} y^{-1})
M_o = sediment mass flux exiting transport segment (g cm^{-1} y^{-1})
$M_i(L)$ = sediment mass flux entering transport segment at distance L down piedmont (g cm^{-1} y^{-1})
$M_p(x)$ = sediment mass flux (±) from piedmont at distance x down piedmont (g cm^{-2} y^{-1})
$\rho(L,z)$ = depth and distance dependant density field (g cm^{-3})

$u(L,z)$ = depth and distance dependant velocity field (cm y^{-1})
ρ = density (g cm^{-3})
$\hat{u}(L)$ = vertically averaged velocity at distance L down piedmont (cm y^{-1})
h = depth (cm)
$M_p(L)$ = sediment mass flux (±) from piedmont at distance x down piedmont (g cm^{-2} y^{-1})
L = distance down piedmont (cm)
A_i = nuclide flux entering transport segment (atoms cm^{-1} y^{-1})
A_p = nuclide flux (±) from piedmont (atoms cm^{-1} y^{-1})
P_{ATL} = nuclide production in ATL during transport (atoms cm^{-1} y^{-1})
A_o = nuclide flux exiting transport segment (atoms cm^{-1} y^{-1})
$A_i(L)$ = nuclide flux entering transport segment at distance L down piedmont (atoms cm^{-1} y^{-1})
$C_i(L)$ = nuclide abundance of sediment entering transport segment at distance L down piedmont (atoms cm^{-1} y^{-1})
$A_p(L)$ = nuclide flux (±) from piedmont at distance L down piedmont (atoms cm^{-1} y^{-1})
$C_p(x)$ = nuclide abundance of piedmont sediment at distance x down piedmont (atoms g^{-1})
$C_p(L)$ = nuclide abundance of piedmont sediment at distance L down piedmont (atoms g^{-1})
$P_{ATL}(L)$ = nuclide production in ATL during transport at distance L down piedmont (atoms g^{-1} y^{-1})
$P_{avg}(x)$ = average nuclide production over ATL thickness at distance x down piedmont (atoms g^{-1} y^{-1})
P_o = nuclide production rate at sea level and high latitude (atoms g^{-1} y^{-1})
z = depth below surface (cm)
$C(L,z)$ = depth and distance dependant nuclide abundance field (atoms g^{-1})
$C(x)$ = nuclide abundance at distance x down piedmont (atoms g^{-1})
$M_i(x)$ = sediment mass flux entering transport segment at distance x down piedmont (g cm^{-1} y^{-1})
$\hat{u}(x)$ = vertically averaged velocity at distance L down piedmont (cm y^{-1})
N = abundance of nuclides (atoms g^{-1})
s = sediment deposition rate (cm y^{-1})
C_i = inherited nuclide abundance at location of soil pit (atoms g^{-1})
C = predicted nuclide abundance (atoms g^{-1})

9.0. Acknowledgements

We thank D. Santos and C. Massey for field assistance, D. Howell for statistical assistance, and B. Copans and S. Neis for laboratory assistance. Funding for this project was provided by U.S. Army Research Office grants DAAG559710180 and DAAH049610036.

10.0 References Cited

Bierman, P.R. and Steig, E.J., 1996. Estimating rates of denudation using cosmogenic isotope abundances in sediment. Earth surface processes and landforms, 21: 125-139.

Birkland, P.W., 1984. Soils and geomorphology. Oxford University Press, New York, 372 pp.

Brown, E.T., Stallard, R.F., Larsen, M.C., Raisbeck, G.M. and Yiou, F., 1995. Denudation rates determined from the accumulation of in situ-produced ^{10}Be in the Luquilo Experimental Forest, Puerto Rico. Earth and Planetary Science Letters, 129: 193-202.

Bull, W.B., 1977. The alluvial-fan environment. Progress in Physical Geography, 1: 222-270.

Bull, W.B., 1991. Geomorphic responses to climatic change. Oxford University Press, New York, 326 pp.

Bull, W.B. and Schick, A.P., 1979. Impact of climatic change on an arid watershed: Nahal Yael, southern Israel. Quaternary Research, 11: 153-171.

Clapp, E.M., Bierman, P.R. and Caffee, M., 1997. Rates of erosion determined using in situ produced cosmogenic isotopes in a small arroyo basin, northwestern New Mexico. Geological Society of America annual meeting Abstracts with Programs, 29: 371-372.

Clapp, E.M., Bierman, P.R., Pavich, M. and Caffee, M., in review. Rates of sediment supply to arroyos from upland erosion determined using *in situ*-produced cosmogenic ^{10}Be and ^{26}Al. Quaternary Research.

Clark, D.H., Bierman, P.R. and Larsen, P., 1995. Improving *in situ* cosmogenic chronometers. Quaternary Research, 44: 367-377.

Cooke, R.U. and Warren, A., 1973. Geomorphology in deserts. University of California Press, Berkeley, 394 pp.

Denny, C.S., 1967. Fans and pediments. American Journal of Science, 265: 81-105.

Dohrenwend, J.C., 1987. Basin and range. In: W.L. Graf (Editor), Geomorphic Systems of North America. Decade of North America Geology. Geological Society of America, Boulder, Colorado, pp. 303-342.

Gilbert, G.K., 1877. Geology of the Henry Mountains (Utah). U.S. Geographical and Geological Survey of the Rocky Mountain Region. Washington D.C.

Granger, D.E., Kirchner, J.W. and Finkel, R., 1996. Spatially averaged long-term erosion rates measured from *in situ* produced cosmogenic nuclides in alluvial sediment. The Journal of Geology, 104: 249-257.

Greenbaum, N., Salmon, O., Gerson, R. and Schick, A.P., 1999. Slope runoff in a hyperarid region. In: J. Lekach and M.A. Hassan (Editors), International Conference on Drainage Basin Dynamics and Morphology. Geological Survey of Israel, Jerusalem, Israel, pp. 201.

Heimsath, A.M., Dietrich, W.E., Nishiizumi, K. and Finkel, R.C., 1999. Cosmogenic nuclides, topography, and the spatial variation of soil depth. Geomorphology, 27(1-2): 151-172.

Hooke, R.L., 1968. Steady-state relationships on arid-region alluvial fans in closed basins. American Journal of Science, 266: 609-629.

Kohl, C.P. and Nishiizumi, K., 1992. Chemical isolation of quartz for measurement of *in situ*-produced cosmogenic nuclides. Geochimica et Cosmochimica Acta, 56: 3583-3587.

Lal, D., 1988. *In situ*-produced cosmogenic isotopes in terrestrial rocks. Annual Reviews of Earth and Planetary Science, 16: 355-388.

Lal, D., 1991. Cosmic ray labeling of erosion surfaces: *In situ* nuclide production rates and erosion models. Earth and Planetary Science Letters, 104: 424-439.

Laronne, J.B., Reid, I., Yitshak, Y. and Frostick, L.E., 1994. The non-layering of gravel streambeds under ephemeral flood regimes. Journal of Hydrology, 159: 353-363.

Laronne, J.B. and Reid, I., 1993. Very high rates of bedload sediment transport by ephemeral desert rivers. Nature, 366: 148-150.

Lekach, J., Amit, R., Grodek, T. and Schick, A.P., 1998. Fluvio-pedogenic processes in an ephemeral stream channel, Nahal Yael, Southern Negev, Israel. Geomorphology, 23: 353-369.

Lekach, J. and Schick, A.P., 1999. Sediment transport and sediment yield. In: J. Lekach and M.A. Hassan (Editors), International Conference on Drainage Basin Dynamics and Morphology. Geological Survey of Israel, Jerusalem, Israel, pp. 201.

Machette, M., 1986. Calcium and magnesium carbonates. In: M.J. Singer and P. Janitzky (Editors), Field and laboratory procedures used in a soil chronosequence study. U. S. Geological Survey, Reston, Virginia, pp. 30-33.

Mayer, L. and Bull, W.B., 1981. Impact of Pleistocene-Holocene climatic change on particle size distribution of fan deposits in southwestern Arizona. Geological Society of America Abstracts with Programs, 13: 95.

McFadden, L.D., Ritter, J.B. and Wells, S.G., 1989. Use of multiparameter relative-age methods for age estimation and correlation of alluvial fansurfaces on a desert piedmont, eastern Mojave Desert, California. Quaternary Research, 32: 276-290.

Monaghan, M. C., McKean, J., Dietrich, W., and Klein, J., 1992, ^{10}Be chronometry of bedrock-to-soil conversion rates: Earth and Planetary Science Letters, v. 111, p. 483-492.

Nichols, K.K. and Bierman, P.R., in press. Fifty-four years of ephemeral channel response to intense military activity at Camp Iron Mountain, Mojave Desert, California. In: R. Harmon and J. Ehlen (Editors), The Environmental Legacy of Military Operations. Geological Society of America.

Nishiizumi, K. et al., 1989. Cosmic ray production rates of ^{10}Be and ^{26}Al in quartz from glacially polished rocks. Journal of Geophysical Research, 94(B12): 17,907-17,915.

NOAA, 1982. Monthly normals of temperature, precipitation, and heating and cooling degree days 1951-1980, California., NOAA (National Oceanic and Atmospheric Administration), Asheville, N.C.

Oberlander, T.M., 1974. Landscape inheritance and the pediment problem in the Mojave Desert of southern California. American Journal of Science, 274: 849-875.

Paige, S., 1912. Rock-cut surfaces in desert ranges. Journal of Geology, 20: 442-450.

Phillips, W. M., McDonald, E. V., Reneau, S.L. and Poths, J., 1998. Dating soils and alluvium with cosmogenic ^{21}Ne depth profiles: case studies from the Pajarito Plateau, New Mexico, USA. Earth and Planetary Science Letters, 160: 209-223.

Rachocki, A., 1981. Alluvial fans an attempt at an empirical approach. John Wiley & Sons, New York, 161 pp.

Reid, I. and Laronne, J.B., 1995. Bed load sediment transport in an ephemeral stream and a comparison with seasonal and perennial counterparts. Water Resources Research, 31(3): 773-781.

Ritter, D.F., 1978. Process geomorphology. WM. C. Brown, Debuque, Iowa, 603 pp.

Small, E.E., Anderson, R.S. and Hancock, G.S., 1999. Estimates of the rate of regolith production using ^{10}Be and ^{26}Al from an alpine hillslope. Geomorphology, 27: 131-150.

Spaulding, W.G. and Graumlich, L.J., 1986. The last pluvial climatic episodes in the deserts of southwestern North America. Nature, 320: 441-444.

Spaulding, W.G., Leopold, E.B. and Devender, T.R.V., 1983. Late Wisconsin paleoecology of the American southwest. In: J. H. E. Wright (Editor), Late-Quaternary Environments of the United States. Stephen C. Porter. University of Minnesota Press, Minneapolis, pp. 407.

Warnke, D.A., 1969. Pediment evolution in the Halloran Hills, Central Mojave Desert, California. Zeitschrift für Geomorphologie, 13: 357-389.

Wells, S.G., McFadden, L.D. and Dohrenwend, J.C., 1987. Influence of Late Quaternary climatic changes on geomorphic and pedogenic processes on a desert piedmont, eastern Mojave Desert, California. Quaternary Research, 27: 130-146.

Yair, A., 1999. Sede Boquer research site. In: J. Lekach and M.A. Hassan (Editors), International Conference on Drainage Basin Dynamics and Morphology. Geological Survey of Israel, Jerusalem, Israel, pp. 201.

Figure Captions

Fig. 1. A.) Location of the Iron and Granite Mountains in the Mojave Desert, California. B.) Oblique aerial photograph of the Iron and Granite Mountains and respective piedmonts looking to the southwest. Granite Mountains are on the left (south) and the Iron Mountains are on the right (west). Steep, narrow source basins for each piedmont penetrate mountains normal to rangefront. View is ~10 km wide.

Fig. 2. Map of the Iron and Granite Mountain piedmonts. Straight black lines represent transect locations on the piedmont surfaces. IMT = Iron Mountain transect samples, GMT = Granite Mountain transect samples, IMT-2H = Iron Mountain

transect where additional shallow pits were dug, but no sediment samples collected. Black squares represent soil pit locations. Gray circles represent valley sample locations. IMV = Iron Mountain valley samples, and GMV = Granite Mountain valley samples. CRA = Colorado River Aqueduct. Contour interval is 50 m. Map based on the Granite Pass and East of Granite Pass U.S.G.S. 1:24,000 quadrangles, 1985.

Fig. 3. Grain size and carbonate distribution of sediment collected from Iron and Granite Mountain piedmonts. G = gravel and larger, CS = coarse sand, MS = medium sand, and FS = fine sand and smaller. A.) Iron Mountain transects. No clear down piedmont fining trend is observed. B.) Granite Mountain transects. No clear down piedmont fining trend is observed. C.) Soil Pit 1. Grain size is uniform except for a gravel layers at depths of 10 to 20 cm and 76 to 86 cm. D.) Soil pit 2. Grain size is uniform except for gravel layer at depth of 28 to 40 cm. E.) Soil pit 1 carbonate percentage on less than 80 μm fraction. Highest percentage is from 20 to 30 cm. F.) Soil pit 2 carbonate percentage. Highest percentage is from 71 to 80 cm.

Fig. 4. Photograph of ephemeral channels and terraces located near IMT-3. Unvegetated channel bottom contains most recently transported sediment. Low-terraces have sparse vegetation. There is no desert pavement. Channel in middle of photograph is ~2 m wide. Photograph taken looking southwest with the Iron Mountains in the right background.

Fig. 5. Reproducibility of sediment samples. GMT-0A and GMT-0B were collected independently. IMT-3 and IMT-3DUP are laboratory replicates.

Fig. 6. ^{10}Be and ^{26}Al data are well-correlated ($r^2 = 0.98$). Slope of 5.8 ± 0.2 (68% confidence level) is consistent with production ratio of 6.0 (Nishiizumi et al., 1989) and suggests that sediment samples were not buried for significant periods of time ($> 10^5$ years).

Fig. 7. Transect (closed symbols) and valley (open symbols) data from Iron (circles) and Granite (squares) Mountain piedmonts. A.) ^{10}Be transect data. r^2 is 0.98 and 0.99 for the Iron and Granite Mountain piedmonts, respectively. B.) ^{26}Al transect data. r^2 is 0.96 and 0.93 for the Iron and Granite Mountain piedmonts, respectively. Slopes for isotope abundance as a function of distance from rangefront are indistinguishable at the 68% confidence level. Error bars represent 1σ analytical error. Error bars for valley samples are same size as symbols.

Fig. 8. Different geomorphic units along the same transect have similar nuclide abundances. IMT-1CHAN and IMT-4CHAN = channel sediment, IMT-1TERR and IMT-4TERR = terrace sediment, and IMT-1CRIT and IMT-4CRIT = animal burrow sediment exposed at surface. Error bars represent 1σ analytical error.

Fig. 9. Soil pit samples have increasing nuclide abundances at depth. A.) ^{10}Be soil pit data for pit 1 (circles) ~2.2 km from the Iron Mountain rangefront and pit 2 (squares) ~4.7 km from the Iron Mountain rangefront. B.) ^{26}Al soil pit data for pit 1 (circles) and pit 2 (squares). Horizontal bars represent 1σ analytical uncertainty. Vertical bars represent thickness of integrated sample.

Fig. 10. Continuity models for A) mass balance and B) nuclide balance divide the piedmont into transport segments of a unit width, the ATL thickness, and an arbitrary length. Flux of mass and nuclides into each segment must equal the flux

of mass and nuclides exiting each segment. Nuclide balance model has additional input of nuclides by production during sediment transport down piedmont. Transport times are sufficiently rapid that decay of ^{10}Be and ^{26}Al is inconsequential.

Fig. 11. Stable surfaces (squares) and eroding surfaces (circles) have nuclide abundances that decrease at depth. Depositional surfaces (triangles) have nuclide abundances that increase with depth. Squares represent a stable surface after 50,000 years of exposure. Circles represent a surface eroding at 38 m Ma^{-1}. Triangles represent a 70 m Ma^{-1} depositional surface.

Fig. 12. Predicted deposition rates using A.) ^{10}Be and B.) ^{26}Al data for soil pit 1 (circles) and soil pit 2 (squares). ^{10}Be and ^{26}Al data are consistent with similar deposition rates for respective soil pits. Nuclide data for soil pit 1 suggest uniform deposition (15 m Ma^{-1}) from the bottom of the soil pit to ~20 cm. A discontinuity in nuclide abundance at 20 cm suggests deposition stopped. Nuclide data for soil pit 2 suggests uniform deposition at 40 m Ma^{-1} for entire soil pit.

Fig. 13. ^{10}Be data for Iron Mountain piedmont (diamonds and thick black line) and predicted results of endmember processes. Surface of transport endmember (open squares) generates nuclide abundances that are lower than transect data, implying sediment velocities are too fast. Open triangles represent deposition endmember (15 m Ma^{-1}). ^{10}Be abundances are lower than transect data for IMT-0, and are higher than transect data for IMT-3 and IMT-4. Open circles represent erosion endmember (5 m Ma^{-1}). ^{10}Be abundances for erosion endmember are lower than surface of transport abundances.

Fig. 14. ^{10}Be data for Iron Mountain piedmont (open circles) and predicted results of steady deposition (15 m Ma^{-1}) followed by 5000 years of transport (black dashes). Predicted results fit transect data well except for IMT-0 and imply the Iron Mountain piedmont has a history that includes changing surface behavior.

Table 1
^{10}Be and ^{26}Al data for the Iron and Granite Mountain piedmonts

Sample[a]	Elevation[b] (m)	Northing[c,d]	Easting[c,d]	Measured nuclide concentration (10^6 atoms g^{-1})[e]		Ratio ^{26}Al/^{10}Be	Description
				^{10}Be	^{26}Al		
GMV-1	485	3766547	671919	0.168 ± 0.009	1.02 ± 0.06	6.08 ± 0.48	integrated valley sediment
GMV-2	600	3764501	672404	0.131 ± 0.005	0.82 ± 0.04	6.22 ± 0.40	integrated valley sediment
GMV-3	550	3765000	672274	0.148 ± 0.005	0.98 ± 0.05	6.65 ± 0.41	integrated valley sediment
GMT-0A	450	3767980	670920	0.188 ± 0.009	1.15 ± 0.06	6.10 ± 0.46	integrated transect sediment (20 sites)
		3766620	674540				
GMT-0B				0.191 ± 0.010	1.06 ± 0.10	5.58 ± 0.59	field replicate of GMT-0A
GMT-1	415	3768900	671270	0.213 ± 0.015	1.11 ± 0.16	5.21 ± 0.86	integrated transect sediment (20 sites)
		3767530	674920				
GMT-2	380	3769820	671640	0.243 ± 0.010	1.57 ± 0.08	6.46 ± 0.42	integrated transect sediment (20 sites)
		3768440	675260				
GMT-3	350	3770760	672000	0.290 ± 0.011	1.66 ± 0.10	5.71 ± 0.41	integrated transect sediment (20 sites)
		3769400	675620				
GMT-4	320	3771680	672360	0.316 ± 0.012	1.95 ± 0.10	6.18 ± 0.39	integrated transect sediment (20 sites)
		3770320	675970				
IMV-1	530	3776603	666643	0.140 ± 0.004	0.91 ± 0.06	6.46 ± 0.46	integrated valley sediment
IMV-2	495	3776515	667054	0.162 ± 0.005	1.13 ± 0.07	6.93 ± 0.47	integrated valley sediment
IMV-3	510	3775699	666478	0.143 ± 0.004	0.99 ± 0.06	6.89 ± 0.45	integrated valley sediment
IMT-0	425	3777034	668460	0.226 ± 0.010	1.38 ± 0.08	6.14 ± 0.45	integrated transect sediment (20 sites)
		3773103	668011				
IMT-0FAN	440	3777034	668460	0.212 ± 0.008	1.37 ± 0.11	6.46 ± 0.57	integrated alluvial fan sediment (4 sites)
		3776442	668402				
IMT-1	400	3776958	669428	0.245 ± 0.008	1.46 ± 0.07	5.98 ± 0.36	integrated transect sediment (20 sites)
		3773033	669010				
IMT-1CHAN				0.252 ± 0.011	1.51 ± 0.08	6.00 ± 0.42	integrated channel sediment (20 sites)
IMT-1CRIT				0.259 ± 0.008	1.68 ± 0.09	6.51 ± 0.40	integrated animal burrow sediment (20 sites)
IMT-1TERR				0.258 ± 0.011	1.53 ± 0.10	5.95 ± 0.46	integrated terrace sediment (20 sites)
IMT-2	355	3776816	670422	0.286 ± 0.009	1.87 ± 0.11	6.54 ± 0.43	integrated transect sediment (20 sites)
		3772997	669974				
IMT-3	320	3776850	671359	0.320 ± 0.013	2.04 ± 0.12	6.37 ± 0.46	integrated transect sediment (20 sites)
		3772898	670988				
IMT-3DUP				0.325 ± 0.010	1.90 ± 0.10	5.86 ± 0.35	laboratory replicate of IMT-3
IMT-4	290	3776693	672391	0.367 ± 0.100	2.38 ± 0.12	6.49 ± 0.36	integrated transect sediment (20 sites)
		3772847	671975				
IMT-4CHAN				0.393 ± 0.019	2.16 ± 0.13	5.49 ± 0.42	integrated channel sediment (20 sites)
IMT-4CRIT				0.392 ± 0.019	2.24 ± 0.12	5.71 ± 0.41	integrated animal burrow sediment (20 sites)

Table 1 cont.

IMT-4TERR				0.380 ± 0.020	2.24 ± 0.12	5.89 ± 0.43	integrated terrace sediment (20 sites)
PIT1 0-10	405	3774990	679030	0.194 ± 0.015	1.10 ± 0.08	5.67 ± 0.57	integrated soil pit sediment
PIT1 10-20				0.193 ± 0.007	1.21 ± 0.08	6.29 ± 0.45	integrated soil pit sediment
PIT1 20-30				0.299 ± 0.014	1.73 ± 0.11	5.80 ± 0.44	integrated soil pit sediment
PIT1 30-40				0.328 ± 0.011	2.01 ± 0.10	6.12 ± 0.38	integrated soil pit sediment
PIT1 40-50				0.352 ± 0.011	2.09 ± 0.11	5.94 ± 0.36	integrated soil pit sediment
PIT1 50-66				0.385 ± 0.013	2.51 ± 0.13	6.52 ± 0.40	integrated soil pit sediment
PIT1 66-76				0.403 ± 0.020	2.44 ± 0.14	6.06 ± 0.45	integrated soil pit sediment
PIT1 76-86				0.427 ± 0.026	2.51 ± 0.13	5.89 ± 0.47	integrated soil pit sediment
PIT2 0-14	310	3774990	671500	0.404 ± 0.012	2.54 ± 0.13	6.29 ± 0.38	integrated soil pit sediment
PIT2 0-14DUP				0.441 ± 0.013	2.38 ± 0.12	5.38 ± 0.32	laboratory replicate of PIT2 0-14
PIT2 14-28				0.411 ± 0.016	2.65 ± 0.15	6.44 ± 0.44	integrated soil pit sediment
PIT2 28-40				0.468 ± 0.015	2.74 ± 0.14	5.86 ± 0.36	integrated soil pit sediment
PIT2 40-50				0.473 ± 0.015	2.99 ± 0.15	6.33 ± 0.38	integrated soil pit sediment
PIT2 50-60				0.479 ± 0.016	2.91 ± 0.16	6.08 ± 0.40	integrated soil pit sediment
PIT2 60-71				0.477 ± 0.014	2.84 ± 0.16	5.95 ± 0.37	integrated soil pit sediment
PIT2 71-80				0.496 ± 0.015	3.00 ± 0.15	6.05 ± 0.34	integrated soil pit sediment
PIT2 80-90				0.513 ± 0.015	3.00 ± 0.15	5.84 ± 0.33	integrated soil pit sediment

[a] GMV = Granite Mountain valley samples, GMT = Granite Mountain transect samples, IMV = Iron Mountain valley samples IMT = Iron Mountain transect samples, IMT-0FAN = sediment from higher alluvial surface, IMT-#CHAN = Iron Mountain channel sediment, IMT-#CRIT = Iron Mountain animal burrow sediment, IMT-#TERR = Iron Mountain low terrace sediment, PIT1 = soil pit 1 sediment, PIT2 = soil pit 2 sediment, DUP = laboratory replicate

[b] measured from Granite Pass and East of Granite Pass U.S.G.S. quadrangles, 1985, average elevation for transect samples

[c] measured using Garmin 12 GPS, UTM zone 11S, NAD 27 coordinate system

[d] transect samples are denoted by the two endpoint coordinates

[e] error is counting statistics of AMS, with 2% uncertainty for stable Be and 4% uncertainty for stable Al combined quadratically

Table 2
Distribution of geomorphic unit samples[a]

Geomorphic unit	IMT-0	IMT-1	IMT-2	IMT-3	IMT-4	GMT-0A	GMT-0B	GMT-1	GMT-2	GMT-3	GMT-4
Terrace	11	13	13	9	15	13	10	12	12	11	11
Channel bottom	5	4	6	10	5	5	7	8	8	6	6
Channel bank	0	1	0	0	0	2	1	0	0	2	2
Road	0	0	1	1	0	0	1	0	0	1	1
Animal burrow	0	0	0	0	0	0	1	0	0	0	0
Alluvial fan	4	2	0	0	0	0	0	0	0	0	0

[a]each sample consists of 20 sub-samples collected along each transect

Table 3

^{10}Be and ^{26}Al erosion rates and associated sediment production rates[a]

Valley location	Basin Area (km^2)	Production rate[b] (atoms g^{-1} y^{-1})		erosion rate[c] (m Ma^{-1})		Sediment generation rate[d] (10^{-2} g cm^{-2} y^{-1})		Sediment flux[e] (m^3 y^{-1} m^{-1})	
		^{26}Al[f]	^{10}Be[g]	^{26}Al	^{10}Be	^{26}Al	^{10}Be	^{26}Al	^{10}Be
Iron Mountain	8.1	55.8	9.4	35	39	0.90	1.03	0.12	0.14
Granite Mountain	5.7	56.4	9.5	38	40	1.04	1.08	0.10	0.10

[a]averages for IMV-1,2,3 and GMV-2,3.

[b]basin wide, weighted average production rate

[c]rock equivalent (2.7 g cm^{-2})

[d]sediment density = 1.55 g cm^{-2}

[e]per unit length of rangefront (m)

[f]based on high latitude sea-level production rate of 36.8 atoms g^{-1} y^{-1} (Nishiizimi et al., 1989)

[g]based on high latitude sea-level production rate of 6.03 atoms g^{-1} y^{-1} (Nishiizimi et al., 1989)

Figure 1A

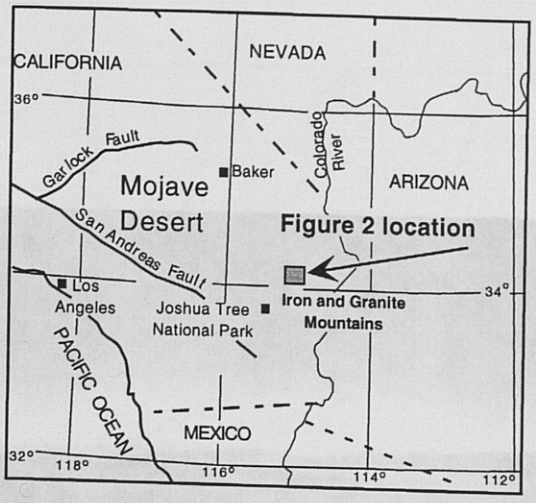
CALIFORNIA
NEVADA
36°
Garlock Fault
Mojave Desert
Baker
Colorado River
ARIZONA
San Andreas Fault
Figure 2 location
Los Angeles
Joshua Tree National Park
Iron and Granite Mountains
34°
PACIFIC OCEAN
MEXICO
32°
118°
116°
114°
112°

Figure 1B

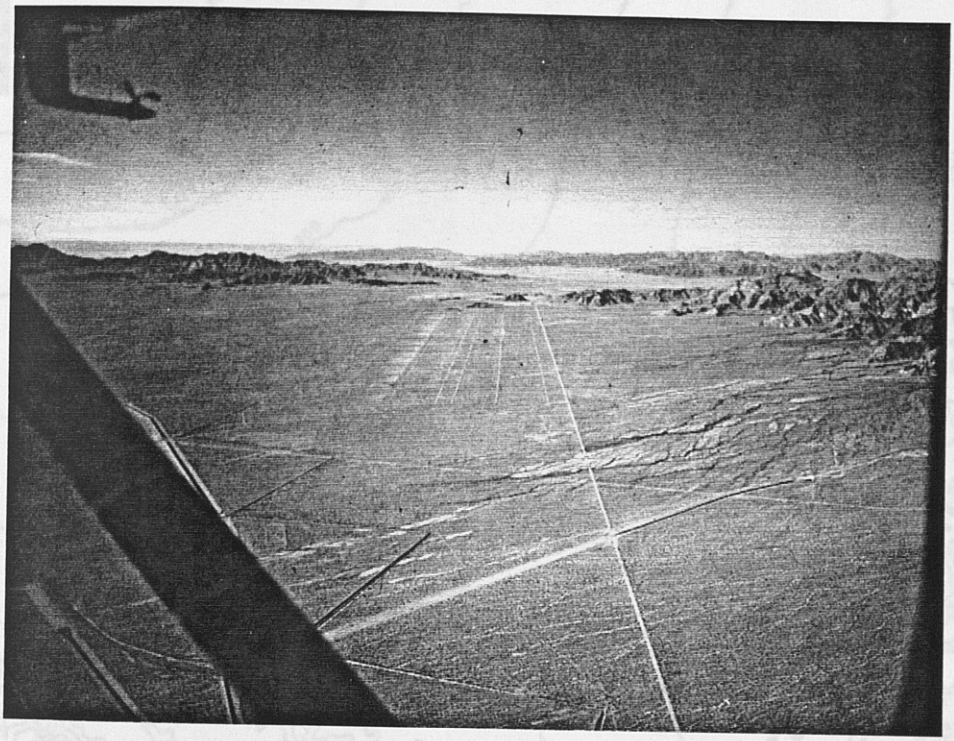

Figure 2

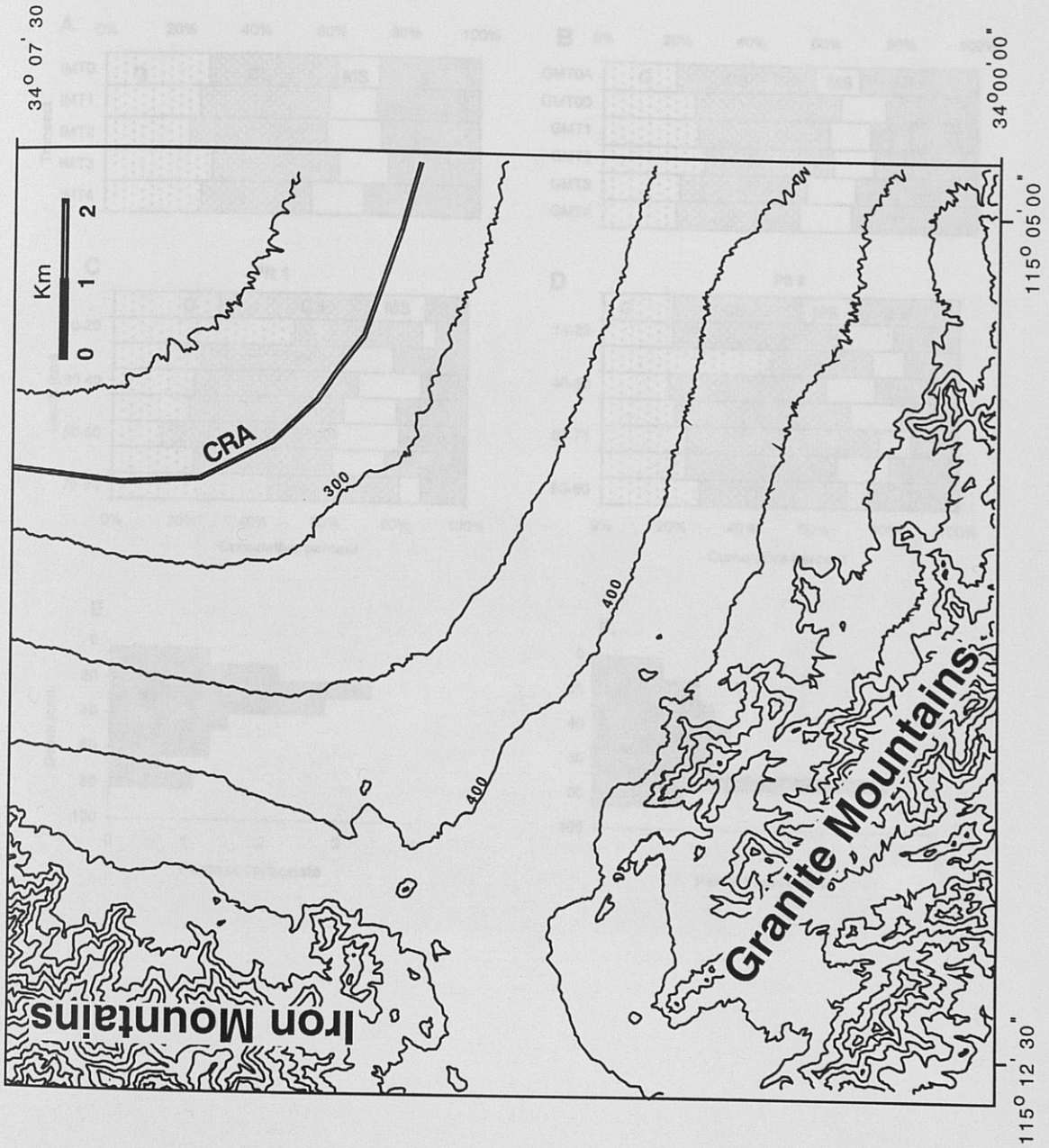
34° 07' 30
34°00'00"
115° 12' 30"
115° 05' 00"
Km
0 1 2
CRA
300
400
400
Iron Mountains
Granite Mountains

Figure 3

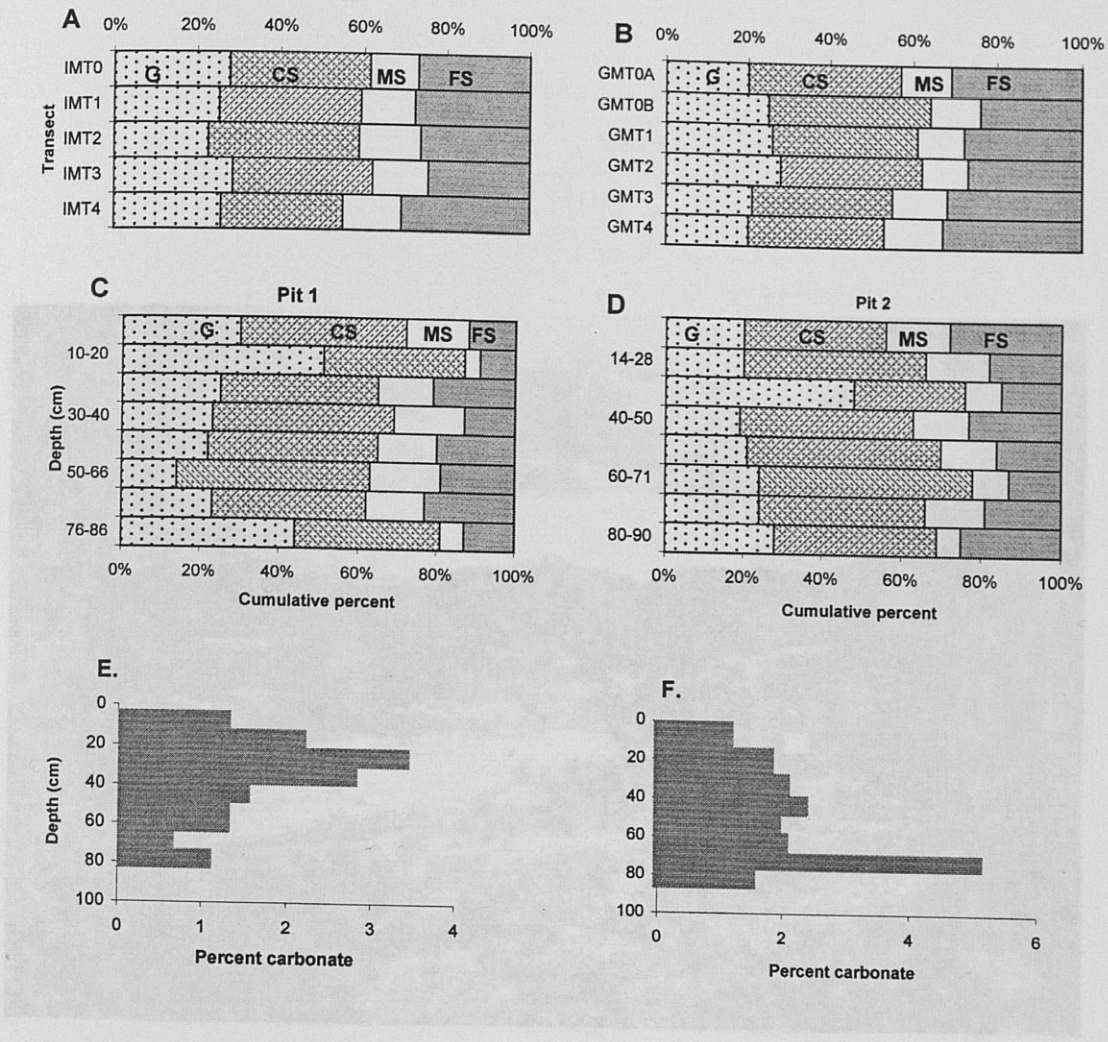
A
0%
20%
40%
60%
80%
100%
IMT0
IMT1
IMT2
IMT3
IMT4
Transect
G
CS
MS
FS
B
GMT0A
GMT0B
GMT1
GMT2
GMT3
GMT4
C
Pit 1
10-20
30-40
50-66
76-86
Depth (cm)
Cumulative percent
D
Pit 2
14-28
40-50
60-71
80-90
E.
0
20
40
60
80
100
Percent carbonate
F.
2
4
6

Figure 4

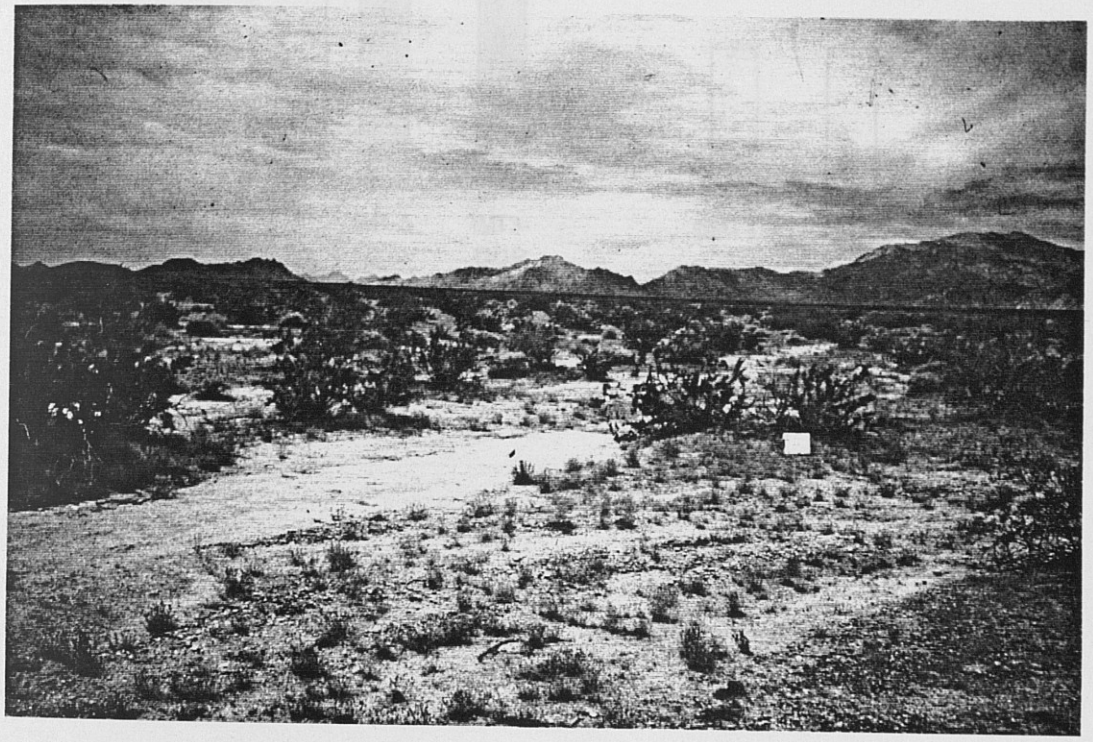

Figure 5

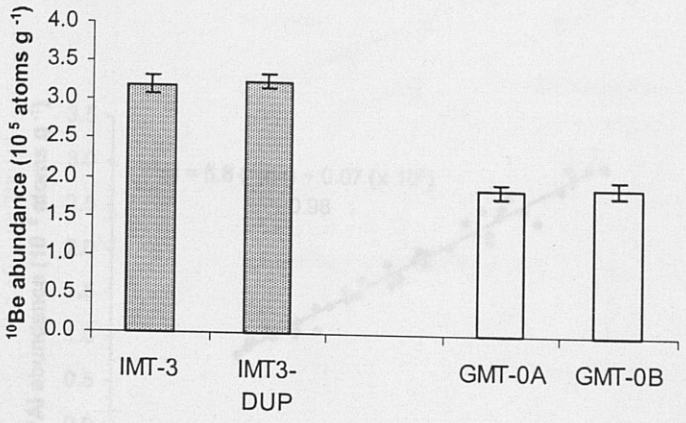
^{10}Be abundance (10^5 atoms g^{-1})
4.0
3.5
3.0
2.5
2.0
1.5
1.0
0.5
0.0
IMT-3
IMT3-DUP
GMT-0A
GMT-0B

Figure 6

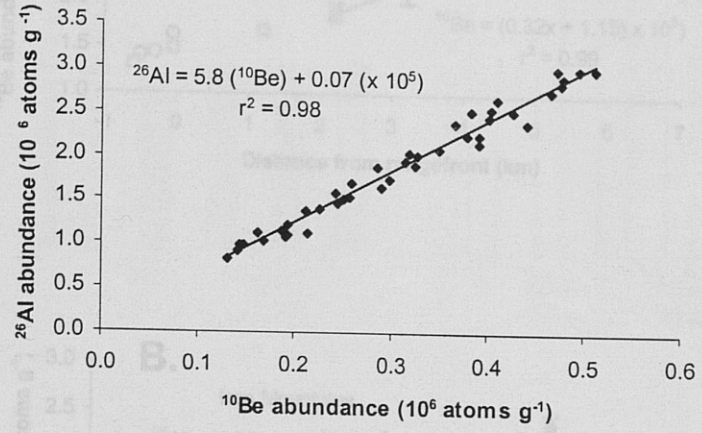
^{26}Al = 5.8 (^{10}Be) + 0.07 (x 10^{5})
r^{2} = 0.98
^{26}Al abundance (10 ^{6} atoms g^{-1})
^{10}Be abundance (10^{6} atoms g^{-1})
0.0
0.5
1.0
1.5
2.0
2.5
3.0
3.5
0.0
0.1
0.2
0.3
0.4
0.5
0.6

Figure 7

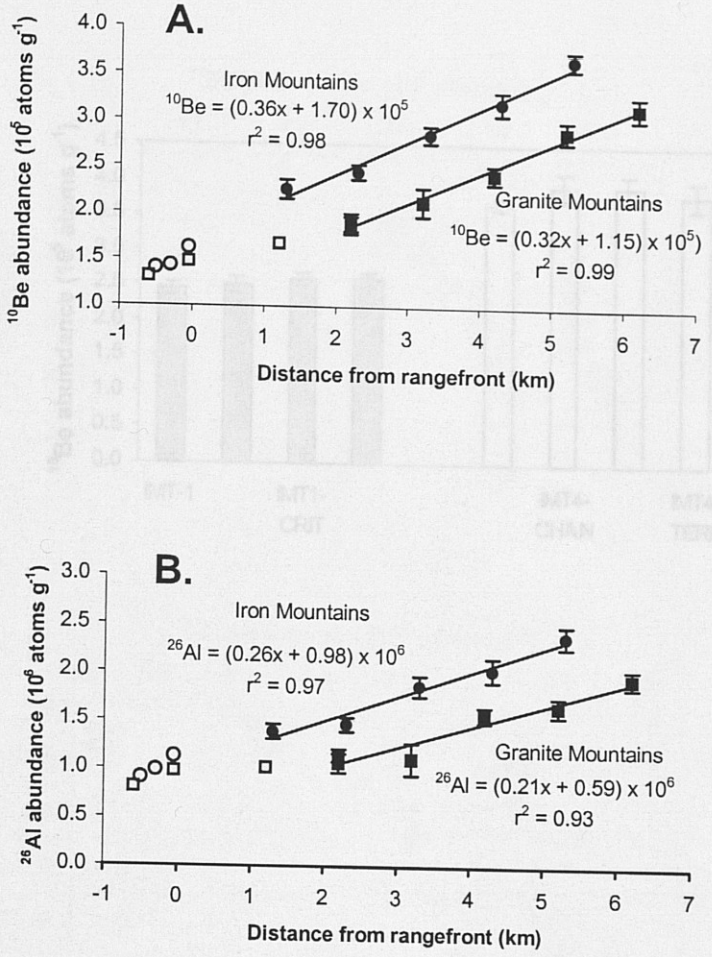
A.
Iron Mountains
$^{10}Be = (0.36x + 1.70) \times 10^5$
$r^2 = 0.98$
Granite Mountains
$^{10}Be = (0.32x + 1.15) \times 10^5$
$r^2 = 0.99$
^{10}Be abundance (10^5 atoms g^{-1})
Distance from rangefront (km)
B.
Iron Mountains
$^{26}Al = (0.26x + 0.98) \times 10^6$
$r^2 = 0.97$
Granite Mountains
$^{26}Al = (0.21x + 0.59) \times 10^6$
$r^2 = 0.93$
^{26}Al abundance (10^6 atoms g^{-1})
Distance from rangefront (km)

Figure 8

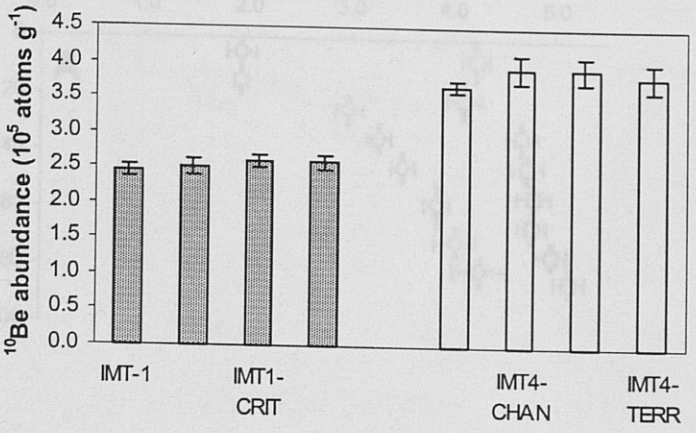
^{10}Be abundance (10^5 atoms g^{-1})
4.5
4.0
3.5
3.0
2.5
2.0
1.5
1.0
0.5
0.0
IMT-1
IMT1-CRIT
IMT4-CHAN
IMT4-TERR

Figure 9

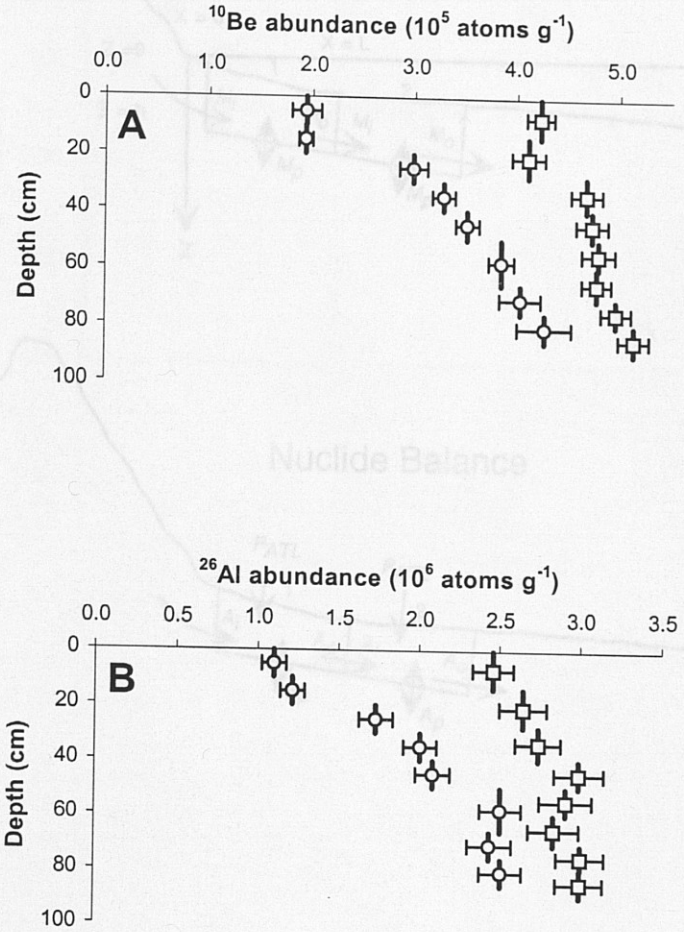
^{10}Be abundance (10^5 atoms g^{-1})
0.0
1.0
2.0
3.0
4.0
5.0
A
Depth (cm)
0
20
40
60
80
100
^{26}Al abundance (10^6 atoms g^{-1})
0.0
0.5
1.0
1.5
2.0
2.5
3.0
3.5
B
Depth (cm)
0
20
40
60
80
100

Figure 10

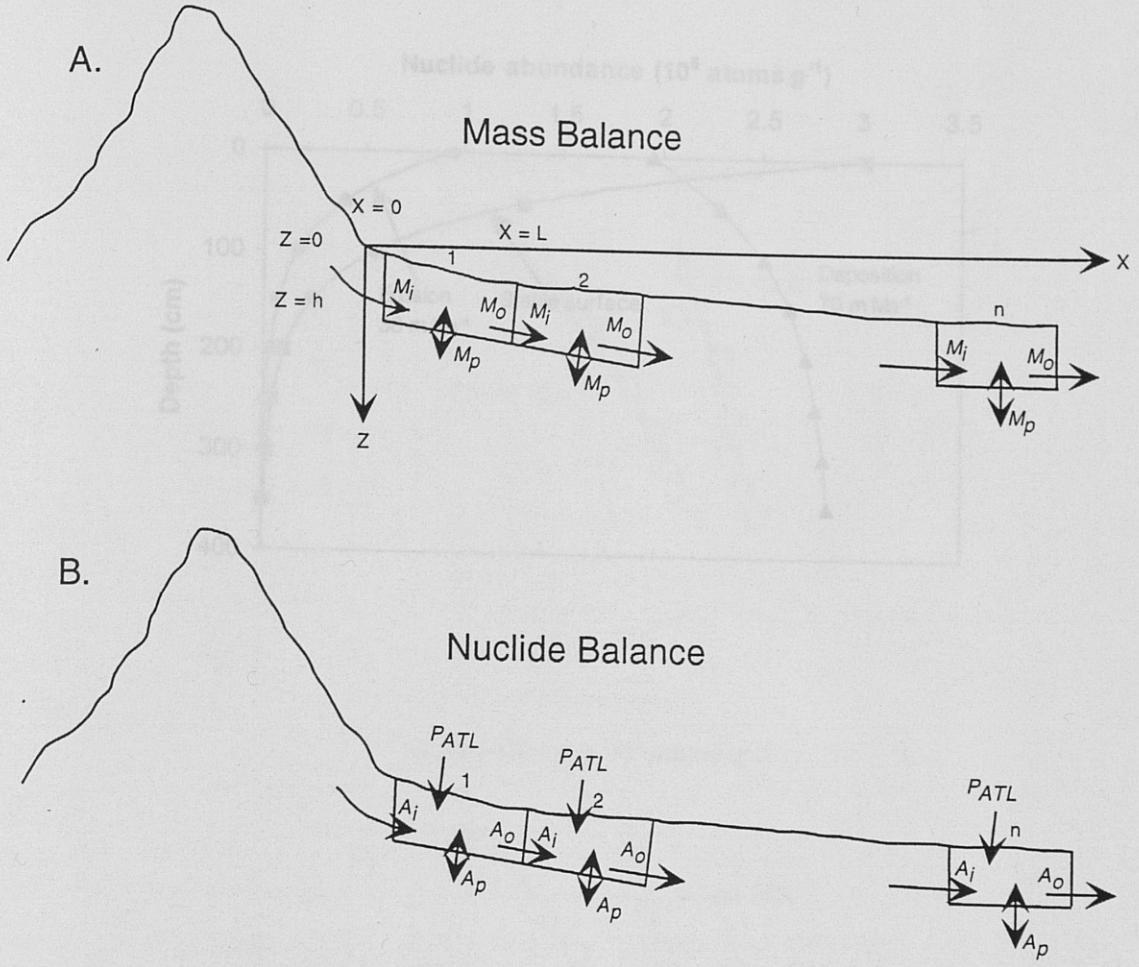
A.
Mass Balance
X = 0
Z =0
X = L
X
Z = h
1
2
n
M_i
M_o
M_p
Z
B.
Nuclide Balance
P_{ATL}
A_i
A_o
A_p

Figure 11

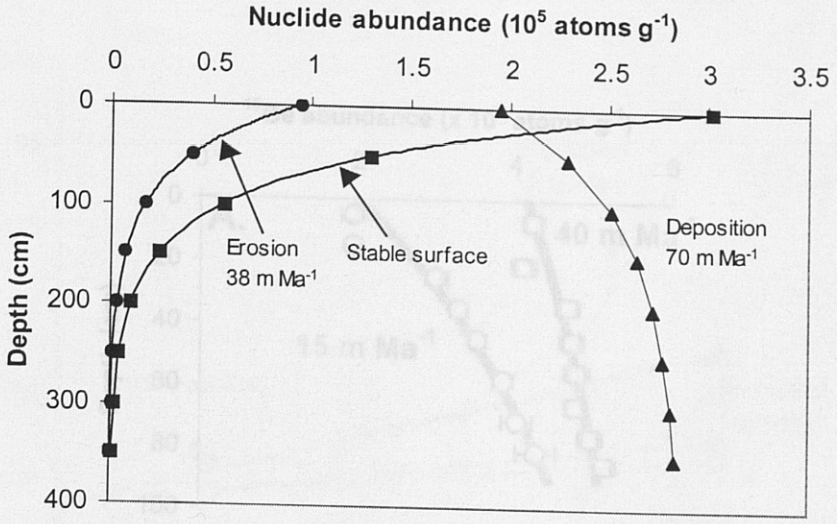
Nuclide abundance (10^5 atoms g^{-1})
0
0.5
1
1.5
2
2.5
3
3.5
0
100
200
300
400
Depth (cm)
Erosion
38 m Ma-1
Stable surface
Deposition
70 m Ma-1

Figure 12

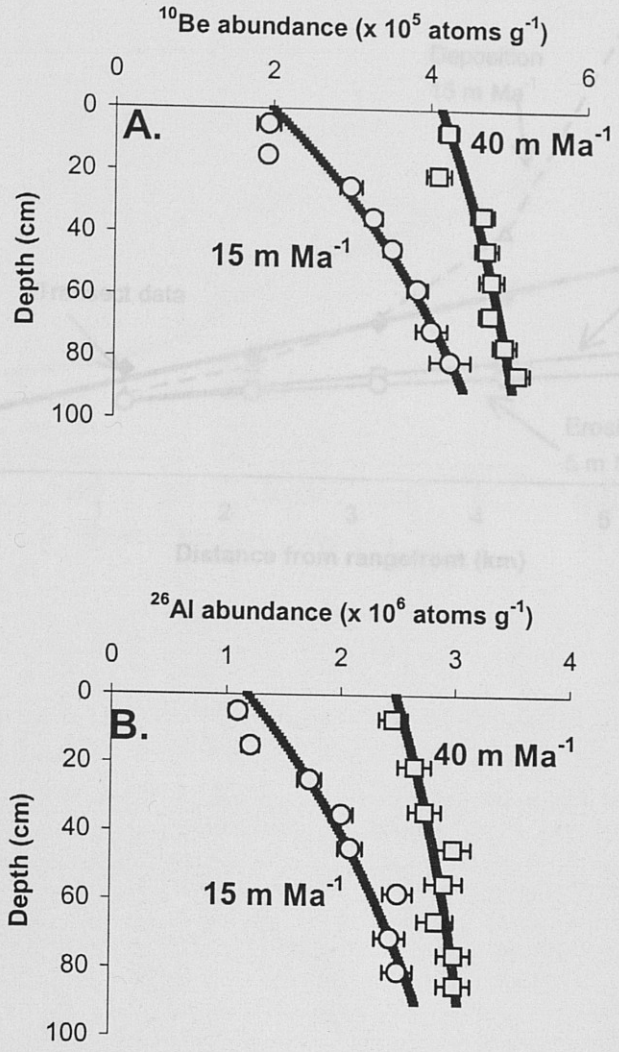
^{10}Be abundance (x 10^5 atoms g^{-1})
0
2
4
6
0
20
40
60
80
100
Depth (cm)
A.
40 m Ma^{-1}
15 m Ma^{-1}
^{26}Al abundance (x 10^6 atoms g^{-1})
0
1
2
3
4
0
20
40
60
80
100
Depth (cm)
B.
40 m Ma^{-1}
15 m Ma^{-1}

Figure 13

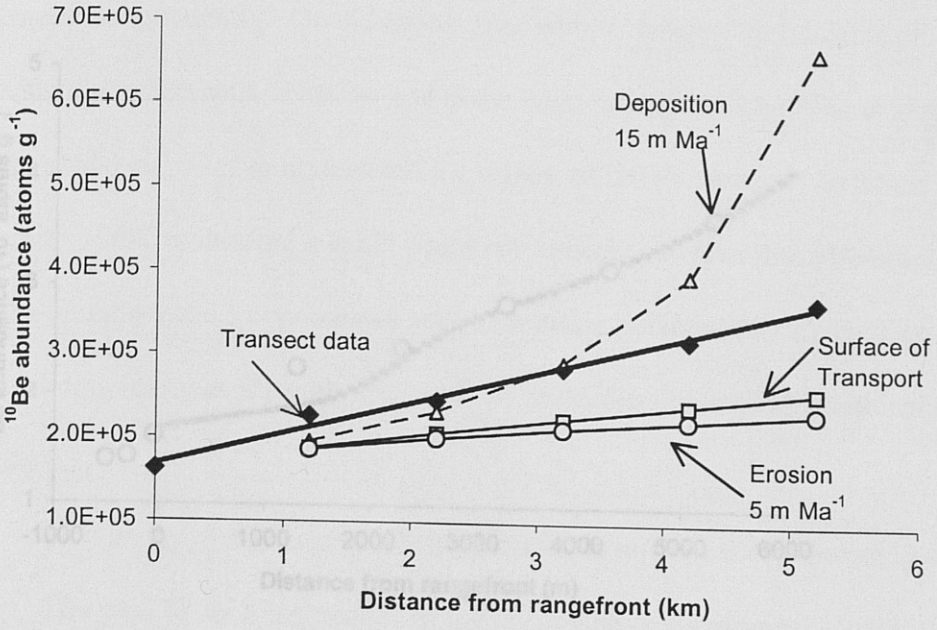
7.0E+05
6.0E+05
5.0E+05
4.0E+05
3.0E+05
2.0E+05
1.0E+05
^{10}Be abundance (atoms g^{-1})
Deposition
15 m Ma^{-1}
Transect data
Surface of
Transport
Erosion
5 m Ma^{-1}
0
1
2
3
4
5
6
Distance from rangefront (km)

Figure 14

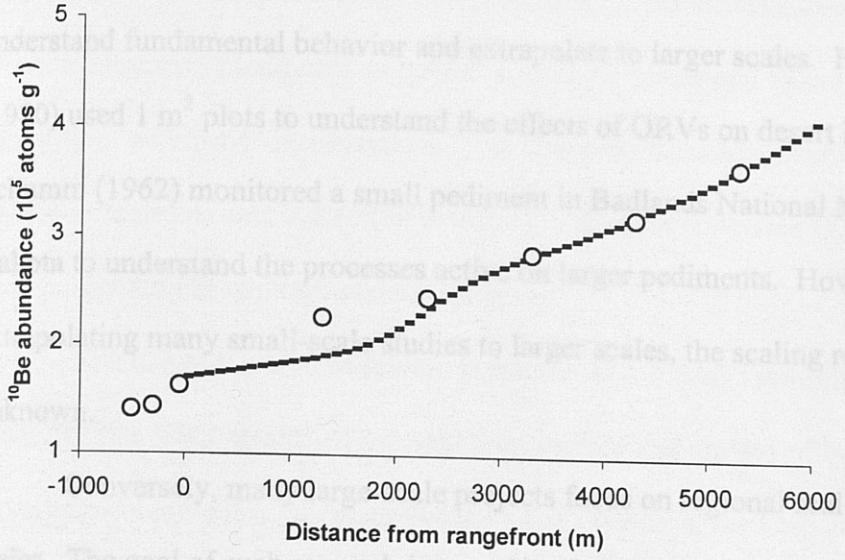
5
4
3
2
1
^{10}Be abundance (10^5 atoms g^{-1})
-1000
0
1000
2000
3000
4000
5000
6000
Distance from rangefront (m)

CHAPTER 5: Integrating different temporal- and spatial-scales

Most geomorphic research investigates small-scale processes and large-scale processes independently. Geomorphologists who investigate small-scale processes try to understand fundamental behavior and extrapolate to larger scales. For example, Iverson (1980) used 1 m^2 plots to understand the effects of ORVs on desert hillslope processes. Schumm (1962) monitored a small pediment in Badlands National Monument of South Dakota to understand the processes active on larger pediments. However, in extrapolating many small-scale studies to larger scales, the scaling relationships are unknown.

Conversely, many large-scale projects focus on regional scales and / or long-time scales. The goal of such research is to understand large geomorphic systems. Many studies focus on large-scale observations and theory at the expense of data analysis. This is due probably to the difficult (logistical and time effective) collection and analysis of data for large areas. Such studies assume small-scale processes to determine their large-scale goals. The desert geomorphology literature is dominated by such theoretical research where each author assumes different small-scale processes to support their theories (Abrahams et al., 1984; Denny, 1967; Gilbert, 1877; Howard, 1942; Mabbutt, 1966; McGee, 1897; Moss, 1977; Paige, 1912). The difficulty in determining the importance of various small-scale processes is in part due to unpredictable periods of rain and runoff, which account for much of the geomorphic change in arid regions.

Cosmogenic isotopes now allow geomorphologists to collect data over a range of spatial scales (point locations to many km^2) and over long-time scales (> 10^3 years).

Such long-term data coupled with short-term data allow for a better understanding of many geomorphic systems.

In order to understand fully the Iron and Granite Mountain piedmonts, one must understand both active and long-term processes. Field observations of the Iron and Granite Mountain piedmonts suggest that shallow ephemeral channels transport the majority of sediment. Furthermore, these channels are active over 98% of the surface. I used two scales of data collection in order to understand the rate at which these channels transport sediment and mix surface sediment.

The use of the Iron Mountain piedmont as a Desert Training Center base camp from 1942 to 1944 smoothed the piedmont surface and destroyed most channels. Topographic surveying of channels inside and outside of the base camp allowed quantification of channel response to anthropogenic influence. I found that channels had not recovered more than a half century after the military last occupied the area. Field observations, reveal that over half of the rock alignments and road berms are still intact suggesting that more than a century is needed for piedmont processes to erase military influences.

Cosmogenic isotope data collected along 4-km long transects are statistically indistinguishable for different geomorphic surfaces (channel sediment and terrace sediment). This implies that the surface is reworked by the ephemeral channels at time-scales comparable to or less than the detection limits of the isotopes (< 1000 years). Thus, 1000 years is the upper time limit of channels reworking the surface of the Iron Mountain piedmont. From these two data sets we constrain the thorough mixing of sediment on the Iron Mountain piedmont surface at the 10^2 year time-scale.

The nature of sediment transport is another example illustrating the utility of a multi-scale approach. Topographic mapping of channel formation inside Camp Iron Mountain reveals that some channels have extended more than 60 m from the channel head in approximately 50 years. Other channels only extend a few meters before they diffuse into the piedmont surface. If we assume that channel head sediment is transported the length of each channel, sediment transport rates are extremely variable (a few meters to over 60 m) during the last 50 years, with most sediment in adjacent terraces not transported at all. Using the cosmogenic isotope transect data, we see that the abundance of nuclides increases in a regular fashion down piedmont. Furthermore, the models suggest that sediment velocities average 35 ± 15 cm y^{-1}. From the cosmogenic isotope data set alone, one would not understand the stochastic nature of sediment transport at small-scales and short time frames. Likewise, from the survey data one would not understand that over the 10^3 year time-scale, the rate and pattern of sediment transport is uniform and predictable.

Soil pit data are another example of multi-scale analysis. Visual logs of soil pits reveal a sharp contact from grey cross-bedded sand to reddened homogenous soil. From a soils analysis we infer that this contact is an unconformity overlain by more recently transported sediment. The cosmogenic isotope data reveal an isotopic unconformity and that the sediment above it is well-mixed. We can also use cosmogenic isotopes to estimate that the unconformity represents a time gap lasting between 5,000 and 15,000 years. Although there is uncertainty in the estimation of time represented by the unconformity, I have constrained the end of deposition. However, if I only used the cosmogenic isotope data from the two soil pits, without knowing the large-scale spatial

distribution of the B-horizon depths across the piedmont surface (from the shallow soil pits), or knowing the maximum channel depths from the 9000 topographic survey points, I would not understand the large-scale significance of the unconformity or the depth of the mixed-layer (ATL) suggested by the cosmogenic isotope data. Likewise, only using the large-scale spatial distribution of the B-horizon, without the small-scale cosmogenic isotope soil profiles, I would not know the time represented by the unconformity or the status of the soil mixing.

This project also shows the disadvantage of only quantifying deposition rates at point locations (small-scale) rather than over a large area. Ideally, a wider distribution of soil pits would better define the spatial distribution of deposition rates and the associated duration of the unconformities. Such data would show the depositional trends or depositional variability of the piedmont. However, I only know two deposition rates and cannot infer accurately large-scale depositional trends along the piedmont. Realistically, more cosmogenic isotope analyses would greatly increase the cost of similar projects.

As the four examples above illustrate, using cosmogenic isotopes in conjunction with a multi-scale analysis is paramount to understanding the styles and rates of desert piedmont processes. Cosmogenic isotopes are effective at determining long-term averaged rates, over either small areas (e.g. soil-pit profiles, surface dating, bedrock erosion rates, or dating terraces) or large areas (basin-wide erosion rates, basin-wide sediment generation rates, and now piedmont-wide sediment transport rates and piedmont-wide surface mixing). By investigating a multitude of scales, one can obtain the best understanding of geomorphic systems.

Future direction of research

This thesis advances the understanding of processes that modify desert piedmonts. The same technique applied to other piedmonts will quantify the range of process rates on desert piedmont over different slopes, lithologies, climatic conditions, and tectonic environments.

The cosmogenic isotope technique utilized in Chapter 4 should be tested further. The variability of cosmogenic isotope abundance along each transect should be tested by analyzing separate collection sites and comparing results to the amalgamated sample. Such a test would illustrate the variability hidden in each amalgamated transect sample, and the variability of individual samples down piedmont. Also, as mentioned before, more soil profiles would better constrain deposition rates and unconformities.

The use of cosmogenic isotope on desert piedmonts is in its infancy. Cosmogenic isotopes can be used to determine deposition rates of different segments of alluvial fans by following the soil pit profile described in Chapter 4. Such deposition rates coupled with surface age estimates could resolve the effects of climatic change on deposition and sediment yield to piedmonts.

There is the potential to use cosmogenic isotopes to quantify rates of piedmont modification. Soil profiles of sediment mantled pediments (Mabbutt, 1966; Moss, 1977) could determine the rate at which pediments are unearthed. Direct measurements of rock-floored pediments could reveal average erosion rates, which could be compared with mountain mass erosion rates. Transects of bedrock erosion from piedmont junctions to mountain peaks could resolve the parallel retreat hypothesis of rangefronts.

The possibilities of using cosmogenic isotopes to address the "piedmont problem" are plentiful. I have only scratched the surface by quantifying sediment transport rates, sediment deposition rates, and sediment residence times for one piedmont. Further interest in rejuvenating piedmont research will answer many questions that are over 100 years old. However, to fully understand piedmont processes a multi-scale analysis appears most promising.

COMPREHENSIVE BIBLIOGRAPHY

Abrahams, A. D., Parsons, A. J., Cooke, R. U., and Reeves, R. W., 1984, Stone movement on hillslopes in the Mojave Desert, California: A 16-year record: Earth Surface Processes and Landforms, v. 9, p. 365-370.

Anderson, R. S., Repka, J. L., and Dick, G. S., 1996, Explicit treatment of inheritance in dating depositonal surfaces using in situ ^{10}Be and ^{26}Al: Geology, v. 24, p. 47-51.

Beaty, C. B., 1970, Age and estimated rate of accumulation of an alluvial fan, White Mountains, California, U.S.A.: American Journal of Science, v. 268, p. 50-77.

Bierman, P. R., 1994, Using in situ produced cosmogenic isotopes to estimate rates of landscape evolution: A review from the geomorphic perspective: Journal of Geophysical Research, v. 99, p. 13,885-13,896.

Bierman, P. R., and Steig, E., 1992, Using cosmogenic isotopes to measure basin-scale rates of erosion: Geological Society of America Abstracts with Programs Annual Meeting, v. 24, p. 122.

Bierman, P. R., and Steig, E. J., 1996, Estimating rates of denudation using cosmogenic isotope abundances in sediment: Earth surface processes and landforms, v. 21, p. 125-139.

Birkland, P. W., 1984, Soils and geomorphology: New York, Oxford University Press, 372 p.

BLM, 1986, Desert Training center California-Arizona Maneuver Area interpretive plan: Bureau of Land Management, California District.

Brook, E. J., Kurz, M. D., Denton, G. H., and Ackert, R. P. J., 1993, Chronology of Taylor Glacier advances in Arena Valley, Antarctica using in situ cosmogenic ^{3}He and ^{10}Be: Quaternary Research, v. 39, p. 11-23.

Brown, E. T., Stallard, R. F., Larsen, M. C., Raisbeck, G. M., and Yiou, F., 1995, Denudation rates determined from the accumulation of in situ-produced ^{10}Be in the Luquilo Experimental Forest, Puerto Rico: Earth and Planetary Science Letters, v. 129, p. 193-202.

Bull, W. B., 1964, Alluvial fans and near-surface subsidence in western Fresno County, California.: United States Geological Survey, 352-E.

Bull, W. B., 1977, The alluvial-fan environment: Progress in Physical Geography, v. 1, p. 222-270.

Bull, W. B., 1991, Geomorphic responses to climate change: New York, Oxford University Press, 326 p.

Bull, W. B., and Schick, A. P., 1979, Impact of climatic change on an arid watershed: Nahal Yael, southern Israel: Quaternary Research, v. 11, p. 153-171.

Clapp, E. M., and Bierman, P.R., 1996, Cosmo-Calibrate - a program for calibrating cosmogenic expoaure ages: Radiocarbon, v.38, no.1, p. 151.

Clapp, E. M., Bierman, P. R., and Caffee, M., 1997, Rates of erosion determined using in situ produced cosmogenic isotopes in a small arroyo basin, northwestern New Mexico: Geological Society of America annual meeting Abstracts with Programs, v. 29, p. 371-372.

Clapp, E. M., Bierman, P. R., and Caffee, M. W., 1999, Sediment generation and export rates in the Nahal Yael drainage basin, determined from cosmogenic ^{10}Be and

^{26}Al, Negev Desert, southern Israel, *in* Lekach, J., and Hassan, M. A., eds., Drainage Basin Dynamics and Morphology Conference Excursion - Negev Desert: Jerusalem, Geological Survey of Israel, p. 98-104.

Clapp, E. M., Bierman, P. R., Pavich, M., and Caffee, M., in review a, Rates of sediment supply to arroyos from upland erosion determined using *in situ*-produced cosmogenic ^{10}Be and ^{26}Al: Quaternary Research.

Clapp, E. M. Bierman, P. R., and Caffee, M.W., in review b, Using ^{10}Be and ^{26}Al to determine sediment generation rates and identify sediment source areas in an arid region drainage: Geomorphology.

Clark, D. H., Bierman, P. R., and Larsen, P., 1995, Improving *in situ* cosmogenic chronometers: Quaternary Research, v. 44, p. 367-377.

Cooke, R. U., 1970, Morphometric analysis of pediments and associated landforms in the western Mojave Desert, California: American Journal of Science, v. 269, p. 26-38.

Cooke, R. U., and Reeves, R. W., 1972, Relations between debris size and the slope of mountain fronts and pediments in the Mojave Desert, California: Zeitschrift für Geomorphologie, v. 16, p. 76-82.

Cooke, R. U., and Warren, A., 1973, Geomorphology in deserts: Berkeley, University of California Press, 394 p.

Davis, R., and Schaeffer, O. A., 1955, Chlorine-36 in nature.: Annals of New York Academy of Science, v. 62, p. 105-122.

Denny, C. S., 1967, Fans and pediments: American Journal of Science, v. 265, p. 81-105.

Doehring, D. O., 1970, Discrimination of pediments and alluvial fans from topographic maps: Geological Society of America Bulletin, v. 81, p. 3109-3116.

Dohrenwend, J. C., 1987, Basin and range, *in* Graf, W. L., ed., Geomorphic Systems of North America: Decade of North America Geology: Boulder, Colorado, Geological Society of America, p. 303-342.

Dunne, T., 1980, Formation and controls of channel networks: Progress in Physical Geography, v. 4, p. 211-239.

Dunne, T., and Leopold, L. B., 1978, Water in environmental planning: San Francisco, W. H. Freeman, 818 p.

Gilbert, G. K., 1877, Geology of the Henry Mountains (Utah): U.S. Geographical and Geological Survey of the Rocky Mountain Region.

Gosse, J. C., Evenson, E. B., Klein, J., Lawn, B., and Middleton, R., 1995a, Precise cosmogenic ^{10}Be measurements in western North America: Support for a global Younger Dryas cooling event: Geology, v. 23, p. 877-880.

Gosse, J. C., Klein, J., Evenson, E. B., Lawn, B., and Middleton, R., 1995b, Beryllium-10 dating of the duration and retreat of the last Pinedale glacial sequence: Science, v. 268, p. 1329-1333.

Gran, S. E., Matmon, A., Bierman, P., Enzel, Y., Caffee, M., and Rizzo, D., in review, Displacement history of a limestone normal fault scarp, northern Israel, from cosmogenic ^{36}Cl: Journal of Geophysical Research, Solid Earth.

Granger, D. E., Kirchner, J. W., and Finkel, R., 1996, Spatially averaged long-term erosion rates measured from *in situ* produced cosmogenic nuclides in alluvial sediment: The Journal of Geology, v. 104, p. 249-257.

Granger, D. E., Kirchner, J. W., and Finkel, R. C., 1997, Quaternary downcutting rate of the New River, Virginia, measured from differential decay of cosmogenic ^{26}Al and ^{10}Be in cave-deposited alluvium: Geology, v. 25, p. 107-110.

Greenbaum, N., Salmon, O., Gerson, R., and Schick, A. P., 1999, Slope runoff in a hyperarid region, *in* International Conference on Drainage Basin Dynamics and Morphology, Jerusalem, Israel, p. 201.

Hadley, R. F., 1967, Pediments and pediment-forming processes: Journal of Geological Education, v. 15, p. 83-89.

Harvey, A. M., 1984, Debris flows and fluvial deposits in Spanish Quaternary alluvial fans: implications for fan morphology, *in* Koster, E. H., and Steel, R. J., eds., Gravels and Conglomerates. Canadian Society of Petroleum Geologists Memoir, p. 123-132.

Heimsath, A. M., Dietrich, W. E., Nishiizumi, K., and Finkel, R. C., 1999, Cosmogenic nuclides, topography, and the spatial variation of soil depth: Geomorphology, v. 27, no. 1-2, p. 151-172.

Henley, D. C., 1989, "The land that God forgot..." The saga of Gen. George Patton's Desert Training Center, Western American History Series, 54 p.

Hillel, D., 1980, Fundamental of soil physics: New York, Academic Press, 486 p.

Hooke, R. L., 1967, Processes on arid-region alluvial-fans: Journal of Geology, v. 75, p. 438-460.

Hooke, R. L., 1968, Steady-state relationships on arid-region alluvial fans in closed basins: American Journal of Science, v. 266, p. 609-629.

Hooke, R. L., 1972, Geomorphic evidence for Late-Wisconsin and Holocene tectonic deformation, Death Valley, California: Bulletin of the Geological Society of America, v. 83, p. 2073-2098.

Horton, R., 1945, Erosional development of streams and their drainage basins: hydrophysical approach to quantitative morphology: Bulletin of the Geological Society of America, v. 57, p. 275-370.

Howard, A. D., 1942, Pediment passes and the pediment problem: Journal of Geomorphology, v. 5, no. 1, p. 3-31.

Iverson, R. M., 1980, Processes of accelerated pluvial erosion on desert hillslopes modified by vehicular traffic: Earth Surface Processes, v. 5, p. 369-388.

Iverson, R. M., Hinckley, B. S., Webb, R. M., and Hallet, B., 1981, Physical effects of vehicular disturbances on arid landscapes: Nature, v. 212, p. 915-917.

Kohl, C. P., and Nishiizumi, K., 1992, Chemical isolation of quartz for measurement of *in situ*-produced cosmogenic nuclides: Geochimica et Cosmochimica Acta, v. 56, p. 3583-3587.

Lal, D., 1988, *In situ*-produced cosmogenic isotopes in terrestrial rocks: Annual Reviews of Earth and Planetary Science, v. 16, p. 355-388.

Lal, D., 1991, Cosmic ray labeling of erosion surfaces: *In situ* nuclide production rates and erosion models: Earth and Planetary Science Letters, v. 104, p. 424-439.

Lal, D., and Arnold, J. R., 1985, Tracing quartz through the environment: Proceeding of the Indian Academy of Science, v. 94, no. 1, p. 1-5.

Laronne, J. B., Reid, I., Yitshak, Y., and Frostick, L. E., 1994, The non-layering of gravel streambeds under ephemeral flood regimes: Journal of Hydrology, v. 159, p. 353-363.

Laronne, J. B., and Reid, I., 1993, Very high rates of bedload sediment transport by ephemeral desert rivers: Nature, v. 366, no. November 11, p. 148-150.

Larsen, P. L., 1996, In-situ production rates of cosmogenic ^{10}Be and ^{26}Al over the past 21,500 years determined from the terminal moraine of the Laurentide Ice Sheet, north-central New Jersey [Masters thesis]: University of Vermont.

Lathrop, E. W., 1983, Recovery of perennial vegetation in military maneuver areas, *in* Webb, R. H., and Wilshire, H. G., eds., Environmental Effects of Off-Road Vehicles: New York, Springer-Verlag, p. 153-166.

Lawson, A. C., 1915, The epigene of the desert: University of California Publications Bulletin of the Department of Geology, v. 9, p. 23-48.

Lecce, S. A., 1990, The alluvial fan problem, *in* Rachocki, A. H., and Church, M., eds., Alluvial Fans A Field Approach: New York, John Wiley & Sons, p. 3-24.

Lekach, J., Amit, R., Grodek, T., and Schick, A. P., 1998, Fluvio-pedogenic processes in an ephemeral stream channel, Nahal Yael, Southern Negev, Israel: Geomorphology, v. 23, p. 353-369.

Lekach, J., and Schick, A. P., 1999, Sediment transport and sediment yield, *in* International Conference on Drainage Basin Dynamics and Morphology, Jerusalem, Israel, p. 201.

Mabbutt, J. A., 1966, Mantle-controlled plantation of pediments: American Journal of Science, v. 264, p. 78-91.

Mabbutt, J. A., 1977, Desert Landforms, An Introduction to Systematic Geomorphology: Cambridge, Massachusetts, The MIT Press, 81-100 p.

Machette, M., 1986, Calcium and magnesium carbonates, *in* Singer, M. J., and Janitzky, P., eds., Field and laboratory procedures used in a soil chronosequence study: Reston, Virginia, U. S. Geological Survey, p. 30-33.

Mammerickx, J., 1964, Quantitative observations on pediments in the Mojave and Sonoran Deserts (Southwestern United States): American Journal of Science, v. 262, p. 414-435.

Marsella, K. A., 1998, Timing and extent of glaciation in the Pangnirtung Fjord region, Baffin Island: Determined using *in situ* produced cosmogenic ^{10}Be and ^{26}Al [M. S. thesis]: University of Vermont, 135 p.

Mayer, L., and Bull, W. B., 1981, Impact of Pleistocene-Holocene climatic change on particle size distribution of fan deposits in southwestern Arizona: Geological Society of America Abstracts with Programs, v. 13, p. 95.

McFadden, L. D., Ritter, J. B., and Wells, S. G., 1989, Use of multiparameter relative-age methods for age estimation and correlation of alluvial fansurfaces on a desert piedmont, eastern Mojave Desert, California: Quaternary Research, v. 32, p. 276-290.

McGee, W. J., 1897, Sheetflood erosion: Bulletin of the Geological Society of America, v. 8, p. 87-112.

McKean, J. A., Dietrich, W. E., Finkel, R. C., Southon, J. R., and Caffee, M. W., 1993, Quantification of soil production and downslope creep rates from cosmogenic ^{10}Be accumulations on a hillslope profile: Geology, v. 21, p. 343-346.

Miller, D. H., Howard, K. A., and Anderson, J. L., 1981, Mylontic gneiss related to emplacement of a Cretaceous batholith: U..S. Geological Survey Open File Report.

Monaghan, M. C., McKean, J., Dietrich, W., and Klein, J., 1992, ^{10}Be chronometry of bedrock-to-soil conversion rates: Earth and Planetary Science Letters, v. 111, p. 483-492.

Montgomery, D. R., 1994, Road surface drainage, channel initiation, and slope instability: Water Resources Research, v. 30, no. 6, p. 1925-1932.

Montgomery, D. R., and Dietrich, W. E., 1994, Landscape dissection and drainage area-slope thresholds, *in* Krikby, M. J., ed., Process Models and Theoretical Geomorphology: New York, John Wiley & Sons Ltd., p. 221-246.

Moss, J. H., 1977, The formation of pediments: scarp backwearing or surface downwasting?, *in* Geomorphology in arid regions. 8th Binghamton symposium in geomorphology, Binghamton, NY, p. 51-78.

Nichols, K. K., and Bierman, P. R., in press, Fifty-four years of ephemeral channel response to intense military activity at Camp Iron Mountain, Mojave Desert, California, *in* Harmon, R., and Ehlen, J., eds., The environmental legacy of military operations.

Nilsen, T. H., and Moore, T. E., 1984, Bibliography of Alluvial-Fan Deposits: Norwich, Geo Books, 96 p.

Nishiizumi, K., Winterer, E. L., Kohl, C. P., Klein, J., Middleton, R., Lal, D., and Arnold, J. R., 1989, Cosmic ray production rates of ^{10}Be and ^{26}Al in quartz from glacially

polished rocks: Journal of Geophysical Research, v. 94, no. B12, p. 17,907-17,915.

NOAA, 1982, Monthly normals of temperature, precipitation, and heating and cooling degree days 1951-1980, California.: NOAA (National Oceanic and Atmospheric Administration).

Oberlander, T. M., 1972, Morphogensis of granitic boulder slopes in the Mojave Desert, California: The Journal of Geology, v. 80, p. 1-20.

Oberlander, T. M., 1974, Landscape inheritance and the pediment problem in the Mojave Desert of southern California: American Journal of Science, v. 274, p. 849-875.

Paige, S., 1912, Rock-cut surface in the desert ranges: Journal of Geology, v. 20, p. 442-450.

Parsons, A. J., and Abrahams, A. D., 1984, Mountain mass denudation and piedmont formation in the Mojave and Sonoran Deserts: American Journal of Science, v. 284, p. 255-271.

Phillips, F. M., Zreda, M. G., Smith, S. S., Elmore, D., Kubik, P. W., and Sharma, P., 1990, Cosmogenic Chlorine-36 chronology for glacial deposits at Bloody Canyon, eastern Sierra Nevada: Science, v. 248, p. 1529-1532.

Phillips, W. M., McDonald, E. V., Reneau, S. L., and Poths, J., 1998, Dating soils and alluvium with cosmogenic ^{21}Ne depth profiles: case studies from the Pajarito Plateau, New Mexico, USA: Earth and Planetary Science Letters, v. 160, p. 209-223.

Prose, D. V., 1985, Persisting effects of armored military maneuvers on some soils of the Mojave Desert: Environmental Geology Water Science, v. 7, p. 163-170.

Prose, D. V., Metzger, S. K., and Wilshire, H. G., 1987, Effects on substrate disturbance on secondary plant succession; Mojave Desert, California: Journal of Applied Ecology, v. 24, p. 305-313.

Rachocki, A., 1981, Alluvial fans an attempt at an empirical approach: New York, John Wiley & Sons, 161 p.

Reid, I., and Laronne, J. B., 1995, Bed load sediment transport in an ephemeral stream and a comparison with seasonal and perennial counterparts: Water Resources Research, v. 31, no. 3, p. 773-781.

Rich, J. L., 1935, Origin and evolution of rock fans and pediments: Bulletin of the Geological Society of America, v. 46, p. 999-1024.

Ritter, D. F., 1978, Process geomorphology: Debuque, Iowa, WM. C. Brown, 603 p.

Santos, D. L., 1999, Channel head initiation on a former WWII base camp Mojave desert, California [Senior thesis]: University of Vermont.

Schlesinger, W. H., Fonteyn, P. J., and Reiners, W. A., 1989, Effects of overland flow on plant water relations, erosion, and soil water percolation on a Mojave Desert Landscape: Soil Science Society of America Journal, v. 53, p. 1167-1172.

Schumm, S. A., 1962, Erosion of miniature pediments in Badlands National Monument, South Dakota: Geological Society of America Bulletin, v. 73, p. 719-724.

Small, E. E., Anderson, R. S., and Hancock, G. S., 1999, Estimates of the rate of regolith production using ^{10}Be and ^{26}Al from an alpine hillslope: Geomorphology, v. 27, p. 131-150.

Spaulding, W. G., and Graumlich, L. J., 1986, The last pluvial climatic episodes in the deserts of southwestern North America: Nature, v. 320, no. April 3, p. 441-444.

Spaulding, W. G., Leopold, E. B., and Devender, T. R. V., 1983, Late Wisconsin paleoecology of the American southwest, *in* H. E. Wright, J., ed., Late-Quaternary Environments of the United States: Stephen C. Porter: Minneapolis, University of Minnesota Press, p. 407.

Tarbuck, E. J., and Lutgens, F. K., 1996, Earth An Introduction to Physical Geology: Upper Saddle River, New Jersey, Prentice Hall, 605 p.

Thompson, G. R., and Turk, J., 1991, Modern Physical Geology: Philadelphia, Saunders College Publishing, 608 p.

Warnke, D. A., 1969, Pediment evolution in the Halloran Hills, Central Mojave Desert, California: Zeitschrift fur Geomorphologie, v. 13, p. 357-389.

Webb, R. H., Steiger, J. W., and Wilshire, H. G., 1986, Recovery of compacted soils in Mojave Desert ghost towns: Soil Science Society of America Journal, v. 50, p. 1341-1344.

Wells, S. G., and Harvey, A. M., 1987, Sedimentologic and geomorphic variations in storm-generated alluvial fans, Howgill Fells, northwest England.: Geological Society of America Bulletin, v. 98, p. 182-198.

Wells, S. G., McFadden, L. D., and Dohrenwend, J. C., 1987, Influence of Late Quaternary climatic changes on geomorphic and pedogenic processes on a desert piedmont, eastern Mojave Desert, California: Quaternary Research, v. 27, p. 130-146.

Wemple, B. C., Jones, J. A., and Grant, G. E., 1996, Channel network extension by logging roads in two basins, Western Cascades, Oregon: Water Resources Bulletin, v. 32, no. 6, p. 1195-1207.

Whipple, K. V., and Dunne, T., 1992, Debris-flow fans in Owens Valley, California: Geological Society of America Bulletin, v. 104.

Whitaker, C. R., 1973, Pediments: A Bibliography: Norwich, England, GeoAbstracts Ltd., 95 p.

Whitaker, C. R., 1979, The use of the term "pediment" and related terminology: Zeitschrift für Geomorphologie, v. 23, p. 427-439.

Wilshire, H. G., and Webb, R. H., 1980, Recovery of soils and vegetation in a Mojave Desert ghost town, Nevada, U.S.A.: Journal of Arid Environments, v. 3, p. 1-15.

Yair, A., 1999, Sede Boquer research site, *in* International Conference on Drainage Basin Dynamics and Morphology, Jerusalem, Israel, p. 201.

APPENDIX A: Survey data

All plot locations are arbitrary. Control plots were randomized by dropping pebbles onto field map. Walkway and road plots were chosen by criteria described in Methods section of Chapter 3. Upper boundary for control and walkway plots was set orthogonal to steepest gradient. Upper boundary for road plots was the defined as the road berm.

Control Plot 1

Northing [a]	Easting [a]	Elevation [b]	Feature code [c]	Depth (m) [d]	Width (m) [e]	Cross (m^2) [f]
3775837.128	670515.23	345.344	CH1 LT	0.35	2.95	0.79
3775835.795	670516.064	344.993	CH1 LB			
3775835.259	670516.248	344.99	CH1 RB	0.18		
3775834.516	670516.606	345.173	CH1 RT			
3775834.938	670518.804	345.078	CH1 RT	0.15	2.87	0.46
3775835.961	670518.582	344.925	CH1 RB			
3775836.556	670518.219	344.92	CH1 LB	0.16		
3775837.674	670517.945	345.085	CH1 LT			
3775843.34	670511.468	345.286	HEAD			
3775843.469	670513.472	345.255	CH2 LT	0.07	1.96	0.27
3775843.028	670513.29	345.189	CH2 LB			
3775842.471	670513.195	345.186	CH2 RB	0.21		
3775841.583	670512.931	345.399	CH2 RT			
3775841.521	670514.406	345.183	CH2 RT	0.09	1.33	0.08
3775841.662	670514.557	345.097	CH2 RB			
3775842.026	670514.887	345.129	CH2 LB	0.04		
3775842.389	670515.413	345.169	CH2 LT			
3775839.82	670512.45	345.444	HEAD			
3775838.731	670516.512	345.261	CH2 RT	0.26	2.11	0.37
3775839.232	670517.139	345.005	CH2 RB			
3775839.704	670517.512	344.979	CH2 LB	0.10		
3775840.162	670518.058	345.079	CH2 LT			
3775837.075	670522.736	344.86	CH2 LT	0.08	1.77	0.11
3775836.683	670522.674	344.778	CH2 LB			
3775836.199	670522.432	344.777	CH2 RB	0.04		
3775835.368	670522.26	344.816	CH2 RT			
3775833.894	670525.326	344.799	CH2 RT	0.12	1.27	0.13
3775834.201	670525.371	344.682	CH2 RB			
3775834.775	670525.492	344.668	CH2 LB	0.09		
3775835.099	670525.728	344.758	CH2 LT			
3775835.433	670528.884	344.673	CH2 LT	0.10	1.23	0.13
3775835.22	670528.898	344.573	CH2 LB			
3775834.767	670529.029	344.563	CH2 RB	0.11		
3775834.213	670529.018	344.675	CH2 RT			
3775835.166	670531.172	344.609	CH2 RT	0.13	0.86	0.11
3775835.417	670531.042	344.478	CH2 RB			
3775835.661	670530.926	344.493	CH2 TB	0.13		
3775835.922	670530.76	344.621	CH2 LT			
3775836.78	670529.533	344.634	HEAD			
3775835.995	670533.923	344.431	CH2 LT	0.08	1.82	0.13

3775835.694	670533.842	344.353	CH2 LB			
3775834.927	670533.685	344.355	CH2 RB	0.06		
3775834.189	670533.73	344.416	CH2 RT			
3775833.833	670535.29	344.384	CH2 RT	0.12	1.40	0.19
3775833.982	670535.444	344.26	CH2 RB			
3775834.44	670535.778	344.251	CH2 LB	0.15		
3775834.909	670536.179	344.402	CH2 LT			
3775837.504	670496.63	346.349	BERM T			
3775842.169	670490.743	346.388	BERM T			
3775845.789	670486.231	346.509	BERM T			
3775845.58	670485.428	346.446	BERM B			
3775841.845	670489.937	346.237	BERM B			
3775837.951	670494.14	346.028	BERM B			
3775838.616	670484.156	346.553	BERM RB			
3775841.167	670480.821	346.708	BERM RB			
3775840.668	670480.485	346.842	BERM RT			
3775838.579	670482.619	346.75	BERM RT			
3775848.782	670482.536	346.417	HEAD			
3775849.943	670485.8	346.374	CH3 LT	0.14	1.63	0.25
3775849.587	670485.864	346.235	CH3 LB			
3775848.841	670486.017	346.211	CH3 RB	0.17		
3775848.392	670486.302	346.384	CH3 RT			
3775848.123	670489.104	346.166	CH3 RT	0.13	0.94	0.12
3775848.221	670489.314	346.033	CH3 RB			
3775848.468	670489.566	346.047	CH3 LB	0.12		
3775848.798	670489.76	346.163	CH3 LT			
3775847.492	670491.528	346.08	CH3 LT	0.08	1.65	0.24
3775847.133	670491.625	345.997	CH3 LB			
3775846.464	670491.663	345.958	CH3 RB	0.21		
3775845.851	670491.679	346.165	CH3 RT			
3775845.821	670495.684	345.935	CH3 RT	0.13	1.72	0.24
3775846.369	670495.887	345.801	CH3 RB			
3775847.077	670496.007	345.794	CH3 LB	0.15		
3775847.541	670495.742	345.942	CH3 LT			
3775848.137	670501.257	345.687	CH3 LT	0.10	2.15	0.20
3775847.626	670501.382	345.586	CH3 LB			
3775846.628	670501.302	345.567	CH3 RB	0.09		
3775845.989	670501.333	345.655	CH3 RT			
3775845.321	670508.66	345.427	CH3 RT	0.05	2.52	0.29
3775845.551	670508.71	345.377	CH3 RB			
3775847.05	670509.035	345.353	CH3 LB	0.18		
3775847.742	670509.343	345.535	CH3 LT			
3775846.303	670517.679	345.381	CH3 LT	0.27	2.80	0.46
3775845.571	670517.759	345.114	CH3 LB			
3775844.304	670517.472	345.12	CH3 RB	0.06		
3775843.53	670517.321	345.18	CH3 RT			
3775841.733	670520.37	345.115	CH3 RT	0.16	2.60	0.40
3775842.287	670520.492	344.952	CH3 RB			
3775842.86	670520.733	344.939	CH3 LB	0.14		
3775844.05	670521.56	345.082	CH3 LT			

3775842.747	670528.063	344.828	CH3 LT	0.13	2.14	0.29
3775842.055	670527.967	344.699	CH3 LB			
3775840.988	670527.687	344.712	CH3 RB	0.14		
3775840.644	670527.679	344.853	CH3 RT			
3775839.361	670534.94	344.453	CH3 RW		1.58	
3775840.852	670535.458	344.463	CH3 LW			
3775840.206	670540.354	344.314	CH3 LW		2.78	0.23
3775837.943	670540.375	344.27	CH3 RB	0.16		
3775837.426	670540.264	344.434	CH3 RT			
3775860.017	670483.467	346.533	CH4 RT	0.13	3.05	0.54
3775860.631	670483.527	346.402	CH4 RB			
3775862.229	670483.936	346.377	CH4 LB	0.22		
3775862.983	670484.193	346.601	CH4 LT			
3775860.302	670488.028	346.292	CH4 LT	0.11	3.53	0.44
3775859.802	670487.752	346.179	CH4 LB			
3775857.669	670486.837	346.229	CH4 RB	0.14		
3775857.108	670486.524	346.368	CH4 RT			
3775855.948	670491.627	346.23	CH4 RT	0.19	2.78	0.43
3775856.301	670491.601	346.041	CH4 RB			
3775857.36	670491.675	346.007	CH4 LB	0.12		
3775858.534	670492.635	346.125	CH4 LT			
3775857.739	670496.397	345.971	CH4 LW		2.67	0.30
3775855.673	670496.492	345.853	CH4 RB	0.22		
3775855.075	670496.491	346.078	CH4 RT			
3775859.169	670497.1	346.029	HEAD			
3775856.965	670501.894	345.792	CH4 LW		2.43	0.10
3775855.081	670501.857	345.697	CH4 RB	0.08		
3775854.541	670501.733	345.781	CH4 RT			
3775853.457	670504.995	345.727	CH4 RW		3.05	0.12
3775855.961	670505.634	345.61	CH4 LB	0.08		
3775856.435	670505.643	345.688	CH4 LT			
3775855.632	670509.148	345.561	CH4 LW		2.74	0.22
3775853.467	670509.551	345.512	CH4 RB	0.16		
3775852.934	670509.603	345.673	CH4 RT			
3775851.808	670515.257	345.46	CH4 RT	0.08	4.72	0.35
3775852.094	670515.113	345.381	CH4 RB			
3775855.406	670518.099	345.202	CH4 LB	0.07		
3775855.644	670518.002	345.272	CH4 LT			
3775854.611	670521.349	345.123	CH4 RW		4.50	
3775859.11	670521.417	345.037	CH4 LW			
3775860.362	670524.453	345.049	CH4 LT	0.14	1.42	0.16
3775860.084	670524.522	344.904	CH4 LB			
3775859.172	670524.431	344.926	CH4 RB	0.08		
3775858.943	670524.513	345.002	CH4 RT			
3775858.121	670530.1	344.778	CH4 RT	0.08	2.97	0.12
3775858.328	670530.065	344.697	CH4 RB			
3775861.06	670530.527	344.754	CH4 LW			
3775861.653	670537.784	344.496	CH4 LB	0.08		
3775861.84	670537.886	344.575	CH4 LT		2.93	
3775859.214	670537.379	344.437	CH4 RB	0.03		

3775858.958	670537.365	344.467	CH4 RT			
3775856.886	670542.532	344.37	CH4 RT	0.14	2.99	0.32
3775857.463	670542.623	344.229	CH4 RB			
3775859.384	670542.85	344.253	CH4 LB	0.07		
3775859.848	670542.974	344.327	CH4 LT			
3775868.734	670543.96	344.572	CH5 LT	0.17	2.41	0.33
3775867.703	670543.806	344.406	CH5 LB			
3775867.201	670543.737	344.387	CH5 RB	0.11		
3775866.369	670543.498	344.498	CH5 RT			
3775866.952	670540.492	344.727	CH5 RT	0.19	1.89	0.23
3775867.882	670540.44	344.541	CH5 RB			
3775868.358	670540.671	344.484	CH5 LB	0.06		
3775868.831	670540.672	344.542	CH5 LT			
3775868.063	670538.895	344.578	HEAD			
3775833.061	670540.196	344.527	BENCH CK			
3775833.056	670540.188	344.535	CK BENCH			
3775870.558	670484.522	346.609	CH6 LT	0.15	2.00	0.36
3775870.198	670484.417	346.458	CH6 LB			
3775869.309	670484.322	346.468	CH6 RB	0.20		
3775868.57	670484.276	346.672	CH6 RT			
3775866.416	670489.182	346.454	CH6 RT	0.12	2.72	0.35
3775866.68	670489.301	346.337	CH6 RB			
3775867.966	670489.895	346.247	CH6 LB	0.14		
3775868.978	670490.083	346.386	CH6 LT			
3775865.325	670495.606	346.195	CH6 LT	0.12	1.70	0.21
3775865.095	670495.559	346.072	CH6 LB			
3775863.97	670495.068	346.058	CH6 RB	0.12		
3775863.735	670495.003	346.178	CH6 RT			
3775860.562	670500.986	345.94	CH6 RT	0.07	2.00	0.18
3775860.827	670501.062	345.865	CH6 RB			
3775861.899	670501.932	345.849	CH6 LB	0.11		
3775862.148	670502.212	345.957	CH6 LT			
3775858.464	670506.364	345.8	CH6 LT	0.14		
3775858.164	670506.205	345.663	CH6 LB			
3775856.798	670526.244	344.969	HEAD			
3775856.753	670525.137	345.009	HEAD			
3775857.834	670522.861	345.045	HEAD			
3775854.771	670526.913	344.911	HEAD			
3775853.558	670531.312	344.791	CH7 RT	0.09	2.00	0.20
3775853.919	670531.598	344.704	CH7 RB			
3775854.922	670531.957	344.663	CH7 LB	0.11		
3775855.322	670532.257	344.772	CH7 LT			
3775852.356	670537.253	344.588	CH7 LT	0.10	2.18	0.26
3775851.898	670536.926	344.484	CH7 LB			
3775850.794	670536.256	344.46	CH7 RB	0.14		
3775850.526	670536.064	344.595	CH7 RT			
3775847.252	670541.566	344.306	CH7 RT	0.09	1.68	0.22
3775847.72	670541.743	344.215	CH7 RB			
3775848.447	670541.915	344.154	CH7 LB	0.17		
3775848.895	670541.899	344.326	CH7 LT			

3775861.395	670518.876	345.164	HEAD			
3775866.134	670513.107	345.448	HEAD			
3775865.556	670522.042	345.136	CH8 LT	0.05	1.71	0.10
3775865.393	670522.133	345.085	CH8 LB			
3775864.188	670522.456	345.036	CH8 RB	0.07		
3775863.897	670522.457	345.107	CH8 RT			
3775863.976	670529.375	344.91	CH8 RT	0.07	1.82	0.17
3775864.173	670529.394	344.836	CH8 RB			
3775865.196	670529.887	344.826	CH8 LB	0.12		
3775865.572	670530.245	344.944	CH8 LT			
3775862.736	670533.326	344.712	CH8 LT	0.08		
3775862.466	670533.199	344.63	CH8 LB			
3775877.372	670485.302	346.691	CH9 LT	0.04	1.58	0.10
3775876.902	670485.133	346.646	CH9 LB			
3775876.305	670484.983	346.632	CH9 RB	0.08		
3775875.864	670484.82	346.712	CH9 RT			
3775873.758	670491.173	346.463	CH9 RT	0.07	1.44	0.09
3775874.147	670491.303	346.396	CH9 RB			
3775874.759	670491.505	346.377	CH9 LB	0.05		
3775875.121	670491.648	346.429	CH9 LT			
3775873.364	670498.454	346.2	CH9 LT	0.08	1.67	
3775873.151	670498.445	346.121	CH9 LB			
3775871.69	670498.443	346.102	CH9 RW			
3775870.685	670502.374	345.951	CH9 RT	0.05	1.17	0.08
3775871.08	670502.421	345.902	CH9 RB			
3775871.588	670502.624	345.902	CH9 LB	0.09		
3775871.833	670502.613	345.993	CH9 LT			
3775870.843	670514.262	345.594	CH9 LT	0.12	1.21	0.12
3775870.441	670514.171	345.474	CH9 LB			
3775870.016	670513.981	345.454	CH9 RB	0.07		
3775869.733	670513.77	345.525	CH9 RT			
3775865.972	670517.826	345.298	CH9 RT	0.10	1.24	0.13
3775866.231	670517.966	345.196	CH9 RB			
3775866.627	670518.457	345.216	CH9 LB	0.11		
3775866.927	670518.618	345.322	CH9 LT			
3775885.837	670486.185	346.627	CH10 LT	0.11	3.17	0.36
3775885.206	670486.186	346.515	CH10 LB			
3775883.083	670485.928	346.505	CH10 RB	0.11		
3775882.663	670486.185	346.618	CH10 RT			
3775882.228	670493.339	346.324	CH10 RT	0.03	3.34	0.26
3775882.402	670493.329	346.293	CH10 RB			
3775885.122	670493.606	346.241	CH10 LB	0.13		
3775885.563	670493.564	346.368	CH10 LT			
3775882.402	670501.338	345.999	CH10 LT	0.03	1.43	0.06
3775882.265	670501.28	345.968	CH10 LB			
3775881.147	670501.204	345.999	CH10 RB	0.05		
3775880.978	670501.187	346.048	CH10 RT			
3775879.487	670508.883	345.715	CH10 RW		6.02	
3775884.156	670512.676	345.592	CH10 LW			
3775880.334	670522.42	345.264	CH10 LT	0.01	4.23	0.03

3775880.172	670522.406	345.249	CH10 LB			
3775876.193	670523.274	345.231	CH10 RW			
3775875.542	670532.007	344.97	CH10 RW		8.21	
3775883.73	670531.394	344.923	CH10 LW			
3775884.285	670543.477	344.533	CH10 LW			
3775883.469	670545.384	344.534	CH10 LT	0.05	6.56	0.44
3775883.225	670545.345	344.482	CH10 LB			
3775877.347	670544.644	344.407	CH10 RB	0.08		
3775876.966	670544.52	344.489	CH10 RT			
3775889.436	670486.835	346.608	CH11 RT	0.08	1.66	0.11
3775889.632	670486.87	346.525	CH11 RB			
3775890.891	670487.078	346.532	CH11 LB	0.05		
3775891.074	670487.12	346.585	CH11 LT			
3775890.302	670494.04	346.376	CH11 LT	0.09	2.70	0.15
3775889.986	670493.862	346.289	CH11 LB			
3775887.969	670494.242	346.281	CH11 RB	0.02		
3775887.608	670494.134	346.305	CH11 RT			
3775885.358	670499.17	346.075	CH11 RW		2.94	
3775887.17	670501.481	346.02	CH11 LW			
3775894.767	670498.602	346.162	HEAD			
3775893.148	670501.904	346.12	CH12 LT	0.07	1.24	0.08
3775892.93	670501.798	346.051	CH12 LB			
3775892.231	670501.834	346.045	CH12 RB	0.05		
3775891.913	670501.771	346.099	CH12 RT			
3775890.163	670506.469	345.915	CH12 RW		6.05	
3775893.868	670511.248	345.717	CH12 LW			
3775894.079	670515.504	345.524	CH12 LT	0.08	1.05	0.09
3775893.827	670515.649	345.446	CH12 LB			
3775893.361	670515.884	345.458	CH12 RB	0.10		
3775893.107	670515.897	345.56	CH12 RT			
3775892.971	670519.793	345.395	CH12 RT	0.13	1.55	0.15
3775893.467	670520.085	345.26	CH12 RB			
3775894.243	670520.332	345.296	CH12 LB	0.06		
3775894.443	670520.275	345.361	CH12 LT			
3775890.499	670528.986	345.052	CH12 LT	0.05	1.41	0.10
3775890.204	670528.834	344.998	CH12 LB			
3775889.479	670528.558	344.972	CH12 RB	0.08		
3775889.174	670528.518	345.055	CH12 RT			
3775888.643	670523.684	345.208	HEAD			
3775885.287	670532.608	344.893	CH12 RW		4.84	
3775886.837	670537.198	344.773	CH12 LW			
3775883.819	670542.328	344.552	CH12 LW		3.71	
3775882.163	670539.003	344.625	CH12 RW			
3775894.599	670524.665	345.268	HEAD			
3775892.917	670529.771	345.132	CH13 LT	0.10	1.27	0.08
3775892.428	670529.61	345.033	CH13 LB			
3775892.147	670529.411	345.04	CH13 RB	0.02		
3775891.756	670529.246	345.059	CH13 RT			
3775890.025	670533.733	344.919	CH13 RW		2.20	0.08
3775891.238	670535.571	344.966	CH13 LT	0.07		

3775890.862	670535.446	344.897	CH13 LB			
3775887.002	670540.754	344.617	CH13 LB	0.04		
3775887.124	670540.936	344.661	CH13 LT		1.93	
3775885.207	670540.68	344.605	CH13 RW			
3775896.287	670510.996	345.739	CH14 RT	0.06	1.28	0.07
3775896.551	670511.155	345.68	CH14 RB			
3775896.809	670511.715	345.651	CH14 LB	0.05		
3775896.935	670512.096	345.704	CH14 LT			
3775896.362	670515.269	345.605	CH14 LT	0.10	1.10	0.09
3775896.232	670515.119	345.509	CH14 LB			
3775895.669	670514.932	345.483	CH14 RB	0.07		
3775895.416	670514.703	345.553	CH14 RT			
3775894.445	670515.891	345.487	CH14 RT	0.08	1.51	0.13
3775894.723	670516	345.41	CH14 RB			
3775895.25	670516.42	345.429	CH14 LB	0.10		
3775895.645	670516.807	345.526	CH14 LT			
3775833.055	670540.198	344.526	BENCH CK			

[a] Determined using Trimble 4400 differential Global Positioning System with NAD State Plane 27 datum. Data are percise to centimeter-scale, however are accurate to ± 30 m because GPS was not tied to real coordinates.

[b] Elevations are not tied into real elevations

[c] CH = channel number, R = right, L = left, B = bottom bank, T = top bank W = wash, HEAD = channel head, BERM =road berm, BAR = channel bar, ROCK = rock alignment, TOPO = topographic points, BENCH = benchmark

[d] determined by subtracting bottom bank points from top bank points

[e] determined using Pythagreom theorem on Northing and Easting coordinates

[f] determined by multiplying average depth by width

Control Plot 2

Northing	Easting	Elevation	Feature code	Depth (m)	Width (m)	Cross (m^2)
3773773.825	668327.584	421.898	HEAD			
3773775.104	668328.701	421.886	HEAD			
3773774.197	668329.47	421.871	CH1 LT	0.08	1.05	0.09
3773774.111	668329.427	421.794	CH1 LB			
3773773.325	668329.41	421.775	CH1 RB	0.10		
3773773.162	668329.283	421.875	CH1 RT			
3773773.185	668330.289	421.842	CH1 RT	0.09	0.89	0.07
3773773.235	668330.275	421.754	CH1 RB			
3773773.888	668330.328	421.762	CH1 LB	0.07		
3773774.071	668330.341	421.835	CH1 LT			
3773773.908	668336.039	421.612	DEL			
3773772.678	668335.242	421.682	CH1 LT	0.06	1.61	0.09
3773772.581	668335.206	421.627	CH1 LB			
3773771.495	668334.492	421.62	CH1 RB	0.06		
3773771.261	668334.486	421.675	CH1 RT			
3773769.795	668336.425	421.632	CH1 RT	0.11	1.06	0.09
3773769.856	668336.438	421.525	CH1 RB			
3773770.501	668337.15	421.538	CH1 LB	0.07		

3773766.635	668343.172	421.303	CH1 RB	0.08		
3773766.485	668342.841	421.388	CH1 RT			
3773774.366	668329.69	421.836	CH2 RT	0.04	0.85	0.05
3773774.554	668329.68	421.795	CH2 RB			
3773775.087	668329.891	421.765	CH2 LB	0.08		
3773775.183	668329.917	421.842	CH2 LT			
3773787.539	668318.117	422.315	CH3 LT	0.04	1.05	0.06
3773787.444	668318.068	422.274	CH3 LB			
3773786.768	668317.907	422.281	CH3 RB	0.07		
3773786.557	668317.749	422.353	CH3 RT			
3773783.41	668321.773	422.185	CH3 RT	0.07	1.71	0.09
3773783.657	668321.866	422.118	CH3 RB			
3773784.798	668322.595	422.115	CH3 LB	0.03		
3773784.842	668322.716	422.148	CH3 LT			
3773779.147	668330.114	421.813	CH3 LW		1.87	0.07
3773777.683	668329.533	421.803	CH3 LRB	0.07		
3773777.43	668329.384	421.877	CH3 RT			
3773772.905	668335.38	421.628	CH3 RT	0.04	1.26	
3773773.091	668335.57	421.591	CH3 RB			
3773773.92	668336.123	421.615	CH3 LW			
3773771.551	668338.618	421.471	CH3 LW		1.21	0.05
3773770.978	668337.693	421.5	CH3 RB	0.08		
3773770.97	668337.551	421.578	CH3 RT			
3773773.596	668339.194	421.618	TOPO			
3773771.28	668342.177	421.555	TOPO			
3773774.111	668339.393	421.545	TOPO			
3773778.511	668333.887	421.719	TOPO			
3773778.271	668332.969	421.827	TOPO			
3773782.542	668328.496	422.05	TOPO			
3773783.149	668328.744	421.953	TOPO			
3773790.371	668330.923	421.978	TOPO			
3773789.665	668349.828	421.224	HEAD			
3773788.615	668352.235	421.176	CH4 LT	0.06	0.71	0.05
3773788.563	668352.192	421.115	CH4 LB			
3773788.199	668351.935	421.105	CH4 RB	0.07		
3773788.028	668351.832	421.172	CH4 RT			
3773786.368	668353.386	421.063	CH4 RT	0.06	0.51	0.03
3773786.409	668353.428	421.003	CH4 RB			
3773786.633	668353.685	421.012	CH4 LB	0.04		
3773786.658	668353.806	421.053	CH4 LT			
3773785.939	668354.847	420.983	CH4 LT	0.05	0.68	0.04
3773785.775	668354.806	420.935	CH4 LB			
3773785.434	668354.718	420.927	CH4 RB	0.06		
3773785.272	668354.72	420.991	CH4 RT			
3773784.284	668359.424	420.803	CH4 RW		0.62	
3773784.899	668359.464	420.81	CH4 LW			
3773784.757	668362.07	420.755	CH4 LT	0.06	0.61	0.03
3773784.611	668362.01	420.694	CH4 LB			
3773784.374	668361.811	420.699	CH4 RB	0.02		
3773784.203	668361.807	420.723	CH4 RT			

3773780.641	668364.787	420.601	CH4 RT	0.13	1.25	0.15
3773780.931	668364.852	420.472	CH4 RB			
3773781.487	668365.183	420.489	CH4 LB	0.11		
3773781.698	668365.453	420.597	CH4 LT			
3773779.533	668369.09	420.433	CH4 LT	0.11	1.13	0.13
3773779.449	668369.017	420.327	CH4 LB			
3773778.883	668368.587	420.344	CH4 RB	0.12		
3773778.585	668368.466	420.459	CH4 RT			
3773775.363	668376.359	420.142	CH4 RT	0.07	1.49	0.13
3773775.424	668376.367	420.076	CH4 RB			
3773776.653	668376.876	420.043	CH4 LB	0.10		
3773776.728	668376.96	420.146	CH4 LT			
3773775.132	668373.107	420.278	HEAD			
3773775.5	668373.656	420.251	CH5 LT	0.04	0.67	0.03
3773775.391	668373.731	420.206	CH5 LB			
3773775.174	668373.942	420.195	CH5 RB	0.04		
3773775.074	668374.17	420.237	CH5 RT			
3773789.227	668357.935	421.039	HEAD			
3773787.56	668359.774	420.931	CH6 LT	0.07	0.64	0.04
3773787.522	668359.703	420.864	CH6 LB			
3773787.296	668359.393	420.877	CH6 RB	0.06		
3773787.19	668359.251	420.94	CH6 RT			
3773786.348	668350.698	421.208	HEAD			
3773786.569	668352.631	421.11	CH7 LT	0.09	0.73	0.05
3773786.482	668352.541	421.019	CH7 LB			
3773786.075	668352.159	421.053	CH7 RB	0.06		
3773785.982	668352.189	421.111	CH7 RT			
3773805.487	668330.969	422.01	HEAD			
3773804.552	668332.964	421.966	CH8 LT	0.08	0.61	0.05
3773804.517	668332.941	421.886	CH8 LB			
3773804.109	668332.667	421.882	CH8 RB	0.08		
3773804.023	668332.669	421.961	CH8 RT			
3773801.582	668335.817	421.828	CH8 RT	0.05	0.67	0.05
3773801.622	668335.828	421.775	CH8 RB			
3773802.15	668335.89	421.771	CH8 LB	0.08		
3773802.246	668335.858	421.855	CH8 LT			
3773833.024	668329.316	422.469	CH8 LT	0.06	6.53	0.46
3773832.879	668329.277	422.405	CH8 LB			
3773826.831	668327.776	422.468	CH8 RB	0.08		
3773826.71	668327.66	422.546	CH8 RT			
3773824.602	668333.183	422.375	CH8 RT	0.07	7.78	0.28
3773824.672	668333.178	422.302	CH8 RB			
3773831.439	668336.904	422.201	CH8 LW			
3773828.751	668335.914	422.218	CH8-9SPLITW			
3773826.27	668341.4	421.993	CH8 LW		3.55	0.27
3773823.102	668340.406	422.017	CH8 RB	0.15		
3773822.882	668340.355	422.17	CH8 RT			
3773819.891	668345.958	421.91	CH8 RT	0.08	4.52	0.18
3773820.132	668346.031	421.832	CH8 RB			
3773823.605	668348.534	421.833	CH8 LW			

3773820.948	668354.918	421.631	CH8 LW		5.51	0.16
3773816.222	668352.715	421.531	CH8 RB	0.06		
3773815.948	668352.603	421.59	CH8 RT			
3773810.002	668361.032	421.305	CH8 RT	0.09	7.03	0.31
3773810.108	668361.084	421.217	CH8 RB			
3773816.105	668364.513	421.284	CH8 LW			
3773808.983	668370.074	420.972	CH8 LW		3.62	
3773805.66	668368.635	420.976	CH8 RW			
3773795.958	668381.249	420.478	CH8 RT	0.09	2.07	0.09
3773796.085	668381.21	420.392	CH8 RB			
3773797.793	668382.203	420.439	CH8 LW			
3773818.082	668387.323	420.587	CH9 TR	0.09		
3773818.328	668387.386	420.494	CH9 RB			
3773819.281	668385.003	420.548	CH9-10 SPLITB			
3773819.083	668385.363	420.604	CH9-10 SPLITT			
3773817.724	668384.99	420.55	CH10 RB	0.08		
3773817.39	668385.063	420.634	CH10 RT			
3773816.71	668385.918	420.597	CH10 RT	0.10	1.38	0.12
3773817.004	668386.019	420.498	CH10 RB			
3773817.644	668386.536	420.504	CH10 LB	0.08		
3773817.86	668386.689	420.585	CH10 LT			
3773817.841	668387.221	420.598	TOPO			
3773818.113	668386.83	420.62	TOPO			
3773817.299	668387.525	420.47	TOPO			
3773817.606	668387.63	420.569	TOPO			
3773816.878	668387.458	420.436	TOPO			
3773816.636	668387.354	420.437	TOPO			
3773816.138	668387.269	420.536	TOPO			
3773815.864	668387.018	420.574	TOPO			
3773820.171	668380.91	420.761	CH9 RT	0.07		
3773820.388	668380.979	420.695	CH9 RB			
3773821.232	668377.063	420.844	CH9 RB	0.08		
3773821.087	668376.987	420.923	CH9 RT			
3773822.726	668370.398	421.126	CH9 RT	0.09		
3773822.763	668370.43	421.031	CH9 RB			
3773824.403	668366.908	421.141	CH9 RB	0.07		
3773824.39	668366.821	421.207	CH9 RT			
3773828.961	668346.836	421.921	CH9 RW			
3773826.92	668343.065	421.997	CH9 RW			
3773826.929	668342.031	422.036	CH9 RW			
3773828.961	668337.721	422.167	CH9 RW			
3773808.571	668381.681	420.598	HEAD			
3773807.49	668384.252	420.528	CH11 LW		0.85	
3773806.688	668383.97	420.541	CH11 RW			

Control Plot 3

Northing	Easting	Elevation	Feature code	Depth (m)
3775600.152	669973.556	369.374	CH2 RT	0.06

3775600.398	669973.822	369.313	CH2 RB	
3775599.305	669975.973	369.232	CH2 RB	0.10
3775598.987	669975.983	369.33	CH2 RT	
3775598.427	669978.106	369.219	CH2 RT	0.10
3775598.698	669978.164	369.116	CH2 RB	
3775599.135	669980.014	369.057	CH2 RB	0.08
3775598.897	669980.066	369.136	CH2 RT	
3775597.223	669983.145	368.964	CH2 RT	0.06
3775597.356	669983.228	368.907	CH2 RB	
3775596.117	669985.097	368.831	CH2 RB	0.14
3775596.005	669984.984	368.971	CH2 RT	
3775595.506	669985.683	368.937	CH2 RT	0.11
3775595.488	669985.757	368.828	CH2 RB	
3775595.193	669985.315	368.946	CH2 RT	0.10
3775595.109	669985.511	368.843	CH2 RB	
3775594.612	669984.793	368.921	CH2 RB	0.04
3775594.717	669984.737	368.96	CH2 RT	
3775594.651	669983.838	369.004	CH2 RT	0.03
3775594.545	669983.837	368.973	CH2 RB	
3775594.432	669983.275	369.036	HEAD	
3775594.269	669984.14	368.976	CH2 RT	0.04
3775594.389	669984.226	368.94	CH2 RB	
3775594.434	669985.189	368.904	CH2 RB	0.04
3775594.336	669985.204	368.946	CH2 RT	
3775594.933	669986.099	368.886	CH2 RT	0.11
3775595.071	669986.185	368.776	CH2 RB	
3775594.557	669987.188	368.735	CH2 RB	0.12
3775594.509	669987.146	368.855	CH2 RT	
3775593.119	669989.044	368.786	CH2 RT	0.11
3775593.174	669989.06	368.677	CH2 RB	
3775591.177	669991.243	368.621	CH2 RB	0.05
3775591.076	669991.179	368.673	CH2 RT	
3775592.416	669996.846	368.634	CH2 LT	0.10
3775592.33	669996.771	368.531	CH2 LB	
3775593.678	669994.918	368.587	CH2 LB	0.12
3775593.954	669995.065	368.703	CH2 LT	
3775595.417	669993.113	368.769	CH2 LT	0.16
3775595.034	669992.784	368.613	CH2 LB	
3775596.935	669989.579	368.686	CH2 LB	0.17
3775597.099	669989.924	368.855	CH2 LT	
3775599.618	669986.479	368.88	CH2 LT	0.06
3775599.531	669986.341	368.815	CH2 LB	
3775603.751	669982.497	369.035	CH2 LB	0.10
3775604.163	669982.748	369.136	CH2 LT	
3775605.141	669981.233	369.159	WASH	
3775605.001	669979.299	369.253	CH2 LT	0.06
3775604.952	669979.273	369.197	CH2 LB	
3775605.089	669977.589	369.222	CH2 LB	0.15
3775605.557	669977.725	369.367	CH2 LT	
3775604.627	669974.252	369.39	CH2 LT	0.10

3775604.496	669974.213	369.294	CH2 LB	
3775604.963	669972.553	369.338	CH2 LB	0.12
3775605.21	669972.647	369.461	CH2 LT	
3775605.993	669991.733	368.768	HEAD	
3775605.438	669992.283	368.759	CH3 RT	0.03
3775605.49	669992.36	368.732	CH3 RB	
3775604.627	669994.097	368.638	CH3 RB	0.07
3775604.423	669994.054	368.704	CH3 RT	
3775603.691	669994.977	368.645	CH3 RT	0.05
3775603.727	669995.02	368.592	CH3 RB	
3775602.86	669995.778	368.582	CH3 RB	0.04
3775602.845	669995.652	368.623	CH3 RT	
3775601.735	669998.187	368.597	CH3 RT	0.09
3775601.813	669998.198	368.51	CH3 RB	
3775602.318	670000.217	368.412	CH3 RB	0.05
3775602.042	670000.221	368.458	CH3 RT	
3775601.941	670001.337	368.43	CH3 RT	0.07
3775602.047	670001.376	368.364	CH3 RB	
3775600.087	670006.061	368.184	CH3 RB	0.03
3775599.9	670006.023	368.212	CH3 RT	
3775598.703	670008.928	368.147	CH3 RT	0.04
3775598.807	670009.038	368.111	CH3 RB	
3775597.649	670011.167	367.99	CH3 RB	0.06
3775597.514	670011.225	368.052	CH3 RT	
3775596.858	670012.019	367.987	CH3 RT	0.04
3775596.821	670012.136	367.951	CH3 RB	
3775596.751	670011.485	367.994	CH3 RB	0.04
3775596.798	670011.56	368.035	CH3 RT	
3775597.189	670010.314	368.076	CH3 RT	0.02
3775597.072	670010.336	368.053	CH3 RB	
3775597.109	670009.977	368.101	HEAD	
3775596.831	670010.42	368.08	CH3 RT	0.02
3775596.929	670010.478	368.055	CH3 RB	
3775596.397	670012.304	367.963	CH3 RB	0.06
3775596.353	670012.27	368.02	CH3 RT	
3775596.109	670013.89	367.953	CH3 RT	0.04
3775596.207	670013.876	367.908	CH3 RB	
3775594.802	670015.428	367.783	CH3 RB	0.08
3775594.659	670015.337	367.864	CH3 RT	
3775592.707	670018.011	367.729	CH3 RT	0.05
3775592.787	670018.072	367.68	CH3 RB	
3775591.259	670020.439	367.575	CH3 RB	0.07
3775591.144	670020.374	367.645	CH3 RT	
3775590.173	670023.393	367.524	CH3 RT	0.07
3775590.232	670023.365	367.456	CH3 RB	
3775591.977	670025.187	367.433	CH3 LB	0.06
3775592.101	670025.271	367.498	CH3 LT	
3775592.185	670021.131	367.643	CH3 LT	0.06
3775592.134	670021.141	367.58	CH3 LB	
3775593.583	670018.061	367.683	CH3 LB	0.09

3775593.709	670018.09	367.77	CH3 LT	
3775595.022	670016.541	367.839	CH3 LT	
3775595.009	670016.539	367.841	CH3 LT	0.08
3775594.977	670016.404	367.762	CH3 LB	
3775595.442	670016.658	367.806	CH3 LB	0.05
3775595.479	670016.815	367.854	CH3 LT	
3775595.927	670016.608	367.881	CH3 LT	0.08
3775595.868	670016.422	367.799	CH3 LB	
3775596.256	670015.798	367.826	CH3 LB	0.08
3775596.343	670015.821	367.906	CH3 LT	
3775597.695	670013.573	367.962	CH3 LT	0.05
3775597.62	670013.488	367.911	CH3 LB	
3775598.104	670013.465	367.947	CH3 LB	0.04
3775598.216	670013.531	367.985	CH3 LT	
3775597.48	670012.356	367.995	CH3 LT	0.03
3775597.414	670012.374	367.965	CH3 LB	
3775598.292	670010.503	368.042	CH3 LB	0.05
3775598.411	670010.53	368.091	CH3 LT	
3775600.123	670007.378	368.193	CH3 LT	0.03
3775600.037	670007.357	368.164	CH3 LB	
3775602.195	670002.622	368.344	CH3 LB	0.05
3775602.36	670002.637	368.394	CH3 LT	
3775602.747	670001.388	368.451	CH3 LT	0.06
3775602.608	670001.378	368.392	CH3 LB	
3775602.665	669997.655	368.518	CH3 LB	0.06
3775602.776	669997.611	368.582	CH3 LT	
3775602.911	669996.575	368.587	CH3 LT	0.05
3775602.891	669996.534	368.54	CH3 LB	
3775604.894	669994.312	368.645	CH3 LB	0.09
3775605.034	669994.402	368.735	CH3 LT	
3775605.945	669992.41	368.788	CH3 LT	0.05
3775605.817	669992.333	368.74	CH3 LB	
3775629.881	669968.585	369.927	CH3 RT	0.18
3775630.133	669968.907	369.747	CH3 RB	
3775629.099	669970.049	369.668	CH3 RB	0.21
3775628.999	669969.455	369.874	CH3 RT	
3775628.667	669969.442	369.816	CH3 RT	0.06
3775628.383	669969.436	369.756	CH3 RB	
3775628.493	669968.68	369.867	CH3 RB	0.11
3775628.785	669968.569	369.977	CH3 RT	
3775628.419	669967.614	369.982	HEAD	
3775627.542	669968.343	369.957	CN4 T	0.09
3775627.837	669968.562	369.868	CH3 RB	
3775628.19	669969.646	369.742	CH3 RB	0.12
3775627.827	669969.829	369.862	CH3 RT	
3775628.054	669970.871	369.725	CH3 RT	0.09
3775628.554	669971.09	369.633	CH3 RB	
3775627.89	669971.339	369.673	CH3 RB	0.10
3775627.601	669970.968	369.776	CH3 RT	
3775627.052	669970.671	369.805	CH3 RT	0.04

3775626.94	669970.814	369.763	CH3 RB	
3775626.127	669969.962	369.918	HEAD	
3775626.69	669970.967	369.747	CH3 RB	0.09
3775626.524	669971.125	369.833	CH3 RT	
3775627.318	669972.243	369.72	CH3 RT	0.14
3775627.719	669972.513	369.58	CH3 RB	
3775627.403	669972.868	369.581	CH3 RB	0.14
3775627.092	669972.552	369.717	CH3 RT	
3775626.905	669972.575	369.696	CH3 RB	
3775626.096	669971.824	369.81	HEAD	
3775626.588	669972.711	369.76	CH3 RT	0.05
3775626.692	669972.63	369.714	CH3 RB	
3775627.401	669973.363	369.518	CH3 RB	0.14
3775626.92	669973.052	369.662	CH3 RT	
3775624.834	669976.132	369.586	CH3 RT	0.19
3775625.368	669976.435	369.401	CH3 RB	
3775621.713	669983.414	369.154	CH3 RB	0.21
3775620.839	669982.953	369.363	CH3 RT	
3775619.002	669987.523	369.17	CH3 RT	0.13
3775619.596	669987.744	369.039	CH3 RB	
3775619.231	669991.291	368.912	CH3 RB	0.14
3775618.702	669991.259	369.05	CH3 RT	
3775620.521	669995.441	368.831	CH3 RT	0.07
3775620.679	669995.326	368.759	CH3 RB	
3775623.531	669999.732	368.577	CH3 RB	0.15
3775623.164	669999.991	368.731	CH3 RT	
3775623.462	670001.116	368.685	CH3 RT	0.15
3775623.754	670001.321	368.531	CH3 RB	
3775622.834	670004.03	368.386	CH3 RB	0.11
3775622.606	670003.778	368.495	CH3 RT	
3775621.627	670004.87	368.477	CH3 RT	0.11
3775621.705	670005.125	368.365	CH3 RB	
3775621.39	670004.523	368.444	CH3 RB	0.04
3775621.544	670004.476	368.489	CH3 RT	
3775621.125	670003.373	368.529	HEAD	
3775621.339	670005.352	368.427	CH3 RT	0.09
3775621.589	670005.412	368.333	CH3 RB	
3775621.09	670006.343	368.304	CH3 RB	0.14
3775620.892	670006.202	368.443	CH3 RT	
3775620.545	670007.41	368.358	CH3 RT	0.07
3775620.536	670007.602	368.285	CH3 RB	
3775620.306	670007.142	368.354	CH3 RB	0.04
3775620.392	670007.094	368.393	CH3 RT	
3775619.838	670006.868	368.392	HEAD	
3775620.203	670008.086	368.402	CH3 RT	0.10
3775620.322	670008.071	368.302	CH3 RB	
3775621.379	670009.615	368.146	CH3 RB	0.14
3775621.172	670009.761	368.284	CH3 RT	
3775620.143	670014.238	368.148	CH3 RT	0.16
3775620.297	670014.291	367.988	CH3 RB	

3775619.641	670019.112	367.876	CH3 RB	0.04
3775619.424	670018.959	367.915	CH3 RT	
3775617.951	670026.289	367.699	CH3 RT	0.08
3775618.431	670026.495	367.623	CH3 RB	
3775616.291	670031.776	367.445	CH3 RB	0.05
3775615.937	670031.739	367.499	CH3 RT	
3775617.61	670032.875	367.44	CH3 LT	0.01
3775617.334	670032.745	367.432	CH3 LB	
3775618.41	670029.853	367.533	CH3 LB	0.06
3775618.911	670029.794	367.592	CH3 LT	
3775620.115	670025.759	367.728	CH3 LT	0.07
3775619.628	670025.427	367.653	CH3 LB	
3775621.574	670022.354	367.823	CH3 LB	0.13
3775622.064	670022.333	367.95	CH3 LT	
3775622.633	670019.701	367.926	CH 4 LT	0.06
3775622.3	670019.649	367.869	CH 4 LB	
3775623.117	670018.928	367.949	CH 4 LB	0.08
3775623.432	670019.078	368.033	CH 4 LT	
3775623.621	670018.361	368.053	CH 4 LT	0.06
3775623.559	670018.53	367.989	CH 4 LB	
3775622.551	670018.874	367.947	CH 4 LB	0.14
3775622.72	670018.416	368.088	CH 4 LT	
3775622.982	670015.481	368.061	CH 4 LT	0.06
3775622.865	670015.273	368.002	CH 4 LB	
3775624.521	670013.477	368.094	CH 4 LB	0.12
3775624.788	670013.707	368.214	CH 4 LT	
3775627.151	670010.887	368.399	CH 4 LT	0.07
3775627.048	670010.815	368.333	CH 4 LB	
3775629.251	670008.217	368.503	CH 4 LB	0.09
3775629.594	670008.296	368.595	CH 4 LT	
3775630.75	670006.694	368.715	CH 4 LW	
3775628.331	670008.548	368.532	CH 4 LT	0.07
3775628.449	670008.623	368.462	CH 4 LB	
3775625.588	670012.221	368.185	CH 4 LB	0.11
3775625.467	670012.035	368.294	CH 4 LT	
3775622.856	670014.06	368.098	CH 4 LT	0.07
3775622.625	670014.076	368.024	CH 4 LB	
3775622.162	670011.023	368.037	CH 4 LB	0.11
3775622.433	670010.963	368.151	CH 4 LT	
3775624.011	670009.024	368.346	CH 4 LT	0.13
3775624.021	670008.873	368.218	CH 4 LB	
3775627.362	670004.348	368.433	CH 4 LB	0.13
3775627.709	670004.553	368.564	CH 4 LT	
3775629.134	670002.207	368.725	CH 4 LT	0.14
3775629.339	670002.02	368.582	CH 4 LB	
3775631.131	670002.523	368.699	CH 4 LB	0.07
3775631.174	670002.676	368.765	CH 4 LT	
3775632.79	670001.685	368.857	CH 4 LW	
3775631.749	670002.094	368.863	CH 4 LT	0.11
3775631.783	670002.218	368.753	CH 4 LB	

3775629.959	670001.394	368.651	CH 4 LB	0.09
3775630.046	670001.469	368.742	CH 4 LT	
3775631.757	669999.736	368.823	CH 4 LT	0.10
3775631.419	669999.613	368.722	CH 4 LB	
3775633.534	669996.887	368.955	CH 4 LB	0.09
3775633.304	669996.922	368.867	CH 4 LB	
3775634.766	669994.985	368.954	CH 4 LB	0.12
3775635.054	669995.158	369.075	CH 4 LT	
3775634.479	669994.538	369.088	CH 4 LT	0.13
3775634.631	669994.678	368.96	CH 4 LB	
3775630.795	669998.758	368.8	CH 4 LB	0.10
3775630.536	669998.759	368.904	CH 4 LT	
3775626.459	670003.586	368.631	CH 4 LT	0.17
3775626.711	670003.683	368.457	CH 4 LB	
3775624.251	670007.434	368.294	CH 4 LB	0.13
3775623.969	670007.199	368.424	CH 4 LT	
3775625.304	670002.561	368.663	CH 4 LT	0.11
3775625.021	670002.555	368.558	CH 4 LB	
3775624.965	670000.443	368.556	CH 4 LB	0.17
3775625.434	670000.535	368.729	CH 4 LT	
3775627.568	669996.731	368.845	CH 4 LT	0.09
3775627.398	669996.657	368.76	CH 4 LB	
3775631.156	669992.303	369.04	CH 4 LB	0.14
3775631.959	669992.68	369.179	CH 4 LT	
3775634.855	669988.136	369.318	CH 4 LT	0.07
3775634.505	669987.839	369.244	CH 4 LB	
3775633.794	669987.789	369.294	CH 4 LT	
3775628.747	669993.617	369.109	CH 4 LT	0.10
3775628.89	669994.02	369.006	CH 4 LB	
3775625.918	669998.495	368.615	CH 4 LB	0.23
3775625.218	669998.22	368.847	CH 4 LT	
3775624.301	669999.085	368.752	CH 4 LT	0.15
3775623.52	669999.094	368.604	CH 4 LB	
3775621.475	669995.011	368.774	CH 4 LB	0.21
3775622.251	669994.988	368.989	CH 4 LT	
3775624.477	669990.278	369.112	CH 4 LT	0.12
3775624.293	669990.138	368.991	CH 4 LB	
3775626.584	669986.844	369.306	CH 4 LT	0.12
3775626.285	669987.186	369.185	CH 4 LB	
3775625.582	669987.301	369.282	CH 4 LT	
3775622.903	669990.771	369.112	CH 4 LT	0.16
3775623.237	669991.038	368.956	CH 4 LB	
3775621.148	669994.886	368.751	CH 4 LB	0.10
3775621.224	669994.648	368.848	CH 4 LT	
3775621.076	669986.884	369.228	CH 4 LT	0.18
3775620.813	669986.745	369.047	CH 4 LB	
3775624.962	669978.441	369.318	CH 4 LB	0.27
3775626.057	669978.585	369.587	CH 4 LT	
3775631.639	669968.605	370.035	CH 4 LT	0.26
3775631.084	669968.675	369.776	CH 4 LB	

3775631.841	669965.126	370.018	CH 4 LB	
3775632.771	669963.728	370.18	CH 4 LW	
3775630.687	669964.823	370.016	CH 4 LB	0.21
3775630.983	669964.591	370.223	CH 4 LT	
3775631.914	669957.963	370.475	CH 4 LT	0.10
3775631.557	669957.936	370.375	CH 4 LB	
3775631.727	669956.102	370.482	CH 4 LW	
3775630.523	669960.009	370.282	CH 4 LB	0.15
3775630.127	669959.64	370.432	CH 4 LT	
3775629.716	669964.664	370.202	CH 4 LT	0.16
3775630.134	669964.63	370.043	CH 4 LB	
3775630.657	669968.109	369.851	CH 4 RB	0.18
3775630.31	669967.785	370.034	CH 4 RT	
3775639.036	669971.023	369.993	CH 5 RT	0.10
3775639.298	669971.211	369.893	CH 5 RB	
3775637.961	669975.613	369.676	CH 5 RB	0.18
3775637.571	669975.603	369.852	CH 5 RT	
3775634.527	669985.866	369.469	CH 5 RT	0.11
3775635.059	669985.837	369.355	CH 5 RB	
3775635.444	669993.898	368.983	CH 5 RB	0.09
3775634.961	669993.677	369.073	CH 5 RT	
3775637.362	669994.234	369.2	CH 5 LT	0.14
3775637.055	669994.098	369.063	CH 5 LB	
3775638.33	669985.979	369.305	CH 5 LB	0.11
3775638.869	669985.913	369.415	CH 5 LT	
3775640.387	669979.982	369.593	CH 5 LT	0.10
3775640.082	669979.995	369.497	CH 5 LB	
3775641.578	669972.539	369.822	CH 5 LB	0.09
3775642.194	669972.704	369.917	CH 5 LT	
3775643.271	669969.249	370.049	CH 5 LT	0.10
3775642.973	669969.147	369.949	CH 5 LB	
3775634.989	670000.254	368.902	HEAD	
3775635.029	670002.284	368.859	CH 6 RT	0.06
3775635.234	670002.152	368.799	CH 6 RB	
3775638.957	670009.204	368.346	CH 6 RB	0.11
3775638.46	670009.281	368.459	CH 6 RT	
3775638.025	670012.17	368.28	CH 6 RT	0.06
3775638.304	670012.151	368.219	CH 6 RB	
3775637.82	670012.194	368.246	CH 6 RB	
3775637.623	670010.614	368.358	CH 6 RB	
3775637.409	670011.398	368.337	CH 6 RT	0.05
3775637.483	670011.737	368.284	CH 6 RB	
3775636.003	670009.748	368.487	CH 6 RB	
3775637.585	670012.97	368.239	CH 6 RB	
3775637.363	670013.003	368.372	CH 6 RT	
3775636.091	670018.634	368.166	CH 6 RT	0.12
3775636.499	670018.555	368.045	CH 6 RB	
3775636.778	670021.568	367.893	CH 6 RB	0.11
3775636.665	670021.622	368.003	CH 6 RT	
3775633.791	670024.416	367.908	CH 6 RT	0.18

3775634.065	670024.648	367.733	CH 6 RB	
3775629.555	670030.465	367.482	CH 6 RB	0.13
3775629.352	670030.172	367.61	CH 6 RT	
3775626.488	670033.439	367.462	CH 6 RT	0.17
3775626.388	670033.734	367.294	CH 6 RB	
3775626.387	670028.8	367.684	CH 6 R	
3775624.939	670029.181	367.645	CH 6 R	
3775625.882	670030.177	367.527	CH 6 RT	0.08
3775625.966	670030.574	367.45	CH 6 RB	
3775625.769	670031.562	367.402	CH 6 RB	0.09
3775625.661	670031.604	367.494	CH 6 RT	
3775624.668	670035.58	367.409	CH 6 RT	0.19
3775624.937	670035.622	367.218	CH 6 RB	
3775626.704	670035.904	367.314	CH 6 LB	0.10
3775627.241	670036.26	367.412	CH 6 LT	
3775631.965	670030.479	367.69	CH 6 LT	0.18
3775631.662	670030.17	367.509	CH 6 LB	
3775634.533	670026.254	367.725	CH 6 LB	0.10
3775634.586	670026.433	367.822	CH 6 LT	
3775639.537	670020.527	368.091	CH 6 LT	0.10
3775639.309	670020.372	367.991	CH 6 LB	
3775641.467	670016.74	368.225	CH 6 LW	
3775640.346	670017.863	368.131	CH 6 LB	
3775638.604	670019.882	368.09	CH 6 LT	
3775638.475	670020.185	367.972	CH 6 LT	
3775638.766	670014.286	368.296	CH 6 LT	0.099
3775638.564	670014.338	368.197	CH 6 LB	
3775639.075	670011.52	368.277	CH 6 LB	0.072
3775639.42	670011.683	368.349	CH 6 LT	
3775640.328	670009.835	368.414	CH 6 L CH	
3775639.278	670010.89	368.352	CH 6 LT	0.108
3775638.912	670011.195	368.244	CH 6 LB	
3775639.04	670008.794	368.382	CH 6 LB	0.097
3775639.264	670008.403	368.479	CH 6 LT	
3775636.843	670005.568	368.64	CH 6 LT	0.067
3775637.121	670006.167	368.573	CH 6 LB	
3775595.643	670034.179	367.511	BENCH	

Control Plot 4

Northing	Easting	Elevation	Feature code	Depth (m)	Width (m)	Cross (m^2)
3774786.884	671098.745	304.314	CHLT	0.08	0.71	0.05
3774786.694	671098.964	304.235	CH1 LB			
3774786.501	671099.121	304.242	CH1 RB	0.05		
3774786.342	671099.205	304.291	CH1 RT			
3774786.006	671101.627	304.251	CH1 RT	0.08	0.89	0.06
3774786.259	671101.572	304.171	CH1 RB			
3774786.69	671101.651	304.146	CH1 LB	0.06		
3774786.896	671101.595	304.21	CH1 LT			
3774789	671099.619	304.291	HEAD			

3774788.549	671100.961	304.262	CH2 LT	0.06	0.89	0.06
3774788.426	671100.789	304.207	CH2 LB			
3774788.022	671100.465	304.204	CH2 RB	0.07		
3774787.91	671100.343	304.275	CH2 RT			
3774786.854	671101.738	304.212	CH2 RT	0.05	0.64	0.04
3774786.914	671101.842	304.167	CH2 RB			
3774787.22	671102.117	304.159	CH2 LB	0.07		
3774787.363	671102.127	304.231	CH2 LT			
3774787.427	671103.474	304.142	CH2 LT	0.09	0.63	0.07
3774787.349	671103.57	304.047	CH2 LB			
3774787.122	671103.69	304.031	CH2 RB	0.12		
3774786.875	671103.773	304.149	CH2 RT			
3774786.833	671105.979	304.075	CH2 RT	0.07	1.15	0.11
3774787.013	671105.988	304.004	CH2 RB			
3774787.705	671105.994	303.964	CH2 LB	0.13		
3774787.983	671105.908	304.091	CH2 LT			
3774787.903	671108.227	303.948	CH2 LT	0.03	1.23	0.09
3774787.799	671108.301	303.914	CH2 LB			
3774787.258	671108.799	303.93	CH2 RB	0.12		
3774787.156	671109.207	304.047	CH2 RT			
3774789.747	671100.313	304.286	HEAD			
3774788.842	671102.529	304.203	CH2 LT	0.08	0.69	0.05
3774788.669	671102.549	304.123	CH2 LB			
3774788.359	671102.365	304.15	CH2 RB	0.07		
3774788.174	671102.362	304.221	CH2 RT			
3774790.666	671100.846	304.256	HEAD			
3774789.755	671104.942	304.125	CH4 LT	0.07	1.13	0.08
3774789.606	671104.908	304.054	CH4 LB			
3774788.742	671104.753	304.072	CH4 RB	0.07		
3774788.648	671104.722	304.147	CH4 RT			
3774788.071	671108.071	303.982	CH4 RT	0.06	0.95	0.07
3774788.218	671108.141	303.925	CH4 RB			
3774788.532	671108.512	303.896	CH4 LB	0.10		
3774788.788	671108.69	303.997	CH4 LT			
3774788.748	671110.076	303.871	CH4 LT	0.03	1.35	0.08
3774788.583	671110.118	303.838	CH4 LB			
3774787.729	671110.228	303.852	CH4 RB	0.08		
3774787.433	671110.398	303.935	CH4 RT			
3774792.696	671104.974	304.174	HEAD			
3774791.614	671108.719	304.05	CH5 LT	0.07	0.91	0.03
3774791.462	671108.662	303.981	CH5 LB			
3774790.769	671108.375	303.972	CH5 RW			
3774789.365	671109.802	303.919	CH5 RT	0.04	0.64	0.05
3774789.41	671109.936	303.878	CH5 RB			
3774789.56	671110.188	303.857	CH5 LB	0.11		
3774789.729	671110.323	303.967	CH5 LT			
3774788.658	671113.176	303.93	CH5 LT	0.19	1.63	0.19
3774788.313	671113.131	303.744	CH5 LB			
3774787.322	671113.022	303.791	CH5 RB	0.05		
3774787.053	671112.912	303.84	CH5 RT			

3774785.873	671118.993	303.702	CH5 RT	0.05	1.67	0.04
3774786.023	671118.975	303.65	CH5 RB			
3774787.541	671119.109	303.649	CH5 LW			
3774788.077	671122.812	303.57	CH5 LT	0.06	1.90	0.16
3774787.451	671122.831	303.512	CH5 LB			
3774786.556	671123.018	303.548	CH5 RB	0.11		
3774786.217	671123.175	303.66	CH5 RT			
3774787.8	671127.035	303.465	CH5 RT	0.07	1.16	0.04
3774788.134	671126.904	303.392	CH5 RB			
3774788.901	671126.677	303.427	CH5 LW			
3774788.534	671130.74	303.363	CH5 LT	0.04	1.73	0.10
3774788.356	671130.668	303.322	CH5 LB			
3774787.067	671130.543	303.28	CH5 RB	0.07		
3774786.82	671130.511	303.354	CH5 RT			
3774783.087	671139.76	303.036	CH5 RW			
3774785.054	671140.605	303.033	CH5 LW			
3774781.316	671148.985	302.781	CH5 LW			
3774780.702	671148.57	302.753	CH5 RW			
3774804.463	671100.335	304.373	CH6 LT	0.05	3.75	0.35
3774804.245	671100.216	304.327	CH6 LB			
3774801.045	671099.241	304.323	CH6 RB	0.14		
3774800.886	671099.2	304.462	CH6 RT			
3774797.532	671107.368	304.145	CH6 RT	0.07	3.24	0.21
3774797.661	671107.445	304.07	CH6 RB			
3774799.96	671108.926	304.024	CH6 LB	0.05		
3774800.318	671109.026	304.078	CH6 LT			
3774797.46	671113.436	303.926	CH6 LT	0.05	3.11	0.38
3774797.243	671113.38	303.881	CH6 LB			
3774795.082	671112.52	303.823	CH6 RB	0.20		
3774794.567	671112.3	304.025	CH6 RT			
3774791.551	671119.855	303.782	CH6 RT	0.10	2.52	0.21
3774791.718	671119.904	303.683	CH6 RB			
3774793.71	671120.704	303.616	CH6 LB	0.06		
3774793.915	671120.742	303.68	CH6 LT			
3774790.414	671127.206	303.457	CH6 LT	0.04	1.31	0.08
3774790.302	671127.107	303.413	CH6 LB			
3774789.518	671126.607	303.404	CH6 RB	0.08		
3774789.315	671126.495	303.48	CH6 RT			
3774794.988	671119.548	303.756	CH7 RW			
3774794.625	671126.367	303.526	CH7 RW			
3774794.251	671134.899	303.249	CH7 RW			
3774790.818	671139.34	303.081	CH7 RW			
3774785.618	671145.19	302.907	CH7 RW			
3774781.305	671154.603	302.602	CH7 RW			
3774788.757	671156.604	302.503	CH7 LW			
3774791.191	671147.691	302.823	CH7 LB	0.07		
3774791.442	671147.697	302.897	CH7 LT			
3774794.213	671140.063	303.123	CH7 LT	0.03		
3774794.061	671140.007	303.094	CH7 LB			
3774797.048	671133.922	303.34	CH7 LW			

3774800.302	671126.438	303.59	CH7 LB	0.06		
3774800.471	671126.439	303.65	CH7 LT			
3774803.767	671116.024	303.948	CH7 LT	0.03		
3774803.507	671115.945	303.921	CH7 LB			
3774803.425	671104.586	304.242	CH7 LW			
3774800.678	671108.856	304.098	CH7 BAR			
3774800.248	671117.049	303.893	CH7 BAR			
3774796.696	671117.514	303.815	CH7 BAR			
3774796.267	671122.234	303.669	CH7 BAR			
3774798.966	671122.919	303.682	CH7 BAR			
3774796.484	671128.449	303.498	CH7 BAR			
3774788.49	671145.167	302.907	CH7 BAR			
3774784.88	671151.027	302.757	CH7 BAR			
3774786.575	671152.799	302.664	CH7 BAR			
3774786.256	671157.417	302.498	CH7 BAR			
3774781.972	671155.912	302.546	CH7 BAR			
3774805.115	671126.646	303.587	HEAD			
3774804.856	671129.085	303.495	CH8 LT	0.06	0.74	0.05
3774804.698	671129.11	303.439	CH8 LB			
3774804.306	671128.981	303.449	CH8 RB	0.07		
3774804.152	671128.848	303.522	CH8 RT			
3774802.383	671136.583	303.209	CH8 RT	0.02	0.60	0.02
3774802.438	671136.631	303.185	CH8 RB			
3774802.792	671136.769	303.194	CH8 LB	0.04		
3774802.958	671136.755	303.237	CH8 LT			
3774801.107	671145.335	303.003	CH8 LT	0.11	1.29	0.11
3774800.925	671145.337	302.895	CH8 LB			
3774800.056	671145.249	302.9	CH8 RB	0.06		
3774799.821	671145.299	302.959	CH8 RT			
3774797.539	671154.234	302.684	CH8 RT	0.09	1.54	0.16
3774797.822	671154.263	302.592	CH8 RB			
3774798.686	671154.362	302.611	CH8 LB	0.11		
3774799.067	671154.386	302.723	CH8 LT			
3774799.116	671158.891	302.576	CH8 LT	0.07	2.03	0.16
3774798.932	671158.845	302.505	CH8 LB			
3774797.379	671158.622	302.489	CH8 RB	0.08		
3774797.107	671158.596	302.573	CH8 RT			
3774810.372	671100.897	304.398	CH9 RT	0.08	1.72	0.10
3774810.716	671100.885	304.323	CH9 RB			
3774811.943	671101.023	304.327	CH9 LB	0.04		
3774812.096	671100.908	304.368	CH9 LT			
3774813.257	671108.063	304.179	CH9 LW			
3774810.473	671108.501	304.156	CH9 RW			
3774808.133	671114.402	303.954	CH9 RW		6.59	0.19
3774814.396	671116.072	303.968	CH9 LB	0.06		
3774814.508	671116.084	304.027	CH9 LT			
3774812.715	671117.005	303.899	CH9 LW			
3774807.278	671115.894	303.902	CH9 RW			
3774805.675	671122.707	303.677	CH9 RW		4.30	0.19
3774809.036	671123.992	303.575	CH9 LB	0.09		

3774809.738	671124.101	303.664	CH9 LT			
3774809.969	671129.587	303.59	CH9 LT	0.11	2.56	0.25
3774809.676	671129.563	303.477	CH9 LB			
3774807.598	671130.216	303.42	CH9 RB	0.09		
3774807.504	671130.266	303.506	CH9 RT			
3774807.753	671136.211	303.3	CH9 RT	0.09	2.31	0.19
3774808.146	671136.283	303.212	CH9 RB			
3774809.687	671136.912	303.218	CH9 LB	0.08		
3774809.943	671136.941	303.294	CH9 LT			
3774807.3	671142.548	303.139	CH9 LT	0.11	2.06	0.23
3774807.016	671142.511	303.029	CH9 LB			
3774805.541	671142.047	303.025	CH9 RB	0.11		
3774805.343	671141.901	303.138	CH9 RT			
3774804.243	671148.586	302.913	CH9 RT	0.08	1.74	0.17
3774804.365	671148.621	302.833	CH9 RB			
3774805.824	671148.853	302.814	CH9 LB	0.12		
3774805.971	671148.788	302.932	CH9 LT			
3774806.13	671155.022	302.776	CH9 LT	0.14	3.22	0.36
3774805.13	671154.758	302.636	CH9 LB			
3774803.302	671154.253	302.666	CH9 RB	0.08		
3774803.016	671154.211	302.747	CH9 RT			
3774800.973	671159.227	302.541	CH9 RT	0.06	2.32	0.18
3774801.266	671159.295	302.482	CH9 RB			
3774802.942	671159.593	302.468	CH9 LB	0.09		
3774803.252	671159.655	302.563	CH9 LT			
3774806.917	671121.557	303.716	CH9 BAR			
3774807.09	671118.702	303.778	CH9 BAR			
3774808.415	671119.45	303.778	CH9 BAR			
3774808.857	671116.432	303.861	CH9 BAR			
3774810.586	671116.718	303.852	CH9 BAR2			
3774810.92	671113.941	303.981	CH9 BAR2 T	0.03		
3774810.753	671113.908	303.95	CH9 BAR2 B			
3774812.298	671114.635	303.942	CH9 BAR2 B	0.07		
3774812.043	671114.584	304.016	CH9 BAR2 T			
3774812.496	671111.293	304.062	CH9 BAR2			
3774818.269	671101.574	304.383	CH10 LT	0.09	1.14	0.07
3774817.899	671101.698	304.296	CH10 LB			
3774817.36	671101.769	304.334	CH10 RB	0.03		
3774817.151	671101.813	304.367	CH10 RT			
3774818.004	671106.327	304.179	CH10 RT	0.04	0.98	0.07
3774818.088	671106.35	304.138	CH10 RB			
3774818.543	671106.569	304.149	CH10 LB	0.09		
3774818.891	671106.737	304.243	CH10 LT			
3774818.04	671111.813	304.02	CH10 LT	0.05	1.21	0.10
3774817.77	671111.9	303.972	CH10 LB			
3774817.018	671112.003	303.971	CH10 RB	0.12		
3774816.843	671111.971	304.093	CH10 RT			
3774817.805	671121.679	303.779	CH10 RT	0.07	1.71	0.11
3774817.959	671121.71	303.71	CH10 RB			
3774819.328	671121.704	303.713	CH10 LB	0.06		

3774819.51	671121.572	303.772	CH10 LT			
3774819.426	671128.305	303.562	CH10 LT	0.05	1.99	0.11
3774819.255	671128.267	303.508	CH10 LB			
3774817.725	671128.317	303.516	CH10 RB	0.06		
3774817.433	671128.292	303.575	CH10 RT			
3774817.117	671137.532	303.293	CH10 RT	0.05		
3774817.266	671137.545	303.245	CH10 RB			
3774818.98	671137.894	303.266	CH10 LW			
3774819.459	671147.839	302.957	CH10 LW			
3774816.202	671147.76	302.979	CH10 RW			
3774815.314	671153.77	302.76	CH10 RW			
3774819.041	671154.587	302.733	CH10 LB	0.04		
3774819.168	671154.552	302.772	CH10 LT			
3774817.619	671161.3	302.578	CH10 LT	0.02	4.10	0.10
3774817.521	671161.293	302.558	CH10 LB			
3774813.731	671160.824	302.538	CH10 RB	0.03		
3774813.544	671160.886	302.568	CH10 RT			
3774824.715	671102.477	304.348	CH11 RT	0.04	1.35	0.07
3774824.925	671102.428	304.312	CH11 RB			
3774825.617	671102.367	304.296	CH11 LB	0.07		
3774826.069	671102.425	304.368	CH11 LT			
3774825.084	671107.756	304.223	CH11 LT	0.08	1.08	0.08
3774824.905	671107.889	304.139	CH11 LB			
3774824.387	671108.135	304.122	CH11 RB	0.07		
3774824.148	671108.297	304.195	CH11 RT			
3774826.273	671113.937	303.997	CH11 RT	0.06	1.91	0.17
3774826.458	671113.954	303.932	CH11 RB			
3774827.955	671113.596	303.982	CH11 LB	0.12		
3774828.139	671113.537	304.098	CH11 LT			
3774826.192	671118.94	303.865	CH11 LT	0.07	1.28	0.09
3774825.961	671118.821	303.793	CH11 LB			
3774825.253	671118.285	303.828	CH11 RB	0.07		
3774825.139	671118.204	303.895	CH11 RT			
3774823.267	671123.802	303.729	CH11 RT	0.06	2.02	0.11
3774823.417	671123.705	303.67	CH11 RB			
3774825.133	671124.175	303.65	CH11 LB	0.05		
3774825.256	671124.156	303.701	CH11 LT			
3774825.787	671129.93	303.56	CH11 LT	0.06	3.19	0.09
3774825.554	671129.959	303.505	CH11 LB			
3774822.596	671130.066	303.536	CH11 RW			
3774823.084	671134.824	303.367	CH11 RW			
3774825.059	671135.757	303.335	CH11 LW			
3774820.238	671141.765	303.127	CH11 LW			
3774819.41	671139.595	303.184	CH11 RW			
3774833.011	671106.423	304.256	HEAD			
3774832.632	671111.191	304.147	CH12 LT	0.06	1.08	0.06
3774832.282	671111.219	304.084	CH12 LB			
3774831.808	671111.138	304.076	CH12 RB	0.05		
3774831.553	671111.155	304.125	CH12 RT			
3774830.581	671116.407	303.944	CH12 RW			

3774831.377	671116.612	303.94	CH12 LW			
3774829.719	671120.372	303.855	CH12 LT	0.07	0.83	0.05
3774829.543	671120.267	303.784	CH12 LB			
3774829.229	671120.082	303.799	CH12 RB	0.04		
3774829.006	671119.94	303.843	CH12 RT			
3774826.505	671123.377	303.743	CH12 RT	0.09	0.94	0.06
3774826.728	671123.459	303.652	CH12 RB			
3774827.13	671123.741	303.663	CH12 LB	0.04		
3774827.327	671123.827	303.703	CH12 LT			
3774838.746	671103.479	304.438	CH13 LT	0.21	4.28	0.73
3774838.033	671103.337	304.23	CH13 LB			
3774834.781	671103.193	304.284	CH13 RB	0.13		
3774834.475	671103.24	304.415	CH13 RT			
3774835.169	671106.225	304.354	CH13 RT	0.11	3.88	0.59
3774835.292	671106.167	304.243	CH13 RB			
3774838.536	671105.484	304.156	CH13 LB	0.19		
3774838.988	671105.516	304.347	CH13 LT			
3774839.536	671106.565	304.293	CH13 LT	0.18	2.09	0.26
3774839.081	671106.783	304.116	CH13 LB			
3774838.182	671107.135	304.084	CH13 RB	0.07		
3774837.582	671107.319	304.155	CH13 RT			
3774838.771	671110.351	304.111	CH13 RT	0.09	1.91	0.26
3774839.254	671110.198	304.021	CH13 RB			
3774840.429	671110.275	304.015	CH13 LB	0.18		
3774840.676	671110.36	304.197	CH13 LT			
3774841.846	671114.042	304.043	CH13 LT	0.09	2.24	0.20
3774841.687	671114.083	303.949	CH13 LB			
3774840.098	671114.516	303.871	CH13 RB	0.09		
3774839.648	671114.47	303.956	CH13 RT			
3774842.959	671103.604	304.427	CH14 RT	0.12	1.32	0.08
3774843.276	671103.569	304.305	CH14 RB			
3774844.267	671103.77	304.357	CH14 LW			
3774843.963	671107.79	304.214	CH14 LT	0.06	1.07	0.08
3774843.637	671107.86	304.152	CH14 LB			
3774843.213	671107.874	304.217	CH14 RB	0.09		
3774842.896	671107.839	304.306	CH14 RT			
3774844.626	671105.685	304.382	CH15 RT	0.06	2.19	0.13
3774844.769	671105.736	304.317	CH15 RB			
3774844.387	671107.869	304.139	CH15 RB	0.05		
3774844.028	671107.794	304.193	CH15 RT			
3774842.602	671109.981	304.226	CH15 RT	0.14	1.96	0.14
3774842.988	671110	304.085	CH15 RB			
3774844.508	671110.433	304.127	CH15 LW			
3774843.475	671114.644	304.057	CH15 LT	0.11	1.74	0.18
3774842.918	671114.394	303.945	CH15 LB			
3774842	671114.086	303.961	CH15 RB	0.10		
3774841.853	671114.025	304.061	CH15 RT			
3774839.089	671117.691	303.866	CH15 RT	0.06	2.83	0.30
3774839.519	671117.737	303.804	CH15 RB			
3774841.38	671118.605	303.837	CH15 LB	0.15		

3774841.712	671118.742	303.985	CH15 LT			
3774839.312	671125.361	303.719	CH15 LT	0.12	2.45	0.31
3774838.737	671125.195	303.6	CH15 LB			
3774837.027	671124.838	303.653	CH15 RB	0.13		
3774836.915	671124.838	303.784	CH15 RT			
3774834.221	671134.351	303.451	CH15 RT	0.18	2.17	0.27
3774834.399	671134.45	303.275	CH15 RB			
3774836.02	671134.646	303.354	CH15 LB	0.07		
3774836.376	671134.61	303.427	CH15 LT			
3774836.158	671141.315	303.222	CH15 LW		5.09	0.16
3774831.375	671140.773	303.23	CH15 RB	0.06		
3774831.103	671140.718	303.291	CH15 RT			
3774831.796	671145.711	303.115	CH15 RT	0.05	4.54	0.14
3774831.996	671145.795	303.069	CH15 RB			
3774836.146	671145.842	303.102	CH15 LB	0.01		
3774836.334	671145.81	303.116	CH15 LT			
3774836.733	671148.339	303.04	CH15 LT	0.03	3.98	0.06
3774836.575	671148.258	303.01	CH15 LB			
3774832.755	671148.34	302.951	CH15 RW			
3774832.866	671149.259	303.076	CH15 RT	0.13		
3774832.991	671149.376	302.943	CH15 RB			
3774834.419	671148.737	302.899	CH15 BAR B			
3774835.836	671148.868	302.952	CH15 LB	0.07		
3774836.02	671148.883	303.025	CH15 LT			
3774836.056	671152.407	302.916	CH15 LT	0.10	3.10	0.35
3774835.822	671152.462	302.82	CH15 LB			
3774833.215	671152.39	302.818	CH15 RB	0.13		
3774832.959	671152.373	302.947	CH15 RT			
3774832.234	671158.371	302.701	CH15 RT	0.07	4.06	0.28
3774832.36	671158.367	302.631	CH15 RB			
3774836.102	671158.813	302.619	CH15 LB	0.07		
3774836.273	671158.737	302.687	CH15 LT			
3774835.844	671162.709	302.639	CH15 LT	0.13	4.52	0.30
3774835.436	671162.788	302.507	CH15 LB			
3774831.37	671162.033	302.553	CH15 RW			
3774834.054	671160.479	302.544	CH15 BAR B	0.06		
3774833.985	671160.051	302.607	CH15 BAR T			
3774832.968	671157.482	302.699	CH15 BAR T	0.02		
3774832.838	671157.532	302.681	CH15 BAR B			
3774834.338	671157.403	302.689	CH15 BAR B	0.05		
3774834.164	671157.39	302.742	CH15 BAR T			
3774833.809	671154.699	302.784	CH15 BAR T	0.02		
3774833.762	671154.335	302.768	CH15 BAR B			
3774834.967	671149.728	302.905	CH15 BAR B	0.06		
3774835.112	671149.41	302.964	CH15 BAR T			
3774835.48	671148.475	303.017	CH15 BAR T	0.07		
3774835.624	671148.618	302.947	CH15 BAR B			
3774834.541	671148.552	302.931	CH15 BAR B	0.07		
3774834.805	671148.372	303.002	CH15 BAR T			
3774834.627	671145.531	303.094	CH15 BAR T	0.03		

3774834.499	671145.473	303.062	CH15 BAR B			
3774835.682	671145.612	303.109	CH15 BAR			
3774835.294	671144.439	303.14	CH15 BAR B	0.07		
3774835.194	671144.765	303.206	CH15 BAR T			
3774841.55	671144.384	303.135	CH16 LT	0.10	1.17	0.06
3774841.234	671144.084	303.031	CH16 LB			
3774840.691	671143.597	303.064	CH16 RW			
3774839.538	671145.603	303.143	CH16 RT	0.18	1.00	0.09
3774839.781	671145.671	302.959	CH16 RB			
3774840.455	671146.009	303.037	CH16 LW			
3774838.728	671152.338	302.887	CH16 LT	0.06	1.41	0.11
3774838.469	671152.281	302.826	CH16 LB			
3774837.622	671152.248	302.829	CH16 RB	0.09		
3774837.33	671152.14	302.921	CH16 RT			
3774836.546	671159.011	302.685	CH16 RT	0.03	1.30	0.02
3774836.664	671158.986	302.653	CH16 RB			
3774837.69	671159.618	302.647	CH16 LW			
3774835.465	671160.606	302.556	CH16-15			
3774834.449	671129.089	303.609	HEAD			
3774840.273	671126.151	303.739	HEAD			

Control Plot 5

Northing	Easting	Elevation	Feature code	Depth (m)	Width (m)	Cross (m^2)
3776206.277	672505.073	320.172	CH1 LT	0.11	1.52	0.17
3776206.204	672504.886	320.061	CH1 LB			
3776206.422	672503.773	320.055	CH1 RB	0.05		
3776206.197	672503.555	320.101	CH1 RT			
3776207.771	672498.375	320.295	CH1 RT	0.08	1.23	0.10
3776208.122	672498.488	320.211	CH1 RB			
3776208.489	672498.439	320.235	CH1 LB	0.10		
3776208.992	672498.524	320.331	CH1 LT			
3776209.066	672492.1	320.532	CH1 LT	0.10	1.35	0.13
3776208.704	672492.208	320.436	CH1 LB			
3776208.117	672492.591	320.38	CH1 RB	0.05		
3776207.84	672492.654	320.43	CH1 RT			
3776208.821	672488.797	320.615	CH1 LT	0.09		
3776208.534	672488.876	320.53	CH1 LB			
3776213.355	672506.804	320.117	CH2 RT	0.06	2.04	0.12
3776213.695	672506.769	320.057	CH2 RB			
3776214.992	672506.468	320.052	CH2 LB	0.05		
3776215.373	672506.478	320.106	CH2 LT			
3776214.973	672499.467	320.318	CH2 LT	0.08	2.94	0.23
3776214.59	672499.599	320.239	CH2 LB			
3776212.447	672499.393	320.239	CH2 RB	0.08		
3776212.037	672499.423	320.322	CH2 RT			
3776211.128	672492.744	320.522	CH2 RT	0.07	2.80	0.20
3776211.348	672492.777	320.451	CH2 RB			
3776213.243	672491.882	320.464	CH2 LB	0.08		
3776213.641	672491.519	320.542	CH2 LT			

3776213.78	672484.48	320.723	CH2 LT	0.07	2.91	0.22
3776213.488	672484.372	320.648	CH2 LB			
3776211.529	672483.657	320.667	CH2 RB	0.11		
3776210.973	672483.701	320.774	CH2 RT			
3776212.684	672475.371	320.975	CH2 RT	0.13	2.33	0.30
3776213.175	672475.458	320.846	CH2 RB			
3776214.7	672475.273	320.88	CH2 LB	0.11		
3776215.014	672475.383	320.985	CH2 LT			
3776217.016	672468.335	321.157	CH2 LT	0.09	2.24	0.21
3776216.749	672468.202	321.063	CH2 LB			
3776215.846	672466.944	321.072	CH2 RB	0.12		
3776215.639	672466.571	321.192	CH2 RT			
3776217.994	672458.08	321.416	CH2 RT	0.11	2.81	0.30
3776218.427	672458.207	321.31	CH2 RB			
3776220.158	672457.484	321.36	CH2 LB	0.18		
3776220.748	672457.524	321.537	CH2 LT			
3776223.68	672451.473	321.632	CH2 LT	0.07	2.25	0.16
3776223.331	672451.218	321.561	CH2 LB			
3776222.432	672450.154	321.562	CH2 RB	0.15		
3776222.058	672449.913	321.717	CH2 RT			
3776223.479	672447.915	321.767	CH2 RT	0.16	2.07	0.34
3776223.763	672448.031	321.603	CH2 RB			
3776224.992	672448.257	321.661	CH2 LB	0.12		
3776225.503	672448.357	321.782	CH2 LT			
3776219.485	672447.379	321.758	CH3 LT	0.10	0.97	0.10
3776219.109	672447.253	321.657	CH3 LB			
3776218.865	672447.254	321.696	CH3 RB	0.05		
3776218.559	672447.082	321.751	CH3 RT			
3776217.507	672450.476	321.706	CH3 RT	0.11	0.99	0.11
3776217.737	672450.539	321.595	CH3 RB			
3776218.257	672450.682	321.588	CH3 LB	0.11		
3776218.408	672450.882	321.698	CH3 LT			
3776217.08	672454.895	321.541	CH3 LT	0.07	1.05	0.07
3776216.802	672455.02	321.473	CH3 LB			
3776216.4	672455.152	321.436	CH3 RB	0.14		
3776216.082	672455.214	321.577	CH3 RT			
3776217.382	672457.044	321.455	CH3 RT	0.04	1.01	0.04
3776217.547	672456.943	321.413	CH3 RB			
3776217.959	672456.639	321.381	CH3 LB	0.07		
3776218.216	672456.478	321.452	CH3 LT			
3776214.886	672452.249	321.603	CH4 LT	0.02	0.88	0.01
3776214.652	672452.318	321.586	CH4 LB			
3776214.347	672452.438	321.594	CH4 RB	0.05		
3776214.057	672452.536	321.645	CH4 RT			
3776215.403	672455.906	321.578	CH4 RT	0.06	0.78	0.05
3776215.621	672455.652	321.518	CH4 RB			
3776215.797	672455.488	321.507	CH4 LB	0.04		
3776215.941	672455.336	321.548	CH4 LT			
3776222.051	672473.342	321.01	HEAD			
3776221.737	672475.305	320.987	CH5 RW		1.31	

3776222.675	672475.34	320.946	CH5 LB	0.07		
3776223.048	672475.344	321.018	CH5 LT			
3776223.14	672478.194	320.886	CH5 LW		0.93	
3776222.615	672478.143	320.851	CH5 W			
3776222.214	672478.17	320.896	CH5 RW			
3776222.27	672484.825	320.624	HEAD			
3776223.195	672487.266	320.644	CH6 LT	0.07	1.14	0.08
3776222.795	672487.358	320.576	CH6 LB			
3776222.343	672487.265	320.573	CH6 RB	0.06		
3776222.058	672487.399	320.632	CH6 RT			
3776222.708	672488.117	320.551	CH6 W			
3776225.53	672500.488	320.185	HEAD			
3776225.839	672502.471	320.149	CH7 LT	0.04	0.69	0.03
3776225.569	672502.527	320.107	CH7 LB			
3776225.358	672502.597	320.116	CH7 RB	0.05		
3776225.171	672502.633	320.168	CH7 RT			
3776225.817	672504.823	320.074	CH7 RT	0.05	0.76	0.04
3776226.012	672504.677	320.022	CH7 RB			
3776226.318	672504.415	320.013	CH7 LB	0.02		
3776226.419	672504.363	320.035	CH7 LT			
3776227.456	672503.821	320.107	HEAD			
3776228.069	672508.594	320.103	CH7 LT	0.21	1.04	0.22
3776227.599	672508.69	319.89	CH7 LB			
3776227.257	672508.866	319.899	CH7 RB	0.08		
3776227.071	672508.895	319.983	CH7 RT			
3776231.404	672509.431	319.96	CH8 RT	0.05	0.69	0.03
3776231.701	672509.462	319.914	CH8 RB			
3776231.803	672509.573	319.909	CH8 LB	0.06		
3776232.058	672509.636	319.968	CH8 LT			
3776233.067	672506.346	320.13	CH8 LT	0.08	0.78	0.06
3776232.806	672506.349	320.05	CH8 LB			
3776232.474	672506.303	320.05	CH8 RB	0.07		
3776232.288	672506.344	320.116	CH8 RT			
3776234.059	672503.335	320.176	HEAD			
3776231.168	672508.969	319.935	CH9 LT	0.05	0.78	0.04
3776230.977	672509.099	319.884	CH9 LB			
3776230.792	672509.127	319.905	CH9 RB	0.16		
3776230.471	672509.316	320.067	CH9 RT			
3776228.557	672504.202	320.206	CH9 RT	0.10	1.46	0.15
3776228.936	672504.091	320.104	CH9 RB			
3776229.674	672504.01	320.089	CH9 LB	0.06		
3776230.004	672504.006	320.149	CH9 LT			
3776229.457	672494.141	320.445	CH9 LT	0.10	1.69	0.17
3776229.122	672494.201	320.344	CH9 LB			
3776228.234	672494.184	320.355	CH9 RB	0.06		
3776227.766	672494.161	320.418	CH9 RT			
3776227.035	672485.411	320.666	CH9 RT	0.08	1.54	0.12
3776227.519	672485.805	320.586	CH9 RB			
3776228.063	672486.032	320.574	CH9 LB	0.06		
3776228.304	672486.286	320.632	CH9 LT			

3776230.499	672481.511	320.788	CH9 LT	0.07	1.45	0.10
3776230.128	672481.703	320.717	CH9 LB			
3776229.454	672481.615	320.744	CH9 RB	0.06		
3776229.058	672481.633	320.802	CH9 RT			
3776226.355	672476.777	320.958	CH9 RT	0.09	0.95	0.08
3776226.664	672476.505	320.87	CH9 RB			
3776226.864	672476.283	320.891	CH9 LB	0.02		
3776227.035	672476.115	320.908	CH9 LT			
3776227.903	672474.583	320.979	HEAD			
3776225.406	672471.58	321.092	CH9 LT	0.05	1.00	0.05
3776225.042	672471.547	321.042	CH9 LB			
3776224.769	672471.502	321.033	CH9 RB	0.05		
3776224.403	672471.535	321.086	CH9 RT			
3776224	672467.253	321.209	CH9 RT	0.04	1.04	0.05
3776224.438	672467.161	321.165	CH9 RB			
3776224.632	672467.053	321.172	CH9 LB	0.09		
3776225.011	672467.015	321.265	CH9 LT			
3776224.285	672464.1	321.333	HEAD			
3776229.895	672479.647	320.799	CH10 RT	0.02	1.02	0.03
3776230.171	672479.767	320.774	CH10 RB			
3776230.43	672480	320.755	CH10 LB	0.09		
3776230.741	672480.21	320.843	CH10 LT			
3776231.098	672478.488	320.854	CH10 LT	0.05	0.83	0.04
3776230.951	672478.384	320.807	CH10 LB			
3776230.651	672478.179	320.822	CH10 RB	0.06		
3776230.476	672477.934	320.885	CH10 RT			
3776232.794	672476.018	320.92	HEAD			
3776232.067	672474.856	320.929	CH10 RT	0.02	0.78	0.02
3776231.838	672474.723	320.909	CH10 RB			
3776231.726	672474.381	320.923	CH10 LB	0.08		
3776231.522	672474.301	321.001	CH10 LT			
3776235.482	672467.548	321.247	CH10 LT	0.10	1.39	0.14
3776235.18	672467.43	321.147	CH10 LB			
3776234.439	672467.323	321.143	CH10 RB	0.05		
3776234.116	672467.283	321.192	CH10 RT			
3776235.212	672459.231	321.502	CH10 RT	0.10	1.35	0.14
3776235.547	672459.202	321.4	CH10 RB			
3776236.208	672459.348	321.408	CH10 LB	0.08		
3776236.532	672459.491	321.486	CH10 LT			
3776237.458	672450.611	321.753	CH10 LT	0.04	1.48	0.07
3776237.024	672450.687	321.708	CH10 LB			
3776236.431	672450.482	321.712	CH10 RB	0.10		
3776235.989	672450.403	321.807	CH10 RT			
3776243.389	672451.45	321.746	CH11 RT	0.08		
3776243.912	672451.445	321.662	CH11 RB			
3776244.624	672451.437	321.651	CH11 BAR			
3776244.381	672455.777	321.578	CH11 BAR			
3776245.451	672458.673	321.485	CH11 BAR			
3776247.397	672461.19	321.452	CH11 BAR			
3776248.012	672457.84	321.557	CH11 BAR			

3776247.498	672455.19	321.612	CH11 BAR			
3776246.995	672452.325	321.648	CH11 BAR			
3776247.876	672452.1	321.722	CH11 LT	0.07		
3776247.58	672452.138	321.654	CH11 LB			
3776249.405	672459.257	321.707	CH11 LT	0.28	4.13	1.17
3776248.718	672459.302	321.423	CH11 LB			
3776245.901	672460.641	321.39	CH11 RB	0.10		
3776245.563	672460.784	321.492	CH11 RT			
3776248.025	672468.752	321.27	CH11 RT	0.08	1.53	0.13
3776248.416	672468.682	321.185	CH11 RB			
3776249.22	672468.604	321.181	CH11 LB	0.07		
3776249.541	672468.547	321.254	CH11 LT			
3776251.295	672475.604	321.126	CH11 LT	0.16	1.43	0.23
3776250.791	672475.676	320.968	CH11 LB			
3776250.156	672475.809	321.007	CH11 RB	0.05		
3776249.873	672475.788	321.053	CH11 RT			
3776249.322	672484.583	320.785	CH11 RT	0.03	1.23	0.04
3776249.603	672484.594	320.753	CH11 RB			
3776250.259	672484.487	320.765	CH11 LB	0.06		
3776250.538	672484.397	320.826	CH11 LT			
3776247.01	672491.05	320.634	CH11 LT	0.08	1.52	0.12
3776247.102	672491.124	320.554	CH11 LB			
3776247.953	672491.881	320.598	CH11 RB	0.13		
3776248.197	672491.993	320.723	CH11 RT			
3776245.297	672495.453	320.449	CH11 RT	0.02		
3776244.917	672495.37	320.432	CH11 RB			
3776244.259	672495.851	320.406	CH11 BAR			
3776242.821	672495.446	320.375	CH11 RB	0.08		
3776242.453	672495.358	320.452	CH11 RT			
3776238.809	672499.67	320.338	CH11 RT	0.08	8.52	0.65
3776239.178	672499.948	320.262	CH11 RB			
3776246.22	672503.274	320.247	CH11 LB	0.04		
3776246.5	672503.325	320.287	CH11 LT			
3776244.656	672507.942	320.185	CH11 LT	0.08	8.80	0.74
3776244.073	672507.542	320.101	CH11 LB			
3776236.532	672505.475	320.075	CH11 RB	0.14		
3776236.23	672505.405	320.211	CH11 RT			
3776235.38	672510.117	320.041	CH11 RT	0.11	6.46	0.68
3776235.583	672510.26	319.935	CH11 RB			
3776241.168	672511.316	319.96	CH11 LB	0.05		
3776241.705	672511.415	320.007	CH11 LT			
3776239.937	672511.02	319.977	CH11 BAR1			
3776242.088	672507.617	320.088	CH11 BAR1			
3776243.699	672504.611	320.184	CH11 BAR1			
3776244.356	672500.402	320.305	CH11 BAR1			
3776241.531	672500.977	320.281	CH11 BAR1			
3776240.483	672505.427	320.145	CH11 BAR1			
3776237.567	672510.552	320.036	CH11 BAR1			
3776237.756	672508.324	320.002	CH11 BAR2			
3776238.628	672506.764	320.056	CH11 BAR2			

3776237.094	672506.331	320.054	CH11 BAR2			
3776237.661	672503.137	320.173	CH11 BAR2			
3776239.477	672502.792	320.162	CH11 BAR2			
3776239.869	672500.6	320.277	CH11 BAR2			
3776258.506	672453.992	321.74	CH12 LT	0.04	1.00	0.04
3776258.168	672453.887	321.701	CH12 LB			
3776257.774	672453.868	321.702	CH12 RB	0.04		
3776257.52	672453.836	321.744	CH12 RT			
3776255.582	672458.782	321.61	CH12 RT	0.06	0.93	0.06
3776255.876	672458.893	321.549	CH12 RB			
3776256.076	672459.016	321.563	CH12 LB	0.03		
3776256.478	672459.042	321.595	CH12 LT			
3776257.611	672464.774	321.421	CH12 LT	0.02	1.11	0.02
3776257.192	672464.751	321.401	CH12 LB			
3776256.777	672464.832	321.408	CH12 RB	0.03		
3776256.52	672464.968	321.437	CH12 RT			
3776258.276	672462.738	321.507	HEAD			
3776257.458	672470.714	321.272	CH12 LT	0.05	0.88	0.04
3776257.244	672470.717	321.223	CH12 LB			
3776257.011	672470.639	321.203	CH12 RB	0.04		
3776256.591	672470.577	321.246	CH12 RT			
3776254.764	672478.402	321.044	CH12 RT	0.04	1.16	0.05
3776255.08	672478.442	320.999	CH12 RB			
3776255.389	672478.671	321.006	CH12 LB	0.12		
3776255.856	672478.795	321.122	CH12 LT			
3776253.878	672483.467	320.941	CH12 LT	0.08	0.73	0.06
3776253.472	672483.16	320.864	CH12 LB			
3776253.379	672483.075	320.868	CH12 RB	0.05		
3776253.319	672482.994	320.919	CH12 RT			
3776251.098	672484.362	320.807	CH12 RT	0.02	0.97	0.02
3776251.173	672484.615	320.784	CH12 RB			
3776251.268	672484.985	320.771	CH12 LB	0.07		
3776251.532	672485.234	320.837	CH12 LT			
3776251.989	672513.466	320.033	CH13 LT	0.07	1.77	0.13
3776251.842	672513.416	319.961	CH13 LB			
3776250.726	672512.682	320	CH13 RB	0.04		
3776250.425	672512.627	320.037	CH13 RT			
3776251.645	672505.534	320.298	CH13 RT	0.09	3.09	0.27
3776251.98	672505.501	320.211	CH13 RB			
3776254.561	672505.053	320.238	CH13 LB	0.11		
3776254.663	672504.892	320.344	CH13 LT			
3776257.018	672496.381	320.563	CH13 LT	0.07	3.38	0.23
3776256.542	672496.254	320.494	CH13 LB			
3776254.373	672495.02	320.471	CH13 RB	0.15		
3776253.954	672494.96	320.621	CH13 RT			
3776256.336	672488.763	320.793	CH13 RT	0.12	2.92	0.34
3776256.78	672488.707	320.677	CH13 RB			
3776258.867	672488.84	320.66	CH13 LB	0.14		
3776259.245	672488.984	320.803	CH13 LT			
3776260.05	672486.07	320.863	CH13 LT	0.13	3.00	0.38

3776259.698	672485.86	320.736	CH13 LB			
3776257.757	672484.425	320.8	CH13 RB	0.05		
3776257.617	672484.322	320.854	CH13 RT			
3776258.285	672477.821	321.098	CH13 RT	0.11	3.15	0.34
3776258.854	672477.847	320.99	CH13 RB			
3776261.11	672478.131	321.007	CH13 LB	0.09		
3776261.396	672478.343	321.099	CH13 LT			
3776263.694	672470.501	321.262	CH13 LT	0.08	3.71	0.30
3776263.383	672470.433	321.18	CH13 LB			
3776260.732	672468.945	321.213	CH13 RB	0.14		
3776260.454	672468.7	321.351	CH13 RT			
3776262.996	672463.187	321.485	CH13 RT	0.08	3.01	0.25
3776263.455	672463.314	321.401	CH13 RB			
3776265.356	672463.586	321.402	CH13 LB	0.06		
3776265.929	672463.872	321.463	CH13 LT			
3776269.47	672458.893	321.753	CH13 LT	0.10	3.86	0.40
3776269.254	672458.804	321.649	CH13 LB			
3776266.45	672457.067	321.594	CH13 RB	0.08		
3776266.15	672456.93	321.677	CH13 RT			
3776260.537	672485.755	320.93	CH14 RT	0.12	3.24	0.40
3776260.414	672485.312	320.807	CH14 RB			
3776260.446	672482.839	320.868	CH14 LB	0.06		
3776260.392	672482.514	320.926	CH14 LT			
3776263.278	672479.334	321.075	CH14 LT	0.08		
3776263.755	672479.519	320.994	CH14 LB			
3776264.773	672479.917	321.049	CH14 RT			
3776267.404	672476.111	321.202	CH14 RT	0.11	1.39	0.15
3776267.131	672475.878	321.094	CH14 RB			
3776266.809	672475.348	321.1	CH14 LB	0.08		
3776266.485	672475.074	321.178	CH14 LT			
3776269.852	672469.518	321.395	CH14 LT	0.13	1.24	0.17
3776270.253	672469.56	321.261	CH14 LB			
3776270.768	672469.675	321.293	CH14 RB	0.13		
3776271.074	672469.703	321.42	CH14 RT			
3776272.058	672466.314	321.445	CH14 RT	0.11	1.41	0.15
3776271.832	672466.151	321.337	CH14 RB			
3776271.191	672465.804	321.405	CH14 RB	0.18		
3776270.881	672465.546	321.583	CH14 RT			
3776271.94	672462.922	321.578	CH14 RT	0.09		
3776272.271	672462.866	321.486	CH14 RB			
3776273.172	672462.911	321.495	CH14 LB	0.12		
3776273.483	672462.95	321.612	CH14 LT		1.90	
3776273.17	672462.737	321.486	CH14 LB			
3776272.603	672462.136	321.515	CH14 RB	0.13		
3776272.203	672461.542	321.646	CH14 RT			
3776273.764	672455.918	321.757	HEAD			
3776274.792	672456.288	321.741	HEAD			
3776271.151	672459.911	321.665	HEAD			

Control Plot 6

Northing	Easting	Elevation	Feature code	Depth (m)	Width (m)	Cross (m^2)
3772751.151	671736.654	328.457	CH1 LT	0.02	1.13	0.04
3772751.065	671736.745	328.439	CH1 LB			
3772750.665	671737.126	328.389	CH1 RB	0.05		
3772750.357	671737.451	328.436	CH1 RT			
3772743.101	671742.338	328.455	CH1 RW		5.72	
3772747.771	671739.028	328.457	CH1 LW			
3772745.485	671736.252	328.512	CH1 LT	0.06	6.90	0.21
3772745.389	671736.29	328.452	CH1 LB			
3772740.791	671741.303	328.493	CH1 RW			
3772737.21	671735.713	328.615	CH1 RW		5.59	0.11
3772740.701	671731.666	328.608	CH1 LB	0.04		
3772740.9	671731.513	328.646	CH1 LT			
3772737.631	671728.996	328.741	CH1 LT	0.05	2.29	0.06
3772737.594	671729.068	328.69	CH1 LB			
3772735.836	671730.424	328.696	CH1 RW			
3772746.111	671740.336	328.441	CHBAR T			
3772746.395	671740.063	328.37	CH1 BAR B			
3772744.622	671735.847	328.484	CH1 BAR B			
3772743.867	671736.732	328.517	CH1 BAR B	0.05		
3772743.641	671736.867	328.57	CH1 BAR T			
3772740.473	671734.219	328.6	CH1 BAR			
3772737.871	671732.288	328.677	CH1 BAR			
3772739.163	671737.672	328.566	CH1 BAR			
3772741.618	671740.846	328.496	CH1 BAR			
3772743.954	671741.687	328.45	CH1 BAR			
3772741.118	671741.625	328.527	CH1 RW			
3772733.008	671726.637	328.769	CH1 RW			
3772734.553	671724.892	328.818	CH1 LW			
3772731.2	671718.2	329.032	CH1 LT	0.11	2.41	0.19
3772730.721	671718.39	328.92	CH1 LB			
3772729.011	671718.643	328.984	CH1 RB	0.05		
3772728.842	671718.705	329.032	CH1 RT			
3772727.697	671713.61	329.112	CH1 RT	0.06	2.17	0.14
3772727.861	671713.569	329.048	CH1 RB			
3772729.195	671712.607	329.063	CH1 LB	0.06		
3772729.472	671712.359	329.128	CH1 LT			
3772724.954	671703.668	329.324	CH1 LT	0.08	2.15	0.17
3772724.576	671703.81	329.242	CH1 LB			
3772723.421	671704.674	329.265	CH1 RB	0.08		
3772723.171	671704.864	329.344	CH1 RT			
3772719.297	671700.065	329.434	CH1 RT	0.09	2.33	0.19
3772719.56	671699.962	329.346	CH1 RB			
3772720.667	671698.772	329.38	CH1 LB	0.07		
3772720.946	671698.416	329.453	CH1 LT			
3772717.186	671694.718	329.626	CH1 LT	0.13	1.86	0.20
3772717.087	671694.744	329.5	CH1 LB			
3772715.942	671695.421	329.482	CH1 RB	0.09		
3772715.626	671695.728	329.574	CH1 RT			
3772714.254	671693.778	329.662	CH1 RT	0.10	1.83	0.29

3772714.614	671693.572	329.563	CH1 RB			
3772715.535	671693.011	329.523	CH1 LB	0.22		
3772715.827	671692.84	329.744	CH1 LT			
3772715.079	671691.505	329.752	CH1 LT	0.23	3.67	0.68
3772714.569	671691.962	329.518	CH1 LB			
3772712.497	671693.895	329.619	CH1 RB	0.14		
3772712.443	671694.059	329.756	CH1 RT			
3772711.289	671693.161	329.767	CH1 RT	0.15	4.09	0.59
3772711.416	671693.08	329.619	CH1 RB			
3772714.318	671691.297	329.587	CH1 LB	0.14		
3772714.757	671690.987	329.729	CH1 LT			
3772717.79	671689.186	329.679	HEAD			
3772719.242	671690.568	329.653	CH3 LT	0.05	0.70	0.04
3772719.157	671690.631	329.603	CH3 LB			
3772718.765	671690.895	329.601	CH3 RB	0.06		
3772718.678	671690.985	329.656	CH3 RT			
3772720.192	671694.633	329.551	CH3 RT	0.07	0.75	0.06
3772720.369	671694.574	329.476	CH3 RB			
3772720.623	671694.429	329.487	CH3 LB	0.08		
3772720.876	671694.325	329.572	CH3 LT			
3772721.012	671695.795	329.497	CH3 LT	0.05	0.79	0.08
3772720.827	671695.81	329.448	CH3 LB			
3772720.561	671695.717	329.424	CH3 RB	0.17		
3772720.243	671695.604	329.589	CH3 RT			
3772719.992	671698.112	329.392	CH3 RT	0.05	0.70	0.05
3772720.093	671698.157	329.347	CH3 RB			
3772720.312	671698.161	329.346	CH3 LB	0.11		
3772720.691	671698.196	329.455	CH3 LT			
3772702.336	671699.223	329.711	CH4 LT	0.02	0.91	0.03
3772702.206	671699.34	329.694	CH4 LB			
3772701.72	671699.77	329.676	CH4 RB	0.04		
3772701.656	671699.831	329.717	CH4 RT			
3772706.012	671704.267	329.592	CH4 RW		1.18	
3772706.755	671703.356	329.579	CH4 LW			
3772706.396	671703.751	329.562	CH4 END			
3772710.651	671706.716	329.474	HEAD			
3772711.591	671707.932	329.431	CH5 LT	0.04	0.93	0.04
3772711.49	671707.993	329.391	CH5 LB			
3772711.222	671708.515	329.381	CH5 RB	0.05		
3772711.128	671708.741	329.435	CH5 RT			
3772713.754	671710.358	329.352	CH5 RT	0.05	0.52	0.03
3772713.826	671710.339	329.298	CH5 RB			
3772714.024	671710.062	329.305	CH5 LB	0.06		
3772714.07	671709.941	329.368	CH5 LT			
3772717.602	671713.217	329.241	CH5 LW		0.68	
3772717.241	671713.795	329.249	CH5 RW			
3772719.435	671715.662	329.17	CH5 RW		0.77	0.05
3772719.816	671715.407	329.182	CH5 LB	0.12		
3772720.155	671715.384	329.301	CH5 LT			
3772721.641	671718.242	329.193	CH5 LT	0.11	0.78	0.04

3772721.485	671718.508	329.083	CH5 LB			
3772721.168	671718.856	329.098	CH5 RW			
3772727.481	671722.111	328.934	CH5 RT	0.02	0.51	0.02
3772727.539	671722.031	328.919	CH5 RB			
3772727.63	671721.842	328.927	CH5 LB	0.06		
3772727.749	671721.681	328.989	CH5 LT			
3772730.647	671723.172	328.854	CH5 LT	0.04	0.50	0.02
3772730.604	671723.29	328.81	CH5 LB			
3772730.6	671723.451	328.848	CH5 RB	0.05		
3772730.576	671723.662	328.898	CH5 RT			
3772691.679	671707.013	329.825	CH6 RT	0.09	1.33	0.11
3772691.952	671706.886	329.736	CH6 RB			
3772692.509	671706.5	329.718	CH6 LB	0.08		
3772692.82	671706.339	329.795	CH6 LT			
3772694.218	671709.464	329.647	CH6 LT	0.03	1.17	0.06
3772694.122	671709.618	329.618	CH6 LB			
3772693.406	671710.105	329.665	CH6 RB	0.08		
3772693.346	671710.24	329.746	CH6 RT			
3772695.833	671714.144	329.608	CH6 RT	0.06	1.44	0.09
3772695.879	671714.117	329.547	CH6 RB			
3772697.033	671713.837	329.55	CH6 LB	0.07		
3772697.212	671713.725	329.62	CH6 LT			
3772698.604	671717.293	329.547	CH6 LT	0.08	1.39	0.10
3772698.512	671717.399	329.467	CH6 LB			
3772698.016	671718.337	329.454	CH6 RB	0.07		
3772697.98	671718.537	329.522	CH6 RT			
3772702.402	671721.879	329.342	CH6 RT	0.12	1.70	0.19
3772702.781	671721.506	329.221	CH6 RB			
3772703.453	671720.866	329.299	CH6 LB	0.11		
3772703.718	671720.797	329.405	CH6 LT			
3772707.022	671726.361	329.167	CH6 LT	0.05	1.62	0.16
3772706.92	671726.507	329.119	CH6 LB			
3772705.924	671727.411	329.091	CH6 RB	0.15		
3772705.85	671727.478	329.243	CH6 RT			
3772710.073	671732.134	329.042	CH6 RT	0.10	1.55	0.12
3772710.165	671732.005	328.939	CH6 RB			
3772711.134	671731.086	328.985	CH6 LB	0.05		
3772711.179	671731.052	329.036	CH6 LT			
3772717.814	671738.264	328.83	CH6 LT	0.09	1.41	0.09
3772717.652	671738.325	328.74	CH6 LB			
3772716.962	671739.094	328.786	CH6 RB	0.03		
3772716.796	671739.237	328.819	CH6 RT			
3772722.557	671746.895	328.611	CH6 RW		1.28	0.03
3772723.634	671746.665	328.597	CH6 LB	0.05		
3772723.815	671746.653	328.643	CH6 LT			
3772726.898	671753.552	328.489	CH6 LT	0.09	1.17	0.11
3772726.749	671753.57	328.403	CH6 LB			
3772726.103	671754.005	328.373	CH6 RB	0.10		
3772725.892	671754.147	328.477	CH6 RT			
3772717.095	671735.698	328.886	HEAD			

3772717.492	671737.274	328.838	CH7 LT	0.02	0.60	0.02
3772717.266	671737.191	328.815	CH7 LB			
3772717.061	671737.065	328.811	CH7 RB	0.04		
3772716.962	671737.001	328.847	CH7 RT			
3772702.243	671717.367	329.494	HEAD			
3772701.718	671718.487	329.437	CH8 LT	0.04	0.74	0.04
3772701.606	671718.391	329.396	CH8 LB			
3772701.249	671718.23	329.402	CH8 RB	0.06		
3772701.141	671718.02	329.462	CH8 RT			
3772700.1	671719.801	329.355	TOPO			
3772699.992	671719.866	329.473	TOPO			
3772681.679	671713.42	329.826	CH9 LT	0.07	1.23	0.11
3772681.455	671713.632	329.759	CH9 LB			
3772681.025	671714.064	329.758	CH9 RB	0.11		
3772680.714	671714.18	329.872	CH9 RT			
3772682.59	671715.168	329.753	CH9 RT	0.04	1.11	0.07
3772682.827	671715.059	329.709	CH9 RB			
3772683.316	671714.734	329.701	CH9 LB	0.09		
3772683.548	671714.601	329.789	CH9 LT			
3772686.39	671719.494	329.643	CH9 LT	0.05	0.92	0.07
3772686.338	671719.681	329.59	CH9 LB			
3772686.018	671720.089	329.567	CH9 RB	0.09		
3772685.877	671720.261	329.658	CH9 RT			
3772688.404	671719.976	329.615	CH9 RT	0.19	0.71	0.11
3772688.39	671719.677	329.427	CH9 RB			
3772688.308	671719.574	329.425	CH9 LB	0.13		
3772688.212	671719.295	329.551	CH9 LT			
3772685.158	671714.046	329.772	HEAD			
3772686.986	671715.91	329.71	CH10 LT	0.07	0.69	0.06
3772686.837	671715.934	329.636	CH10 LB			
3772686.582	671716.126	329.647	CH10 RB	0.10		
3772686.391	671716.256	329.742	CH10 RT			
3772689.167	671720.207	329.592	CH10 RT	0.12	1.05	0.11
3772689.257	671719.971	329.469	CH10 RB			
3772689.446	671719.547	329.508	CH10 LB	0.09		
3772689.504	671719.211	329.602	CH10 LT			
3772695.002	671723.325	329.445	CH10 LT	0.08	0.81	0.05
3772694.891	671723.47	329.369	CH10 LB			
3772694.529	671723.793	329.381	CH10 RB	0.04		
3772694.409	671723.876	329.422	CH10 RT			
3772695.783	671732.903	329.227	CH10 RT	0.11	1.17	0.11
3772696.057	671732.808	329.113	CH10 RB			
3772696.776	671732.815	329.183	CH10 LB	0.07		
3772696.954	671732.817	329.25	CH10 LT			
3772697.843	671740.584	329.097	CH10 LT	0.14	1.50	0.21
3772697.585	671740.865	328.958	CH10 LB			
3772697.15	671741.39	328.989	CH10 RB	0.14		
3772696.75	671741.609	329.126	CH10 RT			
3772703.656	671745.005	328.979	CH10 RT	0.10	1.51	0.15
3772703.751	671744.859	328.877	CH10 RB			

3772704.463	671743.98	328.912	CH10 LB	0.09		
3772704.55	671743.788	329.006	CH10 LT			
3772709.116	671748.172	328.856	CH10 LT	0.09	1.84	0.15
3772708.963	671748.475	328.765	CH10 LB			
3772708.587	671749.762	328.759	CH10 RB	0.07		
3772708.563	671749.93	328.828	CH10 RT			
3772714.94	671753.716	328.63	CH10 RW		1.87	0.05
3772716.621	671753.28	328.634	CH10 LB	0.06		
3772716.786	671753.403	328.69	CH10 LT			
3772716.317	671755.366	328.558	CH10 LW		2.19	0.07
3772714.337	671755.681	328.599	CH10 RB	0.07		
3772714.155	671755.683	328.666	CH10 RT			
3772715.506	671758.973	328.533	CH10 RT	0.03	2.17	0.13
3772715.556	671758.943	328.499	CH10 RB			
3772717.155	671757.98	328.484	CH10 LB	0.08		
3772717.332	671757.804	328.567	CH10 LT			
3772719.122	671758.596	328.449	CH10 LW		2.23	0.07
3772717.506	671759.715	328.425	CH10 RB	0.06		
3772717.33	671759.922	328.49	CH10 RT			
3772692.059	671749.682	328.922	HEAD			
3772692.107	671751.258	328.91	CH11 LT	0.07	0.64	0.04
3772691.927	671751.227	328.843	CH11 LB			
3772691.635	671751.191	328.842	CH11 RB	0.07		
3772691.472	671751.154	328.914	CH11 RT			
3772692.327	671754.429	328.832	CH11 RT	0.06	0.71	0.06
3772692.41	671754.359	328.77	CH11 RB			
3772692.711	671754.239	328.764	CH11 LB	0.11		
3772692.967	671754.122	328.871	CH11 LT			
3772703.172	671770.835	328.533	BENCH C6			

Road Plot 1

Northing	Easting	Elevation	Feature code	Depth (m)
3775540.687	670895.831	329.968	CH 1 RT	0.11
3775541.251	670895.894	329.858	CH 1 RB	
3775541.598	670894.576	329.912	CH 1 RB	0.18
3775541.063	670894.498	330.096	CH 1 RT	
3775541.529	670892.072	330.137	CH 1 RT	0.10
3775542.177	670892.24	330.034	CH 1 RB	
3775542.773	670890.032	330.108	CH 1 RB	0.12
3775542.321	670889.878	330.229	CH 1 RT	
3775543.398	670887.854	330.222	CH 1 RT	0.09
3775543.94	670888.042	330.136	CH 1 RB	
3775545.58	670885.344	330.239	CH 1 RB	0.10
3775545.099	670885.133	330.338	CH 1 RT	
3775547.882	670883.461	330.413	CH 1 RT	0.13
3775548.255	670883.897	330.281	CH 1 RB	
3775550.189	670881.91	330.362	CH 1 RB	0.20
3775549.934	670881.245	330.56	CH 1 RT	
3775551.212	670878.95	330.548	CH 1 RT	0.09

3775551.734	670879.272	330.46	CH 1 RB	
3775553.558	670876.821	330.517	CH 1 RB	0.19
3775553.166	670876.567	330.711	CH 1 RT	
3775555.113	670873.262	330.805	CH 1 RT	0.17
3775555.766	670873.392	330.638	CH 1 RB	
3775556.249	670870.965	330.741	CH 1 RB	0.18
3775555.775	670870.762	330.925	CH 1 RT	
3775569.895	670856.319	331.502	CH 1 LT	0.21
3775569.423	670856.367	331.292	CH 1 LB	
3775569.598	670858.436	331.234	CH 1 LB	0.14
3775570.072	670858.354	331.377	CH 1 LT	
3775569.873	670861.875	331.252	CH 1 LT	0.12
3775569.246	670861.915	331.129	CH 1 LB	
3775568.902	670864.421	331.048	CH 1 LB	0.11
3775569.919	670864.528	331.155	CH 1 LT	
3775569.593	670866.88	331.084	CH 1 LT	0.09
3775569.679	670867.374	330.99	CH 1 LB	
3775570.779	670866.369	331.018	CH 1 LT	
3775571.279	670864.607	331.081	CH 1 LT	
3775572.026	670863.548	331.085	HEAD	
3775572	670865.318	331.059	CH 1 LT	
3775571.74	670868.67	330.975	CH 1 LT	
3775571.253	670871.484	330.886	CH 1 LT	
3775570.905	670871.705	330.845	CH 1 LB	
3775571.554	670874.241	330.789	CH 1 LB	0.13
3775572.041	670874.297	330.921	CH 1 LT	
3775572.71	670876.843	330.821	CH 1 LT	0.15
3775572.162	670876.994	330.67	CH 1 LB	
3775572.919	670879.875	330.567	CH 1 LB	0.09
3775573.565	670880.004	330.658	CH 1 LT	
3775573.583	670882.294	330.573	CH 1 LT	0.07
3775573.306	670882.347	330.5	CH 1 LB	
3775572.745	670883.952	330.507	CH 1 LB	0.05
3775573.225	670884.035	330.553	CH 1 LT	
3775571.615	670886.205	330.527	CH 1 LT	0.10
3775571.15	670886.11	330.424	CH 1 LB	
3775570.071	670887.955	330.318	CH 1 LB	0.14
3775570.782	670888.155	330.462	CH 1 LT	
3775570.429	670889.814	330.441	CH 1 LT	0.22
3775569.678	670889.796	330.223	CH 1 LB	
3775569.365	670893.143	330.119	CH 1 LB	0.13
3775569.694	670893.403	330.25	CH 1 LT	
3775569.252	670895.808	330.152	CH 1 LT	0.13
3775568.871	670895.758	330.026	CH 1 LB	
3775567.225	670897.716	329.917	CH 1 LB	0.17
3775567.696	670898.27	330.085	CH 1 LT	
3775566.943	670899.653	329.984	CH 1 LT	0.13
3775566.412	670899.805	329.855	CH 1 LB	
3775566.97	670902.195	329.758	CH 1 LB	0.08
3775567.347	670902.327	329.833	CH 1 LT	

3775567.836	670904.814	329.767	CH 1 LT	0.14
3775567.33	670904.912	329.623	CH 1 LB	
3775567.493	670906.91	329.555	CH 1 LB	0.15
3775567.885	670907.044	329.701	CH 1 LT	
3775567.791	670909.895	329.584	CH 1 LT	0.13
3775567.403	670910.024	329.457	CH 1 LB	
3775567.981	670912.456	329.353	CH 1 LB	0.10
3775568.151	670912.259	329.457	CH 1 LT	
3775568.594	670911.556	329.486	CH 1 LT	0.08
3775568.865	670911.547	329.405	CH 1 LB	
3775570.208	670910.382	329.481	HEAD	
3775570.19	670911.547	329.495	CH 1 LT	0.05
3775569.856	670911.451	329.446	CH 1 LB	
3775568.101	670913.111	329.355	CH 1 LB	0.17
3775568.504	670913.417	329.526	CH 1 LT	
3775568.447	670914.35	329.371	CH 1 LT	0.07
3775568.526	670914.62	329.302	CH 1 LB	
3775570.54	670913.511	329.448	HEAD	
3775568.901	670915.353	329.447	CH 1 LT	0.17
3775568.493	670915.553	329.278	CH 1 LB	
3775568.806	670917.938	329.22	CH 1 LB	0.13
3775569.263	670917.96	329.354	CH 1 LT	
3775564.755	670914.719	329.355	CH 1 BAR 1 T	
3775564.905	670912.045	329.445	CH 1 BAR 1 T	
3775564.969	670908.448	329.536	CH 1 BAR 1 T	
3775564.566	670904.959	329.655	CH 1 BAR 1 T	
3775563.618	670907.353	329.671	CH 1 BAR 1 T	
3775563.189	670909.686	329.6	CH 1 BAR 1 T	
3775561.794	670912.436	329.462	CH 1 BAR 1 T	
3775557.036	670908.736	329.668	CH 1 BAR 1 T	
3775557.7	670905.877	329.721	CH 1 BAR 1 T	
3775557.923	670903.483	329.795	CH 1 BAR 1 T	
3775557.227	670900.956	329.904	CH 1 BAR 1 T	
3775556.544	670898.391	329.969	CH 1 BAR 1 T	
3775556.507	670894.555	330.203	CH 1 BAR 1 T	0.15
3775556.841	670894.431	330.054	CH 1 BAR 1 B	
3775556.687	670890.991	330.18	CH 1 BAR 1 B	0.09
3775556.283	670890.935	330.274	CH 1 BAR 1 T	
3775555.955	670888.093	330.246	CH 1 BAR 1 T	
3775555.242	670891.342	330.252	CH 1 BAR 1 T	0.06
3775554.933	670891.244	330.197	CH 1 BAR 1 B	
3775553.931	670893.795	330.105	CH 1 BAR 1 B	0.08
3775554.419	670894.017	330.185	CH 1 BAR 1 T	
3775552.978	670897.172	330.084	CH 1 BAR 1 T	0.12
3775552.475	670897.377	329.961	CH 1 BAR 1 B	
3775551.35	670900.953	329.828	CH 1 BAR 1 B	0.10
3775551.826	670901.191	329.928	CH 1 BAR 1 T	
3775551.717	670903.368	329.838	CH 1 BAR 1 T	0.10
3775551.399	670903.557	329.734	CH 1 BAR 1 B	
3775551.452	670904.543	329.704	CH 1 BAR 1 B	0.07

3775551.722	670904.556	329.771	CH 1 BAR 1 T	
3775547.259	670901.105	329.832	CH 1 BAR 2 T	0.13
3775547.662	670901.366	329.701	CH 1 BAR 2 B	
3775547.643	670901.06	329.734	CH 1 BAR 2 B	
3775548.983	670898.806	329.83	CH 1 BAR 2 B	0.07
3775548.48	670898.61	329.896	CH 1 BAR 2 T	
3775550.006	670895.29	330.108	CH 1 BAR 2 T	0.18
3775550.67	670895.347	329.93	CH 1 BAR 2 B	
3775552.215	670891.807	330.127	CH 1 BAR 2 B	0.08
3775551.977	670891.612	330.211	CH 1 BAR 2 T	
3775553.335	670888.305	330.349	CH 1 BAR 2 T	0.09
3775553.657	670888.383	330.258	CH 1 BAR 2 B	
3775554.612	670885.494	330.368	CH 1 BAR 2 T	
3775556.025	670880.558	330.551	CH 1 BAR 2 T	
3775556.531	670877.583	330.647	CH 1 BAR 2 T	
3775553.727	670880.954	330.576	CH 1 BAR 2 T	0.13
3775553.222	670880.744	330.451	CH 1 BAR 2 B	
3775550.282	670883.693	330.369	CH 1 BAR 2 T	
3775547.192	670886.882	330.251	CH 1 BAR 2 T	0.03
3775546.832	670886.69	330.22	CH 1 BAR 2 B	
3775545.825	670888.839	330.167	CH 1 BAR 2 B	0.06
3775546.251	670889.207	330.226	CH 1 BAR 2 T	
3775545.301	670892.102	330.175	CH 1 BAR 2 T	0.15
3775544.725	670892.205	330.022	CH 1 BAR 2 B	
3775545.432	670895.084	329.997	CH 1 BAR 2 T	0.10
3775545.027	670895.205	329.901	CH 1 BAR 2 B	
3775545.558	670898.289	329.788	CH 1 BAR 2 T	
3775545.546	670899.637	329.742	CH 1 BAR 2 T	
3775565.506	670878.03	330.562	CH 1 BAR 3 T	
3775566.645	670876.154	330.686	CH 1 BAR 3 T	
3775567.68	670873.066	330.818	CH 1 BAR 3 T	
3775568.187	670870.003	330.993	CH 1 BAR 3 T	0.12
3775568.768	670870.035	330.877	CH 1 BAR 3 B	
3775567.896	670866.893	330.973	CH 1 BAR 3 B	0.06
3775567.255	670867.156	331.035	CH 1 BAR 3 T	
3775566.793	670865.522	331.048	CH 1 BAR 3 T	
3775565.212	670869.104	331.023	CH 1 BAR 3 T	0.12
3775564.55	670869.369	330.907	CH 1 BAR 3 B	
3775564.777	670871.688	330.834	CH 1 BAR 3 B	0.05
3775565.367	670871.709	330.886	CH 1 BAR 3 T	
3775565.386	670875.635	330.727	CH 1 BAR 3 T	0.05
3775564.935	670875.699	330.677	CH 1 BAR 3 B	
3775569.327	670878.757	330.653	CH 1 BAR 4 B	0.10
3775569.603	670879.188	330.753	CH 1 BAR 4 T	
3775567.229	670881.046	330.609	CH 1 BAR 4 T	0.09
3775566.696	670880.989	330.523	CH 1 BAR 4 B	
3775566.116	670883.276	330.395	CH 1 BAR 4 B	0.07
3775566.806	670883.461	330.465	CH 1 BAR 4 T	
3775566.418	670885.957	330.333	CH 1 BAR 4 T	
3775566.074	670889.013	330.219	CH 1 BAR 4 T	

3775565.835	670893.238	330.067	CH 1 BAR 4 B	0.09
3775566.336	670893.156	330.154	CH 1 BAR 4 T	
3775566.395	670896.486	330.049	CH 1 BAR 4 T	0.11
3775566.137	670896.611	329.943	CH 1 BAR 4 B	
3775568.122	670893.312	330.115	CH 1 BAR 4 B	0.07
3775567.654	670893.102	330.187	CH 1 BAR 4 T	
3775568.243	670890.536	330.316	CH 1 BAR 4 T	0.10
3775568.545	670890.555	330.218	CH 1 BAR 4 B	
3775569.212	670887.301	330.327	CH 1 BAR 4 T	
3775569.03	670884.194	330.476	CH 1 BAR 4 B	0.07
3775568.69	670883.792	330.545	CH 1 BAR 4 T	
3775569.423	670881.33	330.596	CH 1 BAR 4 T	
3775569.303	670879.181	330.682	CH 1 BAR 4 T	
3775539.084	670895.177	330.198	BENCH CH	
3775574.266	670882.816	330.577	CHAN 2 RT	0.07
3775574.527	670882.953	330.503	CHAN 2 R B	
3775574.895	670880.619	330.521	CHAN 2 R B	0.08
3775574.475	670880.654	330.598	CHAN 2 R T	
3775574.195	670878.252	330.69	CHAN 2 R T	0.08
3775574.487	670878.138	330.605	CHAN 2 R B	
3775574.182	670875.929	330.726	HEAD	
3775575.201	670877.297	330.688	CHAN 2 R T	0.09
3775574.834	670878.005	330.593	CHAN 2 R B	
3775575.594	670880.536	330.504	CHAN 2 R B	0.15
3775576.004	670880.612	330.654	CHAN 2 R T	
3775576.045	670882.245	330.53	CHAN 2 R T	0.07
3775575.896	670882.6	330.463	CHAN 2 R B	
3775576.344	670883.274	330.449	CHAN 2 R B	0.11
3775576.74	670883.021	330.563	CHAN 2 R T	
3775576.931	670883.197	330.452	CHAN 2 R B	
3775577.626	670880.445	330.546	CHAN 2 R B	0.08
3775577.317	670880.333	330.626	CHAN 2 R T	
3775577.693	670878.27	330.719	CHAN 2 R T	0.14
3775578.005	670878.269	330.58	CHAN 2 R B	
3775577.531	670875.816	330.718	HEAD	
3775579.509	670877.928	330.754	CHAN 2 RT	0.13
3775578.522	670878.089	330.629	CHAN 2 RB	
3775578.214	670880.075	330.566	CHAN 2 RB	
3775578.623	670880.161	330.627	CHAN 2 RT	0.07
3775578.068	670880.082	330.559	CHAN 2 RB	
3775577.59	670883.026	330.454	CHAN 2 RB	0.10
3775578.121	670883.082	330.555	CHAN 2 RT	
3775574.613	670885.981	330.442	CHAN 2 RT	0.09
3775575.11	670885.931	330.35	CHAN 2 RB	
3775574.993	670888.854	330.245	CHAN 2 RB	0.10
3775574.652	670888.804	330.349	CHAN 2 RT	
3775575.764	670892.204	330.242	CHAN 2 RT	0.09
3775575.934	670892.069	330.148	CHAN 2 RB	
3775576.915	670894.71	330.086	CHAN 2 RB	0.04
3775576.578	670894.779	330.123	CHAN 2 RT	

3775577.844	670898.155	330.043	CHAN 2 RT	0.05
3775578.093	670898.068	329.992	CHAN 2 RB	
3775578.629	670900.569	329.897	CHAN 2 RB	0.06
3775578.132	670900.797	329.957	CHAN 2 RT	
3775577.827	670903.402	329.863	CHAN 2 RT	0.13
3775578.352	670903.571	329.735	CHAN 2 RB	
3775577.006	670906.461	329.668	CHAN 2 RB	0.07
3775576.376	670906.39	329.737	CHAN 2 RT	
3775576.332	670908.996	329.656	CHAN 2 RT	0.09
3775576.722	670909.155	329.562	CHAN 2 RB	
3775575.796	670912.21	329.468	CHAN 2 RB	0.08
3775575.433	670912.339	329.545	CHAN 2 RT	
3775575.153	670914.607	329.444	CHAN 2 RT	0.09
3775575.291	670914.795	329.358	CHAN 2 RB	
3775574.403	670917.697	329.283	CHAN 2 RB	0.15
3775573.902	670917.771	329.431	CHAN 2 RT	
3775574.329	670920.514	329.203	CHAN 2 RT	0.06
3775574.835	670920.614	329.14	CHAN 2 RB	
3775574.652	670923.064	329.087	CHAN 2 RB	0.11
3775573.883	670922.994	329.193	CHAN 2 RT	
3775576.872	670921.694	329.129	CHAN 2 LT	
3775576.163	670919.502	329.318	CHAN 2 LT	0.13
3775575.803	670919.623	329.191	CHAN 2 LB	
3775575.658	670916.456	329.32	CHAN 2 LB	0.13
3775576.072	670916.416	329.447	CHAN 2 LT	
3775576.775	670912.523	329.564	CHAN 2 LT	0.12
3775576.373	670912.457	329.445	CHAN 2 LB	
3775577.2	670909.421	329.543	CHAN 2 LB	0.09
3775577.699	670909.351	329.632	CHAN 2 LT	
3775578.046	670905.893	329.78	CHAN 2 LT	0.06
3775577.767	670905.77	329.718	CHAN 2 LB	
3775579.354	670902.559	329.812	CHAN 2 LB	0.10
3775579.747	670902.522	329.914	CHAN 2 LT	
3775579.864	670898.208	330.019	CHAN 2 LT	0.08
3775579.485	670898.239	329.935	CHAN 2 LB	
3775578.473	670893.058	330.116	CHAN 2 LB	0.05
3775578.781	670892.767	330.168	CHAN 2 LT	
3775577.138	670890.339	330.283	CHAN 2 LT	0.08
3775576.814	670890.449	330.202	CHAN 2 LB	
3775576.216	670887.703	330.288	CHAN 2 LB	0.09
3775576.636	670887.465	330.374	CHAN 2 LT	
3775576.894	670885.322	330.427	CHAN 2 LT	0.08
3775576.614	670885.177	330.346	CHAN 2 LB	
3775576.682	670883.837	330.414	CHAN 2 LB	0.11
3775577.123	670884.151	330.525	CHAN 2 LT	
3775570.389	670919.818	329.243	CHAN 3 RT	0.08
3775570.693	670919.919	329.162	CHAN 3 RB	
3775571.147	670918.358	329.233	CHAN 3 RB	0.05
3775570.487	670918.101	329.278	CHAN 3 RT	
3775571.646	670917.096	329.288	CHAN 3 RT	0.03

3775572.029	670917.277	329.263		CHAN 3 RB	
3775573.56	670914.49	329.38		CHAN 3 RB	0.07
3775573.205	670914.236	329.452		CHAN 3 RT	
3775573.836	670911.206	329.572		CHAN 3 RT	0.08
3775574.226	670911.202	329.491		CHAN 3 RB	
3775574.565	670907.996	329.680	C	HEAD	
3775574.912	670910.608	329.553		CHAN 3 RT	0.03
3775574.574	670910.624	329.522		CHAN 3 RB	
3775574.154	670913.208	329.437		CHAN 3 RB	0.03
3775574.537	670913.291	329.463		CHAN 3 LT	
3775573.376	670916.606	329.367		CHAN 3 LT	0.08
3775573.154	670916.511	329.291		CHAN 3 LB	
3775571.716	670919.011	329.218		CHAN 3 LB	0.07
3775572.101	670919.037	329.287		CHAN 3 LT	
3775577.268	670921.559	329.09		CHAN 4 RT	0.01
3775577.501	670921.696	329.101		CHAN 4 RB	
3775578.831	670919.503	329.181		CHAN 4 RB	0.06
3775578.563	670919.151	329.239		CHAN 4 RT	
3775578.924	670916.702	329.268		CHAN 4 RT	0.03
3775579.289	670916.989	329.233		CHAN 4 RB	
3775579.853	670915.04	329.312		CHAN 4 RB	0.07
3775579.571	670914.891	329.384		CHAN 4 RT	
3775580.716	670911.842	329.496		CHAN 4 RT	0.05
3775581.147	670911.959	329.444		CHAN 4 RB	
3775581.707	670909.205	329.544		CHAN 4 RB	0.07
3775581.253	670909.06	329.616		CHAN 4 RT	
3775582.194	670906.845	329.661		CHAN 4 RT	0.05
3775582.45	670906.927	329.614		CHAN 4 RB	
3775582.68	670904.624	329.722		HEAD	
3775583.175	670906.47	329.703		CHAN 4 RT	0.08
3775582.815	670906.499	329.627		CHAN 4 RB	
3775582.333	670909.703	329.511		CHAN 4 RB	0.09
3775582.771	670909.825	329.599		CHAN 4 RT	
3775582.118	670912.748	329.568		CHAN 4 RT	0.17
3775581.679	670912.646	329.394		CHAN 4 RB	
3775580.621	670914.81	329.312		CHAN 4 RB	0.10
3775581.206	670914.645	329.411		CHAN 4 RT	
3775582.338	670913.833	329.514		CHAN 4 LT	0.07
3775582.493	670914.163	329.445		CHAN 4 LB	
3775583.405	670913.125	329.551		HEAD	
3775582.97	670914.488	329.507		CHAN 4 LT	0.06
3775582.723	670914.358	329.444		CHAN 4 LB	
3775580.967	670915.272	329.337		CHAN 4 LB	0.07
3775581.28	670915.679	329.404		CHAN 4 LT	
3775580.19	670918.821	329.274		CHAN 4 LT	0.06
3775579.665	670918.649	329.212		CHAN 4 LB	
3775578.909	670921.252	329.139		CHAN 4 LB	0.08
3775579.327	670921.677	329.22		CHAN 4 LT	
3775578.096	670924.058	329.102		CHAN 4 LT	0.03
3775577.706	670923.892	329.069		CHAN 4 LB	

3775577.132	670925.024	329.036	CHAN 4 LB	0.06
3775577.596	670925.32	329.097	CHAN 4 LT	
3775586.186	670884.886	330.512	CHAN 5 RW	
3775586.838	670882.497	330.62	CHAN 5 RW	
3775587.765	670880.183	330.686	CHAN 5 RB	0.11
3775587.383	670879.793	330.791	CHAN 5 RT	
3775588.316	670878.055	330.868	CHAN 5 RT	0.12
3775588.535	670878.185	330.753	CHAN 5 RB	
3775589.715	670876.467	330.766	CHAN 5 RB	0.13
3775589.215	670876.213	330.897	CHAN 5 RT	
3775590.507	670874.436	330.894	CHAN 5 RT	0.04
3775590.732	670874.523	330.853	CHAN 5 RB	
3775591.463	670872.799	330.932	HEAD	
3775591.085	670875.745	330.906	CHAN 5 LT	0.06
3775590.824	670875.643	330.841	CHAN 5 LB	
3775589.829	670877.444	330.781	CHAN 5 LB	0.07
3775590.211	670877.805	330.851	CHAN 5 LT	
3775588.692	670880.317	330.764	CHAN 5 LT	0.07
3775588.209	670880.33	330.697	CHAN 5 LB	
3775588.041	670883.233	330.61	CHAN 5 L W	
3775591.137	670889.663	330.349	HEAD	
3775591.482	670892.127	330.283	CHAN 6 RT	0.04
3775591.654	670892.009	330.243	CHAN 6 RB	
3775593.241	670893.727	330.145	CHAN 6 RB	0.07
3775592.731	670893.942	330.212	CHAN 6 RT	
3775591.624	670896.057	330.119	CHAN 6 RT	0.05
3775591.886	670896.135	330.074	CHAN 6 RB	
3775590.847	670900.015	329.964	CHAN 6 RB	0.13
3775590.406	670900.004	330.089	CHAN 6 RT	
3775589.842	670903.18	329.982	CHAN 6 RT	0.12
3775590.173	670903.239	329.862	CHAN 6 RB	
3775590.272	670906.393	329.785	CHAN 6 RB	0.10
3775589.8	670906.479	329.887	CHAN 6 RT	
3775591.183	670908.663	329.827	CHAN 6 RT	0.13
3775591.507	670908.613	329.692	CHAN 6 RB	
3775592.844	670910.733	329.59	CHAN 6 RB	0.11
3775591.928	670910.981	329.703	CHAN 6 RT	
3775591.978	670913.948	329.595	CHAN 6 RT	0.09
3775592.319	670913.938	329.506	CHAN 6 RB	
3775592.508	670916.521	329.448	CHAN 6 RB	0.12
3775592.005	670916.579	329.564	CHAN 6 RT	
3775593.847	670918.283	329.56	CHAN 6 RT	0.16
3775594.053	670918.22	329.399	CHAN 6 RB	
3775594.629	670921.151	329.283	CHAN 6 RB	0.11
3775594.284	670921.348	329.395	CHAN 6 RT	
3775597.372	670917.729	329.466	CHAN 6 LB	
3775597.166	670917.701	329.405	CHAN 6 LB	
3775595.612	670915.339	329.458	CHAN 6 LB	0.09
3775595.874	670915.166	329.547	CHAN 6 LT	
3775593.797	670909.562	329.726	CHAN 6 LT	0.07

3775593.489	670909.714	329.657	CHAN 6 LB	
3775592.91	670907.525	329.701	CHAN 6 LB	0.11
3775593.248	670907.609	329.807	CHAN 6 LT	
3775592.251	670906.072	329.838	CHAN 6 LT	0.07
3775591.956	670906.217	329.768	CHAN 6 LB	
3775592.321	670904.625	329.818	CHAN 6 LB	0.06
3775592.575	670904.55	329.88	CHAN 6 LT	
3775592.708	670902.184	329.954	HEAD	
3775591.949	670903.64	329.859	CHAN 6 LB	0.06
3775591.367	670903.613	329.922	CHAN 6 LT	
3775591.074	670905.364	329.866	CHAN 6 LT	0.06
3775591.46	670905.273	329.808	CHAN 6 LB	
3775590.699	670905.866	329.801	CHAN 6 LB	0.07
3775590.996	670905.671	329.868	CHAN 6 LT	
3775591.028	670902.106	329.949	CHAN 6 LT	0.05
3775590.888	670902.073	329.899	CHAN 6 LB	
3775591.405	670898.218	330.034	CHAN 6 LB	0.03
3775591.78	670898.178	330.063	CHAN 6 LT	
3775593.657	670895.176	330.269	CHAN 6 LT	0.12
3775593.391	670894.993	330.152	CHAN 6 LB	
3775592.769	670892.813	330.196	CHAN 6 LB	0.15
3775593.886	670892.629	330.342	CHAN 6 LT	
3775593.808	670890.244	330.343	HEAD	0.03
3775593.629	670890.364	330.312	CHAN 6 LB	
3775603.725	670869.384	331.077	CHAN 7 RB	0.18
3775603.271	670869.555	331.255	CHAN 7 RT	
3775604.332	670872.178	331.101	CHAN 7 RT	0.09
3775604.649	670872.19	331.009	CHAN 7 RB	
3775603.62	670876.179	330.908	CHAN 7 RB	0.02
3775603.03	670876.12	330.927	CHAN 7 RT	
3775601.678	670880.247	330.808	CHAN 7 RT	0.04
3775601.979	670880.422	330.764	CHAN 7 RB	
3775601.32	670884.132	330.58	CHAN 7 RB	0.07
3775600.852	670884.345	330.652	CHAN 7 RT	
3775601.104	670888.224	330.506	CHAN 7 RT	0.04
3775601.398	670888.232	330.467	CHAN 7 RB	
3775600.781	670892.865	330.298	CHAN 7 RB	0.04
3775600.166	670892.989	330.336	CHAN 7 RT	
3775600.322	670897.04	330.2	CHAN 7 RT	0.01
3775600.665	670897.092	330.187	CHAN 7 RB	
3775599.879	670900.944	330.029	CHAN 7 RB	0.04
3775599.214	670900.811	330.068	CHAN 7 RT	
3775596.928	670904.685	329.925	CHAN 7 RT	0.05
3775597.096	670904.921	329.873	CHAN 7 RB	
3775595.198	670907.494	329.72	CHAN 7 RB	0.11
3775594.672	670907.377	329.827	CHAN 7 RT	
3775593.99	670909.414	329.725	CHAN 7 RT	0.06
3775594.248	670909.674	329.665	CHAN 7 RB	
3775595.485	670913.532	329.55	CHAN 7 RB	0.04
3775596.011	670913.649	329.589	CHAN 7 RT	

3775597.559	670911.914	329.76	CHAN 7 RT	0.12
3775597.21	670911.573	329.644	CHAN 7 RB	
3775598.385	670907.761	329.809	CHAN 7 RB	0.07
3775598.911	670907.673	329.875	CHAN 7 RT	
3775599.957	670903.439	330.036	CHAN 7 RT	0.07
3775599.531	670903.185	329.965	CHAN 7 RB	
3775600.281	670901.505	330.036	CHAN 7 RB	0.05
3775600.509	670901.233	330.083	CHAN 7 RT	
3775600.723	670903.197	330.05	CHAN 7 RT	0.12
3775601.038	670903.195	329.933	CHAN 7 RB	
3775601.724	670904.291	329.891	CHAN 7 RB	0.17
3775601.495	670904.414	330.062	CHAN 7 RT	
3775602.206	670905.406	329.877	CHAN 7 RT	0.05
3775602.589	670905.539	329.831	CHAN 7 RB	
3775602.206	670908.681	329.736	CHAN 7 RB	0.09
3775601.76	670908.859	329.821	CHAN 7 RT	
3775601.023	670911.165	329.735	CHAN 7 RT	0.06
3775601.57	670911.434	329.672	CHAN 7 RB	
3775604.664	670908.456	329.736	CHAN 7 LB	0.10
3775605.053	670908.129	329.837	CHAN 7 LT	
3775604.433	670905.279	329.907	CHAN 7 LT	0.12
3775604.144	670905.324	329.784	CHAN 7 LB	
3775604.792	670903.743	329.884	CHAN 7 LB	0.13
3775605.383	670903.671	330.009	CHAN 7 LT	
3775605.455	670901.969	329.998	HEAD	
3775603.986	670903.452	329.926	CHAN 7 LT	0.06
3775603.98	670903.723	329.867	CHAN 7 LB	
3775604.047	670902.053	329.92	CHAN 7 LB	0.06
3775604.463	670901.981	329.978	CHAN 7 LT	
3775604.467	670899.869	330.066	CHAN 7 LT	0.07
3775604.224	670899.874	329.997	CHAN 7 LB	
3775604.225	670897.308	330.146	HEAD	
3775603.013	670900.486	330.024	CHAN 7 LT	0.06
3775603.232	670900.543	329.969	CHAN 7 LB	
3775603.007	670902.905	329.901	CHAN 7 LB	0.05
3775602.617	670902.957	329.951	CHAN 7 LT	
3775602.518	670904.078	329.925	CHAN 7 LT	
3775601.462	670902.586	330.067	CHAN 7 LT	0.07
3775601.175	670902.725	329.996	CHAN 7 LB	
3775601.528	670898.453	330.151	CHAN 7 LB	0.01
3775601.96	670898.37	330.164	CHAN 7 LT	
3775602.199	670894.447	330.323	CHAN 7 LT	0.04
3775601.911	670894.386	330.281	CHAN 7 LB	
3775602.115	670890.547	330.391	CHAN 7 LB	0.07
3775602.561	670890.296	330.464	CHAN 7 LT	
3775602.472	670886.173	330.626	CHAN 7 LT	0.08
3775602.128	670886.319	330.544	CHAN 7 LB	
3775601.776	670883.059	330.653	CHAN 7 LB	0.05
3775602.127	670883.174	330.703	CHAN 7 LT	
3775603.173	670880.643	330.776	CHAN 7 LT W	

3775604.596	670878.911	330.948	CHAN 7 LT	0.13		
3775604.171	670878.605	330.822	CHAN 7 LB			
3775605.282	670875.36	330.928	CHAN 7 LB	0.07		
3775605.974	670875.487	330.999	CHAN 7 LT			
3775606.864	670873.002	331.113	CHAN 7 LT	0.08		
3775606.401	670872.818	331.029	CHAN 7 LB			
3775609.015	670889.727	330.432	HEAD			
3775609.13	670891.34	330.327	CHAN 8 RB	0.08		
3775608.77	670891.324	330.411	CHAN 8 RT			
3775608.963	670893.769	330.294	CHAN 8 RT	0.05		
3775609.312	670893.713	330.244	CHAN 8 RB			
3775609.107	670895.682	330.179	CHAN 8 RB	0.08		
3775608.736	670895.987	330.254	CHAN 8 RT			
3775608.586	670899.056	330.133	CHAN 8 RT	0.05		
3775609.213	670898.969	330.084	CHAN 8 RB			
3775609.192	670901.21	330.02	CHAN 8 RB	0.10		
3775608.885	670901.239	330.123	CHAN 8 RT			
3775609	670902.914	330.036	CHAN 8 RT	0.06		
3775609.221	670902.884	329.973	CHAN 8 RB			
3775610.392	670901.047	329.977	CHAN 8 LB	0.11		
3775610.598	670900.813	330.082	CHAN 8 LT			
3775610.723	670897.658	330.155	CHAN 8 LT	0.03		
3775610.399	670897.552	330.12	CHAN 8 LB			
3775611.07	670894.389	330.242	CHAN 8 LB	0.08		
3775611.461	670894.198	330.321	CHAN 8 LT			
3775611.249	670892.821	330.358	CHAN 8 LT	0.07		
3775611	670892.879	330.287	CHAN 8 LB			
3775611.236	670891.722	330.322	CHAN 8 LB	0.06		
3775611.447	670891.805	330.38	CHAN 8 LT			
3775610.898	670890.6	330.388	HEAD			
3775610.121	670891.228	330.413	CHAN 8 LT	0.10		
3775610.432	670891.303	330.311	CHAN 8 LB			
3775610.463	670892.521	330.295	CHAN 8 LB	0.04		
3775610.25	670892.495	330.331	CHAN 8 LT			
3775609.805	670892.435	330.348	CHAN 8 LT	0.06		
3775609.621	670892.446	330.286	CHAN 8 LB			
3775609.653	670891.288	330.325	CHAN 8 LB	0.07		
3775609.834	670891.45	330.399	CHAN 8 LT			
3775539.097	670895.183	330.19	BENCH CH			

Road Plot 2

Northing	Easting	Elevation	Feature code	Depth (m)	Width (m)	Cross (m^2)
3775616.139	670955.755	328.258	CH1RT	0.03		
3775616.433	670955.756	328.223	CH1 RB			
3775621.302	670957.015	328.157	CH1 LB	0.04		
3775621.481	670957.052	328.201	CH1 LT			
3775621.05	670953.006	328.366	CH1 LT	0.08		
3775620.87	670953.011	328.288	CH1 LB			
3775624.958	670946.807	328.567	CH2 RW			
3775627.611	670947.278	328.58	CH2 LW			

3775629.677	670943.2	328.717	CH2 LW			
3775631.257	670940.034	328.843	CH2 LB	0.04		
3775631.407	670939.974	328.887	CH2 LT			
3775627.803	670950.851	328.426	CH2 LW			
3775629.379	670953.098	328.313	CH2 LW			
3775624.479	670955.42	328.303	CH2 RW			
3775626.145	670959.853	328.152	CH2 RB	0.05		
3775625.952	670959.978	328.204	CH2 RT			
3775630.608	670958.892	328.195	CH2 LT	0.06		
3775630.465	670958.922	328.136	CH2 LB			
3775630.711	670956.349	328.227	CH2 LB	0.04		
3775630.743	670956.318	328.267	CH2 LT			
3775630.813	670962.141	327.999	CH2 LW			
3775630.654	670966.14	327.854	CH2 LB	0.10		
3775630.926	670966.208	327.952	CH2 LT			
3775627.33	670963.423	328	CH2 RW			
3775627.341	670961.065	328.091	CH2 RB	0.08		
3775626.97	670961.142	328.172	CH2 RT			
3775627.886	670960.029	328.094	CH2 BAR			
3775627.438	670956.163	328.249	CH2 BAR			
3775626.995	670954.101	328.35	CH2 BAR			
3775625.442	670954.934	328.338	CH2 BAR			
3775625.751	670956.515	328.295	CH2 BAR T	0.05		
3775625.533	670956.579	328.249	CH2 BAR B			
3775626.292	670958.067	328.238	CH2 BAR			
3775626.648	670956.746	328.321	TOPO			
3775626.588	670955.581	328.351	TOPO			
3775623.819	670950.244	328.429	CH2 BAR			
3775624.54	670949.247	328.545	CH2 BAR T	0.07		
3775624.717	670949.291	328.472	CH2 BAR B			
3775624.998	670946.962	328.564	CH2 BAR B			
3775623.19	670948.56	328.466	CH2 BAR B	0.08		
3775623.377	670948.619	328.546	CH2 BAR T			
3775624.876	670947.108	328.569	CH2 BAR			
3775630.025	670962.659	327.979	CH2 BAR			
3775630.596	670964.008	327.995	CH2 BAR T	0.10		
3775630.708	670964.046	327.896	CH2 BAR B			
3775629.305	670964.518	327.897	CH2 BAR B	0.03		
3775629.544	670964.592	327.93	CH2 BAR T			
3775629.089	670965.24	327.898	CH2 BAR			
3775629.912	670965.692	327.87	CH2 BAR			
3775632.007	670946.689	328.611	HEAD			
3775631.977	670948.524	328.535	CH3 LT	0.02	0.77	0.03
3775631.777	670948.518	328.515	CH3 LB			
3775631.407	670948.416	328.508	CH3 RB	0.05		
3775631.25	670948.257	328.561	CH3 RT			
3775629.713	670951.195	328.455	CH3 RT	0.04	1.49	0.09
3775629.865	670951.255	328.415	CH3 RB			
3775630.867	670951.68	328.377	CH3 LB	0.08		
3775631.093	670951.765	328.46	CH3 LT			

3775636.799	670948.383	328.565	HEAD			
3775636.899	670949.625	328.522	CH4 LT	0.04	0.75	0.03
3775636.759	670949.586	328.483	CH4 LB			
3775636.346	670949.523	328.512	CH4 RB	0.04		
3775636.161	670949.484	328.554	CH4 RT			
3775634.625	670954.237	328.361	CH4 RT	0.04	0.74	0.02
3775634.764	670954.217	328.318	CH4 RB			
3775635.224	670954.186	328.318	CH4 LB	0.02		
3775635.364	670954.258	328.338	CH4 LT			
3775634.11	670957.845	328.268	CH4 LT	0.05	1.31	0.03
3775634.033	670957.78	328.216	CH4 LB			
3775632.845	670957.498	328.213	CH4 RW			
3775631.239	670962.305	328.006	CH4 RW		1.79	0.01
3775631.998	670960.682	328.076	CH4 LT	0.01		
3775631.932	670960.658	328.064	CH4 LB			
3775642.914	670924.485	329.412	CH5 LB	0.04		
3775642.991	670924.47	329.453	CH5 LT		1.37	0.03
3775641.719	670924.983	329.436	CH5 RT	0.04		
3775641.803	670924.966	329.399	CH5 RB			
3775641.458	670932.943	329.152	CH5 RT	0.03	1.19	0.04
3775641.628	670932.946	329.125	CH5 RB			
3775642.287	670932.781	329.12	CH5 LB	0.03		
3775642.638	670932.805	329.154	CH5 LT			
3775642.929	670936.782	329.056	CH5 LT	0.08	1.87	0.08
3775642.775	670936.839	328.974	CH5 LB			
3775641.197	670937.494	328.994	CH5 RW			
3775641.515	670942.953	328.801	CH5 RW		0.91	0.03
3775642.127	670943.188	328.824	CH5 LB	0.07		
3775642.398	670943.19	328.89	CH5 LT			
3775641.603	670949.89	328.675	CH5 LT	0.09	1.43	0.07
3775641.321	670949.774	328.583	CH5 LB			
3775640.171	670949.821	328.599	CH5 RW			
3775638.078	670954.756	328.387	CH5 RW		0.81	0.01
3775638.227	670955.371	328.37	CH5 LB	0.03		
3775638.328	670955.522	328.402	CH5 LT			
3775634.81	670959.758	328.159	CH5 LT	0.02	0.97	0.05
3775634.689	670959.682	328.143	CH5 LB			
3775634.131	670959.434	328.131	CH5 RB	0.08		
3775633.962	670959.294	328.209	CH5 RT			
3775632.826	670962.585	328.061	CH5 LT	0.04		
3775632.713	670962.582	328.023	CH5 LB			
3775637.185	670963.014	328.1	HEAD			
3775637.709	670964.752	328.093	CH6 LT	0.08	0.95	0.04
3775637.438	670964.79	328.018	CH6 LB			
3775636.81	670965.055	328.01	CH6 RW			
3775636.693	670970.678	327.827	CH6 RT	0.03	0.99	0.05
3775636.852	670970.693	327.799	CH6 RB			
3775637.265	670970.815	327.786	CH6 LB	0.07		
3775637.644	670970.941	327.853	CH6 LT			
3775659.077	670927.411	329.544	HEAD			

3775658.741	670928.272	329.538	CH7 LT	0.06	0.86	0.04
3775658.555	670928.14	329.478	CH7 LB			
3775658.169	670927.991	329.456	CH7 RB	0.03		
3775658.023	670927.796	329.49	CH7 RT			
3775656.375	670928.785	329.428	CH7 RW		1.52	0.06
3775657.292	670929.361	329.384	CH7 LB	0.08		
3775657.577	670929.721	329.469	CH7 LT			
3775656.221	670931.917	329.306	CH7 LW		1.80	
3775654.506	670931.356	329.321	CH7 RW			
3775655.294	670931.708	329.281	CH7END			
3775650.664	670940.135	328.968	HEAD			
3775650.449	670941.416	328.949	CH8 LT	0.06	0.61	0.03
3775650.29	670941.164	328.885	CH8 LB			
3775650.107	670941.02	328.88	CH8 RB	0.03		
3775650.046	670940.956	328.908	CH8 RT			
3775647.288	670944.604	328.776	CH8 RT	0.06	1.08	0.06
3775647.431	670944.615	328.719	CH8 RB			
3775648.066	670944.886	328.726	CH8 LB	0.06		
3775648.306	670944.966	328.781	CH8 LT			
3775647.48	670949.95	328.639	CH8 LT	0.06	1.18	0.04
3775647.269	670949.957	328.578	CH8 LB			
3775646.306	670950.072	328.605	CH8 RW			
3775646.208	670954.931	328.446	CH8 RT	0.05	1.00	0.06
3775646.28	670954.961	328.399	CH8 RB			
3775646.958	670954.941	328.411	CH8 LB	0.07		
3775647.199	670955.075	328.486	CH8 LT			
3775646.112	670960.304	328.329	CH8 LT	0.10	0.92	0.09
3775645.814	670960.156	328.227	CH8 LB			
3775645.408	670959.986	328.226	CH8 RB	0.09		
3775645.241	670960.004	328.312	CH8 RT			
3775643.321	670964.168	328.139	CH8 RT	0.05	1.30	0.06
3775643.491	670964.141	328.091	CH8 RB			
3775644.414	670964.406	328.065	CH8 LB	0.04		
3775644.599	670964.397	328.102	CH8 LT			
3775644.489	670965.312	328.062	CH8 LT	0.03	0.95	0.06
3775644.45	670965.343	328.031	CH8 LB			
3775643.778	670965.196	328.043	CH8 RB	0.11		
3775643.548	670965.206	328.148	CH8 RT			
3775654.327	670951.959	328.636	HEAD			
3775654.055	670953.707	328.595	CH9 LT	0.06	0.66	0.04
3775653.952	670953.638	328.534	CH9 LB			
3775653.539	670953.565	328.518	CH9 RB	0.07		
3775653.403	670953.61	328.592	CH9 RT			
3775651.636	670955.651	328.52	CH9 RT	0.06	1.88	0.14
3775651.808	670955.689	328.457	CH9 RB			
3775653.058	670956.732	328.458	CH9 LB	0.09		
3775653.158	670956.755	328.544	CH9 LT			
3775651.559	670957.812	328.448	CH9 LT	0.07	0.94	0.06
3775651.379	670957.654	328.374	CH9 LB			
3775650.966	670957.28	328.378	CH9 RB	0.06		

3775650.852	670957.189	328.436	CH9 RT			
3775648.605	670960.183	328.331	CH9 RT	0.09	1.47	0.10
3775648.832	670960.352	328.24	CH9 RB			
3775649.533	670960.774	328.248	CH9 LB	0.05		
3775649.91	670960.856	328.296	CH9 LT			
3775647.155	670963.899	328.221	CH9 LT	0.09	1.22	0.10
3775647.02	670963.86	328.131	CH9 LB			
3775646.359	670963.312	328.125	CH9 RB	0.08		
3775646.285	670963.042	328.202	CH9 RT			
3775641.474	670969.468	327.918	CH9 RT	0.04	2.15	0.15
3775641.6	670969.484	327.879	CH9 RB			
3775643.097	670970.293	327.866	CH9 LB	0.11		
3775643.438	670970.343	327.971	CH9 LT			
3775654.519	670957.122	328.554	HEAD			
3775653.615	670959.515	328.465	CH10 LT	0.04	0.77	0.03
3775653.556	670959.453	328.427	CH10 LB			
3775653.082	670959.19	328.42	CH10 RB	0.04		
3775652.964	670959.106	328.458	CH10 RT			
3775649.004	670963.043	328.287	CH10 LT	0.06		
3775649.04	670962.918	328.228	CH10 LB			
3775659.592	670977.299	327.751	HEAD			
3775658.354	670983.298	327.588	CH11 LT	0.05	1.02	0.06
3775658.172	670983.225	327.534	CH11 LB			
3775657.612	670982.972	327.475	CH11 RB	0.06		
3775657.416	670982.908	327.54	CH11 RT			
3775655.656	670985.78	327.388	CH11 RT	0.06	1.19	0.09
3775655.908	670985.887	327.329	CH11 RB			
3775656.325	670986.093	327.35	CH11 LB	0.09		
3775656.71	670986.323	327.437	CH11 LT			
3775663.611	670987.336	327.455	HEAD			
3775663.584	670988.732	327.432	CH12 LT	0.04	0.70	0.04
3775663.504	670988.668	327.388	CH12 LB			
3775663.115	670988.631	327.39	CH12 RB	0.06		
3775662.891	670988.663	327.447	CH12 RT			
3775663.298	670990.086	327.404	CH12 RT	0.06	0.81	0.04
3775663.366	670990.008	327.341	CH12 RB			
3775663.797	670989.717	327.325	CH12 LB	0.03		
3775663.938	670989.584	327.356	CH12 LT			
3775665.455	670990.715	327.292	CH12 LT	0.05	0.73	0.03
3775665.337	670990.858	327.241	CH12 LB			
3775665.083	670991.165	327.226	CH12 RB	0.04		
3775664.942	670991.239	327.267	CH12 RT			
3775665.292	670921.404	329.783	CH13 RT	0.13	2.79	0.27
3775665.815	670921.455	329.656	CH13 RB			
3775667.41	670921.907	329.621	CH13 LB	0.07		
3775667.912	670922.363	329.687	CH13 LT			
3775667.916	670931.225	329.452	CH13 LT	0.07	2.81	0.18
3775667.624	670931.078	329.385	CH13 LB			
3775665.312	670930.679	329.35	CH13 RB	0.06		
3775665.154	670930.689	329.414	CH13 RT			

3775663.018	670941.434	329.027	CH13 RW	
3775661.43	670950.667	328.737	CH13 RW	
3775662.569	670959.049	328.459	CH13 RW	
3775663.992	670966.656	328.21	CH13 RT	0.08
3775664.082	670966.665	328.126	CH13 RB	
3775666.256	670972.539	327.93	CH13 RW	
3775666.402	670977.99	327.681	CH13 RB	0.09
3775666.084	670977.973	327.77	CH13 RT	
3775665.216	670983.443	327.585	CH13 RW	
3775667.231	670985.556	327.5	CH13 RW	
3775615.272	670955.636	328.415	R2 BENCH	
3775667.898	670987.751	327.425	CH13 RT	0.05
3775668.137	670987.604	327.379	CH13 RB	
3775669.417	670986.85	327.369	CH13 LB	0.11
3775669.666	670986.8	327.475	CH13 LT	
3775669.501	670981.86	327.566	CH13 LT	0.03
3775669.365	670981.877	327.535	CH13 LB	
3775669.62	670978.879	327.654	CH13 LB	0.10
3775669.693	670978.833	327.754	CH13 LT	
3775669.034	670973.639	328.003	CH13 LT	0.18
3775668.719	670973.56	327.828	CH13 LB	
3775670.267	670968.149	328.091	CH13 LB	0.06
3775670.404	670968.056	328.149	CH13 LT	
3775667.007	670962.541	328.311	CH13 LW	
3775667.366	670958.834	328.441	CH13 LB	0.04
3775667.569	670958.894	328.484	CH13 LT	
3775668.64	670949.915	328.815	CH13 LT	0.08
3775668.497	670949.894	328.734	CH13 LB	
3775665.549	670944.639	328.949	CH13 LB	0.04
3775665.801	670944.639	328.985	CH13 LT	
3775665.891	670938	329.21	CH13 LT	0.04
3775665.838	670937.969	329.169	CH13 LB	
3775667.774	670928.406	329.467	CH13 LB	0.05
3775667.921	670928.396	329.52	CH13 LT	
3775667.384	670920.448	329.865	CH13 LT	0.21
3775667.134	670920.471	329.655	CH13 LB	
3775667.487	670917.572	329.809	TOPO	
3775665.172	670914.311	329.879	TOPO	
3775664.794	670944.015	329.003	CH13 BAR	
3775663.917	670947.783	328.897	CH13 BAR T	0.04
3775663.806	670947.798	328.857	CH13 BAR B	
3775663.711	670953.456	328.641	CH13 BAR	
3775664.88	670958.142	328.543	CH13 BAR T	0.04
3775664.711	670958.159	328.499	CH13 BAR B	
3775665.91	670962.913	328.328	CH13 BAR	
3775666.49	670958.951	328.496	CH13 BAR T	0.05
3775666.749	670959.025	328.445	CH13 BAR B	
3775668.387	670955.077	328.579	CH13 BAR	
3775667.784	670949.934	328.784	CH13 BAR T	0.01
3775667.935	670949.872	328.773	CH13 BAR B	

3775665.947	670946.863	328.874	CH13 BAR			
3775665.586	670963.493	328.326	CH13 BAR			
3775664.853	670966.94	328.187	CH13 BAR T	0.09		
3775664.733	670966.999	328.093	CH13 BAR B			
3775665.455	670968.601	328.058	CH13 BAR B	0.01		
3775665.614	670968.587	328.069	CH13 BAR T			
3775667.069	670969.732	328.081	CH13 BAR T	0.06		
3775666.926	670969.794	328.025	CH13 BAR B			
3775667.389	670970.826	327.95	CH13 BAR			
3775669.195	670968.69	328.07	CH13 BAR			
3775667.768	670967.078	328.187	CH13 BAR			
3775666.173	670965.237	328.243	CH13 BAR			
3775666.251	670964.312	328.267	CH13 BAR			
3775668.101	670976.344	327.76	CH13 BAR			
3775667.041	670979.128	327.733	CH13 BAR T	0.05		
3775666.863	670979.073	327.688	CH13 BAR B			
3775666.372	670982.371	327.582	CH13 BAR B	0.05		
3775666.585	670982.364	327.629	CH13 BAR T			
3775667.537	670984.209	327.579	CH13 BAR T	0.10		
3775667.347	670984.245	327.478	CH13 BAR B			
3775668.408	670985.433	327.432	CH13 BAR			
3775669.142	670982.27	327.544	CH13 BAR B	0.04		
3775669.027	670982.263	327.588	CH13 BAR T			
3775669.132	670978.872	327.706	CH13 BAR			
3775678.454	670939.493	329.133	HEAD			
3775678.852	670940.519	329.106	CH15LT	0.07	0.62	0.04
3775678.772	670940.491	329.034	CH15 LB			
3775678.353	670940.624	329.057	CH15 RB	0.05		
3775678.237	670940.577	329.105	CH15 RT			
3775678.514	670943.126	328.999	CH15 RT	0.04	0.88	0.05
3775678.706	670943.168	328.964	CH15 RB			
3775679.136	670943.239	328.974	CH15 LB	0.09		
3775679.373	670943.302	329.064	CH15 LT			
3775676.639	670956.038	328.542	HEAD			
3775676.89	670957.403	328.503	CH16 LT	0.03	0.56	0.02
3775676.762	670957.35	328.469	CH16 LB			
3775676.487	670957.336	328.483	CH16 RB	0.04		
3775676.327	670957.369	328.52	CH16 RT			
3775677.065	670962.052	328.346	CH16 RT	0.08	0.74	0.06
3775677.266	670962.056	328.267	CH16 RB			
3775677.61	670962.132	328.265	CH16 LB	0.07		
3775677.799	670962.155	328.335	CH16 LT			
3775677.667	670968.371	328.142	CH16 LT	0.09	0.83	0.05
3775677.517	670968.321	328.049	CH16 LB			
3775677.134	670968.138	328.042	CH16 RB	0.03		
3775676.881	670968.119	328.069	CH16 RT			
3775672.878	670974.767	327.815	CH16 RW		1.11	
3775673.889	670975.23	327.819	CH16 LW			
3775673.53	670978.103	327.815	CH16 LT	0.10	1.04	0.05
3775673.402	670978.006	327.714	CH16 LB			

3775672.596	670977.637	327.727	CH16 RW			
3775670.383	670980.259	327.654	CH16 RT	0.03	1.19	0.02
3775670.438	670980.335	327.622	CH16 RB			
3775671.138	670981.175	327.62	CH16 LW			
3775680.383	670963.785	328.401	HEAD			
3775678.842	670966.634	328.287	CH17 RT	0.07	0.93	0.07
3775679.002	670966.699	328.214	CH17 RB			
3775679.508	670966.534	328.203	CH17 LB	0.09		
3775679.77	670966.636	328.29	CH17 LT			
3775678.385	670968.941	328.165	CH17 LT	0.07		
3775678.386	670968.822	328.096	CH17 LB			
3775673.155	670959.471	328.399	HEAD			
3775673.559	670962.024	328.354	CH18 LT	0.06	0.71	0.05
3775673.425	670962.014	328.297	CH18 LB			
3775673.001	670962.015	328.265	CH18 RB	0.07		
3775672.874	670961.854	328.336	CH18 RT			
3775670.976	670963.969	328.246	CH18 RT	0.06	1.20	0.07
3775671.139	670964.121	328.191	CH18 RB			
3775671.509	670964.739	328.2	CH18 LB	0.05		
3775671.675	670964.945	328.254	CH18 LT			

Road Plot 3

Northing	Easting	Elevation	Feature code	Depth (m)	Width (m)	Cross (m^2)
3774637.256	670623.947	360.574	CH1 LT	0.04		
3774637.129	670623.883	360.539	CH1 LB			
3774635.363	670630.439	360.348	CH1 LW			
3774634.349	670634.994	360.234	CH1 LT	0.05		
3774634.098	670634.903	360.187	CH1 LB			
3774631.911	670638.286	360.086	CH1 LW			
3774624.978	670639.474	360.045	CH1 RW			
3774626.303	670643.478	359.937	CH1 RW			
3774628.686	670643.966	359.932	CH1 LT	0.03		
3774628.636	670643.993	359.906	CH1 LB			
3774628.932	670649.517	359.794	CH1 LT	0.07		
3774628.818	670649.484	359.723	CH1 LB			
3774623.835	670648.455	359.677	CH1 RB	0.08		
3774623.624	670648.396	359.761	CH1 RT			
3774621.094	670655.36	359.462	CH1 RW			
3774628.469	670657.111	359.452	CH1 LB	0.08		
3774628.575	670657.143	359.53	CH1 LT			
3774627.088	670663.338	359.315	CH1 LT	0.06		
3774626.995	670663.304	359.258	CH1 LB			
3774618.071	670661.469	359.296	CH1 RW			
3774626.228	670665.075	359.181	CH1 LB	0.09		
3774626.625	670665.178	359.266	CH1 LT			
3774625.212	670665.771	359.149	CH1 BAR			
3774626.192	670663.779	359.255	CH1 BAR T	0.03		
3774626.32	670663.861	359.224	CH1 BAR B			
3774626.929	670661.294	359.349	CH1 BAR			
3774626.781	670660.084	359.433	CH1 BAR T	0.04		

3774626.862	670660.12	359.397	CH1 BAR B	
3774627.246	670658.047	359.496	CH1 BAR	
3774625.997	670660.168	359.376	CH1 BAR	
3774625.628	670662.474	359.304	CH1 BAR T	0.05
3774625.52	670662.483	359.258	CH1 BAR B	
3774625.598	670664.534	359.283	CH1 BAR T	0.07
3774625.549	670664.511	359.213	CH1 BAR B	
3774625.582	670664.754	359.263	TOPO	
3774625.742	670663.993	359.29	TOPO	
3774625.963	670663.977	359.295	TOPO	
3774625.996	670663.445	359.303	TOPO	
3774626.535	670662.461	359.314	TOPO	
3774626.105	670662.437	359.326	TOPO	
3774626.411	670661.346	359.368	TOPO	
3774626.594	670659.993	359.445	TOPO	
3774624.061	670665.326	359.156	CH1 BAR	
3774624.68	670661.932	359.289	CH1 BAR	
3774623.004	670660.374	359.368	CH1 BAR	
3774622.161	670657.441	359.459	CH1 BAR	
3774620.604	670660.034	359.404	CH1 BAR T	0.09
3774620.452	670660.006	359.317	CH1 BAR B	
3774619.391	670662.11	359.267	CH1 BAR B	0.05
3774619.535	670662.212	359.319	CH1 BAR T	
3774624.486	670660.86	359.334	CH1 BAR	
3774626.906	670657.09	359.502	CH1 BAR	
3774627.82	670655.032	359.558	CH1 BAR	
3774627.324	670651.025	359.75	CH1 BAR T	0.07
3774627.433	670651.05	359.684	CH1 BAR B	
3774627.89	670650.209	359.711	CH1 BAR B	0.04
3774627.84	670650.164	359.748	CH1 BAR T	
3774625.266	670650.126	359.708	CH1 BAR T	0.04
3774625.231	670650.086	359.67	CH1 BAR B	
3774623.387	670653.867	359.59	CH1 BAR	
3774622.863	670657.301	359.463	CH1 BAR	
3774623.482	670659.387	359.428	CH1 BAR	
3774626.309	670646.297	359.826	CH1 BAR	
3774627.503	670645.575	359.858	CH1 BAR	
3774627.48	670644.184	359.914	CH1 BAR	
3774626.374	670645.218	359.841	CH1 BAR	
3774625.954	670650.123	359.762	TOPO	
3774625.87	670649.915	359.715	TOPO	
3774620.226	670659.853	359.294	TOPO	
3774619.676	670661.037	359.266	TOPO	
3774619.107	670661.972	359.24	TOPO	
3774619.808	670662.331	359.313	TOPO	
3774620.533	670660.618	359.396	TOPO	
3774625.994	670637.846	360.061	CH1 BAR	
3774627.116	670640.886	359.977	CH1 BAR	
3774628.485	670638.271	360.11	CH1 BAR T	0.06
3774628.568	670638.354	360.051	CH1 BAR B	

3774631.501	670634.991	360.157	CH1 BAR			
3774633.011	670630.372	360.336	CH1 BAR			
3774634.097	670626.509	360.408	CH1 BAR			
3774633.583	670630.661	360.31	CH1 BAR			
3774632.973	670632.154	360.294	CH1 BAR T	0.05		
3774632.858	670632.12	360.244	CH1 BAR B			
3774632.295	670633.586	360.203	CH1 BAR B	0.03		
3774632.407	670633.593	360.232	CH1 BAR T			
3774632.832	670635.666	360.188	CH1 BAR T	0.03		
3774632.796	670635.708	360.158	CH1 BAR B			
3774633.418	670633.858	360.205	CH1 BAR			
3774633.693	670631.417	360.291	CH1 BAR			
3774633.201	670644.058	359.972	HEAD			
3774634.545	670646.446	359.874	CH2 LT	0.08	0.95	0.06
3774634.205	670646.52	359.79	CH2 LB			
3774633.926	670646.667	359.783	CH2 RB	0.05		
3774633.654	670646.775	359.832	CH2 RT			
3774633.789	670648.459	359.747	CH2 RW		0.72	0.02
3774634.208	670648.82	359.753	CH2 LB	0.05		
3774634.369	670648.879	359.798	CH2 LT			
3774632.543	670651.238	359.648	CH2 LW		0.50	0.02
3774632.219	670651.084	359.653	CH2 RB	0.06		
3774632.088	670651.028	359.716	CH2 RT			
3774639.532	670645.22	359.935	HEAD			
3774639.561	670645.281	359.929	HEAD B			
3774639.288	670646.445	359.899	CH3 LT	0.04	0.93	0.04
3774639.221	670646.46	359.857	CH3 LB			
3774638.613	670647.006	359.856	CH3 RB	0.04		
3774638.551	670647.008	359.899	CH3 RT			
3774639.137	670647.74	359.79	CH3 LT	0.04	0.49	0.03
3774639.072	670647.764	359.755	CH3 LB			
3774638.901	670647.801	359.744	CH3 RB	0.10		
3774638.646	670647.696	359.846	CH3 RT			
3774640.291	670646.066	359.893	HEAD			
3774640.133	670647.028	359.881	CH4 LT	0.07	0.52	0.03
3774640.023	670646.971	359.814	CH4 LB			
3774639.788	670646.836	359.825	CH4 RB	0.04		
3774639.672	670646.798	359.869	CH4 RT			
3774638.539	670649.43	359.754	CH4 RT	0.06	1.09	0.06
3774638.625	670649.426	359.689	CH4 RB			
3774639.492	670649.665	359.765	CH4 LB	0.04		
3774639.593	670649.693	359.807	CH4 LT			
3774638.001	670654.084	359.628	CH4 LT	0.06	0.85	0.05
3774637.815	670653.965	359.573	CH4 LB			
3774637.413	670653.846	359.551	CH4 RB	0.06		
3774637.233	670653.717	359.615	CH4 RT			
3774634.125	670657.672	359.514	CH4 RT	0.08	1.45	0.08
3774634.19	670657.674	359.434	CH4 RB			
3774635.212	670658.108	359.428	CH4 LB	0.04		
3774635.41	670658.342	359.465	CH4 LT			

3774635.2	670660.609	359.399	CH4 LT	0.07	1.11	0.04
3774635.125	670660.606	359.327	CH4 LB			
3774634.106	670660.408	359.322	CH4 RW			
3774633.283	670664.901	359.187	CH4 RW		1.18	
3774634.443	670665.116	359.186	CH4 LW			
3774635.173	670670.662	359.076	CH4 LW		1.70	
3774633.482	670670.506	359.026	CH4 RW			
3774633.175	670671.899	358.975	CH4 RW		1.09	
3774634.254	670672.064	358.975	CH4 LW			
3774646.887	670649.755	359.787	HEAD			
3774647.812	670652.15	359.743	CH5 LT	0.07	0.63	0.04
3774647.561	670652.156	359.675	CH5 LB			
3774647.275	670652.209	359.647	CH5 RB	0.05		
3774647.188	670652.196	359.697	CH5 RT			
3774646.669	670655.951	359.548	CH5 LW		0.42	0.01
3774646.247	670655.951	359.563	CH5 RT	0.04		
3774646.332	670655.95	359.526	CH5 RB			
3774644.619	670659.062	359.447	CH5 RW		0.59	
3774645.175	670659.269	359.462	CH5 LW			
3774642.299	670667.881	359.148	HEAD			
3774644.137	670669.238	359.153	CH6 LT	0.06	1.16	0.05
3774644.061	670669.229	359.096	CH6 LB			
3774643.119	670669.546	359.05	CH6 RB	0.02		
3774643.019	670669.549	359.073	CH6 RT			
3774642.983	670671.654	359.02	CH6 RT	0.06	0.53	0.03
3774643.051	670671.669	358.963	CH6 RB			
3774643.244	670671.854	358.934	CH6 LB	0.04		
3774643.43	670671.94	358.975	CH6 LT			
3774644.901	670670.593	359.116	HEAD			
3774644.772	670671.536	359.101	CH7 LT	0.10	0.72	0.05
3774644.475	670671.352	359.006	CH7 LB			
3774644.287	670671.274	359.033	CH7 RB	0.04		
3774644.14	670671.2	359.073	CH7 RT			
3774643.74	670672.305	359.045	CH7 LT	0.07		
3774643.572	670672.201	358.977	CH7 LB			
3774642.305	670674.729	358.95	CH7 LT	0.04	0.90	0.04
3774642.192	670674.683	358.907	CH7 LB			
3774641.732	670674.355	358.914	CH7 RB	0.05		
3774641.593	670674.183	358.968	CH7 RT			
3774639.846	670675.056	358.908	CH7 RT	0.13	0.77	0.08
3774639.901	670675.142	358.773	CH7 RB			
3774640.085	670675.589	358.785	CH7 LB	0.07		
3774640.16	670675.764	358.853	CH7 LT			
3774639.402	670676.507	358.871	CH7 LT	0.16	0.87	0.13
3774639.099	670676.331	358.71	CH7 LB			
3774638.853	670676.142	358.738	CH7 RB	0.13		
3774638.633	670676.09	358.87	CH7 RT			
3774654.406	670664.405	359.357	HEAD			
3774654.689	670666.288	359.315	CH8 LT	0.07	0.68	0.05
3774654.516	670666.362	359.24	CH8 LB			

3774654.178	670666.482	359.245	CH8 RB	0.07		
3774654.056	670666.524	359.313	CH8 RT			
3774654.196	670669.497	359.189	CH8 RT	0.03	0.94	0.04
3774654.327	670669.551	359.163	CH8 RB			
3774654.905	670669.786	359.156	CH8 LB	0.07		
3774655.038	670669.91	359.222	CH8 LT			
3774653.022	670675.96	358.989	CH8 LT	0.04	0.43	
3774652.606	670675.846	358.947	CH8 RW			
3774652.29	670675.815	358.948	CH8 RW			
3774650.137	670681.005	358.793	CH8 RT	0.05	0.64	0.01
3774650.294	670681.106	358.748	CH8 RB			
3774650.731	670681.249	358.765	CH8 LW			
3774651.172	670685.818	358.656	CH8 LT	0.08	0.83	0.03
3774650.979	670685.764	358.576	CH8 LB			
3774650.354	670685.652	358.588	CH8 RW			
3774653.62	670682.779	358.811	HEAD			
3774653.075	670684.523	358.758	CH9 LT	0.08	0.61	0.04
3774652.906	670684.487	358.678	CH9 LB			
3774652.555	670684.475	358.656	CH9 RB	0.06		
3774652.466	670684.441	358.718	CH9 RT			
3774651.854	670686.2	358.639	CH9 TT	0.05		
3774651.711	670686.094	358.592	CH9 LB			
3774664.617	670661.941	359.617	HEAD			
3774664.169	670664.049	359.54	CH10 LT	0.05	0.57	0.04
3774664.002	670663.987	359.491	CH10 LB			
3774663.728	670663.883	359.495	CH10 RB	0.09		
3774663.613	670663.903	359.587	CH10 RT			
3774663.211	670667.86	359.402	CH10 RW		1.00	
3774664.185	670668.08	359.395	CH10 LW			
3774663.46	670674.933	359.193	CH10 LT	0.04	0.37	0.01
3774663.381	670674.889	359.156	CH10 LB			
3774663.243	670674.846	359.16	CH10 RB	0.03		
3774663.121	670674.784	359.194	CH10 RT			
3774662.961	670677.231	359.092	CH10 RW		0.69	
3774663.6	670677.482	359.102	CH10 LW			
3774658.322	670684.036	358.814	CH10 LW		0.62	
3774657.766	670683.76	358.81	CH10 RW			
3774656.502	670689.823	358.583	CH10 RW		0.90	0.03
3774657.107	670690.001	358.597	CH10 LB	0.06		
3774657.348	670690.137	358.66	CH10 LT			
3774669.476	670672.196	359.208	HEAD			
3774669.172	670673.475	359.174	CH11 LT	0.01	0.36	0.00
3774669.127	670673.509	359.159	CH11 LB			
3774668.824	670673.367	359.168	CH11 RW			
3774668.084	670679.72	358.966	CH11 RW		1.91	
3774669.986	670679.519	358.978	CH11 LW			
3774670.94	670656.584	359.751	HEAD			
3774671.411	670657.318	359.711	CH12 LT	0.05	0.55	0.03
3774671.322	670657.338	359.659	CH12 LB			
3774671.008	670657.407	359.67	CH12 RB	0.05		

3774670.865	670657.416	359.722	CH12 RT			
3774672.737	670656.094	359.758	HEAD			
3774672.621	670656.937	359.748	CH13 LT	0.05	0.47	0.03
3774672.54	670656.885	359.695	CH13 LB			
3774672.247	670656.81	359.694	CH13 RB	0.06		
3774672.176	670656.776	359.755	CH13 RT			
3774671.172	670658.487	359.688	CH13 RT	0.06	0.93	0.05
3774671.424	670658.489	359.63	CH13 RB			
3774672.026	670658.395	359.636	CH13 LB	0.05		
3774672.103	670658.445	359.691	CH13 LT			
3774672.183	670660.195	359.627	CH13 LT	0.04	0.71	0.02
3774672.075	670660.217	359.584	CH13 LB			
3774671.476	670660.229	359.591	CH13 RW			
3774670.832	670663.582	359.495	CH13 RW		0.92	
3774671.677	670663.938	359.521	CH13 LW			
3774610.376	670656.813	359.489	BENCH			

Road Plot 4

Northing	Easting	Elevation	Feature code	Depth (m)	Width (m)	Cross (m^2)
3774487.873	670113.165	377.179	CH1 RT	0.08	1.61	0.15
3774488.404	670113.276	377.102	CH1 RB			
3774489.241	670113.623	377.114	CH1 LB	0.10		
3774489.413	670113.644	377.217	CH1 LT			
3774489.541	670110.529	377.326	CH1 LT			
3774487.644	670119.443	376.944	CH1 LT	0.07	1.46	0.13
3774487.497	670119.339	376.874	CH1 LB			
3774486.62	670118.835	376.907	CH1 RB	0.10		
3774486.37	670118.727	377.009	CH1 RT			
3774484.034	670124.018	376.707	CH1 W			
3774484.655	670124.334	376.658	CH1 W			
3774485.844	670124.311	376.743	CH1 W			
3774479.732	670125.987	376.566	HEAD			
3774479.421	670127.684	376.506	CH2 W			
3774480.069	670127.552	376.493	CH2 W			
3774480.547	670127.357	376.528	CH2 W			
3774480.273	670134.113	376.251	HEAD			
3774479.808	670136.07	376.241	CH3 RT	0.08	1.25	0.08
3774480.062	670136.013	376.165	CH3 RB			
3774480.86	670136.038	376.157	CH3 LB	0.06		
3774481.056	670136.02	376.217	CH3 LT			
3774482.089	670142.11	376.056	CH3 LT	0.10	1.85	0.18
3774481.839	670142.042	375.956	CH3 LB			
3774480.556	670141.852	375.975	CH3 RB	0.09		
3774480.264	670141.813	376.07	CH3 RT			
3774477.996	670147.208	375.763	CH3 RT	0.08	1.33	0.10
3774478.251	670147.23	375.684	CH3 RB			
3774478.873	670147.792	375.735	CH3 LB	0.07		
3774479.14	670147.891	375.801	CH3 LT			
3774475.95	670152.787	375.634	CH3 LT	0.11	1.47	0.13
3774475.667	670152.586	375.525	CH3 LB			

3774474.931	670152.36	375.538	CH3 RB	0.07		
3774474.67	670152.068	375.605	CH3 RT			
3774471.535	670156.344	375.461	CH3 RT	0.12	1.57	0.17
3774471.624	670156.477	375.343	CH3 RB			
3774472.685	670156.735	375.377	CH3 LB	0.09		
3774472.99	670156.923	375.471	CH3 LT			
3774471.524	670161.491	375.274	CH3 LT	0.05	1.79	0.12
3774471.25	670161.495	375.223	CH3 LB			
3774470.022	670161.835	375.187	CH3 RB	0.08		
3774469.74	670161.638	375.267	CH3 RT			
3774467.567	670165.92	375.06	CH3 RT	0.05	1.85	0.12
3774467.825	670166.18	375.007	CH3 RB			
3774469.087	670166.515	375.04	CH3 LB	0.07		
3774469.375	670166.307	375.114	CH3 LT			
3774467.259	670161.705	375.186	CH4 W			
3774467.746	670161.836	375.177	CH4 W			
3774468.105	670162.031	375.19	CH4 W			
3774469.096	670157.643	375.35	CH4 RT	0.08	0.67	0.05
3774469.397	670157.789	375.273	CH4 RB			
3774469.46	670157.875	375.275	CH4 LB	0.08		
3774469.706	670157.93	375.353	CH4 LT			
3774470.622	670155.122	375.468	HEAD			
3774471.094	670152.172	375.575	CH5 W			
3774471.376	670152.351	375.512	CH5 W			
3774471.614	670152.519	375.562	CH5 W			
3774472.764	670150.424	375.651	HEAD			
3774471.587	670146.914	375.766	CH6 W			
3774470.743	670146.295	375.753	CH6 W			
3774469.877	670145.708	375.79	CH6 W			
3774469.724	670143.065	375.942	CH6 RT	0.09	1.71	0.15
3774470.073	670142.931	375.855	CH6 RB			
3774471.031	670142.516	375.855	CH6 LB	0.09		
3774471.342	670142.514	375.948	CH6 LT			
3774471.126	670139.287	376.063	CH6 LT	0.10	1.52	0.15
3774470.71	670139.184	375.965	CH6 LB			
3774469.976	670139.003	375.967	CH6 RB	0.10		
3774469.632	670139.013	376.063	CH6 RT			
3774469.884	670136.401	376.128	CH6 RT	0.05	1.23	0.09
3774470.186	670136.328	376.077	CH6 RB			
3774470.895	670136.44	376.073	CH6 LB	0.10		
3774471.113	670136.513	376.171	CH6 LT			
3774472.818	670129.264	376.404	HEAD			
3774467.397	670142.303	375.991	CH7 LT	0.14	3.15	0.34
3774466.908	670142.26	375.855	CH7 LB			
3774464.843	670143.324	375.766	CH7 RB	0.08		
3774464.443	670143.397	375.845	CH7 RT			
3774464.214	670148.978	375.662	CH7 RT	0.08	1.91	0.14
3774464.295	670149.022	375.585	CH7 RB			
3774465.74	670149.675	375.565	CH7 LB	0.07		
3774465.935	670149.799	375.64	CH7 LT			

3774463.968	670155.52	375.414	CH7 W			
3774461.063	670155.66	375.386	CH7 W			
3774460.731	670159.672	375.261	CH7 RT	0.08	2.24	0.15
3774461.191	670159.857	375.186	CH7 RB			
3774462.723	670159.966	375.262	CH7 LB	0.06		
3774462.941	670160.008	375.318	CH7 LT			
3774456.966	670157.609	375.243	CH8 LT	0.04	1.76	0.11
3774456.747	670157.44	375.206	CH8 LB			
3774455.768	670156.796	375.267	CH8 RB	0.08		
3774455.427	670156.761	375.352	CH8 RT			
3774456.828	670153.038	375.478	CH8 RT	0.08	1.08	0.08
3774457.086	670153.206	375.399	CH8 RB			
3774457.688	670153.212	375.432	CH8 LB	0.07		
3774457.888	670153.25	375.501	CH8 LT			
3774459.774	670150.151	375.581	CH8 LW		0.96	0.02
3774459.165	670149.927	375.573	CH8 RB	0.05		
3774458.824	670149.997	375.622	CH8 RT			
3774479.031	670175.359	374.818	CH9 RT	0.04	1.12	0.02
3774479.274	670175.381	374.775	CH9 RB			
3774480.135	670175.186	374.81	CH9 LW			
3774481.105	670170.171	375.029	CH9 LT	0.07	1.62	0.16
3774480.413	670169.814	374.954	CH9 LB			
3774479.9	670169.599	374.946	CH9 RB	0.12		
3774479.599	670169.573	375.068	CH9 RT			
3774481.747	670164.85	375.204	CH9 RT	0.11	1.47	0.15
3774482.454	670165.18	375.099	CH9 RB			
3774482.778	670165.442	375.117	CH9 LB	0.10		
3774483.017	670165.59	375.214	CH9 LT			
3774485.514	670162.282	375.387	CH9 LT	0.15	1.10	0.14
3774485.143	670161.924	375.235	CH9 LB			
3774485.176	670161.666	375.229	CH9 RB	0.10		
3774485.067	670161.274	375.332	CH9 RT			
3774485.123	670158.488	375.489	HEAD			
3774486.563	670157.773	375.508	CH9 LT	0.08	1.02	0.10
3774487.102	670157.866	375.427	CH9 LB			
3774487.323	670157.921	375.392	CH9 RB	0.11		
3774487.559	670157.97	375.505	CH9 RT			
3774487.641	670155.592	375.617	HEAD			
3774487.337	670159.411	375.375	CH9 RT			
3774489.219	670157.556	375.576	CH9 RT	0.08	0.92	0.09
3774489.526	670157.715	375.494	CH9 RB			
3774489.617	670157.749	375.485	CH9 LB	0.12		
3774490.043	670157.956	375.609	CH9 LT			
3774491.343	670152.516	375.763	HEAD			
3774493.608	670143.705	376.06	CH10 W			
3774493.858	670144.106	376.02	CH10 W			
3774494.162	670144.268	376.069	CH10 W			
3774495.324	670141.307	376.159	CH10 LT	0.05	0.86	0.04
3774495.038	670141.241	376.107	CH10 LB			
3774494.792	670141.16	376.119	CH10 RB	0.05		

3774494.464	670141.231	376.171	CH10 RT			
3774495.685	670139.228	376.246	HEAD			
3774495.376	670134.955	376.392	CH11 W			
3774494.832	670134.939	376.439	CH11 W			
3774495.66	670134.701	376.437	CH11 W			
3774495.502	670133.53	376.492	CH11 LT	0.04	0.66	0.02
3774495.293	670133.575	376.449	CH11 LB			
3774495.044	670133.612	376.471	CH11 RB	0.01		
3774494.844	670133.621	376.481	CH11 RT			
3774494.859	670132.347	376.531	HEAD			
3774499.886	670174.709	374.959	HEAD			
3774499.307	670176.103	374.936	CH12 RT	0.07	0.99	0.09
3774499.582	670176.185	374.865	CH12 RB			
3774499.825	670176.192	374.861	CH12 LB	0.10		
3774500.281	670176.291	374.963	CH12 LT			
3774498.139	670180.748	374.774	CH12 LT	0.06	1.59	0.12
3774497.851	670180.524	374.717	CH12 LB			
3774497.085	670180.652	374.69	CH12 RB	0.09		
3774496.567	670180.486	374.779	CH12 RT			
3774494.935	670184.416	374.628	CH12 RT	0.02	1.43	0.04
3774495.229	670184.525	374.603	CH12 RB			
3774495.799	670184.797	374.603	CH12 LB	0.03		
3774496.263	670184.951	374.629	CH12 LT			
3774495.099	670187.549	374.599	CH12 LT	0.08	1.30	0.13
3774494.745	670187.223	374.519	CH12 LB			
3774494.416	670186.776	374.51	CH12 RB	0.11		
3774494.287	670186.531	374.623	CH12 RT			
3774505.161	670187.597	374.603	CH13 W			
3774506.084	670187.416	374.589	CH13 W			
3774507.33	670186.75	374.562	CH13 W			
3774508.016	670179.631	374.847	CH13 W			
3774505.712	670179.513	374.837	CH13 W			
3774506.532	670175.111	375.002	CH13 LT	0.02	0.48	0.01
3774506.395	670175.161	374.981	CH13 LB			
3774506.234	670175.13	374.977	CH13 RB	0.04		
3774506.056	670175.14	375.013	CH13 RT			
3774506.358	670174.029	375.042	HEAD			
3774506.866	670170.329	375.155	CH14 W			
3774507.58	670170.282	375.153	CH14 W			
3774508.262	670170.259	375.147	CH14 W			
3774508.276	670168.206	375.188	CH14 LT	0.01	1.20	0.06
3774507.861	670168.188	375.174	CH14 LB			
3774507.455	670168.197	375.19	CH14 RB	0.08		
3774507.12	670167.889	375.272	CH14 RT			
3774507.129	670166.463	375.284	CH14 RT	0.05	0.84	0.06
3774507.431	670166.455	375.238	CH14 RB			
3774507.722	670166.358	375.22	CH14 LB	0.09		
3774507.958	670166.306	375.311	CH14 LT			
3774508.031	670164.62	375.366	HEAD			
3774509.493	670165.098	375.363	HEAD			

3774509.48	670166.495	375.328	CH14 LT	0.05	0.71	0.04
3774509.123	670166.41	375.274	CH14 LB			
3774508.928	670166.315	375.266	CH14 RB	0.06		
3774508.785	670166.355	375.322	CH14 RT			
3774509.241	670167.996	375.29	CH14 LT	0.08		
3774508.87	670167.917	375.212	CH14 LB			
3774453.952	670155.774	375.384	BENCH CH			

Road Plot 5

Northing	Easting	Elevation	Feature code	Depth (m)	Width (m)	Cross (m^2)
773869.323	669617.569	388.387	HEAD			
773869.462	669618.972	388.367	CH1 LT	0.01	0.61	0.01
773869.341	669618.993	388.356	CH1 LB			
773869.019	669619.044	388.363	CH1 RB	0.01		
773868.865	669619.075	388.376	CH1 RT			
773868.134	669622.673	388.206	CH1 RW		0.54	
773868.566	669622.998	388.2	CH1 LW			
773867.75	669625.285	388.115	CH1 LW		1.11	
773866.661	669625.511	388.165	CH1 RW			
773868.339	669630.026	387.987	CH1 RT	0.08	0.28	0.01
773868.411	669630.006	387.91	CH1 RB			
773868.558	669629.857	387.919	CH1 LW			
773869.619	669630.63	387.934	CH1 LT	0.05	0.50	0.02
773869.496	669630.676	387.88	CH1 LB			
773869.311	669630.785	387.901	CH1 RB	0.02		
773869.207	669630.906	387.926	CH1 RT			
773869.679	669634.694	387.787	CH1 RT	0.02	0.29	0.01
773869.747	669634.727	387.764	CH1 RB			
773869.866	669634.795	387.763	CH1 LB	0.03		
773869.925	669634.856	387.793	CH1 LT			
773869.67	669637.454	387.682	CH1 LT	0.01	0.36	0.01
773869.594	669637.448	387.673	CH1 LB			
773869.474	669637.482	387.668	CH1 RB	0.04		
773869.315	669637.443	387.71	CH1 RT			
773868.315	669638.746	387.617	CH1 RW		0.44	0.01
773868.552	669638.894	387.597	CH1 LB	0.04		
773868.645	669639.031	387.636	CH1 LT			
773868.474	669639.907	387.6	CH1 LT	0.01	0.60	0.00
773868.335	669639.945	387.591	CH1 LB			
773867.886	669640.04	387.62	CH1 RW			
773869.425	669643.376	387.511	CH1 RW		0.66	0.01
773869.874	669643.266	387.493	CH1 LB	0.04		
773870.046	669643.148	387.53	CH1 LT			
773875.682	669628.88	388.106	HEAD			
773875.338	669629.917	388.091	CH2 LT	0.08	0.52	0.04
773875.312	669629.863	388.009	CH2 LB			
773875.044	669629.679	387.992	CH2 RB	0.08		
773874.899	669629.632	388.074	CH2 RT			
773873.374	669631.665	387.952	CH2 RT	0.02	0.49	0.01
773873.499	669631.683	387.928	CH2 RB			

773873.588	669631.847	387.928	CH2 LB	0.03		
773873.709	669632.023	387.961	CH2 LT			
773871.919	669632.971	387.876	CH2 LT	0.05	0.65	0.04
773871.706	669632.884	387.827	CH2 LB			
773871.433	669632.647	387.864	CH2 RB	0.06		
773871.352	669632.646	387.925	CH2 RT			
773870.247	669636.557	387.714	CH2 RW		0.32	0.01
773870.452	669636.664	387.7	CH2 LB	0.03		
773870.542	669636.671	387.733	CH2 LT			
773860.028	669654.849	387.083	HEAD			
773858.249	669657.371	387.01	CH3 LT	0.03	0.55	0.02
773858.152	669657.28	386.975	CH3 LB			
773857.945	669657.233	386.958	CH3 RB	0.02		
773857.749	669657.145	386.978	CH3 RT			
773857.376	669658.463	386.975	CH3 RT	0.07	0.41	0.01
773857.427	669658.5	386.904	CH3 RB			
773857.787	669658.469	386.945	CH3 LW			
773856.549	669660.103	386.893	CH3 LT	0.02	0.43	0.01
773856.497	669660.048	386.869	CH3 LB			
773856.332	669659.737	386.882	CH3 RW			
773860.448	669606.499	388.751	HEAD			
773861.405	669608.718	388.66	CH4 LW		0.43	
773860.978	669608.778	388.656	CH4 RW			
773861.434	669614.835	388.455	HEAD			
773861.495	669616.766	388.383	CH5 LT	0.03	0.37	0.01
773861.397	669616.725	388.357	CH5 LB			
773861.239	669616.685	388.364	CH5 RB	0.02		
773861.138	669616.68	388.382	CH5 RT			
773859.332	669620.612	388.234	CH5 RT	0.03	0.91	0.03
773859.548	669620.652	388.201	CH5 RB			
773860.193	669620.737	388.212	CH5 LB	0.03		
773860.229	669620.768	388.246	CH5 LT			
773857.322	669624.972	388.055	CH5 LT	0.03	0.56	0.02
773857.247	669624.905	388.024	CH5 LB			
773856.933	669624.882	388.043	CH5 RB	0.04		
773856.793	669624.787	388.081	CH5 RT			
773853.325	669633.221	387.822	CH5 RT	0.06	0.80	0.04
773853.424	669633.228	387.764	CH5 RB			
773853.896	669633.54	387.751	CH5 LB	0.03		
773854.04	669633.585	387.785	CH5 LT			
773850.869	669639.62	387.541	CH5 LW		0.79	0.01
773850.151	669639.497	387.557	CH5 RB	0.03		
773850.093	669639.476	387.588	CH5 RT			
773849.689	669646.415	387.32	CH5 RW		0.61	
773850.286	669646.54	387.311	CH5 LW			
773850.451	669650.729	387.188	CH5 LW		0.89	
773849.751	669651.278	387.176	CH5 RW			
773851.495	669654.054	387.056	CH5 RW		0.89	
773852.38	669653.924	387.027	CH5 LW			
773851.46	669657.518	386.944	CH5 LW		0.73	

773850.813	669657.19	386.949	CH5 RW			
773851.598	669626.099	388.003	HEAD			
773852.051	669628.069	387.933	CH6 LT	0.08	0.34	0.01
773851.821	669628.137	387.851	CH6 LB			
773851.721	669628.133	387.847	CH6 RB			
773850.831	669632.049	387.747	HEAD			
773850.196	669633.114	387.694	CH7 LT	0.10	0.46	0.04
773850.059	669633.008	387.595	CH7 LB			
773849.896	669632.861	387.613	CH7 RB	0.08		
773849.879	669632.784	387.693	CH7 RT			
773848.457	669634.783	387.607	CH7 RT	0.11	0.66	0.07
773848.568	669634.855	387.501	CH7 RB			
773848.858	669635.02	387.544	CH7 LB	0.10		
773848.988	669635.174	387.641	CH7 LT			
773847.211	669640.873	387.42	CH7 LT	0.06	0.50	0.03
773847.018	669640.693	387.36	CH7 LB			
773846.886	669640.652	387.359	CH7 RB	0.05		
773846.794	669640.604	387.412	CH7 RT			
773845.596	669643.332	387.299	CH7 RW		0.63	0.02
773846.014	669643.552	387.264	CH7 LB	0.06		
773846.175	669643.574	387.32	CH7 LT			
773844.908	669648.992	387.077	CH7 LW		0.66	
773844.251	669648.991	387.079	CH7 RW			
773847.376	669633.24	387.684	HEAD			
773848.388	669634.772	387.611	CH8 LT	0.05	0.74	0.05
773848.275	669634.833	387.559	CH8 LB			
773848.165	669635.479	387.509	CH8 RB	0.08		
773848.029	669635.42	387.59	CH8 RT			
773847.724	669634.679	387.627	CH8 RT	0.06	0.51	0.03
773847.902	669634.624	387.571	CH8 RB			
773848.107	669634.523	387.585	CH8 LB	0.06		
773848.19	669634.462	387.645	CH8 LT			
773839.586	669631.96	387.7	HEAD			
773839.772	669633.759	387.666	CH9 LT	0.03	1.28	0.07
773839.63	669633.73	387.635	CH9 LB			
773838.61	669633.655	387.588	CH9 RB	0.08		
773838.501	669633.639	387.666	CH9 RT			
773837.471	669637.515	387.475	CH9 RW		0.42	
773837.865	669637.662	387.476	CH9 LW			
773830.736	669638.968	387.36	HEAD			
773830.535	669640.328	387.319	CH10 LT	0.05	0.54	0.03
773830.362	669640.255	387.265	CH10 LB			
773830.149	669640.142	387.264	CH10 RB	0.05		
773830.04	669640.105	387.31	CH10 RT			
773830.498	669624.199	387.887	HEAD			
773829.675	669625.734	387.859	CH11 LT	0.09	0.43	0.02
773829.629	669625.707	387.769	CH11 LB			
773829.399	669625.608	387.771	CH11 RB	0.02		
773829.321	669625.483	387.791	CH11 RT			
773827.773	669626.915	387.75	CH11 RT	0.04	0.52	0.02

773827.812	669626.997	387.715	CH11 RB			
773827.97	669627.33	387.72	CH11 LB	0.03		
773828.008	669627.378	387.752	CH11 LT			
773826.514	669627.627	387.64	CH11 LT	0.07	0.43	0.03
773826.48	669627.598	387.573	CH11 LB			
773826.151	669627.507	387.633	CH11 RB	0.08		
773826.102	669627.495	387.717	CH11 RT			
773825.648	669630.692	387.571	CH11 RT	0.05	0.65	0.04
773825.692	669630.769	387.52	CH11 RB			
773825.783	669631.013	387.531	CH11 LB	0.08		
773825.97	669631.26	387.612	CH11 LT			
773824.34	669630.846	387.504	CH11 LT	0.04	0.58	0.02
773824.421	669630.649	387.461	CH11 LB			
773824.55	669630.36	387.498	CH11 RB	0.04		
773824.619	669630.335	387.538	CH11 RT			
773821.79	669631.858	387.472	CH11 RT	0.06	1.28	0.07
773821.951	669631.961	387.409	CH11 RB			
773822.73	669632.554	387.389	CH11 LB	0.04		
773822.758	669632.701	387.429	CH11 LT			
773822.659	669633.965	387.408	CH11 LT	0.06	1.59	0.11
773822.264	669633.893	387.351	CH11 LB			
773821.387	669633.449	387.365	CH11 RB	0.07		
773821.163	669633.423	387.44	CH11 RT			
773828.34	669621.049	387.923	HEAD			
773828.593	669622.884	387.876	CH12 LT	0.04	0.45	0.01
773828.495	669622.899	387.837	CH12 LB			
773828.148	669622.877	387.863	CH12 RW			
773827.709	669625.216	387.76	CH12 RW		0.62	0.01
773827.983	669625.542	387.743	CH12 LB	0.04		
773828.135	669625.669	387.781	CH12 LT			
773827.112	669626.863	387.689	CH12 LT	0.04	0.68	0.03
773826.963	669626.793	387.653	CH12 LB			
773826.731	669626.641	387.693	CH12 RB	0.05		
773826.499	669626.564	387.747	CH12 RT			
773824.868	669622.156	387.854	HEAD			
773824.159	669622.849	387.852	CH13 LT	0.08	0.60	0.04
773824.125	669622.757	387.775	CH13 LB			
773824.051	669622.377	387.784	CH13 RB	0.06		
773824.028	669622.261	387.848	CH13 RT			
773823.382	669622.669	387.798	CH13 RT	0.05	0.29	0.01
773823.409	669622.75	387.747	CH13 RB			
773823.46	669622.857	387.735	CH13 LB	0.04		
773823.513	669622.924	387.773	CH13 LT			
773823.361	669623.742	387.762	CH13 LT	0.06	1.05	0.08
773823.184	669623.715	387.701	CH13 LB			
773822.548	669623.671	387.676	CH13 RB	0.10		
773822.309	669623.668	387.775	CH13 RT			
773822.22	669627.041	387.648	CH13 RT	0.05	1.07	0.06
773822.392	669626.974	387.602	CH13 RB			
773823.122	669627.102	387.591	CH13 LB	0.07		

773823.291	669627.073	387.659	CH13 LT			
773824.58	669630.179	387.552	CH13 LT	0.06	1.02	0.03
773824.505	669630.223	387.495	CH13 LB			
773823.61	669630.189	387.497	CH13 RB	0.01		
773823.563	669630.192	387.507	CH13 RT			
773821.606	669615.921	388.057	HEAD			
773821.263	669617.064	388.023	CH14 LT	0.04	0.52	0.03
773821.171	669617.039	387.982	CH14 LB			
773820.852	669617.008	387.962	CH14 RB	0.09		
773820.75	669616.953	388.048	CH14 RT			
773821.059	669618.788	387.981	CH14 RT	0.09	0.50	0.03
773821.095	669618.743	387.892	CH14 RB			
773821.386	669618.691	387.921	CH14 LB	0.03		
773821.541	669618.668	387.948	CH14 LT			
773821.944	669621.353	387.851	CH14 LT	0.05	0.50	0.03
773821.862	669621.363	387.799	CH14 LB			
773821.575	669621.574	387.782	CH14 RB	0.08		
773821.503	669621.588	387.866	CH14 RT			
773822.518	669622.749	387.769	CH14 RT	0.03	0.48	0.03
773822.577	669622.707	387.737	CH14 RB			
773822.834	669622.52	387.734	CH14 LB	0.08		
773822.896	669622.46	387.816	CH14 LT			
773849.328	669605.276	388.716	HEAD			
773851.476	669605.953	388.687	CH15 LT	0.07	0.68	0.04
773851.432	669605.999	388.621	CH15 LB			
773851.033	669606.349	388.601	CH15 RB	0.07		
773850.96	669606.397	388.667	CH15 RT			
773850.847	669608.186	388.55	CH15 RW		0.81	
773851.639	669608.363	388.539	CH15 LW			

Road Plot 6

Northing	Easting	Elevation	Feature code	Depth (m)	Width (m)	Cross (m^2)
773558.243	669260.636	398.421	CH1LT	0.03	1.65	0.03
773557.984	669260.718	398.389	CH1LB			
773557.421	669261.27	398.362	CH1RB	0.12		
773556.883	669261.562	398.48	CH1RT			
773558.394	669267.251	398.373	CH1RT	0.13	2.91	0.20
773558.725	669267.126	398.238	CH1RB			
773560.615	669265.941	398.238	CH1 LB	0.10		
773560.864	669265.71	398.336	CH1 LT			
773560.22	669264.029	398.38	CH1 LT			
773561.955	669262.681	398.403	HEAD			
773561.238	669271.137	398.133	CH1 LT	0.10	1.95	0.09
773560.851	669271.14	398.036	CH1 LB			
773559.735	669271.138	398.091	CH1 RB	0.07		
773559.292	669271.002	398.16	CH1 RT			
773558.618	669275.075	398.072	CH1 RT	0.11	2.88	0.15
773559.036	669274.995	397.966	CH1 RB			
773560.994	669275.462	397.934	CH1 RB	0.08		
773561.491	669275.3	398.01	CH1 RT			

773562.313	669274.834	398.078	HEAD			
773563.016	669277.816	398.038	CH1 RT	0.12		
773562.56	669277.727	397.92	CH1 RB			
773562.076	669277.62	397.941	CH1 BAR1			
773561.41	669276.195	398.037	CH1 BAR1			
773560.472	669275.167	397.977	CH1 BAR1			
773560.104	669277.285	397.897	CH1 BAR1			
773559.75	669279.208	397.835	CH1 BAR1			
773560.514	669281.069	397.851	CH1 LT	0.04	2.94	0.06
773559.945	669280.863	397.811	CH1 LB			
773558.104	669280.464	397.761	CH1 RB	0.06		
773557.689	669280.27	397.817	CH1 RT			
773555.879	669286.207	397.671	CH1 RT	0.12	2.72	0.16
773556.152	669286.33	397.552	CH1 RB			
773557.682	669287.729	397.541	CH1 LB	0.13		
773558.012	669287.895	397.666	CH1 LT			
773556.489	669292.092	397.491	CH1 LT	0.11	4.76	0.26
773555.955	669291.831	397.382	CH1 LB			
773552.194	669291.741	397.389	CH1 RB	0.08		
773551.735	669291.785	397.467	CH1 RT			
773549.174	669299.381	397.13	CH1 RT	0.09	3.66	0.16
773549.615	669299.729	397.04	CH1 RB			
773552.09	669300.746	397.086	CH1 LB	0.11		
773552.451	669301.016	397.196	CH1 LT			
773547.082	669307.175	397.036	CH1 LT	0.19	3.51	0.33
773547.015	669306.76	396.849	CH1 LB			
773544.399	669305.357	396.745	CH1 RB	0.11		
773544.254	669305.09	396.857	CH1 RT			
773549.671	669306.842	396.922	HEAD			
773549.757	669309.417	396.864	CH2 LT	0.04	1.02	0.02
773549.53	669309.401	396.822	CH2 LB			
773549.078	669309.467	396.814	CH2 RB	0.03		
773548.742	669309.436	396.847	CH2 RT			
773552.485	669286.894	397.568	CH3 RT	0.01	3.34	0.03
773552.761	669286.839	397.553	CH3 RB			
773555.437	669285.898	397.581	CH3 LB	0.09		
773555.612	669285.734	397.675	CH3 LT			
773555.018	669277.511	398.012	CH3 LT	0.10	3.58	0.18
773554.762	669277.468	397.909	CH3 LB			
773552.039	669277.078	397.844	CH3 RB	0.13		
773551.458	669277.098	397.974	CH3 RT			
773550.323	669271.354	398.115	CH3 RT	0.07	5.84	0.21
773551.157	669271.232	398.044	CH3 RB			
773555.615	669270.416	398.154	CH3 LB	0.08		
773556.085	669270.398	398.235	CH3 LT			
773556.528	669262.444	398.488	CH3 LT	0.04	4.40	0.09
773556.4	669262.488	398.449	CH3 LB			
773554.061	669265.428	398.277	CH3 RB	0.12		
773553.55	669265.68	398.393	CH3 RT			
773550.296	669269.216	398.221	CH3 RT	0.08		

773550.734	669269.251	398.145	CH3 RB			
773554.243	669264.242	398.37	CH3 BAR2			
773552.445	669266.963	398.349	CH3 BAR2			
773553.354	669270.293	398.156	CH3 BAR2			
773552.327	669270.665	398.169	CH3 BAR2			
773552.818	669274.957	397.931	CH3 BAR2			
773547.048	669279.989	397.738	CH4 LW			
773545.877	669280.055	397.751	CH4 W	0.06		
773545.274	669279.813	397.807	CH4 RW			
773546.573	669283.455	397.753	CH4 LT	0.08	2.87	0.11
773546.162	669283.144	397.674	CH4 LB			
773544.051	669283.015	397.659	CH4 RB	0.13		
773543.807	669282.68	397.792	CH4 RT			
773543.165	669288.146	397.521	CH4 RT	0.05	1.51	0.04
773543.422	669288.155	397.472	CH4 RB			
773544.497	669288.158	397.481	CH4 LB	0.05		
773544.674	669288.21	397.529	CH4 LT			
773546.891	669296.594	397.222	CH4 LT	0.05	1.52	0.04
773546.653	669296.442	397.172	CH4 LB			
773545.688	669296.635	397.181	CH4 RB	0.06		
773545.367	669296.628	397.238	CH4 RT			
773543.008	669302.067	397.005	CH4 RT	0.10	1.89	0.09
773543.084	669302.28	396.907	CH4 RB			
773543.366	669303.548	396.897	CH4 LB	0.04		
773543.523	669303.888	396.934	CH4 LT			
773542.479	669305.004	396.881	CH4 LT	0.05	1.73	0.05
773542.392	669304.888	396.829	CH4 LB			
773541.179	669304.276	396.813	CH4 RB	0.08		
773541.011	669304.083	396.893	CH4 RT			
773541.156	669303.993	396.882	CH5 BAR3			
773540.386	669303.602	396.918	CH5 BAR3			
773540.367	669300.919	397.009	CH5 BAR3			
773541.069	669300.469	396.989	CH5 BAR3			
773540.252	669298.2	397.058	CH5 BAR3			
773539.346	669293.289	397.241	CH5 BAR4			
773538.841	669291.314	397.326	CH5 BAR4			
773537.1	669290.564	397.411	CH5 BAR4			
773537.048	669287.675	397.518	CH5 BAR4			
773538.101	669287.047	397.506	CH5 BAR4			
773538.487	669285.019	397.596	CH5 BAR4			
773540.261	669285.638	397.59	CH5 LT	0.04	5.96	0.11
773539.661	669285.913	397.552	CH5 LB			
773535.759	669288.822	397.455	CH5 RB	0.08		
773535.415	669289.1	397.534	CH5 RT			
773536.85	669292.463	397.334	CH5 RT	0.05	3.28	0.08
773537.072	669292.335	397.285	CH5 RB			
773539.826	669292.685	397.229	CH5 LB	0.05		
773540.122	669292.662	397.283	CH5 LT			
773540.859	669296.004	397.222	CH5 LT	0.12	1.73	0.10
773540.349	669295.973	397.106	CH5 LB			

773539.758	669296.549	397.107	CH5 RB	0.05		
773539.298	669296.755	397.156	CH5 RT			
773539.11	669301.95	397.052	CH5 RT	0.13	3.32	0.21
773539.475	669301.942	396.924	CH5 RB			
773542.109	669301.864	396.932	CH5 LB	0.11		
773542.428	669301.782	397.038	CH5 LT			
773574.889	669293.111	397.514	HEAD			
773574.728	669294.588	397.448	CH6 LW			
773574.177	669294.413	397.466	CH6 RW			
773573.524	669296.787	397.36	HEAD			
773573.293	669300.586	397.267	CH7 LT	0.06	1.19	0.03
773572.907	669300.479	397.212	CH7 LB			
773572.489	669300.585	397.194	CH7 RB	0.07		
773572.103	669300.51	397.26	CH7 RT			
773570.049	669306.797	397.036	CH7 RT	0.05	1.36	0.03
773570.264	669306.741	396.989	CH7 RB			
773571.012	669307.161	396.989	CH7 LB	0.04		
773571.345	669307.194	397.028	CH7 LT			
773570.649	669312.241	396.853	CH7 LT	0.05	1.87	0.04
773570.451	669312.261	396.808	CH7 LB			
773569.147	669312.277	396.838	CH7 RB	0.11		
773568.78	669312.37	396.948	CH7 RT			
773569.66	669318.129	396.626	CH7 RT	0.05	0.55	0.02
773569.942	669318.163	396.571	CH7 RB			
773570.093	669318.187	396.574	CH7 LB	0.03		
773570.207	669318.165	396.605	CH7 LT			
773572.168	669326.742	396.414	CH7 LT	0.13	1.77	0.12
773571.573	669326.855	396.282	CH7 LB			
773570.733	669326.794	396.302	CH7 RB	0.06		
773570.397	669326.701	396.361	CH7 RT			
773575.37	669323.023	396.673	HEAD			
773574.131	669325.266	396.647	CH8 LT	0.10	1.07	0.06
773573.966	669324.911	396.544	CH8 LB			
773573.934	669324.583	396.536	CH8 RB	0.05		
773573.843	669324.236	396.587	CH8 RT			
773572.636	669314.792	396.815	CH9 RT	0.08	0.94	0.04
773572.846	669315.033	396.735	CH9 RB			
773573.019	669315.24	396.733	CH9 LB	0.10		
773573.179	669315.557	396.833	CH9 LT			
773576.529	669311.149	396.998	CH9 LT	0.08	1.13	0.05
773576.27	669310.908	396.915	CH9 LB			
773576.003	669310.734	396.909	CH9 RB	0.07		
773575.576	669310.546	396.98	CH9 RT			
773579.159	669303.506	397.224	CH9 RT	0.05	0.63	0.01
773579.424	669303.665	397.179	CH9 RB			
773579.51	669303.568	397.183	CH9 LB	0.06		
773579.743	669303.743	397.246	CH9 LT			
773582.127	669297.712	397.494	CH9 LT	0.10	0.95	0.04
773581.751	669297.657	397.399	CH9 LB			
773581.624	669297.565	397.403	CH9 RB	0.05		

773581.197	669297.542	397.455	CH9 RT			
773583.93	669290.094	397.715	CH9 RT	0.05	0.81	0.02
773584.089	669290.038	397.66	CH9 RB			
773584.372	669290.278	397.672	CH9 LB	0.09		
773584.649	669290.473	397.764	CH9 LT			
773584.4	669290.005	397.739	CH9 W			
773583.727	669287.902	397.807	HEAD			
773585.493	669288.843	397.817	HEAD			
773590.116	669295.138	397.73	HEAD			
773588.85	669295.923	397.682	CH10 RW			
773589.212	669296.276	397.673	CH10 LW			
773583.892	669310.043	397.139	HEAD			
773583.094	669312.228	397.078	CH11 RT	0.02	0.69	0.01
773583.305	669312.228	397.056	CH11 RB			
773583.556	669312.301	397.045	CH11 LB	0.02		
773583.779	669312.311	397.066	CH11 LT			

Walkway Plot 1

Northing	Easting	Elevation	Feature code	Depth (m)	Width (m)	Cross (m^2)
3773262.047	669296.824	278.564	BENCH			
3773286.173	669267.536	279.653	CH1 LW			
3773287.523	669271.339	279.514	CH1 LW			
3773284.19	669269.765	279.557	CH1 RW			
3773284.603	669272.955	279.49	CH1 RW			
3773287.265	669278.609	279.299	CH1 RW		2.59	
3773289.79	669278.053	279.29	CH1 LW			
3773291.178	669281.155	279.157	CH1 LW		2.89	
3773288.695	669282.628	279.147	CH1 RW			
3773291.014	669285.76	278.994	CH1 LW		1.46	
3773289.561	669285.649	278.982	CH1 RW			
3773288.129	669292.042	278.825	CH1 LT	0.03	2.08	0.08
3773287.957	669292.033	278.79	CH1 LB			
3773286.32	669291.458	278.733	CH1 RB	0.04		
3773286.147	669291.419	278.771	CH1 RT			
3773281.649	669300.627	278.488	CH1 RW		2.33	0.06
3773283.425	669301.897	278.461	CH1 LB	0.05		
3773283.529	669302.01	278.509	CH1 LT			
3773280.875	669308.812	278.302	CH1 LT	0.06	3.43	0.11
3773280.709	669308.746	278.239	CH1 LB			
3773277.798	669307.289	278.279	CH1 RW			
3773291.665	669279.301	279.224	HEAD			
3773291.732	669281.671	279.181	CH2 LT	0.07	0.51	0.03
3773291.624	669281.703	279.114	CH2 LB			
3773291.311	669281.626	279.097	CH2 RB	0.05		
3773291.227	669281.617	279.142	CH2 RT			
3773281.462	669282.326	279.198	HEAD			
3773282.322	669282.769	279.164	CH3 LT	0.05	0.60	0.03
3773282.247	669282.842	279.118	CH3 LB			
3773282.034	669283.133	279.111	CH3 RB	0.04		

3773281.932	669283.219	279.149	CH3 RT			
3773282.908	669283.862	279.069	CH3 END			
3773278.853	669290.043	278.858	HEAD			
3773276.319	669294.38	278.747	CH4 LT	0.05	0.62	0.03
3773276.262	669294.299	278.694	CH4 LB			
3773275.933	669293.995	278.699	CH4 RB	0.04		
3773275.87	669293.958	278.74	CH4 RT			
3773272.684	669297.886	278.593	CH4 RT	0.07	0.95	0.08
3773272.841	669297.881	278.525	CH4 RB			
3773273.318	669298.375	278.531	CH4 LB	0.10		
3773273.464	669298.423	278.632	CH4 LT			
3773271.164	669301.384	278.46	CH4 LT	0.09	0.72	0.06
3773271.143	669301.318	278.372	CH4 LB			
3773270.83	669301.09	278.361	CH4 RB	0.09		
3773270.61	669300.928	278.454	CH4 RT			
3773265.214	669294.284	278.625	CH5 RT	0.09	1.28	0.10
3773265.344	669294.204	278.535	CH5 RB			
3773266.306	669294.125	278.552	CH5 LB	0.07		
3773266.472	669294.074	278.62	CH5 LT			
3773266.159	669296.615	278.513	CH5 LT	0.08	0.77	0.05
3773265.979	669296.62	278.434	CH5 LB			
3773265.606	669296.672	278.46	CH5 RB	0.05		
3773265.397	669296.705	278.506	CH5 RT			
3773265.336	669298.136	278.454	CH5 RT	0.09	0.75	0.05
3773265.57	669298.169	278.363	CH5 RB			
3773265.827	669298.199	278.425	CH5 LB	0.05		
3773266.068	669298.318	278.47	CH5 LT			
3773300.585	669263.556	279.855	HEAD			
3773299.232	669265.678	279.742	CH6 LW		0.39	
3773298.97	669265.392	279.737	CH6 RW			
3773297.414	669266.269	279.69	CH6 RW		0.68	
3773297.869	669266.781	279.669	CH6 LW			
3773294.002	669271.327	279.49	CH6 LW		0.58	
3773293.458	669271.115	279.483	CH6 RW			
3773293.265	669274.081	279.411	CH6 RW		1.72	
3773294.917	669274.571	279.395	CH6 LW			
3773294.047	669274.647	279.393	CH6 END			
3773301.453	669277.181	279.456	HEAD			
3773300.658	669278.538	279.392	CH7 LT	0.04	0.68	0.03
3773300.579	669278.491	279.356	CH7 LB			
3773300.314	669278.306	279.354	CH7 RB	0.05		
3773300.094	669278.157	279.401	CH7 RT			
3773298.628	669280.316	279.288	CH7 RW		0.66	
3773299.188	669280.66	279.289	CH7 LW			
3773298.86	669280.609	279.305	CH7 END			
3773310.065	669271.346	279.785	HEAD			
3773309.784	669274.2	279.717	CH8 LT	0.06	0.86	0.05
3773309.699	669274.203	279.66	CH8 LB			
3773309.156	669273.982	279.667	CH8 RB	0.05		
3773308.963	669273.933	279.715	CH8 RT			

3773307.927	669276.323	279.637	CH8 RT	0.08	0.86	0.03
3773308.112	669276.381	279.558	CH8 RB			
3773308.72	669276.65	279.596	CH8 LW			
3773306.637	669281.672	279.392	CH8 LW		1.08	
3773305.801	669280.984	279.414	CH8 RW			
3773304.529	669282.327	279.388	CH8 RW		3.08	
3773307.102	669284.029	279.332	CH8 LW			
3773305.416	669283.938	279.31	CH8 END			
3773296.626	669283.454	279.182	HEAD			
3773296.994	669286.989	279.111	CH9 LT	0.03	0.54	0.01
3773296.912	669286.961	279.079	CH9 LB			
3773296.464	669286.89	279.088	CH9 RW			
3773296.441	669290.794	278.986	CH9 RW		0.80	
3773297.178	669290.481	278.996	CH9 LW			
3773298.39	669292.527	278.964	CH9 LT	0.06	0.50	0.02
3773298.249	669292.498	278.9	CH9 LB			
3773298.045	669292.423	278.894	CH9 RB	0.03		
3773297.902	669292.419	278.922	CH9 RT			
3773294.784	669296.085	278.793	CH9 RW		0.47	
3773295.136	669296.395	278.78	CH9 LW			
3773294.941	669296.289	278.772	CH9 END			
3773292.017	669301.176	278.627	HEAD			
3773290.98	669302.62	278.589	CH10 LT	0.04	0.46	0.01
3773290.893	669302.56	278.552	CH10 LB			
3773290.739	669302.429	278.555	CH10 RB	0.02		
3773290.637	669302.317	278.574	CH10 RT			
3773287.843	669305.744	278.463	CH10 RT	0.04	0.63	0.03
3773287.918	669305.779	278.427	CH10 RB			
3773288.292	669306.075	278.423	CH10 LB	0.06		
3773288.357	669306.1	278.486	CH10 LT			
3773287.982	669306.065	278.395	TOPO			
3773286.701	669306.712	278.427	CH10 RT	0.06	0.78	0.06
3773286.753	669306.732	278.37	CH10 RB			
3773287.157	669306.858	278.324	CH10 LB	0.09		
3773287.432	669306.995	278.412	CH10 LT			
3773284.615	669310.351	278.208	CH10 LW		0.67	
3773284.055	669309.979	278.197	CH10 RW			
3773284.36	669310.25	278.157	TOPO			
3773321.842	669266.282	279.974	CH11 RW		0.89	
3773322.458	669266.931	279.964	CH11 LW			
3773319.307	669271.047	279.848	CH11 LT	0.08	0.57	0.04
3773319.241	669270.974	279.768	CH11 LB			
3773318.909	669270.888	279.794	CH11 RB	0.07		
3773318.781	669270.819	279.864	CH11 RT			
3773319.459	669270.087	279.815	TOPO			
3773318.927	669271.825	279.815	CH11 LT	0.05	0.52	0.02
3773318.878	669271.838	279.769	CH11 LB			
3773318.613	669271.934	279.755	CH11 RB	0.05		
3773318.471	669272.066	279.803	CH11 RT			
3773319.398	669273.84	279.756	CH11 RT	0.09	0.74	0.05

3773319.458	669273.797	279.665	CH11 RB			
3773319.707	669273.479	279.702	CH11 LB	0.05		
3773319.696	669273.16	279.754	CH11 LT			
3773319.501	669272.433	279.761	TOPO			
3773319.694	669272.572	279.802	TOPO			
3773319.767	669271.409	279.845	TOPO			
3773323.765	669268.322	279.947	HEAD			
3773322.915	669270.306	279.897	CH12 LT	0.06	0.49	0.03
3773322.865	669270.27	279.835	CH12 LB			
3773322.648	669270.097	279.853	CH12 RB	0.07		
3773322.522	669270.014	279.927	CH12 RT			
3773320.71	669271.328	279.889	CH12 RT	0.12	1.23	0.09
3773320.725	669271.371	279.773	CH12 RB			
3773321.237	669272.237	279.812	CH12 LB	0.04		
3773321.378	669272.366	279.849	CH12 LT			
3773319.803	669275.826	279.748	CH12 LT	0.13	0.67	0.04
3773319.731	669275.773	279.623	CH12 LB			
3773319.272	669275.411	279.626	CH12 RW			
3773317.988	669276.4	279.577	CH12 RT	0.04	1.42	0.09
3773318.062	669276.562	279.539	CH12 RB			
3773318.686	669277.489	279.586	CH12 LB	0.09		
3773318.775	669277.586	279.679	CH12 LT			
3773317.415	669277.693	279.608	CH12 LT	0.11	0.82	0.08
3773317.341	669277.63	279.503	CH12 LB			
3773316.923	669277.274	279.497	CH12 RB	0.09		
3773316.773	669277.186	279.587	CH12 RT			
3773315.888	669279.335	279.517	CH12 RT	0.11	0.67	0.06
3773316.022	669279.426	279.406	CH12 RB			
3773316.296	669279.664	279.426	CH12 LB	0.06		
3773316.38	669279.794	279.484	CH12 LT			
3773314.296	669282.323	279.454	CH12 LT	0.09	0.94	0.04
3773314.27	669282.189	279.365	CH12 LB			
3773313.732	669281.577	279.334	CH12 RW			
3773311.071	669284.068	279.289	CH12 RT	0.08	1.43	0.11
3773311.162	669284.083	279.211	CH12 RB			
3773312.149	669284.877	279.232	CH12 LB	0.07		
3773312.232	669284.904	279.302	CH12 LT			
3773312.341	669288.721	279.109	CH12 LW		1.22	
3773311.131	669288.849	279.091	CH12 RW			
3773310.064	669292.337	278.994	CH12 RT	0.04	1.28	0.05
3773310.144	669292.394	278.955	CH12 RB			
3773311.201	669292.81	278.969	CH12 LB	0.04		
3773311.264	669292.777	279.005	CH12 LT			
3773309.946	669296.463	278.884	CH12 LW		2.37	0.04
3773308.009	669295.094	278.897	CH12 RT	0.03		
3773308.046	669295.112	278.865	CH12 RB			
3773306.48	669298.519	278.72	CH12 RB	0.08		
3773306.416	669298.488	278.798	CH12 RT		1.62	
3773307.903	669299.122	278.741	CH12 LW			
3773307.457	669297.66	278.781	CH12 BAR			

3773308.978	669296.234	278.832	CH12 BAR			
3773309.597	669294.693	278.891	CH12 BAR			
3773308.291	669295.874	278.837	CH12 BAR			
3773308.763	669295.693	278.895	TOPO			
3773308.306	669296.536	278.875	TOPO			
3773306.862	669303.265	278.643	CH12 LT	0.03	1.35	0.02
3773306.734	669303.289	278.617	CH12 LB			
3773305.529	669303.458	278.602	CH12 RW			
3773305.444	669307.855	278.488	CH12 RW		1.37	
3773306.618	669308.565	278.473	CH12 LW			
3773306.263	669311.576	278.409	CH12 LT	0.03	1.21	0.04
3773306.195	669311.584	278.379	CH12 LB			
3773305.14	669311.557	278.366	CH12 RB	0.03		
3773305.056	669311.549	278.399	CH12 RT			
3773304.038	669313.573	278.331	CH12 RT	0.08	0.74	0.04
3773304.054	669313.605	278.256	CH12 RB			
3773304.653	669313.852	278.305	CH12 LB	0.04		
3773304.717	669313.878	278.344	CH12 LT			
3773302.225	669316.302	278.179	CH12 LW		0.91	0.02
3773301.605	669315.739	278.193	CH12 RB	0.03		
3773301.52	669315.728	278.226	CH12 RT			
3773299.652	669319.805	278.033	CH12 LW		0.91	
3773298.889	669319.302	278.031	CH12 RW			
3773315.735	669272.601	279.732	HEAD	0.09		
3773315.706	669272.632	279.645	HEAD B			
3773315.452	669273.771	279.734	CH13 LT	0.10	0.50	0.05
3773315.344	669273.735	279.638	CH13 LB			
3773315.125	669273.549	279.618	CH13 RB	0.10		
3773315.015	669273.52	279.72	CH13 RT			
3773314.801	669274.547	279.663	CH13 RT	0.06	0.32	0.02
3773314.815	669274.523	279.602	CH13 RB			
3773314.981	669274.529	279.6	CH13 LB	0.05		
3773315.119	669274.529	279.653	CH13 LT			
3773315.443	669277.813	279.576	CH13 LT	0.07	0.69	0.04
3773315.324	669277.857	279.509	CH13 LB			
3773314.846	669277.871	279.524	CH13 RB	0.04		
3773314.757	669277.869	279.565	CH13 RT			
3773303.509	669311.41	278.32	HEAD			
3773302.442	669312.87	278.337	CH14 LT	0.07	0.53	0.03
3773302.377	669312.788	278.266	CH14 LB			
3773302.229	669312.523	278.235	CH14 RB	0.03		
3773302.153	669312.427	278.27	CH14 RT			
3773298.454	669317.629	278.091	CH14 RW		0.74	
3773299.095	669317.991	278.097	CH14 LW			
3773297.449	669320.738	277.968	CH14 LW		0.69	
3773296.789	669320.544	278.011	CH14 RW			
3773297.079	669321.151	277.983	CH14 RW			
3773308.105	669322.26	278.039	HEAD			
3773307.232	669323.067	278.054	CH15 LT	0.08	0.89	0.04
3773307.115	669322.86	277.972	CH15 LB			

3773306.654	669322.389	278.015	CH15 RW			
3773305.967	669323.24	277.974	CH15 RT	0.03	0.54	0.02
3773306.139	669323.375	277.94	CH15 RB			
3773306.366	669323.453	277.937	CH15 LB	0.05		
3773306.455	669323.481	277.991	CH15 LT			
3773304.864	669326.344	277.841	CH15 LT	0.06	0.51	0.03
3773304.808	669326.218	277.779	CH15 LB			
3773304.529	669326.052	277.761	CH15 RB	0.06		
3773304.532	669325.957	277.825	CH15 RT			
3773304.852	669326.061	277.83	TOPO			
3773304.792	669325.855	277.856	TOPO			
3773304.876	669326.183	277.742	TOPO			
3773305.468	669325.791	277.823	TOPO			
3773306.983	669314.715	278.311	HEAD			
3773307.485	669315.959	278.229	CH16 LW		0.70	
3773306.961	669316.419	278.242	CH16 RW			
3773326.402	669286.715	279.382	HEAD			
3773324.58	669288.735	279.253	CH17 LW		0.82	
3773323.928	669288.246	279.265	CH17 RW			
3773317.805	669302.697	278.759	HEAD			
3773318.506	669304.972	278.681	CH18 RW		0.46	
3773318.899	669304.733	278.66	CH18 LW			
3773319.031	669306.412	278.637	CH18 RT	0.05	0.67	0.03
3773319.096	669306.391	278.585	CH18 RB			
3773319.606	669306.642	278.588	CH18 LB	0.03		
3773319.679	669306.581	278.615	CH18 LT			
3773319.302	669308.03	278.624	CH18 LT	0.07	0.79	0.05
3773319.194	669308.006	278.551	CH18 LB			
3773318.819	669307.696	278.556	CH18 RB	0.07		
3773318.685	669307.535	278.622	CH18 RT			
3773317.401	669309.435	278.517	CH18 RT	0.02	1.03	0.01
3773317.549	669309.548	278.498	CH18 RB			
3773318.29	669309.958	278.501	CH18 LW			
3773320.38	669303.171	278.751	HEAD			
3773320.068	669303.914	278.733	CH19 LT	0.03	0.75	0.02
3773319.971	669303.845	278.704	CH19 LB			
3773319.59	669303.721	278.703	CH19 RB	0.03		
3773319.389	669303.588	278.736	CH19 RT			
3773337.81	669281.48	279.687	HEAD			
3773337.825	669281.566	279.566	HEAD			
3773337.565	669281.828	279.497	HEAD			
3773337.39	669282.339	279.497	HEAD			
3773338.028	669282.676	279.486	HEAD			
3773338.726	669281.378	279.706	TOPO			
3773336.099	669281.356	279.71	TOPO			
3773338.281	669283.747	279.59	CH20 LT	0.13	1.15	0.12
3773338.219	669283.775	279.462	CH20 LB			
3773337.317	669284.101	279.507	CH20 RB	0.09		
3773337.189	669284.109	279.594	CH20 RT			
3773336.684	669285.001	279.557	CH20 RT	0.06	1.45	0.15

3773336.731	669285.027	279.496	CH20 RB			
3773338.005	669285.344	279.4	CH20 LB	0.15		
3773338.077	669285.388	279.545	CH20 LT			
3773337.267	669288.7	279.419	CH20 LT	0.04	1.32	0.09
3773337.203	669288.668	279.381	CH20 LB			
3773336.077	669288.431	279.325	CH20 RB	0.10		
3773335.984	669288.395	279.422	CH20 RT			
3773336.261	669291.564	279.232	CH20 RT	0.07	0.86	0.09
3773336.457	669291.592	279.162	CH20 RB			
3773336.772	669291.924	279.203	CH20 LB	0.13		
3773336.961	669292.059	279.333	CH20 LT			
3773335.357	669295.951	279.234	CH20 LT	0.13	0.82	0.09
3773335.294	669295.933	279.102	CH20 LB			
3773334.865	669295.658	279.041	CH20 RB	0.08		
3773334.634	669295.557	279.119	CH20 RT			
3773332.748	669299.167	279.062	CH20 RT	0.12	0.94	0.08
3773332.816	669299.194	278.942	CH20 RB			
3773333.529	669299.541	278.979	CH20 LB	0.06		
3773333.589	669299.581	279.037	CH20 LT			
3773332.788	669301.811	278.95	CH20 LT	0.06	0.94	0.06
3773332.693	669301.768	278.891	CH20 LB			
3773332.005	669301.696	278.862	CH20 RB	0.06		
3773331.867	669301.626	278.922	CH20 RT			
3773331.417	669307.245	278.772	CH20 RW		1.94	0.09
3773332.79	669306.298	278.734	CH20 LB	0.09		
3773333.015	669306.143	278.822	CH20 LT			
3773293.61	669258.181	280.059	ROCK 1			
3773300.157	669263.33	280.226	ROCK 1			
3773292.738	669270.615	279.847	ROCK 1			
3773287.149	669266.475	279.844	ROCK 1			
3773294.143	669271.618	279.811	ROCK 2			
3773301.452	669264.259	280.017	ROCK 2			
3773309.659	669270.659	280.078	ROCK 2			
3773305.911	669280.604	279.784	ROCK 2			
3773307.381	669281.914	279.601	ROCK 3			
3773308.857	669281.905	279.467	ROCK 3			
3773314.512	669274.37	279.733	ROCK 3			
3773311.166	669271.719	279.981	ROCK 3			
3773321.682	669265.096	280.185	ROCK 4			
3773318.055	669269.523	279.918	ROCK 4			
3773316.001	669269.801	279.964	ROCK 4			
3773308.175	669262.635	280.189	ROCK 4			
3773324.942	669268.376	280.035	ROCK 5			
3773312.19	669285.536	279.553	ROCK 5			
3773320.031	669291.395	279.472	ROCK 5			
3773327.436	669284.114	279.643	ROCK 5			
3773318.275	669277.055	279.591	ROCK 5			
3773329.644	669277.467	279.948	ROCK 6			
3773332.281	669274.073	280.038	ROCK 6			
3773328.856	669273.496	279.771	ROCK 7			

3773326.78	669272.014	279.853	ROCK 7
3773324.818	669274.355	279.763	ROCK 7
3773326.925	669276.13	279.786	ROCK 7
3773328.819	669285.244	279.739	ROCK 8
3773321.455	669292.461	279.396	ROCK 8
3773331.984	669300.442	279.122	ROCK 8
3773336.1	669290.473	279.491	ROCK 8
3773348.179	669286.006	279.784	ROCK 9
3773341.614	669294.721	279.576	ROCK 9
3773337.467	669291.526	279.433	ROCK 9
3773333.412	669301.51	279.147	ROCK 9
3773335.435	669302.9	278.996	ROCK 9
3773325.284	669312.747	278.663	ROCK 10
3773310.694	669331.849	277.898	ROCK 10
3773309.445	669330.377	277.872	ROCK 11
3773323.719	669311.589	278.673	ROCK 11
3773313.148	669303.526	278.831	ROCK 11
3773298.922	669321.891	278.03	ROCK 11
3773297.445	669320.839	277.924	ROCK 12
3773311.127	669302.757	278.779	ROCK 12
3773309.948	669303.974	278.669	ROCK 12
3773309.532	669304.679	278.648	ROCK 12
3773308.615	669303.988	278.698	ROCK 12
3773309.295	669303.169	278.75	ROCK 12
3773305.814	669296.176	278.973	ROCK 13
3773299.749	669291.603	279.132	ROCK 13
3773284.113	669312.041	278.302	ROCK 13
3773282.815	669311.13	278.292	ROCK 14
3773297.508	669291.876	279.151	ROCK 14
3773285.672	669282.953	279.198	ROCK 14
3773270.642	669302.258	278.407	ROCK 14
3773269.482	669301.319	278.517	ROCK 15
3773285.098	669280.66	279.309	ROCK 15
3773279.377	669276.177	279.449	ROCK 15
3773290.378	669284.504	279.133	ROCK 16
3773292.914	669281.49	279.315	ROCK 16
3773296.596	669284.309	279.328	ROCK 16
3773294.448	669287.536	279.309	ROCK 16
3773298.384	669290.676	279.206	ROCK 16
3773293.377	669286.292	279.19	ROCK 17
3773294.594	669284.671	279.116	ROCK 17
3773292.826	669283.464	279.252	ROCK 17
3773291.5	669285.138	279.139	ROCK 17
3773262.047	669296.81	278.569	BENCH

Walkway Plot 2

Northing	Easting	Elevation	Feature code	Depth (m)	Width (m)	Cross (m^2)
3773163.465	669010.935	286.4	CH 1 RT	0.02	0.61	0.01
3773163.272	669010.885	286.383	CH 1 RB			
3773163.08	669010.779	286.395	CH 1 LB	0.03		

3773162.938	669010.621	286.42	CH 1 LT			
3773163.578	669016.967	286.194	CH 1 LT	0.03	0.78	0.02
3773163.796	669017.026	286.161	CH 1 LB			
3773164.034	669017.001	286.187	CH 1 RB	0.02		
3773164.354	669017.033	286.208	CH 1 RT			
3773163.237	669019.856	286.08	CH 1 RT	0.00	0.54	0.01
3773163.096	669019.867	286.078	CH 1 RB			
3773162.972	669019.884	286.084	CH 1 LB	0.02		
3773162.694	669019.874	286.107	CH 1 LT			
3773163.159	669022.753	286.01	CH 1 LT	0.02	0.74	0.02
3773163.392	669022.812	285.988	CH 1 LB			
3773163.62	669022.825	285.994	CH 1 RB	0.02		
3773163.892	669022.826	286.015	CH 1 RT			
3773163.181	669025.1	285.944	CH 1 W			
3773162.831	669025.145	285.919	CH 1 W			
3773162.71	669027.069	285.869	CH 1 W			
3773163.255	669025.517	285.925	CH 1 W			
3773163.902	669025.817	285.941	CH 2 W			
3773164.854	669022.808	286.04	CH 2 W			
3773165.495	669022.969	286.025	CH 2 W			
3773166.574	669019.436	286.146	CH 2 W			
3773166.054	669019.169	286.182	CH 2 W			
3773167.484	669018.295	286.25	CH 2 LT	0.05	1.30	0.07
3773167.232	669018.044	286.197	CH 2 LB			
3773166.891	669017.781	286.218	CH 2 RB	0.06		
3773166.493	669017.446	286.273	CH 2 RT			
3773168.865	669015.151	286.356	CH 2 RT	0.06	0.92	0.05
3773169.07	669015.248	286.301	CH 2 RB			
3773169.457	669015.542	286.304	CH 2 LB	0.05		
3773169.65	669015.629	286.351	CH 2 LT			
3773171.232	669013.282	286.409	CH 2 W			
3773170.606	669012.861	286.43	CH 2 W			
3773143.817	669050.078	284.982	HEAD			
3773142.883	669051.295	284.945	CH 3 RT	0.02	0.64	0.02
3773143.137	669051.369	284.927	CH 3 RB			
3773143.376	669051.435	284.918	CH 3 LB	0.05		
3773143.462	669051.569	284.967	CH 3 LT			
3773141.601	669053.913	284.882	CH 3 LT	0.03	0.86	0.03
3773141.48	669053.887	284.855	CH 3 LB			
3773141.13	669053.635	284.858	CH 3 RB	0.05		
3773140.913	669053.402	284.909	CH 3 RT			
3773139.154	669055.727	284.876	CH 3 RT	0.10	0.93	0.08
3773139.522	669055.822	284.773	CH 3 RB			
3773139.801	669055.923	284.762	CH 3 LB	0.07		
3773140.042	669055.989	284.837	CH 3 LT			
3773139.312	669057.832	284.747	CH 3 LT	0.06	0.82	0.05
3773139.005	669057.784	284.685	CH 3 LB			
3773138.798	669057.75	284.71	CH 3 RB	0.07		
3773138.49	669057.767	284.779	CH 3 RT			
3773133.975	669056.454	284.786	HEAD			

3773132.758	669056.606	284.784	CH 4 RT	0.07	0.80	0.06
3773132.883	669056.807	284.717	CH 4 RB			
3773132.92	669057.1	284.696	CH 4 LB	0.08		
3773133.05	669057.356	284.778	CH 4 LT			
3773131.982	669058.051	284.73	CH 4 LT	0.11	0.98	0.11
3773131.883	669057.642	284.624	CH 4 LB			
3773131.904	669057.355	284.636	CH 4 RB	0.11		
3773131.88	669057.081	284.751	CH 4 RT			
3773130.083	669055.801	284.703	CH 4 RT	0.02	1.17	0.08
3773130.269	669055.702	284.68	CH 4 RB			
3773130.585	669055.182	284.667	CH 4 LB	0.11		
3773130.8	669054.874	284.773	CH 4 LT			
3773130.072	669053.765	284.81	CH 4 LT	0.07	1.21	0.10
3773129.763	669053.867	284.74	CH 4 LB			
3773129.305	669053.999	284.734	CH 4 RB	0.09		
3773128.936	669054.171	284.825	CH 4 RT			
3773128.261	669052.872	284.848	CH 4 RT	0.06	0.90	0.03
3773128.604	669052.732	284.785	CH 4 RB			
3773129.067	669052.47	284.827	CH 4 LT			
3773129.932	669052.008	284.881	HEAD			
3773129.064	669049.796	284.934	HEAD			
3773131.087	669053.655	284.836	CH 4 RT	0.11	1.85	0.19
3773131.225	669053.576	284.724	CH 4 RB			
3773132.669	669054.089	284.736	CH 4 LB	0.09		
3773132.915	669053.929	284.825	CH 4 LT			
3773135.535	669054.621	284.856	HEAD			
3773134.813	669052.747	284.885	HEAD			
3773132.17	669050.103	284.912	CH 4 LT	0.12	1.11	0.13
3773132.058	669050.096	284.789	CH 4 LB			
3773131.432	669049.989	284.83	CH 4 RB	0.10		
3773131.085	669049.858	284.934	CH 4 RT			
3773131.238	669045.845	285.031	CH 4 RT	0.12	1.16	0.14
3773131.57	669045.955	284.913	CH 4 RB			
3773131.864	669045.836	284.899	CH 4 LB	0.12		
3773132.38	669046.063	285.021	CH 4 LT			
3773133.152	669044.513	285.077	CH 4 LT	0.10	0.76	0.06
3773133.018	669044.23	284.978	CH 4 LB			
3773132.865	669044.055	285.007	CH 4 RB	0.06		
3773132.684	669043.916	285.065	CH 4 RT			
3773134.447	669042.465	285.165	HEAD			
3773133.032	669043.089	285.131	CH 4 RT	0.05	0.84	0.06
3773133.333	669043.094	285.079	CH 4 RB			
3773133.65	669043.261	285.06	CH 4 LB	0.08		
3773133.821	669043.369	285.142	CH 4 LT			
3773134.907	669044.311	285.108	CH 4 LT	0.06	0.48	0.03
3773134.884	669044.106	285.05	CH 4 LB			
3773134.88	669044.02	285.054	CH 4 RB	0.05		
3773134.827	669043.841	285.101	CH 4 RT			
3773137.258	669043.701	285.165	HEAD			
3773130.753	669031.427	285.424	HEAD			

3773130.001	669033.906	285.38	CH 5 RT	0.04	0.76	0.04
3773130.225	669033.868	285.343	CH 5 RB			
3773130.402	669033.825	285.344	CH 5 LB	0.06		
3773130.733	669033.713	285.408	CH 5 LT			
3773130.865	669037.981	285.32	CH 5 LT	0.09	0.76	0.05
3773130.551	669037.978	285.233	CH 5 LB			
3773130.388	669037.891	285.24	CH 5 RB	0.04		
3773130.122	669037.837	285.284	CH 5 RT			
3773128.625	669040.875	285.153	CH 5 RT	0.05	0.68	0.04
3773128.843	669041.07	285.104	CH 5 RB			
3773129.018	669041.183	285.125	CH 5 LB	0.06		
3773129.139	669041.32	285.188	CH 5 LT			
3773127.262	669043.916	285.111	CH 5 LT	0.06	1.33	0.12
3773126.985	669043.877	285.047	CH 5 LB			
3773126.413	669043.725	284.996	CH 5 RB	0.12		
3773125.996	669043.511	285.119	CH 5 RT			
3773125.488	669047.127	284.946	CH 5 RT	0.06	1.01	0.08
3773125.738	669047.139	284.89	CH 5 RB9			
3773126.087	669047.095	284.888	CH 5 LB	0.09		
3773126.495	669047.246	284.982	CH 5 LT			
3773124.643	669050.54	284.852	CH 5 LT	0.05	1.04	0.08
3773124.484	669050.305	284.8	CH 5 LB			
3773123.982	669049.947	284.817	CH 5 RB	0.09		
3773123.884	669049.835	284.91	CH 5 RT			
3773123.017	669050.7	284.849	CH 5 RT	0.08	1.27	0.09
3773123.467	669050.914	284.771	CH 5 RB			
3773123.812	669051.324	284.792	CH 5 LB	0.06		
3773124.032	669051.467	284.855	CH 5 LT			
3773127.025	669040.055	285.179	HEAD			
3773127.292	669041.551	285.111	CH 5 LT		0.58	
3773126.725	669041.679	285.128	CH 5 RT			
3773143.021	668995.75	286.691	HEAD			
3773143.585	668998.582	286.605	CH 6 RT	0.16	0.42	0.07
3773143.738	668998.513	286.446	CH 6 RB			
3773143.814	668998.488	286.456	CH 6 LB	0.17		
3773143.977	668998.433	286.622	CH 6 LT			
3773143.605	669000.188	286.508	CH 6 LT	0.12	0.53	0.08
3773143.516	669000.062	286.389	CH 6 LB			
3773143.354	668999.939	286.385	CH 6 RB	0.17		
3773143.215	668999.824	286.55	CH 6 RT			
3773144.437	669000.541	286.55	HEAD			
3773143.78	669001.425	286.531	HEAD			
3773143.839	669002.893	286.475	HEAD			
3773142.686	669003.055	286.456	CH 6 LT	0.17	0.68	0.11
3773142.579	669002.917	286.289	CH 6 LB			
3773142.354	669002.721	286.279	CH 6 RB	0.15		
3773142.212	669002.563	286.433	CH 6 RT			
3773140.886	669003.113	286.378	CH 6 RT	0.16	0.85	0.15
3773140.866	669003.351	286.219	CH 6 RB			
3773140.909	669003.675	286.198	CH 6 LB	0.19		

3773141.095	669003.937	286.387	CH 6 LT			
3773140.486	669005.504	286.298	CH 6 LT	0.11	2.19	0.24
3773140.29	669005.433	286.191	CH 6 LB			
3773138.798	669005.479	286.182	CH 6 RB	0.11		
3773138.293	669005.547	286.296	CH 6 RT			
3773136.874	669009.241	286.163	CH 6 RT	0.13	1.20	0.16
3773137.149	669009.29	286.029	CH 6 RB			
3773137.709	669009.478	286.036	CH 6 LB	0.13		
3773138.031	669009.575	286.165	CH 6 LT			
3773135.932	669008.479	286.204	HEAD			
3773134.672	669009.853	286.157	HEAD			
3773135.379	669012.719	286.029	CH 6 RT	0.12	1.85	0.24
3773135.709	669012.998	285.91	CH 6 RB			
3773136.041	669013.717	285.909	CH 6 LB	0.14		
3773136.516	669014.177	286.054	CH 6 LT			
3773133.604	669018.538	285.865	CH 6 LT	0.09	1.46	0.14
3773133.298	669018.367	285.778	CH 6 LB			
3773132.723	669018.095	285.773	CH 6 RB	0.11		
3773132.315	669017.863	285.88	CH 6 RT			
3773128.849	669023.984	285.661	CH 6 RT	0.07	1.15	0.08
3773129.109	669024.191	285.587	CH 6 RB			
3773129.593	669024.459	285.585	CH 6 LB	0.07		
3773129.866	669024.527	285.653	CH 6 LT			
3773129.094	669029.481	285.533	CH 6 LT	0.07	1.14	0.08
3773128.907	669029.483	285.466	CH 6 LB			
3773128.417	669029.538	285.459	CH 6 RB	0.07		
3773127.958	669029.447	285.532	CH 6 RT			
3773127.684	669030.955	285.461	CH 6 RT	0.04	1.30	0.06
3773128.012	669031.046	285.419	CH 6 RB			
3773128.564	669031.526	285.431	CH 6 LB	0.05		
3773128.786	669031.646	285.483	CH 6 LT			
3773127.054	669031.971	285.469	CH 6 LT	0.12	0.91	0.08
3773127.073	669031.854	285.354	CH 6 LB			
3773127.114	669031.49	285.361	CH 6 RB	0.07		
3773127.092	669031.063	285.431	CH 6 RT			
3773124.152	669033.39	285.345	CH 6 RT	0.07	1.87	0.16
3773124.244	669033.589	285.275	CH 6 RB			
3773125.374	669034.399	285.24	CH 6 LB	0.11		
3773125.67	669034.487	285.346	CH 6 LT			
3773123.302	669038.998	285.174	CH 6 LT	0.06	2.04	0.12
3773123.037	669038.873	285.117	CH 6 LB			
3773121.901	669037.939	285.101	CH 6 RB	0.06		
3773121.842	669037.569	285.162	CH 6 RT			
3773120.719	669033.336	285.315	HEAD			
3773121.426	669035.162	285.25	CH 6 LT		0.88	
3773120.58	669035.41	285.246	CH 6 RT			
3773124.603	669039.231	285.191	HEAD			
3773122.492	669041.468	285.102	CH 6 LT	0.05	2.44	0.17
3773122.141	669041.354	285.051	CH 6 LB			
3773120.563	669041.217	285.005	CH 6 RB	0.09		

3773120.085	669041.083	285.092	CH 6 RT			
3773119.3	669044.372	284.983	CH 6 RT	0.09	2.32	0.17
3773119.519	669044.355	284.895	CH 6 RB			
3773120.602	669045.456	284.867	CH 6 LB	0.06		
3773121.186	669045.715	284.928	CH 6 LT			
3773120.321	669048.198	284.85	CH 6 LT	0.06	1.46	0.05
3773119.991	669048.103	284.786	CH 6 LB			
3773119.382	669047.951	284.827	CH 6 RB	0.00		
3773119.009	669047.555	284.828	CH 6 RT			
3773119.206	669048.899	284.877	CH 6 RT	0.12	1.75	0.18
3773119.346	669048.852	284.76	CH 6 RB			
3773120.72	669049.154	284.784	CH 6 LB	0.08		
3773120.959	669048.946	284.867	CH 6 LT			
3773121.957	669049.678	284.785	CH 6 LT			
3773123.201	669048	284.96	HEAD			
3773121.835	669021.605	285.701	HEAD			
3773120.117	669021.01	285.712	HEAD			
3773121.016	669023.279	285.64	CH 7 W			
3773121.929	669023.603	285.654	CH 7 W			
3773120.181	669023.651	285.631	CH 7 W			
3773120.848	669025.079	285.549	CH 7 W			
3773121.803	669025.333	285.603	CH 7 W			
3773140.502	669002.178	286.402	CH 8 LT	0.16	1.22	0.17
3773140.246	669002.28	286.244	CH 8 LB			
3773139.597	669002.539	286.307	CH 8 RB	0.13		
3773139.347	669002.568	286.433	CH 8 RT			
3773139.244	669000.408	286.453	CH 8 RT	0.14	0.78	0.12
3773139.519	669000.487	286.317	CH 8 RB			
3773139.653	669000.517	286.314	CH 8 LB	0.17		
3773140.014	669000.546	286.488	CH 8 LT			
3773138.159	669000.95	286.428	HEAD			
3773139.948	668996.765	286.591	CH 8 RT	0.11	1.50	0.18
3773140.301	668996.793	286.486	CH 8 RB			
3773141.003	668997.044	286.493	CH 8 LB	0.13		
3773141.442	668996.836	286.628	CH 8 LT			
3773141.107	668998.972	286.567	CH 8 LT	0.14	1.77	0.23
3773140.936	668998.961	286.43	CH 8 LB			
3773139.608	668998.925	286.456	CH 8 RB	0.13		
3773139.343	668998.878	286.584	CH 8 RT			
3773139.938	668994.91	286.646	CH 8 RT	0.10	1.17	0.12
3773140.175	668994.851	286.551	CH 8 RB			
3773140.673	668994.707	286.583	CH 8 LB	0.12		
3773141.056	668994.57	286.699	CH 8 LT			
3773142.794	668993.901	286.749	HEAD			
3773141.533	668991.308	286.816	HEAD			
3773139.922	668991.635	286.787	HEAD			
3773110.125	669007.381	286.118	HEAD			
3773109.902	669011.421	285.955	CH 9 LB	0.11		
3773110.111	669011.574	286.067	CH 9 LT		0.75	0.06
3773109.627	669011.307	285.918	CH 9 RB	0.06		

3773109.422	669011.269	285.975	CH 9 RT			
3773105.866	669015.497	285.798	CH 9 RT	0.07	0.56	0.04
3773106.067	669015.559	285.725	CH 9 RB			
3773106.162	669015.669	285.755	CH 9 LB	0.05		
3773106.296	669015.858	285.807	CH 9 RT			
3773103.217	669018.856	285.686	CH 9 RT	0.02	0.88	0.03
3773103.566	669018.916	285.661	CH 9 RB			
3773103.747	669019.091	285.648	CH 9 LB	0.05		
3773103.981	669019.285	285.701	CH 9 LT			
3773100.467	669023.622	285.483	CH 9 W			
3773099.912	669023.293	285.498	CH 9 W			
3773088.316	669024.649	285.518	BENCH			
3773093.98	669028.088	285.21	CH 9 RT	0.07	1.25	0.13
3773094.366	669028.065	285.139	CH 9 RB			
3773094.807	669027.922	285.134	CH 9 LB	0.14		
3773095.104	669027.542	285.276	CH 9 LT			
3773094.455	669023.23	285.407	CH 9 LT	0.13	1.14	0.15
3773094.053	669023.228	285.28	CH 9 LB			
3773093.801	669023.134	285.271	CH 9 RB	0.13		
3773093.428	669022.727	285.403	CH 9 RT			
3773094.634	669019.232	285.552	CH 9 RT	0.06	1.45	0.11
3773094.898	669019.542	285.491	CH 9 RB			
3773095.348	669020.024	285.448	CH 9 LB	0.09		
3773095.695	669020.214	285.535	CH 9 LT			
3773098.23	669016.997	285.669	CH 9 LT	0.06	1.02	0.08
3773097.913	669016.96	285.609	CH 9 LB			
3773097.625	669016.973	285.57	CH 9 RB	0.09		
3773097.208	669017.005	285.657	CH 9 RT			
3773097.237	669015.323	285.703	HEAD			
3773099.676	669013.262	285.765	HEAD			
3773103.002	669008.39	285.978	HEAD			
3773105.401	669009.254	285.974	HEAD			
3773102.956	669010.538	285.85	CH 9 RT			
3773102.13	669012.229	285.846	CH 9 RT	0.06	0.98	0.06
3773102.372	669012.386	285.784	CH 9 RB			
3773102.638	669012.546	285.787	CH 9 LB	0.07		
3773103.009	669012.671	285.854	CH 9 LT			
3773101.748	669016.538	285.725	CH 9 LT	0.11	0.76	0.08
3773101.407	669016.295	285.614	CH 9 LB			
3773101.237	669016.19	285.622	CH 9 RB	0.09		
3773101.072	669016.18	285.712	CH 9 RT			
3773099.064	669017.744	285.604	CH 9 RT	0.05	1.04	0.08
3773099.336	669017.974	285.551	CH 9 RB			
3773099.665	669018.205	285.536	CH 9 LB	0.09		
3773099.825	669018.457	285.627	CH 9 LT			
3773096.139	669022.213	285.427	CH 9 LT	0.05	0.88	0.05
3773095.932	669022.008	285.375	CH 9 LB			
3773095.783	669021.78	285.385	CH 9 RB	0.05		
3773095.634	669021.489	285.435	CH 9 RT			
3773104.304	669036.983	285.142	HEAD			

3773105.642	669037.529	285.209	CH 10 LT	0.17	1.03	0.15
3773105.252	669037.811	285.038	CH 10 LB			
3773105.064	669037.914	285.04	CH 10 RB	0.12		
3773104.742	669038.036	285.161	CH 10 RT			
3773088.299	669024.648	285.517	BECH CH			

Walkway Plot 3

Northing	Easting	Elevation	Feature code	Depth (m)	Width (m)	Cross (m^2)
3775061.22	670439.153	369.372	CH1 RT	0.08		
3775061.595	670439.164	369.292	CH1 RB			
3775062.249	670444.873	369.055	CH1 RB	0.07		
3775062.022	670444.894	369.128	CH1 RT			
3775062.751	670447.695	369.029	CH1 RT	0.08		
3775062.945	670447.577	368.952	CH1 RB			
3775053.983	670434.315	369.484	CH2 RT	0.06	3.77	0.12
3775054.231	670434.384	369.419	CH2 RB			
3775056.73	670436.269	369.353	CH2 LB	0.00		
3775057.148	670436.36	369.354	CH2 LT			
3775056.469	670443.8	369.187	CH2 LT	0.08	2.55	0.22
3775056.083	670443.853	369.104	CH2 LB			
3775054.311	670443.917	369.129	CH2 RB	0.09		
3775053.92	670443.874	369.218	CH2 RT			
3775053.286	670449.802	368.977	CH2 RW		2.39	
3775055.66	670449.557	368.926	CH2 LW			
3775057.101	670455.717	368.728	CH2 LW		2.16	
3775054.944	670455.882	368.81	CH2 RT	0.08		
3775055.26	670455.728	368.728	CH2 RB			
3775054.333	670461.573	368.517	CH2 RW			
3775052.441	670440.986	369.241	HEAD			
3775052.464	670443.551	369.182	CH3 LT	0.04	0.95	0.06
3775052.371	670443.579	369.141	CH3 LB			
3775051.761	670443.554	369.126	CH3 RB	0.09		
3775051.517	670443.533	369.211	CH3 RT			
3775051.424	670445.93	369.121	CH3 RW		1.34	
3775052.542	670446.254	369.084	CH3 LB	0.03		
3775052.72	670446.266	369.112	CH3 LT			
3775051.832	670451.046	368.932	CH3 LW		1.33	
3775050.512	670451.173	368.945	CH3 RW			
3775050.696	670456.705	368.704	CH3 RW		3.10	
3775053.661	670457.618	368.708	CH3 LW			
3775051.598	670464.146	368.442	CH3 LW		3.97	
3775047.625	670464.044	368.406	CH3 RW			
3775046.023	670469.659	368.223	CH3 RW		4.09	
3775050.111	670469.667	368.241	CH3 LT	0.05		
3775049.94	670469.575	368.191	CH3 LB			
3775045.032	670472.206	368.13	CH3 RW			
3775044.621	670477.305	367.897	CH3 RW			
3775041.9	670426.967	369.715	CH4 RT	0.07		
3775042.147	670427.14	369.647	CH4 RB			
3775042.726	670427.586	369.664	CH4 LW			

3775039.479	670431.059	369.55	CH4 LT	0.06	0.85	0.05
3775039.347	670431.007	369.493	CH4 LB			
3775038.9	670430.865	369.5	CH4 RB	0.06		
3775038.651	670430.848	369.564	CH4 RT			
3775038.453	670433.349	369.511	CH4 RT	0.06	0.53	0.04
3775038.532	670433.36	369.447	CH4 RB			
3775038.904	670433.322	369.429	CH4 LB	0.07		
3775038.977	670433.277	369.503	CH4 LT			
3775039.472	670434.692	369.403	CH4 LW		0.83	
3775038.772	670435.141	369.399	CH4 RW			
3775039.114	670434.99	369.374	CH4END			
3775041.6	670454.055	368.759	HEAD			
3775041.853	670455.508	368.722	CH5 LT	0.07	0.51	0.03
3775041.708	670455.462	368.655	CH5 LB			
3775041.466	670455.381	368.675	CH5 RB	0.05		
3775041.388	670455.307	368.727	CH5 RT			
3775041.7	670456.846	368.606	CH5 LW		0.62	
3775041.081	670456.789	368.637	CH5 RW			
3775040.371	670460.64	368.518	HEAD			
3775038.999	670464.057	368.348	CH6 LW		1.20	0.05
3775038.07	670463.624	368.338	CH6 RB	0.08		
3775037.906	670463.553	368.42	CH6 RT			
3775036.75	670468.728	368.194	CH6 RW		1.34	
3775038.07	670468.938	368.2	CH6 LW			
3775037.431	670468.879	368.182	CH6 END			
3775036.712	670473.808	368.048	HEAD			
3775037.25	670474.464	368.037	CH7 LT	0.05	0.57	0.03
3775037.156	670474.433	367.987	CH7 LB			
3775036.807	670474.471	368.001	CH7 RB	0.06		
3775036.678	670474.511	368.063	CH7 RT			
3775037.867	670477.501	367.923	CH7 LT	0.07	1.16	0.04
3775037.7	670477.545	367.854	CH7 LB			
3775036.921	670478.168	367.902	CH7 RW			
3775037.736	670479.078	367.844	CH7 END			
3775042.678	670427.616	369.65	CH8 LT	0.02	1.10	0.05
3775042.407	670427.509	369.628	CH8 LB			
3775041.969	670427.24	369.624	CH8 RB	0.07		
3775041.692	670427.138	369.696	CH8 RT			
3775029.342	670426.19	369.679	HEAD			
3775029.798	670427.497	369.623	CH9 LT	0.04	0.77	0.03
3775029.603	670427.521	369.584	CH9 LB			
3775029.24	670427.6	369.596	CH9 RB	0.04		
3775029.053	670427.7	369.635	CH9 RT			
3775029.093	670429.21	369.528	CH9 END			
3775032.399	670450.646	368.786	HEAD			
3775032.539	670453.226	368.684	CH10 LT	0.06	0.39	0.03
3775032.451	670453.193	368.621	CH10 LB			
3775032.235	670453.214	368.607	CH10 RB	0.08		
3775032.148	670453.19	368.683	CH10 RT			
3775031.965	670455.397	368.618	CH10 RT	0.07	0.52	0.02

3775032.064	670455.379	368.55	CH10 RB			
3775032.482	670455.356	368.57	CH10 LW			
3775032.487	670457.586	368.537	CH10 LT	0.05	1.03	0.05
3775032.323	670457.62	368.483	CH10 LB			
3775031.522	670457.696	368.515	CH10 RB	0.04		
3775031.462	670457.727	368.558	CH10 RT			
3775031.565	670464.846	368.379	CH10 RT	0.07	1.92	0.13
3775031.675	670464.83	368.305	CH10 RB			
3775033.328	670464.842	368.289	CH10 LB	0.06		
3775033.482	670464.813	368.353	CH10 LT			
3775035.543	670476.709	367.967	CH10 LT	0.08	1.60	0.06
3775035.432	670476.641	367.891	CH10 LB			
3775033.953	670476.549	367.898	CH10 RW			
3775032.728	670478.674	367.834	CH10 RW		2.10	0.04
3775034.447	670479.479	367.805	CH10 LB	0.04		
3775034.611	670479.607	367.843	CH10 LT			
3775031.957	670485.491	367.615	CH10 LW		3.38	
3775029.113	670483.656	367.655	CH10 RW			
3775030.374	670484.812	367.661	CH10 END			
3775024.727	670470.052	368.148	HEAD			
3775025.051	670471.882	368.082	CH11 LT	0.05	0.58	0.03
3775024.952	670471.903	368.037	CH11 LB			
3775024.625	670471.993	368.04	CH11 RB	0.05		
3775024.477	670471.95	368.088	CH11 RT			
3775024.628	670474.234	367.996	CH11 RW		0.92	
3775025.546	670474.147	367.999	CH11 LW			
3775024.503	670453.74	368.765	HEAD			
3775025.802	670455.323	368.683	CH12 LT	0.03	0.77	0.03
3775025.737	670455.368	368.657	CH12 LB			
3775025.214	670455.586	368.656	CH12 RB	0.05		
3775025.074	670455.579	368.71	CH12 RT			
3775025.562	670458.366	368.562	CH12 RW		0.85	
3775026.392	670458.207	368.578	CH12 LW			
3775013.266	670464.342	368.173	HEAD			
3775013.365	670466.466	368.134	CH13 LT	0.05	0.73	0.03
3775013.218	670466.484	368.086	CH13 LB			
3775012.843	670466.495	368.084	CH13 RB	0.03		
3775012.641	670466.505	368.111	CH13 RT			
3775029.264	670426.17	369.687	HEAD			
3775029.763	670427.608	369.644	CH14 LT	0.04	0.67	0.03
3775029.628	670427.621	369.6	CH14 LB			
3775029.262	670427.657	369.603	CH14 RB	0.05		
3775029.093	670427.666	369.657	CH14 RT			
3775028.643	670429.204	369.579	CH14 RW		1.78	
3775030.164	670430.138	369.526	CH14 LW			
3775002.816	670459.96	368.243	HEAD			
3775002.797	670461.792	368.191	CH15 LT	0.08	0.68	0.06
3775002.656	670461.768	368.106	CH15 LB			
3775002.367	670461.618	368.101	CH15 RB	0.08		
3775002.165	670461.536	368.185	CH15 RT			

3775001.516	670462.872	368.126	CH15 RT	0.07	0.46	0.03
3775001.612	670462.975	368.055	CH15 RB			
3775001.811	670463.067	368.036	CH15 LB	0.04		
3775001.934	670463.068	368.078	CH15 LT			
3774999.693	670465.667	368.14	CH15 LT	0.12	1.23	0.16
3774999.52	670465.6	368.024	CH15 LB			
3774998.751	670465.06	367.98	CH15 RB	0.14		
3774998.643	670465.027	368.124	CH15 RT			
3774997.82	670466.469	368.039	CH15 RT	0.10	1.00	0.10
3774997.89	670466.502	367.936	CH15 RB			
3774998.464	670467.062	367.973	CH15 LB	0.10		
3774998.475	670467.225	368.075	CH15 LT			
3774997.182	670468.866	367.975	CH15 LT	0.09	0.92	0.07
3774997.118	670468.804	367.89	CH15 LB			
3774996.653	670468.461	367.872	CH15 RB	0.06		
3774996.443	670468.312	367.936	CH15 RT			
3774991.993	670464.421	368.009	HEAD			
3774992.503	670465.609	367.961	CH16 LT	0.06	1.12	0.07
3774992.288	670465.495	367.899	CH16 LB			
3774991.691	670465.202	367.935	CH16 RB	0.06		
3774991.488	670465.14	367.998	CH16 RT			
3775012.418	670422.626	369.691	HEAD			
3775012.883	670423.185	369.688	CH17 LT	0.04	0.29	0.01
3775012.799	670423.173	369.645	CH17 LB			
3775012.694	670423.176	369.649	CH17 RB	0.02		
3775012.598	670423.16	369.67	CH17 RT			
3775011.819	670424.996	369.594	CH17 RT	0.05	0.60	0.03
3775011.917	670425.07	369.546	CH17 RB			
3775012.231	670425.273	369.585	CH17 LB	0.05		
3775012.323	670425.328	369.632	CH17 LT			
3775011.371	670423.963	369.626	HEAD			
3775011.389	670425.138	369.579	CH18 RT	0.03		
3775011.479	670425.069	369.551	CH18 RB			
3775009.888	670427.533	369.485	CH18 RT	0.05	0.69	0.03
3775010.071	670427.651	369.435	CH18 RB			
3775010.347	670427.789	369.44	CH18 LB	0.04		
3775010.5	670427.854	369.476	CH18 LT			
3775008.363	670430.729	369.296	CH18 LW		0.53	0.01
3775008.041	670430.615	369.315	CH18 RB	0.04		
3775007.869	670430.539	369.354	CH18 RT			
3775007.349	670433.476	369.21	CH18 RT	0.04	0.32	0.01
3775007.425	670433.539	369.174	CH18 RB			
3775007.531	670433.638	369.18	CH18 LB	0.01		
3775007.566	670433.705	369.189	CH18 LT			
3775004.852	670436.441	369.009	CH18 LT	0.04	0.39	0.01
3775004.77	670436.4	368.972	CH18 LB			
3775004.589	670436.324	368.983	CH18 RB	0.01		
3775004.496	670436.272	368.994	CH18 RT			
3775004.732	670430.344	369.366	HEAD			
3775004.444	670431.642	369.284	CH19 LT	0.03	0.53	0.01

3775004.344	670431.617	369.254	CH19 LB			
3775004.088	670431.587	369.266	CH19 RB	0.02		
3775003.919	670431.584	369.282	CH19 RT			
3775003.01	670434.822	369.11	CH19 RT	0.02	0.66	0.02
3775003.139	670434.797	369.087	CH19 RB			
3775003.523	670434.619	369.093	CH19 LB	0.02		
3775003.634	670434.597	369.117	CH19 LT			
3775004.212	670436.666	368.955	CH19 RB	0.05		
3775004.032	670436.67	369.007	CH19 RT		2.77	0.14
3775003.998	670439.439	368.915	CH19 LT	0.05		
3775003.877	670439.4	368.869	CH19 LB			
3775003.241	670439.501	368.915	CH19 RW			
3775002.688	670441.737	368.835	CH19 RW		2.98	
3775005.659	670441.996	368.858	CH19 LW			
3775004.593	670445.718	368.653	CH19 LW		1.47	
3775003.127	670445.859	368.694	CH19 RW			
3775003.016	670449.231	368.57	CH19 RW		2.06	
3775005.069	670449.422	368.574	CH19 LW			
3775003.723	670455.22	368.395	CH19 LW		2.49	
3775001.238	670455.054	368.411	CH19 LW			
3775014.111	670442.251	368.967	HEAD			
3775012.183	670443.487	368.903	CH20 LT	0.07	0.55	0.03
3775012.116	670443.364	368.83	CH20 LB			
3775011.99	670443.127	368.839	CH20 RB	0.05		
3775011.889	670443.019	368.888	CH20 RT			
3775009.866	670444.272	368.8	CH20 RT	0.05	1.10	0.04
3775009.923	670444.37	368.754	CH20 RB			
3775010.733	670444.688	368.802	CH20 LB	0.03		
3775010.831	670444.804	368.836	CH20 LT			
3775008.055	670447.04	368.716	CH20 LT	0.03	1.09	0.03
3775007.842	670446.926	368.684	CH20 LB			
3775007.207	670446.748	368.683	CH20 RB	0.03		
3775007.04	670446.655	368.71	CH20 RT			
3775005.307	670449.257	368.595	CH20 RW		1.19	
3775006.309	670449.907	368.595	CH20 LW			
3775020.08	670412.945	370.087	ROCK 1			
3775005.895	670431.37	369.489	ROCK 1			
3775017.95	670440.459	369.171	ROCK 1			
3774995.674	670468.295	367.859	ROCK 1			
3775021.402	670413.852	370.154	ROCK 2			
3775008.504	670430.726	369.518	ROCK 2			
3775016.097	670436.539	369.406	ROCK 2			
3775024.338	670425.785	369.981	ROCK 2			
3775032.123	670429.876	369.756	ROCK 2			
3775034.852	670430.795	369.625	ROCK 2			
3775037.821	670429.243	369.81	ROCK 2			
3775040.35	670426.125	369.867	ROCK 2			
3775044.102	670428.488	369.9	ROCK 3			
3775040.153	670432.338	369.563	ROCK 3			
3775037.053	670434.604	369.666	ROCK 3			

3775032.536	670435.133	369.548	ROCK 3
3775022.27	670429.899	369.575	ROCK 3
3775016.773	670437.143	369.209	ROCK 3
3775019.465	670439.183	369.212	ROCK 3
3775020.028	670438.415	369.335	ROCK 3
3775020.649	670439.095	369.278	ROCK 4
3775020.306	670439.971	369.231	ROCK 4
3775025.535	670443.958	369.23	ROCK 4
3775026.313	670443.172	369.106	ROCK 4
3775027.089	670443.753	369.14	ROCK 5
3775026.55	670444.701	369.12	ROCK 5
3775038.157	670453.504	368.952	ROCK 5
3775038.645	670453.044	368.986	ROCK 5
3775039.684	670453.517	368.884	ROCK 6
3775039.011	670454.177	368.97	ROCK 6
3775042.739	670456.954	368.776	ROCK 6
3775047.31	670450.589	369.151	ROCK 6
3775055.824	670449.131	368.99	ROCK 6
3775063.171	670440.282	369.276	ROCK 6
3775063.988	670442.121	369.292	ROCK 7
3775056.343	670450.941	368.966	ROCK 7
3775048.21	670451.857	369.139	ROCK 7
3775043.971	670457.919	368.82	ROCK 7
3775051.683	670463.624	368.494	ROCK 7
3775050.982	670465.113	368.56	ROCK 8
3775049.237	670463.943	368.418	ROCK 8
3775028.419	670488.687	367.613	ROCK 8
3775027.014	670487.673	367.529	ROCK 9
3775047.744	670462.56	368.619	ROCK 9
3775030.916	670450.095	369.092	ROCK 9
3775010.622	670477.659	367.766	ROCK 9
3775009.136	670476.678	367.863	ROCK 10
3775029.306	670448.835	369.206	ROCK 10
3775019.616	670441.671	369.39	ROCK 10
3774997.114	670469.209	368.077	ROCK 10
3774983.308	670460.873	368.237	BENCH

Walkway Plot 4

Northing	Easting	Elevation	Feature code	Depth (m)	Width (m)	Cross (m^2)
3774728.355	670267.535	373.111	HEAD			
3774727.645	670269.146	373.196	CH1 LT	0.12	1.81	0.18
3774727.47	670268.989	373.076	CH1 LB			
3774726.702	670268.965	373.071	CH1 LB	0.08		
3774727.07	670268.583	373.147	CH1 LT			
3774726.314	670268.167	373.055	CH1 RB	0.15		
3774726.22	670268.026	373.21	CH1 RT			
3774727.988	670265.697	373.267	CH1 RT	0.12	1.09	0.10
3774728.327	670266.024	373.149	CH1 RB			
3774728.539	670266.208	373.105	CH1 LB	0.07		
3774728.867	670266.347	373.176	CH1 LT			

3774732.084	670262.241	373.375	CH1 LT	0.08	1.17	0.12
3774731.876	670262.026	373.294	CH1 LB			
3774731.607	670261.667	373.292	CH1 RB	0.12		
3774731.311	670261.361	373.409	CH1 RT			
3774732.45	670260.485	373.415	CH1 RT	0.06	2.06	0.06
3774732.76	670260.642	373.355	CH1 RB			
3774733.04	670260.622	373.394	CH1 RT			
3774733.377	670258.644	373.535	HEAD			
3774733.974	670260.638	373.394	CH1 LB	0.16		
3774734.225	670260.907	373.554	CH1 LT			
3774737.823	670256.05	373.614	CH1 LT	0.04	1.53	0.08
3774737.688	670255.896	373.577	CH1 LB			
3774737.07	670255.101	373.602	CH1 RB	0.06		
3774736.793	670254.924	373.666	CH1 RT			
3774740.905	670249.777	373.819	CH1 RT	0.03	1.60	0.05
3774741.066	670249.888	373.791	CH1 RB			
3774742.32	670250.234	373.852	CH1 LB	0.03		
3774742.432	670250.265	373.882	CH1 LT			
3774743.712	670249.407	373.883	HEAD			
3774743.502	670248.743	373.881	CH1 LT	0.03	1.43	0.08
3774743.212	670248.762	373.852	CH1 LB			
3774742.445	670248.186	373.865	CH1 RB	0.08		
3774742.222	670248.103	373.944	CH1 RT			
3774745.68	670243.237	374.145	CH1 RT	0.06	1.33	0.08
3774745.866	670243.415	374.088	CH1 RB			
3774746.707	670243.442	374.102	CH1 LB	0.07		
3774746.937	670243.674	374.169	CH1 LT			
3774750.519	670239.275	374.398	CH1 LT	0.04	1.04	0.03
3774750.226	670238.944	374.357	CH1 LB			
3774750.036	670238.667	374.38	CH1 RB	0.02		
3774749.826	670238.496	374.397	CH1 RT			
3774752.486	670234.747	374.621	CH1 RT	0.14	0.92	0.10
3774752.745	670234.837	374.482	CH1 RB			
3774753.101	670234.97	374.531	CH1 LB	0.08		
3774753.312	670235.148	374.612	CH1 LT			
3774756.262	670232.477	374.753	CH1 LT	0.07	0.84	0.06
3774756.188	670232.256	374.678	CH1 LB			
3774755.94	670232.057	374.681	CH1 RB	0.06		
3774755.701	670231.848	374.742	CH1 RT			
3774758.395	670228.701	374.939	CH1 RT	0.12	0.77	0.10
3774758.433	670228.97	374.819	CH1 RB			
3774758.511	670229.227	374.808	CH1 LB	0.13		
3774758.557	670229.457	374.935	CH1 LT			
3774760.233	670228.704	374.952	HEAD			
3774760.611	670226.975	374.985	HEAD			
3774763.38	670220.636	375.137	CH2 W			
3774763.881	670220.905	375.153	CH2 W			
3774764.013	670222.001	375.124	CH2 W			
3774763.372	670222.04	375.118	CH2 W			
3774751.562	670244.164	374.25	HEAD			

3774750.65	670245.805	374.219	CH3 LT	0.03	0.77	0.04
3774750.62	670245.569	374.186	CH3 LB			
3774750.5	670245.363	374.183	CH3 RB	0.07		
3774750.328	670245.106	374.256	CH3 RT			
3774747.398	670246.102	374.121	CH3 RT	0.06	0.76	0.03
3774747.494	670246.312	374.062	CH3 RB			
3774747.612	670246.569	374.089	CH3 LB	0.03		
3774747.714	670246.792	374.118	CH3 LT			
3774735.181	670255.908	373.685	CH3 LT	0.02	0.94	0.04
3774735.081	670255.886	373.66	CH3 LB			
3774734.575	670255.939	373.63	CH3 RB	0.06		
3774734.265	670255.677	373.689	CH3 RT			
3774736.546	670251.3	373.819	CH3 RT	0.03		
3774736.773	670251.356	373.793	CH3 RB			
3774737.916	670251.648	373.793	CH3 LW			
3774741.757	670247.041	373.993	CH3 LW			
3774740.929	670245.58	373.976	CH3 RB	0.03		
3774740.856	670245.521	374.004	CH3 RT			
3774741.703	670244.768	374.047	CH3 RT	0.03	1.87	
3774741.519	670244.788	374.017	CH3 RB			
3774741.561	670242.864	374.094	CH3 RB	0.02		
3774741.777	670242.896	374.11	CH3 RT			
3774741.31	670242.897	374.097	CH3 LB	0.03		
3774741.109	670242.829	374.122	CH3 LT			
3774742.086	670241.11	374.159	HEAD			
3774745.13	670238.814	374.247	CH3 RT	0.01	1.94	0.06
3774745.391	670238.902	374.238	CH3 RB			
3774746.719	670238.669	374.276	CH3 LB	0.06		
3774747.046	670238.513	374.333	CH3 LT			
3774748.257	670237.848	374.363	CH3 W			
3774748.615	670238.15	374.405	CH3 W			
3774749.711	670236.385	374.476	HEAD			
3774748.809	670232.071	374.556	CH3 LT	0.13		
3774748.496	670231.97	374.421	CH3 LB			
3774750.71	670231.223	374.596	HEAD			
3774747.013	670230.011	374.51	CH3 RB	0.07		
3774746.59	670229.534	374.585	CH3 RT			
3774749.388	670228.167	374.636	CH3 LB	0.04		
3774749.57	670228.17	374.675	CH3 LT			
3774750.669	670227.028	374.753	CH3 W			
3774751.202	670227.378	374.747	CH3 W			
3774752.237	670225.184	374.845	HEAD			
3774752.965	670227.094	374.781	CH3 W			
3774753.879	670227.238	374.776	CH3 W			
3774754.971	670224.811	374.863	CH3 W			
3774755.428	670225.005	374.883	CH3 W			
3774756.516	670222.791	374.984	HEAD			
3774750.448	670220.74	375.041	CH3 LT	0.29	2.91	0.57
3774750.09	670220.799	374.749	CH3 LB			
3774747.936	670220.492	374.862	CH3 RB	0.10		

3774747.554	670220.429	374.964	CH3 RT			
3774747.589	670213.653	375.221	CH3 RT	0.19	3.25	0.39
3774748.141	670213.652	375.032	CH3 RB			
3774750.622	670213.898	375.1	CH3 LB	0.05		
3774750.831	670213.851	375.153	CH3 LT			
3774751.74	670214.197	375.195	CH3 LT	0.08		
3774751.641	670214.129	375.112	CH3 LB			
3774752.6	670212.933	375.307	CH3 LT	0.14	0.97	0.11
3774752.276	670212.826	375.168	CH3 LB			
3774751.904	670212.818	375.173	CH3 RB	0.09		
3774751.634	670212.835	375.259	CH3 RT			
3774750.207	670210.685	375.297	CH3 LT	0.08	2.83	0.40
3774749.873	670210.571	375.215	CH3 LB			
3774748.092	670209.505	375.174	CH3 RB	0.20		
3774747.643	670209.477	375.376	CH3 RT			
3774743.397	670206.384	375.465	CH 4 W			
3774744.126	670206.832	375.513	CH 4 W			
3774743.684	670208.066	375.42	CH 4 W			
3774742.921	670207.826	375.417	CH 4 W			
3774739.463	670212.242	375.262	HEAD			
3774740.203	670212.906	375.224	HEAD			
3774738.55	670215.226	375.153	CH 4 LT	0.06	1.00	0.07
3774738.322	670215.015	375.089	CH 4 LB			
3774737.942	670214.836	375.076	CH 4 RB	0.07		
3774737.664	670214.767	375.148	CH 4 RT			
3774738.593	670217.075	375.07	HEAD			
3774737.066	670219.574	374.948	CH 4 LT	0.06	1.21	0.11
3774736.828	670219.593	374.893	CH 4 LB			
3774736.126	670219.771	374.913	CH 4 RB	0.13		
3774735.86	670219.688	375.046	CH 4 RT			
3774732.466	670225.897	374.695	CH 4 RT	0.04	1.18	0.04
3774732.538	670226.08	374.655	CH 4 RB			
3774732.75	670226.546	374.661	CH 4 LB	0.03		
3774733.089	670226.899	374.691	CH 4 LT			
3774728.91	670231.102	374.448	CH 4 LT		1.65	0.03
3774728.792	670230.88	374.453	CH 4 LB			
3774728.014	670230.302	374.466	CH 4 RB	0.03		
3774727.563	670230.153	374.497	CH 4 RT			
3774728.304	670236.731	374.214	CH 4 RT	0.04	0.79	0.04
3774728.603	670236.603	374.174	CH 4 RB			
3774728.74	670236.541	374.173	CH 4 LB	0.05		
3774729.056	670236.485	374.223	CH 4 LT			
3774731.391	670239.498	374.12	CH 4 LT	0.08	2.07	0.15
3774731.067	670239.678	374.044	CH 4 LB			
3774729.679	670239.946	374.08	CH 4 RB	0.07		
3774729.391	670240.013	374.149	CH 4 RT			
3774730.713	670246.585	373.849	CH 4 RT	0.05	1.89	0.24
3774730.943	670246.598	373.803	CH 4 RB			
3774731.926	670247.165	373.811	CH 4 LB	0.21		
3774732.427	670247.375	374.016	CH 4 LT			

3774728.379	670257.376	373.477	CH 4 LT	0.06	0.65	0.04
3774728.108	670257.205	373.419	CH 4 LB			
3774728.032	670257.159	373.434	CH 4 RB	0.05		
3774727.812	670257.057	373.484	CH 4 RT			
3774726.193	670262.644	373.32	CH 4 RT	0.08	0.90	0.06
3774726.447	670262.965	373.243	CH 4 RB			
3774726.63	670263.125	373.255	CH 4 LB	0.06		
3774726.776	670263.326	373.318	CH 4 LT			
3774723.725	670265.752	373.235	CH 4 LT	0.11	1.00	0.12
3774723.489	670265.532	373.122	B			
3774723.136	670265.344	373.123	CH4 RB	0.12		
3774722.884	670265.203	373.243	CH4 RT			
3774716.694	670260.484	373.529	CH4 LT	0.06	1.50	0.09
3774716.566	670260.449	373.464	CH4 LB			
3774715.705	670259.971	373.495	CH4 RB	0.06		
3774715.347	670259.813	373.556	CH4 RT			
3774716.74	670255.426	373.663	CH4 W			
3774717.349	670255.546	373.681	CH4 W			
3774716.812	670255.176	373.673	CH4 W			
3774718.3	670250.832	373.811	CH4 W			
3774718.769	670250.902	373.841	CH4 W			
3774717.943	670247.613	373.999	CH4 RT	0.05	1.11	0.04
3774718.219	670247.667	373.948	CH4 RB			
3774718.77	670247.722	373.951	CH4 LB	0.02		
3774719.047	670247.707	373.971	CH4 LT			
3774718.297	670243.112	374.206	CH4 LT	0.06	1.01	0.06
3774718.062	670243.199	374.146	CH4 LB			
3774717.557	670243.088	374.132	CH4 RB	0.07		
3774717.286	670243.053	374.2	CH4 RT			
3774718.16	670237.328	374.404	CH4 RT	0.11	0.72	0.06
3774718.439	670237.408	374.293	CH4 RB			
3774718.626	670237.462	374.315	CH4 LB	0.06		
3774718.869	670237.451	374.378	CH4 LT			
3774718.707	670235.22	374.454	HEAD			
3774730.426	670197.666	375.704	CH5 RT	0.05	1.19	0.06
3774730.629	670197.848	375.655	CH5 RB			
3774731.123	670198.41	375.644	CH5 LB	0.06		
3774731.27	670198.499	375.701	CH5 LT			
3774728.604	670202.293	375.558	CH5 LT	0.08	0.99	0.07
3774728.221	670202.062	375.48	CH5 LB			
3774727.944	670201.878	375.482	CH5 RB	0.06		
3774727.803	670201.709	375.546	CH5 RT			
3774726.62	670203.424	375.474	CH5 RT	0.06	0.88	0.05
3774726.718	670203.54	375.419	CH5 RB			
3774726.924	670204.059	375.426	CH5 LB	0.06		
3774727.075	670204.179	375.49	CH5 LT			
3774725.247	670202.315	375.504	CH6 LT	0.06	1.11	0.07
3774725.653	670202.287	375.44	CH6 LB			
3774726.134	670202.168	375.474	CH6 LB	0.06		
3774726.34	670202.143	375.538	CH6 LT			

3774727.177	670197.898	375.701	CH6 LT	0.10	1.02	0.09
3774726.801	670197.912	375.598	CH6 LB			
3774726.52	670197.942	375.598	CH6 RB	0.06		
3774726.156	670197.922	375.663	CH6 RT			
3774727.346	670194.466	375.819	HEAD			
3774723.232	670208.164	375.278	CH5 RT	0.05	1.23	0.09
3774723.394	670208.207	375.232	CH5 RB			
3774723.889	670208.581	375.216	CH5 LB	0.11		
3774724.321	670208.736	375.323	CH5 LT			
3774723.576	670214.898	375.048	CH5 LT	0.02	1.05	0.04
3774723.34	670214.892	375.024	CH5 LB			
3774722.769	670215.072	374.994	CH5 RB	0.05		
3774722.539	670215.051	375.044	CH5 RT			
3774722.742	670217.687	374.959	CH5 W			
3774723.784	670217.967	374.949	CH5 W			
3774721.928	670219.567	374.872	CH5 W			
3774723.409	670220.386	374.896	CH5 W			
3774722.564	670222.018	374.859	CH5 W			
3774720.047	670223.932	374.698	CH5 W			
3774718.56	670225.556	374.658	CH5 W			
3774717.184	670228.442	374.507	CH5 W			
3774717.434	670225.999	374.567	CH5 W			
3774719.587	670222.961	374.746	CH5 W			
3774721.335	670219.843	374.873	CH5 W			
3774722.241	670204.607	375.456	HEAD			
3774722.884	670207.047	375.371	CH7 LT	0.075	0.8715739	0.0640607
3774722.641	670206.937	375.296	CH7 LB			
3774722.457	670206.775	375.304	CH7 RB	0.072		
3774722.088	670206.692	375.376	CH7 RT			
3774720.485	670210.949	375.133	CH7 RT	0.017	0.9189042	0.0257293
3774720.596	670211.057	375.116	CH7 RB			
3774720.971	670211.398	375.086	CH7 LB	0.039		
3774721.174	670211.557	375.125	CH7 LT			
3774720.553	670217.573	374.9	CH7 LT	0.029	1.3484287	0.0991095
3774720.31	670217.512	374.871	CH7 LB			
3774719.469	670217.551	374.876	CH7 RB	0.118		
3774719.205	670217.539	374.994	CH7 RT			
3774718.537	670222.408	374.724	CH7 RT	0.059	6.0361883	0.1780676
3774718.822	670222.587	374.665	CH7 RB			
3774718.974	670222.741	374.694	CH7 LB			
3774715.8	670227.788	374.513	CH7 LT	0.017	1.3468248	0.0700349
3774715.627	670227.677	374.496	CH7 LB			
3774714.883	670227.341	374.473	CH7 RB	0.087		
3774714.524	670227.357	374.56	CH7 RT			
3774711.185	670235.7	374.251	CH7 RT	0.065	1.6747967	0.0803902
3774711.55	670235.909	374.186	CH7 RB			
3774711.961	670236.865	374.213	CH7 LB	0.031		
3774712.073	670237.12	374.244	CH7 LT			
3774708.886	670239.666	374.101	CH7 LT	0.028	1.9504994	0.0477872
3774708.524	670239.583	374.073	CH7 LB			

3774707.215	670240.136	374.038	CH7 RB	0.021		
3774706.954	670239.934	374.059	CH7 RT			
3774703.143	670243.966	373.908	CH7 RT	0.044	1.8969291	0.132785
3774703.253	670244.133	373.864	CH7 RB			
3774703.903	670245.202	373.813	CH7 LB	0.096		
3774704.245	670245.51	373.909	CH7 LT			
3774701.98	670248.76	373.757	CH7 LT	0.016	1.5826866	0.0609334
3774701.628	670248.652	373.741	CH7 LB			
3774700.765	670248.368	373.703	CH7 RB	0.061		
3774700.509	670248.176	373.764	CH7 RT			
3774706.341	670240.185	374.032	CH8 LT	0.024	1.3716884	0.0843588
3774706.045	670240.176	374.008	CH8 LB			
3774705.54	670239.665	373.982	CH8 RB	0.099		
3774705.121	670239.558	374.081	CH8 RT			
3774704.114	670237.572	374.147	CH8 RT	0.043	1.0063026	0.0508183
3774704.359	670237.445	374.104	CH8 RB			
3774704.611	670237.032	374.111	CH8 LB	0.058		
3774704.835	670236.87	374.169	CH8 LT			
3774704.171	670235.76	374.193	HEAD			
3774708.007	670234.778	374.207	CH8 RT	0.027	1.5850003	0.0705325
3774708.322	670234.851	374.18	CH8 RB			
3774709.225	670234.6	374.201	CH8 LB	0.062		
3774709.592	670234.777	374.263	CH8 LT			
3774710.844	670229.86	374.516	CH8 LT	0.141	1.8305431	0.2004445
3774710.265	670229.667	374.375	CH8 LB			
3774709.424	670229.351	374.397	CH8 RB	0.078		
3774709.042	670229.538	374.475	CH8 RT			
3774708.408	670226.186	374.593	CH8 RT	0.096	1.3864707	0.129635
3774709.187	670226.012	374.497	CH8 RB			
3774709.371	670225.778	374.508	CH8 LB	0.091		
3774709.734	670225.781	374.599	CH8 LT			
3774708.275	670222.62	374.681	HEAD			
3774712.544	670224.303	374.624	HEAD			
3774711.956	670227.114	374.562	CH8 RT	0.093	0.9418843	0.0711123
3774711.58	670226.963	374.469	CH8 RB			
3774711.459	670226.916	374.487	CH8 LB	0.058		
3774711.051	670226.853	374.545	CH8 LT			

Walkway Plot 5

Northing	Easting	Elevation	Feature code	Depth (m)	Width (m)	Cross (m^2)
3773227.428	669444.05	314.159	CH1 LT	0.04	0.53	0.02
3773227.294	669444.027	314.115	CH1 LB			
3773227.077	669444.123	314.104	CH1 RB	0.04		
3773226.91	669444.139	314.139	CH1 RT			
3773227.285	669444.966	314.134	CH1 RT	0.05	0.74	0.05
3773227.468	669444.822	314.084	CH1 RB			
3773227.718	669444.47	314.055	CH1 LB	0.09		
3773227.729	669444.378	314.141	CH1 LT			
3773238.285	669429.718	314.583	CH2 RWT		0.39	
3773238.566	669429.986	314.564	CH2 LW			

3773236.948	669432.117	314.518	CH2 LW		0.95	
3773236.245	669432.749	314.531	CH2 RW			
3773253.797	669408.613	315.368	CH3 RW		0.69	0.02
3773254.249	669408.863	315.362	CH3 LB	0.05		
3773254.407	669408.933	315.417	CH3 LT			
3773253.656	669410.242	315.307	CH3 LW		0.65	0.02
3773253.217	669410.529	315.284	CH3 RB	0.07		
3773253.092	669410.557	315.359	CH3 RT			
3773259.545	669403.871	315.61	CH4 RT	0.11	0.72	0.10
3773259.679	669403.992	315.502	CH4 RB			
3773259.978	669404.295	315.482	CH4 LB	0.17		
3773260.085	669404.343	315.648	CH4 LT			
3773258.545	669406.184	315.539	CH4 LT	0.09	0.86	0.09
3773258.447	669406.125	315.447	CH4 LB			
3773257.979	669405.761	315.465	CH4 RB	0.11		
3773257.842	669405.682	315.579	CH4 RT			
3773256.643	669407.918	315.449	CH4 RT	0.06	0.58	0.04
3773256.715	669407.973	315.39	CH4 RB			
3773257.043	669408.171	315.408	CH4 LB	0.07		
3773257.141	669408.219	315.475	CH4 LT			
3773255.018	669411.556	315.32	CH4 LW		1.10	
3773254.278	669410.74	315.315	CH4 RW			
3773252.537	669413.435	315.217	CH4 RW		0.77	0.02
3773253.029	669413.915	315.206	CH4 LB	0.06		
3773253.128	669413.934	315.267	CH4 LT			
3773252.099	669415.495	315.143	CH4 LW		0.56	
3773251.538	669415.544	315.19	CH4 RW			
3773252.351	669418.774	315.066	CH4 RW		1.30	
3773253.652	669418.764	315.068	CH4 LW			
3773252.952	669422.74	314.956	CH4 LW		0.90	
3773252.21	669423.245	314.941	CH4 RW			
3773254.192	669427.231	314.834	CH4 RW		1.33	0.03
3773255.428	669427.031	314.846	CH4 LB	0.05		
3773255.496	669426.965	314.894	CH4 LT			
3773256.06	669429.509	314.78	CH4 LW		2.60	
3773253.494	669429.919	314.734	CH4 RW			
3773251.949	669431.884	314.661	CH5 RW		0.61	
3773252.435	669432.246	314.671	CH5 LW			
3773252.162	669434.769	314.551	CH5 LW		0.57	
3773251.632	669434.976	314.57	CH5 RW			
3773248.28	669441.469	314.342	CH6 RW		0.92	
3773249.196	669441.528	314.359	CH6 LW			
3773249.697	669438.347	314.425	CH6 LW		0.96	0.01
3773248.812	669438.192	314.455	CH6 RB	0.02		
3773248.753	669438.166	314.479	CH6 RT			
3773249.007	669435.27	314.551	CH6 RW		0.83	
3773249.836	669435.232	314.512	CH6 LW			
3773250.282	669431.026	314.712	CH6 LT	0.04	0.76	0.03
3773250.177	669431.056	314.674	CH6 LB			
3773249.622	669431.076	314.67	CH6 RB	0.04		

3773249.529	669431.124	314.706	CH6 RT			
3773249.968	669426.443	314.831	CH6 RW		0.38	
3773250.332	669426.55	314.822	CH6 LW			
3773250.454	669425.568	314.872	HEAD			
3773239.173	669431.592	314.573	HEAD			
3773238.395	669432.926	314.511	CH7 LW		0.59	
3773237.947	669432.544	314.495	CH7 RW			
3773235.835	669435.956	314.391	CH7 RW		0.58	0.03
3773236.256	669436.269	314.364	CH7 LB	0.12		
3773236.312	669436.286	314.483	CH7 LT			
3773234.447	669438.009	314.383	CH7 LT	0.09	0.55	0.03
3773234.409	669437.935	314.29	CH7 LB			
3773234.111	669437.568	314.334	CH7 RW			
3773230.838	669440.924	314.288	CH7 RT	0.08	1.24	0.07
3773230.925	669440.989	314.204	CH7 RB			
3773231.656	669441.43	314.191	CH7 LB	0.02		
3773231.827	669441.676	314.215	CH7 LT			
3773228.107	669446.083	314.087	CH7 LT	0.04	1.15	0.05
3773228.057	669446.021	314.045	CH7 LB			
3773227.233	669445.383	314.036	CH7 RB	0.04		
3773227.219	669445.346	314.072	CH7 RT			
3773223.296	669450.812	313.904	CH7 RT	0.06	0.93	0.03
3773223.422	669450.881	313.846	CH7 RB			
3773224.062	669451.183	313.875	CH7 LB	0.01		
3773224.124	669451.228	313.885	CH7 LT			
3773272.688	669413.407	315.388	CHLW		1.18	
3773271.698	669412.769	315.392	CH8 RW			
3773268.677	669416.698	315.226	CH8 RW		0.87	
3773269.332	669417.277	315.226	CH8 LW			
3773267.247	669421.035	315.081	CH8 LW		1.56	
3773265.869	669420.302	315.043	CH8 RW			
3773263.167	669424.052	314.92	CH8 RW		1.33	0.02
3773264.067	669424.935	314.884	CH8 LB	0.04		
3773264.127	669424.969	314.92	CH8 LT			
3773261.511	669428.748	314.756	CH8 LW		0.98	
3773260.653	669428.435	314.759	CH8 RB	0.05		
3773260.583	669428.435	314.812	CH8 RT			
3773257.142	669432.379	314.65	CH8 RT	0.03	1.22	0.02
3773257.19	669432.427	314.623	CH8 RB			
3773257.882	669433.35	314.615	CH8 LW			
3773254.163	669437.805	314.459	CH8 LW		1.20	0.06
3773253.317	669437.044	314.431	CH8 RB	0.09		
3773253.283	669436.992	314.525	CH8 RT			
3773252.043	669438.191	314.522	CH8 RT	0.12	1.55	0.10
3773252.084	669438.332	314.399	CH8 RB			
3773253.164	669439.26	314.423	CH8 LW			
3773251.141	669442.226	314.323	CH8 LW		1.17	0.03
3773250.229	669441.624	314.292	CH8 RB	0.04		
3773250.163	669441.592	314.335	CH8 RT			
3773244.679	669448.415	314.07	CH8 RW		1.37	

3773245.709	669449.325	314.064	CH8 LW			
3773239.989	669456.794	313.764	CH8 LW		0.96	0.05
3773239.278	669456.543	313.782	CH8 RB	0.10		
3773239.108	669456.419	313.884	CH8 RT			
3773236.086	669459.929	313.67	CH8 RW		0.91	
3773236.814	669460.481	313.679	CH8 LW			
3773270.217	669426.278	314.929	HEAD			
3773270.82	669428.597	314.875	CH9 LW		0.81	
3773270.016	669428.644	314.837	CH9 RW			
3773266.691	669431.339	314.746	CH9 RT	0.07	1.17	0.04
3773266.816	669431.466	314.672	CH9 RB			
3773267.499	669432.184	314.733	CH9 LW			
3773266.117	669434.552	314.655	CH9 LT	0.06	3.26	0.21
3773265.984	669434.496	314.59	CH9 LB			
3773263.59	669432.668	314.583	CH9 RB	0.06		
3773263.505	669432.6	314.648	CH9 RT			
3773262.633	669434.946	314.574	CH9 RT	0.07	2.19	0.14
3773262.769	669435.054	314.501	CH9 RB			
3773264.361	669436.011	314.524	CH9 LB	0.05		
3773264.468	669436.14	314.575	CH9 LT			
3773263.508	669436.68	314.523	CH9 LT	0.04	0.75	0.01
3773263.388	669436.611	314.487	CH9 LB			
3773262.835	669436.343	314.449	CH9 RW			
3773261.598	669437.382	314.475	CH9 RW		1.47	0.03
3773262.751	669437.933	314.424	CH9 LB	0.04		
3773262.889	669438.08	314.463	CH9 LT			
3773261.974	669440.08	314.38	CH9 LW		1.63	
3773260.507	669439.378	314.418	CH9 RW			
3773263.579	669435.775	314.556	CH9 BAR T	0.08		
3773263.429	669436.059	314.472	CH9 BAR B			
3773264.832	669434.971	314.572	CH9 BAR B	0.04		
3773264.77	669434.873	314.61	CH9 BAR T			
3773263.786	669434.282	314.605	CH9 BAR T	0.03		
3773263.689	669434.192	314.579	CH9 BAR B			
3773264.753	669433.084	314.62	CH9 BAR B	0.05		
3773264.814	669433.145	314.667	CH9 BAR T			
3773265.604	669433.83	314.658	CH9 BAR T	0.05		
3773265.745	669433.929	314.607	CH9 BAR B			
3773266.39	669432.534	314.676	CH9 BAR			
3773284.47	669427.836	315.08	CH10 LT	0.04	0.69	0.01
3773284.393	669427.87	315.039	CH10 LB			
3773283.986	669428.321	315.023	CH10 RW			
3773284.332	669430.41	314.943	CH10 RW		1.02	
3773285.338	669430.237	314.909	CH10 LW			
3773287.307	669423.495	315.152	CH11 LW		1.29	
3773286.156	669422.909	315.152	CH11 RW			
3773283.625	669426.244	315.077	CH11 RT	0.02	1.30	0.02
3773283.709	669426.291	315.053	CH11 RB			
3773284.679	669427.008	315.058	CH11 LW			
3773281.705	669430.702	314.915	CH11 LW		1.29	0.05

3773280.676	669430.05	314.924	CH11 RB	0.08		
3773280.633	669429.988	315.003	CH11 RT			
3773276.99	669434.898	314.768	CH11 RW		1.22	0.04
3773277.859	669435.624	314.713	CH11 LB	0.06		
3773277.929	669435.67	314.773	CH11 LT			
3773276.157	669438.436	314.759	CH11 LT	0.09	1.45	0.13
3773276.089	669438.347	314.67	CH11 LB			
3773275.012	669437.765	314.655	CH11 RB	0.10		
3773274.913	669437.694	314.751	CH11 RT			
3773270.656	669443.167	314.479	CH11 RT	0.03	1.26	0.02
3773270.742	669443.248	314.446	CH11 RB			
3773271.705	669443.868	314.462	CH11 LW			
3773267.517	669449.516	314.227	CH11 LW		1.08	
3773266.5	669449.138	314.21	CH11 RW			
3773263.66	669453.135	314.046	CH11 RW		0.85	
3773264.13	669453.845	314.068	CH11 LW			
3773261.101	669457.2	313.937	CH11 LW		1.82	
3773259.653	669456.093	313.927	CH11 RW			
3773256.385	669458.846	313.836	CH11 RW		2.39	
3773258.187	669460.419	313.827	CH11 LW			
3773255.795	669464.179	313.663	CH11 LW		1.85	
3773254.027	669463.641	313.68	CH11 RW			
3773251.777	669468.107	313.488	CH11 RW		1.67	
3773252.886	669469.359	313.503	CH11 LW			
3773251.256	669470.745	313.447	CH11 LW		1.31	
3773250.124	669470.083	313.414	CH11 RW			
3773300.064	669432.094	315.044	CH1RT	0.04	0.66	0.01
3773300.168	669432.166	315.008	CH12 RB			
3773300.602	669432.476	315.013	CH12 LW			
3773298.32	669435.976	314.889	CH12 LW		0.88	
3773297.628	669435.429	314.906	CH12 RW			
3773296.028	669438.379	314.779	CH12 LW		0.72	
3773295.381	669438.06	314.775	CH12 RW			
3773291.998	669442.102	314.688	CH12 RT	0.07	1.05	0.04
3773292.116	669442.153	314.615	CH12 RB			
3773292.808	669442.763	314.616	CH12 LW			
3773289.911	669447.189	314.528	CH12 LT	0.09	1.23	0.05
3773289.848	669447.139	314.442	CH12 LB			
3773288.784	669446.698	314.467	CH12 RW			
3773286.47	669450.185	314.346	CH12 RW		0.94	
3773287.047	669450.745	314.28	CH12 LB	0.08		
3773287.164	669450.822	314.362	CH12 LT			
3773283.806	669455.11	314.16	CH12 LW		1.07	
3773282.923	669454.511	314.153	CH12 RW			
3773279.832	669458.285	313.97	CH12 RW		0.41	
3773280.14	669458.55	313.969	CH12 LW			
3773279.15	669460.775	313.934	CH12 LW		0.89	0.03
3773278.447	669460.43	313.916	CH12 RB	0.06		
3773278.379	669460.328	313.976	CH12 RT			
3773276.91	669462.74	313.879	CH12 RT	0.05	0.80	0.03

3773277	669462.726	313.834	CH12 RB			
3773277.479	669463.219	313.831	CH12 LB	0.03		
3773277.551	669463.225	313.859	CH12 LT			
3773274.798	669467.057	313.722	CH12 LW		1.02	0.04
3773273.951	669466.668	313.735	CH12 RB	0.08		
3773273.888	669466.59	313.818	CH12 RT			
3773271.976	669469.622	313.68	CH12 RT	0.04	0.95	0.04
3773272.025	669469.662	313.645	CH12 RB			
3773272.522	669470.296	313.631	CH12 LB	0.05		
3773272.589	669470.351	313.677	CH12 LT			
3773270.123	669472.677	313.536	CH12 LW		1.04	
3773269.272	669472.079	313.519	CH12 RW			
3773264.551	669480.541	313.274	ROCK 1			
3773263.674	669479.13	313.278	ROCK 3			
3773286.516	669448.999	314.423	ROCK 3			
3773287.529	669447.729	314.653	ROCK 2			
3773299.638	669431.91	315.305	ROCK 2			
3773300.794	669432.934	315.074	ROCK 1			
3773296.801	669438.153	314.874	ROCK 1			
3773297.323	669438.732	314.892	ROCK 1			
3773296.658	669439.324	314.842	ROCK 1			
3773296.071	669439.062	314.811	ROCK 1			
3773292.345	669444.187	314.625	ROCK 1			
3773291.715	669445.025	314.699	ROCK 1			
3773292.458	669445.618	314.676	ROCK 1			
3773292.847	669444.722	314.648	ROCK 1			
3773287.549	669423.255	315.232	ROCK 2			
3773286.134	669422.576	315.291	ROCK 4			
3773278.025	669433.096	314.996	ROCK 4			
3773277.325	669433.963	314.91	ROCK 4			
3773276.656	669433.291	314.951	ROCK 4			
3773277.178	669432.551	314.956	ROCK 4			
3773273.566	669439.14	314.682	ROCK 4			
3773272.919	669439.983	314.652	ROCK 4			
3773275.692	669439.009	314.697	ROCK 2			
3773274.91	669440.178	314.746	ROCK 3			
3773251.118	669471.176	313.515	ROCK 3			
3773249.732	669470.266	313.587	ROCK 4			
3773237.123	669460.855	313.755	ROCK 5			
3773235.629	669459.674	313.799	ROCK 6			
3773224.658	669451.762	314.039	ROCK 7			
3773223.069	669450.671	313.973	ROCK 8			
3773259.026	669403.448	315.708	ROCK 8			
3773260.524	669404.519	315.813	ROCK 7			
3773271.675	669412.243	315.585	ROCK 6			
3773273.225	669413.368	315.565	ROCK 5			

Walkway Plot 6

Northing	Easting	Elevation	Feature code	Depth (m)	Width (m)	Cross (m^2)
8763.975	-3509231.97	292.51	CH1 LT	0.00	0.65	

8763.887	-3509232.16	292.507	CH1 LB			
8764.024	-3509232.62	292.541	CH1 RT			
8772.649	-3509235.84	292.808	CH1 RT	0.09	1.16	0.08
8772.628	-3509235.49	292.715	CH1 RB			
8772.635	-3509235.05	292.709	CH1 LB	0.05		
8772.522	-3509234.69	292.762	CH1 LT			
8782.809	-3509242.26	293.108	CH1 LT	0.12	2.23	0.25
8782.59	-3509242.52	292.987	CH1 LB			
8780.822	-3509242.32	293.005	CH1 RB	0.10		
8780.588	-3509242.47	293.106	CH1 RT			
8783.386	-3509242.96	293.126	CH1 LT	0.09		
8783.116	-3509243.13	293.032	CH1 LB			
8784.495	-3509241.52	293.185	HEAD			
8788.191	-3509244.75	293.384	HEAD			
8785.875	-3509245.15	293.283	CH1 RT	0.13	0.86	0.10
8785.952	-3509244.8	293.158	CH1 RB			
8786.143	-3509244.59	293.175	CH1 LB	0.11		
8786.192	-3509244.34	293.286	CH1 LT			
8800.098	-3509253.36	293.742	CH1 RT	0.04	2.66	0.13
8800.35	-3509253.26	293.698	CH1 RB			
8802.462	-3509253.3	293.682	CH1 LB	0.06		
8802.741	-3509253.1	293.739	CH1 LT			
8800.943	-3509247.34	293.575	CH1 LT	0.04	1.38	0.09
8800.697	-3509247.45	293.539	CH1 LB			
8799.988	-3509247.57	293.582	CH1 RB	0.09		
8799.577	-3509247.51	293.675	CH1 RT			
8803.651	-3509251.59	293.73	HEAD			
8807.476	-3509250.69	293.758	HEAD			
8805.006	-3509248.48	293.718	CH2 LT	0.10	1.22	0.06
8804.815	-3509248.71	293.614	CH2 LB			
8804.131	-3509249.33	293.62	CH2 RW			
8800.438	-3509242.62	293.488	CH2 LT	0.05	1.27	0.09
8800.068	-3509242.77	293.439	CH2 LB			
8799.412	-3509243.04	293.4	CH2 RB	0.10		
8799.24	-3509243.04	293.497	CH2 RT			
8796.014	-3509237.56	293.295	CH2 RT	0.04	1.65	0.07
8796.158	-3509237.46	293.254	CH2 RB			
8797.125	-3509236.95	293.306	CH2 LB	0.05		
8797.407	-3509236.68	293.355	CH2 LT			
8798.116	-3509246.59	293.572	HEAD			
8796.246	-3509242.45	293.474	CH2 RT	0.05	0.75	0.04
8796.624	-3509242.45	293.423	CH2 RB			
8796.876	-3509242.51	293.445	CH2 LB	0.06		
8796.989	-3509242.54	293.51	CH2 LT			
8795.071	-3509241.42	293.383	HEAD			
8794.119	-3509238.29	293.304	HEAD			
8794.91	-3509236.92	293.292	CH2 RT	0.04	2.20	0.08
8795.065	-3509236.88	293.254	CH2 RB			
8796.659	-3509236.14	293.292	CH2 LB	0.04		
8796.903	-3509235.99	293.329	CH2 LT			

8792.946	-3509228.42	293.086	CH2 LT	0.04	0.75	0.03
8792.699	-3509228.37	293.048	CH2 LB			
8792.387	-3509228.34	293.058	CH2 RB	0.03		
8792.193	-3509228.37	293.089	CH2 RT			
8791.76	-3509224.22	293.013	CH2 RT	0.08	0.88	0.08
8791.976	-3509224.03	292.936	CH2 RB			
8792.199	-3509223.76	292.933	CH2 LB	0.11		
8792.481	-3509223.72	293.038	CH2 LT			
8791.336	-3509227.72	293.055	HEAD			
8788.801	-3509223.94	292.987	CH2 RT	0.06	0.85	0.04
8789.034	-3509223.74	292.925	CH2 RB			
8789.366	-3509223.62	292.928	CH2 LB	0.02		
8789.585	-3509223.6	292.953	CH2 LT			
8788.115	-3509220.33	292.862	CH2 LT	0.03	2.47	0.16
8787.99	-3509220.38	292.837	CH2 LB			
8786.013	-3509219.65	292.826	CH2 RB	0.10		
8785.715	-3509219.76	292.927	CH2 RT			
8788.111	-3509219.95	292.858	CH2 RT	0.04	1.17	0.07
8788.323	-3509219.85	292.821	CH2 RB			
8788.911	-3509219.43	292.825	CH2 LB	0.08		
8789.001	-3509219.19	292.905	CH2 LT			
8786.185	-3509213.4	292.751	CH2 LT	0.13	1.88	0.24
8785.946	-3509213.55	292.617	CH2 LB			
8785.213	-3509213.93	292.682	CH2 RB	0.12		
8784.615	-3509214.44	292.799	CH2 RT			
8783.443	-3509212.52	292.766	HEAD			
8783.537	-3509206.89	292.609	CH2 RT	0.15	2.39	0.30
8784.052	-3509206.64	292.459	CH2 RB			
8785.537	-3509206.81	292.462	CH2 LB	0.10		
8785.924	-3509206.78	292.56	CH2 LT			
8782.938	-3509197.62	292.357	CH2 LT	0.11	3.04	0.28
8782.685	-3509197.94	292.249	CH2 LB			
8782	-3509200.26	292.345	CH2 RB	0.08		
8781.745	-3509200.42	292.422	CH2 RT			
8793.631	-3509224.25	293.034	CH3 LT	0.03	0.90	0.04
8793.419	-3509224.41	293.003	CH3 LB			
8793.361	-3509224.68	293.005	CH3 RB	0.06		
8793.195	-3509225.04	293.07	CH3 RT			
8797.241	-3509230.36	293.206	CH3 RT	0.02	1.23	0.06
8797.498	-3509230.27	293.19	CH3 RB			
8798.04	-3509230.09	293.172	CH3 LB	0.09		
8798.402	-3509229.96	293.258	CH3 LT			
8801.601	-3509236.35	293.409	CH3 LT	0.03	1.70	0.12
8801.233	-3509236.65	293.383	CH3 LB			
8800.921	-3509237.5	293.355	CH3 RB	0.12		
8800.697	-3509237.79	293.473	CH3 RT			
8804.366	-3509241.11	293.557	CH3 RT	0.08	1.57	0.15
8804.744	-3509241	293.475	CH3 RB			
8805.501	-3509240.72	293.518	CH3 LB	0.10		
8805.861	-3509240.61	293.621	CH3 LT			

8808.449	-3509243.07	293.679	HEAD			
8808.176	-3509244.14	293.705	CH3 LT	0.11	0.90	0.07
8807.966	-3509244.48	293.597	CH3 LB			
8807.706	-3509244.63	293.606	CH3 RB	0.04		
8807.628	-3509244.86	293.647	CH3 RT			
8813.209	-3509247.62	293.817	CH3 RT	0.08	1.45	0.10
8813.381	-3509247.34	293.74	CH3 RB			
8813.837	-3509246.82	293.789	CH3 LB	0.06		
8813.989	-3509246.4	293.844	CH3 LT			
8819.07	-3509248.53	294.02	CH3 LT	0.11	1.16	0.10
8818.957	-3509248.81	293.908	CH3 LB			
8818.871	-3509249.38	293.93	CH3 RB	0.05		
8818.763	-3509249.64	293.983	CH3 RT			
8820.27	-3509250.25	294.024	HEAD			
8818.108	-3509252.73	294.048	HEAD			
8815.546	-3509251.34	294.027	CH4 LT	0.11	1.01	0.11
8815.502	-3509251.66	293.913	CH4 LB			
8815.55	-3509252.14	293.937	CH4 RB	0.10		
8815.597	-3509252.35	294.038	CH4 RT			
8810.733	-3509249.22	293.864	HEAD			
8808.346	-3509248.8	293.835	CH4 RT	0.08	0.83	0.07
8808.453	-3509248.63	293.756	CH4 RB			
8808.626	-3509248.17	293.759	CH4 LB	0.09		
8808.721	-3509248.06	293.845	CH4 LT			
8804.468	-3509246.02	293.673	CH4 LT	0.10	1.20	0.12
8804.437	-3509246.32	293.575	CH4 LB			
8804.261	-3509246.9	293.589	CH4 RB	0.09		
8804.159	-3509247.18	293.683	CH4 RT			
8804.43	-3509238.56	293.528	CH5 RT	0.09	1.61	0.15
8804.255	-3509237.72	293.442	CH5 RB			
8804.207	-3509237.47	293.43	CH5 LB	0.10		
8804.109	-3509236.98	293.531	CH5 LT			
8811.937	-3509239.48	293.782	CH5 LT	0.11	1.49	0.16
8811.818	-3509239.7	293.671	CH5 LB			
8811.196	-3509240.5	293.657	CH5 RB	0.11		
8811.054	-3509240.67	293.764	CH5 RT			
8812.941	-3509242.18	293.775	HEAD			
8818.944	-3509243.74	293.906	CH5 LT	0.11	1.05	0.11
8819.138	-3509243.41	293.8	CH5 LB			
8819.249	-3509243.13	293.815	CH5 RB	0.10		
8819.487	-3509242.84	293.912	CH5 RT			
8825.994	-3509245.61	294.05	CH5 RT	0.03	1.54	0.08
8825.849	-3509245.83	294.018	CH5 RB			
8825.987	-3509246.55	294.015	CH5 LB	0.07		
8825.614	-3509247.1	294.088	CH5 RT			
8836.694	-3509250.68	294.271	HEAD			
8833.913	-3509249.57	294.197	CH5 RT		0.69	0.01
8833.994	-3509249.45	294.198	CH5 RB			
8834.084	-3509249.26	294.21	CH5 LB	0.04		
8834.307	-3509249	294.248	CH5 LT			

8833.679	-3509249.73	294.131	CH5 RB	0.20		
8833.109	-3509250.19	294.335	CH5 RT			
8834.28	-3509254.55	294.346	CH5 RT	0.04	1.13	0.06
8834.481	-3509254.43	294.31	CH5 RB			
8834.869	-3509254.23	294.306	CH5 LB	0.07		
8835.321	-3509254.1	294.378	CH5 LT			
8828.441	-3509243.85	294.051	HEAD			
8826.981	-3509242.19	294.029	CH6 LT	0.10	0.87	0.06
8826.736	-3509242.36	293.925	CH6 LB			
8826.642	-3509242.52	293.988	CH6 RB	0.04		
8826.302	-3509242.74	294.027	CH6 RT			
8819.775	-3509235.23	293.768	HEAD			
8816.927	-3509233.19	293.723	CH6 LT	0.04	0.60	0.03
8816.802	-3509233.46	293.683	CH6 LB			
8816.704	-3509233.63	293.681	CH6 RB	0.07		
8816.662	-3509233.72	293.75	CH6 RT			
8809.667	-3509230.35	293.585	CH6 RT	0.07	1.27	0.08
8809.949	-3509230.25	293.515	CH6 RB			
8810.458	-3509229.75	293.52	CH6 LB	0.06		
8810.78	-3509229.74	293.579	CH6 LT			
8820.36	-3509233.52	293.766	HEAD			
8819.204	-3509231.76	293.709	CH7 RT	0.05	0.52	
8819.337	-3509231.55	293.664	CH7 RB			
8819.35	-3509231.46	293.672	CH7 LB	0.07		
8819.347	-3509231.25	293.741	CH7 LT			
8816.538	-3509229.81	293.647	CH7 LT	0.04	0.81	0.05
8816.417	-3509230.07	293.605	CH7 LB			
8816.311	-3509230.3	293.592	CH7 RB	0.08		
8816.245	-3509230.56	293.672	CH7 RT			
8809.289	-3509226.86	293.457	CH7 RT	0.07	0.89	0.06
8809.56	-3509226.67	293.384	CH7 RB			
8809.878	-3509226.46	293.415	CH7 LB	0.05		
8809.973	-3509226.29	293.469	CH7 LT			
8806.994	-3509224.08	293.325	CH7 RW		1.36	
8807.497	-3509223.82	293.345	CH7 W			
8808.201	-3509223.45	293.328	CH7 LW			
8806.324	-3509220.95	293.249	HEAD			
8805.311	-3509215.13	293.155	CH8 LT	0.07	0.97	0.07
8804.947	-3509215.29	293.087	CH8 LB			
8804.748	-3509215.47	293.101	CH8 RB	0.07		
8804.462	-3509215.6	293.173	CH8 RT			
8801.588	-3509213.15	292.997	CH8 RT	0.06	0.96	0.08
8801.573	-3509212.93	292.939	CH8 RB			
8801.534	-3509212.74	292.933	CH8 LB	0.12		
8801.429	-3509212.21	293.049	CH8 LT			
8803.691	-3509217.68	293.215	CH8 LT	0.11	1.12	0.10
8803.328	-3509217.77	293.1	CH8 LB			
8802.98	-3509217.85	293.122	CH8 RB	0.06		
8802.617	-3509217.99	293.183	CH8 RT			
8804.812	-3509221.79	293.262	HEAD			

8795.196	-3509212.81	292.902	CH8 RT	0.09	1.57	0.14
8795.194	-3509212.45	292.814	CH8 RB			
8795.409	-3509211.97	292.808	CH8 LB	0.09		
8795.838	-3509211.38	292.9	CH8 LT			
8789.403	-3509204.4	292.694	CH8 LT	0.17	1.57	0.20
8789.033	-3509204.75	292.523	CH8 LB			
8788.313	-3509205.14	292.543	CH8 RB	0.08		
8788.177	-3509205.38	292.623	CH8 RT			
8833.384	-3509240.12	294.035	HEAD			
8830.805	-3509239.01	293.972	CH9 RT	0.07	0.56	0.05
8830.912	-3509238.87	293.903	CH9 RB			
8830.951	-3509238.83	293.906	CH9 LB	0.10		
8831.13	-3509238.55	294.004	CH9 LT			
8827.669	-3509236.28	293.914	CH9 LT	0.08	0.67	0.06
8827.503	-3509236.53	293.829	CH9 LB			
8827.453	-3509236.61	293.832	CH9 RB	0.09		
8827.287	-3509236.83	293.923	CH9 RT			
8824.895	-3509232.39	293.783	CH9 LW		1.19	
8824.375	-3509232.57	293.744	CH9 W			
8823.706	-3509232.37	293.766	CH9 RW			
8820.504	-3509221.69	293.49	HEAD			
8819.623	-3509217.75	293.43	CH10 LT	0.17	0.74	0.11
8819.335	-3509217.87	293.26	CH10 LB			
8819.145	-3509217.92	293.286	CH10 RB	0.13		
8818.927	-3509218	293.411	CH10 RT			
8818.85	-3509212.42	293.313	CH10 RT	0.14	0.96	0.14
8819.111	-3509212.7	293.17	CH10 RB			
8819.371	-3509212.93	293.166	CH10 LB	0.14		
8819.294	-3509213.27	293.31	CH10 LT			
8841.102	-3509241.32	294.208	CH11 RT	0.14		
8841.394	-3509241.34	294.066	CH11 RB			
8842.271	-3509238.43	294.091	CH11 RT	0.18	1.30	0.25
8842.624	-3509238.46	293.912	CH11 RB			
8843.18	-3509238.18	293.885	CH11 LB	0.21		
8843.532	-3509238.1	294.096	CH11 LT			
8840.874	-3509232.64	293.961	CH11 LT	0.18	1.42	0.22
8840.545	-3509233.07	293.785	CH11 LB			
8840.123	-3509233.37	293.797	CH11 RB	0.13		
8839.766	-3509233.52	293.927	CH11 RT			
8836.701	-3509227.44	293.754	CH11 RT	0.14	1.33	0.21
8837.017	-3509227.27	293.614	CH11 RB			
8837.257	-3509227.05	293.582	CH11 LB	0.18		
8837.943	-3509226.96	293.757	CH11 LT			
8838.906	-3509225.4	293.778	HEAD			
8841.577	-3509230.9	293.909	CH11 LT	0.11	1.44	0.16
8841.35	-3509231.46	293.8	CH11 LB			
8841.421	-3509231.96	293.801	CH11 RB	0.11		
8841.262	-3509232.31	293.908	CH11 RT			
8845.38	-3509234.07	294.006	CH11 RT	0.11	1.40	0.18
8845.659	-3509233.79	293.899	CH11 RB			

8845.564	-3509233.25	293.907	CH11 LB	0.15		
8845.88	-3509232.76	294.054	CH11 LT			
8836.642	-3509229.36	293.692	HEAD			
8833.557	-3509228.72	293.738	HEAD			
8831.945	-3509228.1	293.743	HEAD			
8833.112	-3509226.89	293.681	CH11 RT	0.07	1.22	0.09
8833.324	-3509226.74	293.611	CH11 RB			
8833.701	-3509226.46	293.588	CH11 LB	0.07		
8834.099	-3509226.17	293.663	CH11 LT			
8835.144	-3509225.28	293.646	CH11 RT	0.14	1.34	0.25
8835.493	-3509224.94	293.503	CH11 RB			
8835.702	-3509224.48	293.509	CH11 LB	0.23		
8836.019	-3509224.27	293.735	CH11 LT			
8831.7	-3509220.13	293.552	CH11 LT	0.12	2.54	0.33
8831.411	-3509220.43	293.434	CH11 LB			
8829.804	-3509221.33	293.419	CH11 RB	0.14		
8829.49	-3509221.39	293.558	CH11 RT			
8835.158	-3509220.96	293.664	HEAD			
8822.462	-3509213.54	293.312	CH11 RT	0.12	2.59	0.32
8822.634	-3509213.26	293.191	CH11 RB			
8824.077	-3509212.22	293.143	CH11 LB	0.12		
8824.57	-3509212.04	293.266	CH11 LT			
8828.37	-3509213.23	293.377	HEAD			
8832.531	-3509215.76	293.515	HEAD			
8831.258	-3509215.18	293.477	CH11 RW		0.54	
8831.541	-3509214.72	293.479	CH11 LW			
8819.682	-3509206.54	293.101	CH11 LT	0.15	3.12	0.44
8819.312	-3509207.07	292.949	CH11 LB			
8817.601	-3509208.34	293.034	CH11 RB	0.13		
8817.367	-3509208.64	293.164	CH11 RT			
8811.549	-3509200.63	292.891	CH11 RT	0.08	3.35	0.25
8811.792	-3509200.39	292.81	CH11 RB			
8812.823	-3509197.89	292.807	CH11 LB	0.07		
8813.051	-3509197.64	292.874	CH11 LT			
8813.387	-3509194.15	292.825	HEAD			
8806.442	-3509191.82	292.63	CH11 LT	0.02	2.38	0.10
8806.19	-3509192.01	292.608	CH11 LB			
8804.574	-3509192.57	292.597	CH11 RB	0.06		
8804.296	-3509192.86	292.661	CH11 RT			
8797.484	-3509188.62	292.495	CH11 RT	0.09	1.98	0.18
8797.582	-3509188.33	292.402	CH11 RB			
8797.797	-3509187.13	292.433	CH11 LB	0.08		
8798.055	-3509186.72	292.518	CH11 LT			
8791.472	-3509183.77	292.311	CH11 LT	0.07	1.99	0.15
8790.892	-3509184.34	292.238	CH11 LB			
8790.307	-3509184.95	292.233	CH11 RB	0.07		
8790.111	-3509185.23	292.306	CH11 RT			
8794.177	-3509189.67	292.405	CH12 RT	0.32	0.62	0.18
8794.421	-3509189.67	292.089	CH12 RB			
8794.497	-3509189.76	292.128	CH12 LB	0.27		

8794.786	-3509189.77	292.401	CH12 LT			
8799.825	-3509195.53	292.628	CH12 LT	0.09	1.53	0.13
8799.573	-3509195.77	292.54	CH12 LB			
8799.201	-3509196.22	292.538	CH12 RB	0.08		
8798.794	-3509196.67	292.622	CH12 RT			
8805.391	-3509189.64	292.606	HEAD			
8801.9	-3509200.94	292.825	CH12 LT	0.07	1.22	0.09
8801.542	-3509201.36	292.751	CH12 LB			
8801.474	-3509201.5	292.752	CH12 RB	0.07		
8801.074	-3509201.84	292.818	CH12 RT			
8803.584	-3509203.97	292.864	HEAD			
8804.069	-3509187.87	292.567	CH13 RT	0.02	0.89	0.04
8804.34	-3509187.75	292.549	CH13 RB			
8804.588	-3509187.56	292.54	CH13 LB	0.06		
8804.841	-3509187.42	292.602	CH13 LT			
8800.395	-3509180.93	292.451	CH13 LT	0.03	0.66	0.03
8800.304	-3509181.08	292.421	CH13 LB			
8800.188	-3509181.23	292.414	CH13 RB	0.06		
8799.929	-3509181.39	292.472	CH13 RT			
8797.122	-3509179.42	292.37	CH13 LT	0.04	1.62	0.06
8796.977	-3509179.61	292.329	CH13 LB			
8796.142	-3509180.2	292.321	CH13 RB	0.03		
8795.907	-3509180.5	292.355	CH13 RT			
8793.889	-3509177.83	292.259	CH13 RT	0.03	1.40	0.05
8794.162	-3509177.53	292.23	CH13 RB			
8794.642	-3509177.15	292.252	CH13 LB	0.04		
8795.036	-3509177.02	292.296	CH13 LT			
8797.802	-3509182.25	292.385	CH13 LT	0.04	0.88	0.06
8797.515	-3509182.54	292.348	CH13 LB			
8797.346	-3509182.68	292.338	CH13 RB	0.09		
8797.163	-3509182.85	292.427	CH13 RT			
8799.153	-3509185.43	292.445	HEAD			
8823.091	-3509199.8	293.095	HEAD			
8821.615	-3509199.33	293.093	CH14 RT	0.05	0.78	0.04
8821.723	-3509199.1	293.045	CH14 RB			
8821.745	-3509198.87	293.038	CH14 LB	0.05		
8821.842	-3509198.58	293.085	CH14 LT			
8855.444	-3509217.38	293.943	CH15 RT	0.12	1.87	0.15
8855.638	-3509217.23	293.82	CH15 RB			
8857.159	-3509216.62	293.858	CH15 LT	0.03		
8856.586	-3509216.72	293.826	CH15 LB			
8855.989	-3509207.62	293.804	CH15 LB			
8855.721	-3509207.64	293.675	CH15 LB			
8854.504	-3509207.22	293.638	CH15 RB	0.14		
8854.037	-3509207.11	293.777	CH15 RT			
8860.63	-3509209.96	293.937	HEAD			
8857.285	-3509207.12	293.844	CH15 RT	0.08	1.12	0.10
8857.509	-3509206.98	293.766	CH15 RB			
8857.628	-3509206.48	293.746	CH15 LB	0.11		
8857.745	-3509206.1	293.851	CH15 LT			

8849.904	-3509202.28	293.607	CH15 LT	0.08	1.91	0.21
8849.786	-3509202.53	293.529	CH15 LB			
8849.063	-3509203.58	293.491	CH15 RB	0.14		
8848.916	-3509203.92	293.632	CH15 RT			
8840.829	-3509200.44	293.43	CH15 RT	0.13	3.70	0.35
8841.049	-3509200.18	293.297	CH15 RB			
8842.136	-3509197.22	293.34	CH15 LB	0.06		
8842.24	-3509197.03	293.398	CH15 LT			
8837.211	-3509191.97	293.264	CH15 LT	0.16	2.63	0.32
8836.765	-3509192.24	293.1	CH15 LB			
8834.963	-3509191.82	293.161	CH15 RB	0.08		
8834.577	-3509191.98	293.241	CH15 RT			
8833.385	-3509194.06	293.222	HEAD			
8828.277	-3509191.32	293.098	CH16 LT	0.03	0.90	0.02
8828.227	-3509191.64	293.073	CH16 LB			
8828.176	-3509191.83	293.077	CH16 RB	0.03		
8827.996	-3509192.18	293.107	CH16 RT			
8821.967	-3509189.6	293.007	CH16 RT	0.07	0.96	0.06
8822.049	-3509189.31	292.938	CH16 RB			
8822.109	-3509188.89	292.933	CH16 LB	0.05		
8822.148	-3509188.66	292.983	CH16 LT			
8817.866	-3509186.74	292.848	CH16 LW		0.82	
8817.688	-3509187.1	292.824	CH16 W			
8817.511	-3509187.48	292.843	CH16 RW			

APPENDIX B: Base station coordinates

Plot Name	Northing	Easting	Elevation	
Control 1	3775866.249	670480.621	346.887	BASE C1
Control 2	3773716.792	668512.953	415.554	BASE 6
Control 3	3774732	669334	388	B
Control 4	3775623.759	670173.34	339.943	C4 BASE
Control 5	3776357.827	673027.319	306.071	BASE 9
Control 6	3772741.046	672610.948	314.138	BASE 8
Walkway 1	3773639.983	668664.202	303.069	CHAPEL BASE
Walkway 2	3773639.983	668664.201	303.069	CHAPEL BASE
Walkway 3	3775221.213	669851.681	391.38	BASE 7
Walkway 4	3775221.213	669851.681	391.38	BASE 7
Walkway 5	3773636.666	668700.884	342.436	CHAPEL BASE
Walkway 6	19845.679	-3554264.8	318.81	CHAPEL BASE
Road 1	3775866.248	670480.621	346.886	BASE 5
Road 2	3775866.248	670480.622	346.886	BASE 5
Road 3	3775221.213	669851.681	391.379	BASE 7
Road 4	3775221.213	669851.681	391.379	BASE 7
Road 5	3773686.549	668657.134	419.853	CHAPEL BASE
Road 6	3773686.549	668657.134	419.853	CHAPEL BASE

Note: All base stations are not tied into real coordinates.
Base locations are marked in the field by 0.75" rebar.
Walkway 6 is not in same coordinates as other plots. It is in Israeli coordinates for reasons unknown to data collector.

APPENDIX C: Grain size data

Iron Mountain Transects

IMV-1

Grain Size (micrometers)	Weight (grams)	Percent of Total Weight
4000	367	11%
2000	770	23%
1410	553	17%
1000	613	18%
710	399	12%
500	290	9%
350	175	5%
250	96	3%
177	36	1%
< 177	44	1%

IMV-2

Grain Size (micrometers)	Weight (grams)	Percent of Total Weight
4000	906	18%
2000	1314	26%
1410	839	17%
1000	769	15%
710	452	9%
500	282	6%
350	204	4%
250	102	2%
177	41	1%
< 177	58	1%

IMV-3

Grain Size (micrometers)	Weight (grams)	Percent of Total Weight
4000	1229	33%
2000	1080	29%
1410	444	12%
1000	381	10%
710	226	6%
500	124	3%
350	124	3%
250	44	1%
177	16	0%
< 177	32	1%

IMT-0

Grain Size (micrometers)	Weight (grams)	Percent of Total Weight
4000	932	14%
2000	918	14%
1410	573	9%
1000	656	10%
710	515	8%
500	489	7%
350	440	7%
250	331	5%
177	217	3%
< 177	1582	24%

IMT-0FAN

Grain Size (micrometers)	Weight (grams)	Percent of Total Weight
4000	443	36%
2000	131	11%
1410	72	6%
1000	77	6%
710	60	5%
500	56	5%
350	47	4%
250	41	3%
177	8	1%
< 177	290	24%

IMT-1

Grain Size (micrometers)	Weight (grams)	Percent of Total Weight
4000	364	11%
2000	485	14%
1410	307	9%
1000	322	10%
710	248	7%
500	264	8%
350	238	7%
250	198	6%
177	128	4%
< 177	808	24%

IMT-1CRIT

Grain Size (micrometers)	Weight (grams)	Percent of Total Weight
4000	194	6%
2000	425	13%
1410	359	11%
1000	436	14%
710	343	11%
500	318	10%
350	264	8%
250	195	6%
177	115	4%
< 177	533	17%

IMT-1TERR

Grain Size (micrometers)	Weight (grams)	Percent of Total Weight
4000	347	11%
2000	415	13%
1410	227	7%
1000	268	9%
710	232	7%
500	247	8%
350	234	7%
250	193	6%
177	125	4%
< 177	837	27%

IMT-1CHAN

Grain Size (micrometers)	Weight (grams)	Percent of Total Weight
4000	368	11%
2000	597	17%
1410	404	12%
1000	458	13%
710	332	10%
500	313	9%
350	269	8%
250	195	6%
177	111	3%
< 177	376	11%

IMT-2

Grain Size (micrometers)	Weight (grams)	Percent of Total Weight
4000	509	9%
2000	803	14%
1410	506	9%
1000	587	10%
710	482	8%
500	500	9%
350	469	8%
250	389	7%
177	246	4%
< 177	1277	22%

IMT-3

Grain Size (micrometers)	Weight (grams)	Percent of Total Weight
4000	1142	14%
2000	1135	14%
1410	662	8%
1000	758	10%
710	600	8%
500	651	8%
350	608	8%
250	470	6%
177	308	4%
< 177	1644	21%

IMT-4

Grain Size (micrometers)	Weight (grams)	Percent of Total Weight
4000	919	12%
2000	1008	13%
1410	522	7%
1000	607	8%
710	512	7%
500	551	7%
350	564	8%
250	484	6%
177	419	6%
< 177	1903	25%

IMT-4CRIT

Grain Size (micrometers)	Weight (grams)	Percent of Total Weight
4000	486	7%
2000	757	11%
1410	680	10%
1000	904	13%
710	743	10%
500	735	10%
350	739	10%
250	495	7%
177	351	5%
< 177	1252	18%

IMT-4TERR

Grain Size (micrometers)	Weight (grams)	Percent of Total Weight
4000	1162	16%
2000	883	12%
1410	390	5%
1000	447	6%
710	371	5%
500	431	6%
350	488	7%
250	482	7%
177	400	6%
< 177	2188	30%

IMT-4CHAN

Grain Size (micrometers)	Weight (grams)	Percent of Total Weight
4000	193	3%
2000	773	12%
1410	590	9%
1000	816	12%
710	785	12%
500	792	12%
350	868	13%
250	647	10%
177	296	4%
< 177	834	13%

Granite Mountain Transects

GMV-1

Grain Size (micrometers)	Weight (grams)	Percent of Total Weight
4000	495	15%
2000	827	26%
1410	444	14%
1000	455	14%
710	281	9%
500	236	7%
350	180	6%
250	121	4%
177	56	2%
< 177	132	4%

GMV-2

Grain Size (micrometers)	Weight (grams)	Percent of Total Weight
4000	1080	36%
2000	655	22%
1410	359	12%
1000	363	12%
710	227	8%
500	160	5%
350	85	3%
250	37	1%
177	13	0%
< 177	29	1%

GMV-3

Grain Size (micrometers)	Weight (grams)	Percent of Total Weight
4000	555	21%
2000	634	24%
1410	305	11%
1000	322	12%
710	216	8%
500	176	7%
350	148	6%
250	112	4%
177	59	2%
< 177	143	5%

GMT-0A

Grain Size (micrometers)	Weight (grams)	Percent of Total Weight
4000	489	7%
2000	923	13%
1410	624	9%
1000	764	11%
710	580	8%
500	549	8%
350	470	7%
250	365	5%
177	213	3%
< 177	1936	28%

GMT-0B

Grain Size (micrometers)	Weight (grams)	Percent of Total Weight
4000	719	10%
2000	980	14%
1410	725	11%
1000	809	12%
710	593	9%
500	587	9%
350	482	7%
250	373	5%
177	220	3%
< 177	1401	20%

GMT-1

Grain Size (micrometers)	Weight (grams)	Percent of Total Weight
4000	875	12%
2000	1061	14%
1410	650	9%
1000	779	11%
710	588	8%
500	538	7%
350	519	7%
250	310	4%
177	226	3%
< 177	1834	25%

GMT-2

Grain Size (micrometers)	Weight (grams)	Percent of Total Weight
4000	732	11%
2000	1057	16%
1410	517	8%
1000	615	9%
710	552	9%
500	537	8%
350	514	8%
250	212	3%
177	219	3%
< 177	1525	24%

GMT-3

Grain Size (micrometers)	Weight (grams)	Percent of Total Weight
4000	302	8%
2000	463	13%
1410	300	8%
1000	342	10%
710	274	8%
500	295	8%
350	264	7%
250	211	6%
177	130	4%
< 177	998	28%

GMT-4

Grain Size (micrometers)	Weight (grams)	Percent of Total Weight
4000	280	8%
2000	449	13%
1410	278	8%
1000	333	9%
710	267	8%
500	286	8%
350	270	8%
250	232	7%
177	140	4%
< 177	1022	29%

Soil Pit 1

PIT1 0-10

Grain Size (micrometers)	Weight (grams)	Percent of Total Weight
4000	531	15%
2000	553	15%
1410	269	7%
1000	405	11%
710	413	11%
500	455	13%
350	373	10%
250	204	6%
177	217	6%
< 177	117	3%
<75	92	3%

PIT1 10-20

Grain Size (micrometers)	Weight (grams)	Percent of Total Weight
4000	416	12%
2000	1394	39%
1410	333	9%
1000	456	13%
710	276	8%
500	195	6%
350	108	3%
250	32	1%
177	97	3%
< 177	113	3%
<75	120	3%

PIT1 20-30

Grain Size (micrometers)	Weight (grams)	Percent of Total Weight
4000	327	9%
2000	535	15%
1410	336	10%
1000	408	12%
710	321	9%
500	330	9%
350	277	8%
250	198	6%
177	163	5%
< 177	413	12%
<75	170	5%

PIT1 30-40

Grain Size (micrometers)	Weight (grams)	Percent of Total Weight
4000	258	7%
2000	628	16%
1410	417	11%
1000	534	14%
710	438	11%
500	444	11%
350	569	15%
250	139	4%
177	146	4%
< 177	240	6%
<75	108	3%

PIT1 40-50

Grain Size (micrometers)	Weight (grams)	Percent of Total Weight
4000	155	6%
2000	405	16%
1410	265	10%
1000	310	12%
710	252	10%
500	263	10%
350	218	9%
250	170	7%
177	136	5%
< 177	242	10%
<75	116	5%

PIT1 50-66

Grain Size (micrometers)	Weight (grams)	Percent of Total Weight
4000	81	3%
2000	312	11%
1410	279	10%
1000	385	14%
710	338	12%
500	343	12%
350	304	11%
250	177	6%
177	199	7%
< 177	239	9%
<75	91	3%

PIT1 66-76

Grain Size (micrometers)	Weight (grams)	Percent of Total Weight
4000	117	9%
2000	187	14%
1410	128	10%
1000	150	11%
710	127	9%
500	123	9%
350	150	11%
250	54	4%
177	125	9%
< 177	134	10%
<75	48	4%

PIT1 76-86

Grain Size (micrometers)	Weight (grams)	Percent of Total Weight
4000	258	22%
2000	257	22%
1410	136	11%
1000	135	11%
710	93	8%
500	71	6%
350	87	7%
250	0	0%
177	74	6%
< 177	61	5%
<75	19	2%

Soil Pit 2

PIT2 0-14

Grain Size (micrometers)	Weight (grams)	Percent of Total Weight
4000	212	6%
2000	547	15%
1410	316	8%
1000	310	8%
710	328	9%
500	386	10%
350	348	9%
250	238	6%
177	192	5%
< 177	696	19%
<75	162	4%

PIT2 14-28

Grain Size (micrometers)	Weight (grams)	Percent of Total Weight
4000	320	8%
2000	502	13%
1410	338	8%
1000	489	12%
710	461	12%
500	512	13%
350	414	10%
250	256	6%
177	202	5%
< 177	404	10%
<75	95	2%

PIT2 28-40

Grain Size (micrometers)	Weight (grams)	Percent of Total Weight
4000	320	8%
2000	502	13%
1410	338	8%
1000	489	12%
710	461	12%
500	512	13%
350	414	10%
250	256	6%
177	202	5%
< 177	404	10%
<75	95	2%

PIT2 40-50

Grain Size (micrometers)	Weight (grams)	Percent of Total Weight
4000	226	6%
2000	506	13%
1410	395	10%
1000	583	15%
710	351	9%
500	398	10%
350	305	8%
250	249	6%
177	373	10%
< 177	405	10%
<75	98	3%

PIT2 50-60

Grain Size (micrometers)	Weight (grams)	Percent of Total Weight
4000	289	7%
2000	584	14%
1410	449	11%
1000	606	14%
710	534	13%
500	503	12%
350	349	8%
250	222	5%
177	187	4%
< 177	450	11%
<75	58	1%

PIT2 60-71

Grain Size (micrometers)	Weight (grams)	Percent of Total Weight
4000	289	7%
2000	584	14%
1410	449	11%
1000	606	14%
710	534	13%
500	503	12%
350	349	8%
250	222	5%
177	187	4%
< 177	450	11%
<75	58	1%

PIT2 71-80

Grain Size (micrometers)	Weight (grams)	Percent of Total Weight
4000	194	8%
2000	391	16%
1410	280	11%
1000	308	13%
710	232	10%
500	195	8%
350	242	10%
250	125	5%
177	139	6%
< 177	298	12%
<75	35	1%

PIT2 80-90

Grain Size (micrometers)	Weight (grams)	Percent of Total Weight
4000	156	9%
2000	306	18%
1410	203	12%
1000	206	12%
710	145	9%
500	130	8%
350	96	6%
250	11	1%
177	133	8%
< 177	210	13%
<75	67	4%